INVESTIGATION OF THE TUMOUR PROMOTING EFFECTS OF CELLULAR SENESCENCE DURING PITUITARY AND LUNG TUMOURIGENESIS

By

Scott Haston

Thesis submitted to University College London for the degree of

Doctor of Philosophy

2019

Developmental Biology and Cancer Programme

GOSH-UCL Institute of Child Health

University College London

DECLARATION

I, Scott Haston, confirm that the work presented in this thesis is my own. Where information has been derived from other sources, I confirm this has been indicated in the thesis.

Scott Haston

UCL student number: 13045754

ABSTRACT

This thesis involves understanding the role that cellular senescence plays during the early stages of adamantinomatous craniopharyngioma (ACP) and non-small cell lung cancer (NSCLC) tumourigenesis using genetically engineered mouse models. The host laboratory has previously shown that when pituitary stem cells are targeted with oncogenic β-catenin, they form clusters of stem cells that show non-cell autonomous tumour inducing potential. Using immunohistochemical and transcriptomic approaches, here I show that cluster cells are molecularly analogous in mouse and human ACP and share a signature of senescence with concomitant activation of the senescence associated secretory phenotype (SASP). I reveal that the tumour-inducing potential of the cluster cells requires a robust SASP. This is evidenced by targeting pituitary stem cells of aged mice (older than 6 months) with oncogenic β -catenin, which results in reduced SASP and decreased tumourigenesis. This suggests that a robust SASP is the likely driver of paracrine tumourigenesis in the pituitary. Further to this, the role of activated MAPK signalling during pituitary development was explored by driving the expression of oncogenic Kras (KrasG12D) and Braf (BrafV600E) in either pituitary progenitors or postnatal adult pituitary stem cells. By demonstrating a cell-autonomous expansion of the embryonic pituitary stem cells compartment with impaired differentiation potential, this study provided insight into the pathogenesis of another pituitary tumour, papillary craniopharyngioma. Finally, during oncogenic Kras-driven (KrasG12D) NSCLC progression in mice, it is observed that the adenoma phase of the tumour does not show a high level of senescence, however senescent cells are found outside and in association with the growing tumours in agreement with the concept of paracrine senescence. To study these senescent cells in vivo a new genetically engineered mouse model (p16FDR) was developed which allows for their visualisation, pharmacogenetic ablation and lineage tracing. Ablation of these senescent cells using p16FDR mice was found to reduce tumour burden and proliferation significantly. Together, these data suggest that senescence can have paracrine pro-tumourigenic properties and their therapeutic ablation may be clinically beneficial.

IMPACT STATEMENT

In this thesis, the function cellular senescence in the early stages of tumour formation was explored. Cellular senescence is classically regarded as a mechanism to restrain the growth of stressed cells, which are at risk of giving rise to tumours. However, senescent cells are known to produce and secrete a number of molecules (collectively termed the senescence associated secretory phenotype (SASP)), which paradoxically has been described to promote the growth of tumour cells. Many cancers and tumours show the presence of senescent cells in both their benign and malignant phases and the function of these cells is poorly understood. This is also true of pituitary adamantinomatous craniopharyngioma (ACP) and non-small cell lung cancer (NSCLC). ACP is the most common non-neuroepithelial brain tumour found in children, associated with significant morbidity and poor quality of life for the survivors, and currently no targeted therapies are available. NSCLC is one of the leading causes of cancer related deaths in adults and while tremendous research efforts are on-going, exploring the biology of the disease to improve targeted therapies, little progress has been made recently in improving patient survival. Therefore, detailed investigations into the role of senescence in cancer biology are of profound importance and may provide insight into the origin of these diseases.

The work in this thesis provides evidence that cellular senescence is acting to promote the growth of lung tumours. Moreover, the SASP from senescent cells acts to drive the formation of ACP-like tumour in the pituitary gland. Therefore, future therapeutic targeting of senescence and SASP pathways may be beneficial in slowing down tumour formation in both of these organ systems. Further to this, this thesis improved our basic understanding of the role a cellular signalling pathway, termed MAPK, plays in orchestrating embryonic development of the pituitary. This work also provided insight into how the mutations found in another pituitary tumour, papillary craniopharyngioma, can lead to the development of the disease. Cancer is an extremely varied and complex class of diseases to clinically manage. Future investigations into the origin of cancer and the involvement of cellular senescence may provide strategies to prevent the occurrence of the disease in the first place. Such a prophylactic approach may circumvent the difficulties faced in treating more advanced forms of the disease.

Dedicated to my grandmother, mother and wife, for everything you have done to help and support me

ACKNOWLEDGEMENTS

Firstly, I would like to extend my deepest gratitude and thanks to my supervisor, Professor Juan Pedro Martinez-Barbera. Your passion for science is an inspiration and I am very fortunate to have been one of your students. My development as a scientist would be significantly worse without the freedom to explore my own hypotheses that you allowed me, as well as the invaluable guidance you provided. I have learned a great deal from you, which I will always carry with me in my scientific career, specifically the “chop chop” mantra and all the stuff about genetics.

I would like to extend my thanks to the Wellcome Trust for providing funding and the opportunity to pursue my PhD. Through the program I was introduced to my first friends in London, Adam Shellard and Rosalyn Flower. You guys have provided invaluable support, joy and laughter during my PhD for which I am grateful. This thesis would not have been possible without the help of a great many people in and associated with the Institute of Child Health. Specifically, I would like to thank Ayad Eddaoudi and Stephanie Canning for their technical expertise in flow cytometry, Debby Mustafa, Ailsa Greppi, and Kyle O’Sullivan for their assistance in working with the mouse lines, John Apps and the staff at UCL genomics for assistance with bioinformatics and sequencing, Massimo Signore for generating chimeras and my first genetically engineered mouse model and the Lamb for many, many double vodkas with red-bull.

I have no words (that doesn’t happen often) to describe my immense love and gratitude to my colleagues and friends in JP’s lab, past and present. I would like to extend my love to my lab partners and friends Dr Gabriela Carreno, Dr Jose Mario Gonzalez-Meljem and Dr Sara Pozzi. You three immediately made me feel welcome in the lab with a shared dark humour and love of alcohol. You all taught me so much. Without you I probably wouldn’t know what end of the pipette the tips go on. I would also like to thank Dr Jean-Marie (Jimmy) Delalande and Saba Manshaei (my first and arguably greatest student) for both sharing many great times with me, inside and outside the lab. Finally, from JP’s group, I would like to thank Leonidas Panousopoulos. Within the lab you have provided more scientific help that I can list and outside you have been a good drinking buddy, an excellent friend and a supportive groomsman. Without your assistance I would not be the scientist I am today and I am grateful to

count you amongst my closest friends. I will forever remember (most of) our many drunken nights in the Lamb/Birkbeck and the mad ideas we all discussed. You all truly are a wonderful assortment of human beings to spend time with.

Finally, I would like to extend my greatest gratitude to my wife, Jennifer Auer-Haston. Absolutely none of this would have been possible without your love, guidance and support (also the delicious cakes!). You have always been there to pick me up in my worst times and cheer me on when I'm at my best. I am glad we have shared this doctoral adventure together and I can't wait for what the future has to bring. You are, and always will be, my favourite "lump of matter".

Thank you all.

TABLE OF CONTENTS

LIST OF FIGURES

LIST OF TABLES

LIST OF PUBLICATIONS

Apps, J. R., Carreno, G., Gonzalez-Meljem, J. M., **Haston, S**., Guiho, R., Cooper, J. E., … Martinez-Barbera, J. P. (2018). Tumour compartment transcriptomics demonstrates the activation of inflammatory and odontogenic programmes in human adamantinomatous craniopharyngioma and identifies the MAPK/ERK pathway as a novel therapeutic target. Acta Neuropathologica, 135(5), 757–777.

Haston, S., Manshaei, S., & Martinez-Barbera, J. P. (2018). Stem/progenitor cells in pituitary organ homeostasis and tumourigenesis. Journal of Endocrinology, 236(1), R1–R13.

Haston, S., Pozzi, S., Carreno, G., Manshaei, S., Panousopoulos, L., Gonzalez-Meljem, J. M., … Martinez-Barbera, J. P. (2017). MAPK pathway control of stem cell proliferation and differentiation in the embryonic pituitary provides insights into the pathogenesis of papillary craniopharyngioma. Development, 144(12), 2141–2152.

Gonzalez-Meljem, J. M., **Haston, S**., Carreno, G., Apps, J. R., Pozzi, S., Stache, C., … Martinez-Barbera, J. P. (2017). Stem cell senescence drives age-attenuated induction of pituitary tumours in mouse models of paediatric craniopharyngioma. Nature Communications, 8(1), 1819.

Carreno, G., Apps, J. R., Lodge, E. J., Panousopoulos, L., **Haston, S**., Gonzalez-Meljem, J. M., … Martinez-Barbera, J. P. (2017). Hypothalamic sonic hedgehog is required for cell specification and proliferation of LHX3/LHX4 pituitary embryonic precursors. Development, 144(18), 3289–3302.

Carreno, G., Gonzalez-Meljem, J. M., **Haston, S**., & Martinez-Barbera, J. P. (2016). Stem cells and their role in pituitary tumorigenesis. Molecular and Cellular Endocrinology, pp. 27–34.

ABBREVIATIONS

AAH - Atypical adenomatous hyperplasias

ACP - Adamantinomatous craniopharyngioma

ACTH - Adenocorticotrophic hormone

AER - Apical ectodermal ridge

AL - Anterior lobe of the pituitary

AML - Acute myeloid leukaemia

ANR - Anterior neural ridge

AP - Alkaline phosphatase

APC - Adenomatous polyposis coli

AVE - Anterior-visceral endoderm

BASCs - Bronchioalveolar stem cells

BrdU - Bromo-deoxy-uridine

CDK - Cyclin-dependent kinase

CDKi - Cyclin-dependent kinase inhibitor

CNS - Central nervous system

CSCs - Cancer stem cells

DDR - DNA-damage response

DMEM - Dulbecco's Modified Eagle's Medium

dpc - days post coitum

DSBs - Double-stand breaks

DTR - Diphtheria toxin receptor

Dvl - Dishevelled

EdU - 5-ethynyl-2'-deoxyuridine

EMT - Epithelial-mesenchymal transition

ER - Endoplasmic reticulum

ESCs - Embryonic stem cells

FCS - Fetal calf serum

FFPE - Formalin-fixed parafin embedded

FSH - Follicle-stimulating hormone

Fz - Frizzled

GH - Growth hormone

GO - gene ontology analysis

GOS - Galacto-oligosaccharides

GSEA - Gene set enrichment analysis

HP - Hypothalamic-pituitary axis

HSC - haematopoietic stem cells

IF - Immunofluorescence

IHC - Immunohistochemistry

IL - Intermediate lobe of the pituitary

ISH - *In situ* hybridisation

LCM - Laser capture microdissection

LH - Lutensing hormone

MAPK - Mitogen activated protein kinase

MEFs - Mouse embryonic fibroblasts

MEFs - Mouse embryonic fibroblasts

MSH - Melanocyte-stiulating hormone

mTOR - Mechanistic target of rapamycin

NC - Neural crest

NSCLC - Non-small-cell lung cancer

OIS - Oncogene induced senescence

PA - Pituitary adeonmas

PAM - Protospacer adjacent motif

PBS - Phosphate-buffered saline

PCA - Principle component analysis

PCP - Papillary craniopharyngipoma

PCR - Polymerase chain reaction

PCR - Polymerase chain reaction

PFA - Paraformaldehyde

PL - Posterior lobe of the pituitary

Pomc1 - Pro-opiomelanocortin

PSCs - Pituitary stem cells

Rb - Retinoblastoma protein

RFP - Red fluorescent protein

ROS - Reactive-oxygen species

RP - Rathke's pouch

SA-β-Gal - Senescence-associated Beta-Galactosidase

SASP - Senescence associated secretory phenotype

SCLC - Small-cell lung cancer

SIPS - Stress-induced premature senescence

TCF/LEF - T cell factor/lymphoid enhancer factor

TSH - Thyroid-stimulating hormone

VD - Ventral diencephalon

YFP - Yellow fluorescent protein

CHAPTER 1: GENERAL INTRODUCTION

1.1 Cellular Senescence

1.1.1 Definition and function of cellular senescence

Cellular senescence is a program characterised by stable/permeant cell cycle arrest and an altered state of gene expression, while maintaining viability and metabolic functions. Cellular quiescence on the other hand, while also being defined by proliferative arrest, is not stable/permeant and cells can re-enter the cell cycle upon stimulation with appropriate mitogenic signals. Generally, cellular quiescence is found in certain differentiated cell types, such as fibroblasts, but is most commonly found as a characteristic of stem cells (Campisi 2013).

Cellular senescence is a process that was first described by Leonard Hayflick and Paul Moorhead in 1962. This was achieved through the observation that fibroblasts had a replicative lifespan during *in vitro* culture and that after serial passage the cells showed a continual decline in their proliferative potential before permanent arrest (Hayflick & Moorhead 1961). From this work it is now appreciated that most cells, under normal conditions, can only undergo a finite number of divisions, known as the 'Hayflick limit'. This phenomenon has come to be termed replicative senescence as it is known to be a consequence of gradual telomere attrition following serial replication (Bodnar et al. 1998).

It has been well established that senescence is a consequence of various persistent cellular stresses. These include; the accumulation of unrepaired DNA damage, ionizing radiation, endoplasmic reticulum (ER) stress response, reactive-oxygen species (ROS) stress, cytotoxic chemical compounds and tumour-suppressor loss such as PTEN (Fitzgerald et al. 2015; Colavitti & Finkel 2005; Le et al. 2010; Liao et al. 2014; Ewald et al. 2010; Matos et al. 2015; Pluquet et al. 2015;

Kuilman et al. 2010; Jan R Dörr et al. 2013). Together these non-telomere related senescent phenotypes are termed as stress-induced premature senescence (SIPS).

Further to SIPS, another form of senescence is oncogene induced senescence (OIS), whereby the expression of oncogenic proteins such as stabilised β-Catenin, BRAF-V600E, KRAS-G12D and HRAS-V12 leads to the acquisition of a senescent phenotype in some cells (Serrano et al. 1997; Collado et al. 2005a; M Collado & Serrano 2010; Gu et al. 2014; Xu et al. 2008a; Wajapeyee et al. 2008). It has been observed that many benign tumours show higher expression of cellular senescence markers than later, more malignant tumours. This has lead to OIS being considered as a potent tumour-suppressive mechanism, which prevents the proliferation of cells harbouring oncogenic mutations (Braig et al. 2005; Z. Chen et al. 2005; Michaloglou et al. 2005).

1.1.1.1 The senescence associated secretory phenotype (SASP)

A prominent and conserved feature of senescent cells is their secretion of a plethora of soluble and insoluble factors, which include; chemokines, cytokines, growth factors and extracellular components, and are collectively known as the senescence associated secretory phenotype (SASP) (Shelton et al. 1999; Coppé et al. 2008a; Coppé, Christopher K Patil, et al. 2010). While the composition of the SASP is known to be heterogeneous depending on the senescence inducing stimuli, time post-senescence induction and cellular context, some factors appear to be more commonly represented. Examples of these factors include: the chemokines IL8, CCL2, CCL5 and CCL20; the interleukins IL1α, IL1β and IL6; inflammatory cytokines: TGFβ, TNFα and MIF as well as growth factors: bFGF, HGF, VEGF (Coppé, Christopher K Patil, et al. 2010; Tchkonia et al. 2013).

The SASP has been shown to mediate pleotropic effects in both senescent cells and in the tissue microenvironment. Generally, SASP is thought to have two main roles; 1) The clearance of senescent cells from sites of damage through the recruitment of immune cells (Iannello & Raulet 2013; Xue et al. 2007a; Kang et al. 2011; Krizhanovsky et al. 2008; Sagiv et al. 2013) and 2) the reinforcement of the senescent phenotype by either autocrine or paracrine signaling (Acosta et al. 2008; Acosta et al. 2013; Hubackova et al. 2012). (Figure 1.1)

1.1.2 Beneficial effects of cellular senescence and the SASP

Cellular senescence and the SASP are generally considered to be a beneficial evolutionary adaptation, which prevents the proliferation of abnormal cells which show signs of stress or persistent DNA damage through immune cell clearance (Sharpless & Sherr 2015).

1.1.2.1 Senescence and embryonic development

Interestingly, recent work has found that cellular senescence is implicated in normal embryonic development. Independent work by two groups identified senescent cell populations in the apical ectodermal ridge (AER) and roof plate of the neural tube in mice, as well as the mesonephros and the endolymphatic sacs of the inner ear in both mouse and human embryos. These developmentally programmed senescent populations are transient and are eliminated either by apoptosis or macrophage clearance. Developmental senescence appears to be important for tissue morphogenesis by promoting the elimination of transient developmental structures as well as aiding in tissue homeostasis and remodelling. Molecularly this developmental senescence is maintained by the cyclin-dependent kinase inhibitor Cdkn1a (p21) and

mice lacking *Cdkn1a* show morphological and patterning defects in developmentally senescent tissues (Storer et al. 2013; Muñoz-Espín et al. 2013).

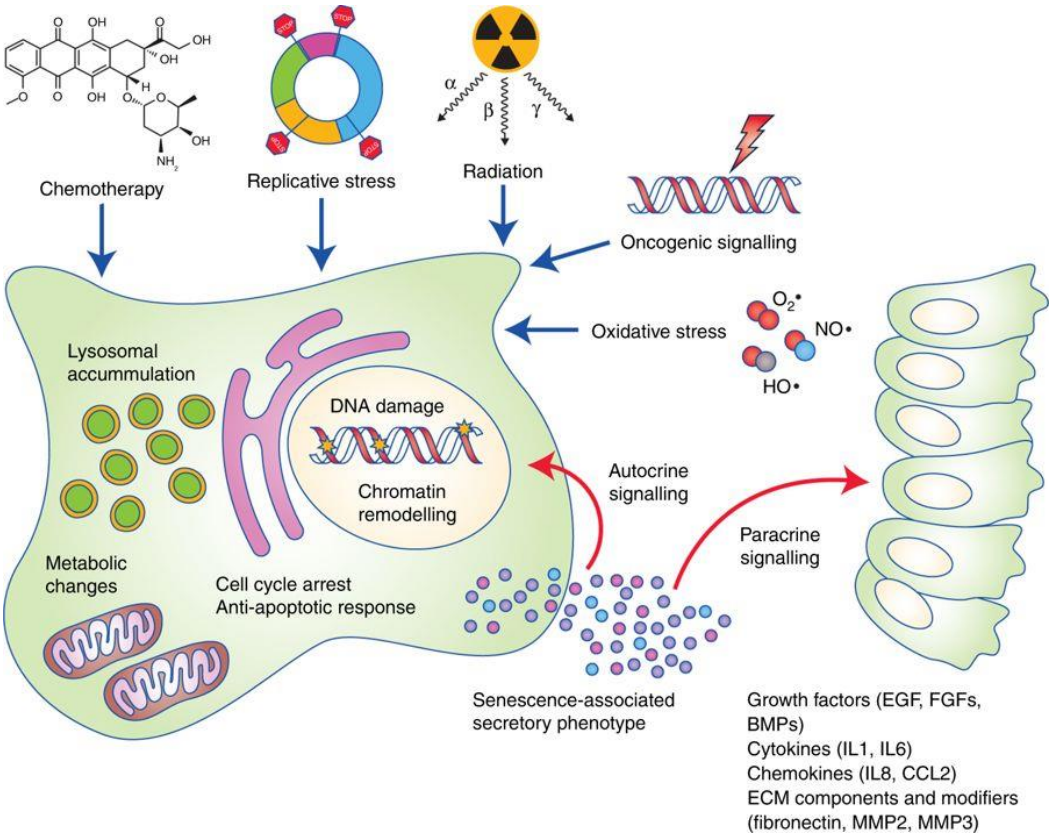

Figure 1.1. Diagram detailing the senescent phenotype. Senescence is induced by cellular stresses including; genotoxic drugs (such as chemotherapeutic agents), replicative stress, ionizing radiation-induced DNA damage, oxidative stress and oncogene signaling. These stresses result in expansion of the lysosomal compartment, metabolic and epigenetic changes, permenant cell cycle arrest with apoptotic resistance and production of the SASP. The SASP can then signal in an autocrine manner to reinforce the senescent state or in a paracrine manner to influence surrounding cells locally and systemically.

1.1.2.2 Senescence and regeneration

Recent evidence has also suggested that cellular senescence is implicated in promoting tissue regeneration following injury. Work by the Campisi group demonstrated that cellular senescence is involved in normal wound healing in mice. Using a novel mouse model (*p16-3MR*) they were able to genetically label p16-

expressing senescent cell populations with monomeric red fluorescent protein (RFP) and ablate them through the administration of the drug ganciclovir. This research found that senescent cells are induced following skin wounding and that they aid in optimal wound closure through the secretion of the SASP factor PDGF-AA, before being cleared (Demaria, Ohtani, Youssef, Rodier, Toussaint, Mitchell, Laberge, Vijg, VanSteeg, Martijn E.T. Dollé, et al. 2014). The view that cellular senescence can be pro-regenerative is bolstered by observations of salamanders during limb regeneration. Many salamander species possess an impressive capability to regenerate complex structures such as the limbs, heart, brain and spinal cord, among other tissues. During limb regeneration it was observed that senescent cells are specifically induced at the site of the injury and they are cleared from the wound site by macrophages. Depletion of macrophages results in persistence of the injury-induced senescent cells, which leads to impaired regeneration (Yun et al. 2015). Recent evidence suggests that the involvement of senescent cells in tissue regeneration appears to be conserved in mammals, as senescent cells at the site of muscle injury in mice enhances *in vivo* reprogramming and promotes muscle regenerations (Chiche et al. 2017). Moreover, further evidence that cellular senescence can promote the dedifferentiation and reprogramming of neighbouring non-senescent cells was appreciated using mice in which the expression of pluripotency reprogramming factors (OCT4, SOX2, KLF4 and cMYC) could be activated in an inducible manner. Expression of these factors resulted in the induction of cellular senescence in non-reprogrammed cells which, through the action of the SASP, particularly IL6, enhanced the reprogramming efficiency of neighbouring non-senescent cells which also harboured the reprogramming factors (Mosteiro et al. 2016). Bolstering these observations, a recent study has shown that transient exposure of mouse keratinocytes to SASP factors results in the aquisition of stem cell markers and increased *in vivo* regenerative capacity. This reinforces the view that the transient induction of cellular senescence can be pro-regenerative through inducing local cellular plasticity (Ritschka et al. 2017).

1.1.3 Detrimental effects of cellular senescence and the SASP

While canonically considered an anti-tumour mechanism, recent research has highlighted the involvement of senescent cells in numerous pathological processes, principally ageing and age-associated diseases as well as cancer (Collado et al. 2007; Muñoz-Espín & Serrano 2014). For further detail of the role of cellular senescence in cancer see section 1.1.5.

1.1.3.1 Senescence, ageing and age-associated diseases

Hayflick and Moorhead originally posited the concept that cellular senescence contributes to the normal ageing process (Hayflick & Moorhead 1961) and senescent cells are observed to accumulate in most ageing tissues. This has been well characterized in the lung, liver, skin and spleen of aging humans, monkeys and mice (Herbig et al. 2006; Wang et al. 2009; Dimri et al. 1995). Further to this, quantification of the senescent cell burden in the intestine and liver allows for the accurate prediction of life-span in mice (Jurk et al. 2014).

The role of cellular senescence during the normal ageing process is currently debated with two main hypotheses being considered. The first postulates that the accumulation of senescent cells and their SASP result in tissue dysfunction leading to an aging phenotype (Hall et al. 2016; Franceschi & Campisi 2014; Salminen et al. 2008; Shaw et al. 2010). The second view is that senescence may reduce the regenerative capacity of adult stem/progenitor cells, which are necessary for tissue homeostatic balance (Flores et al. 2006; Castilho et al. 2009; Pollina & Brunet 2011). These hypotheses are not necessarily mutually exclusive and may act concomitantly during normal aging. Evidence supporting senescence having a causative role in ageing is derived from observations that *p16*^{INK4A} -deficient mice, in which the

senescence program is abrogated, have increased lifespans and reduced incidence of age-associated disease. Notably, this effect is also observed in progeroid or normal mice when senescent cells are ablated genetically or with chemical compounds that specifically target senescent cells (i.e. senolytics) (Darren J. Baker et al. 2011; Baker et al. 2016; Chang et al. 2016; Roos et al. 2016; Farr et al. 2017; Xu et al. 2018). However, further work is required to determine the mechanisms by which senescent cells accumulate during ageing and their specific effects on the tissue microenvironment, which potentially lead to the ageing phenotype. This area of study has been confounded by the lack of available biomarkers and tools to study these processes *in vivo*.

1.1.3.2 Senescence, SASP and the promotion of tumourigenesis

Over recent years there has been accumulating evidence that senescence and SASP can, counter-intuitively, act in a pro-tumourigenic manner. This was first appreciated by the fact that the SASP production from senescent fibroblasts is able to promote the growth and tumourigenic ability of premalignant epithelial cells (deficient for p53), but not normal epithelial cells (Coppé, Christopher K Patil, et al. 2010; Krtolica et al. 2001). Senescent cells, through SASP production, are now known to promote tumourigenesis by two non-mutually exclusive means: 1) Direct signaling to malignant or pre-malignant cells or 2) Indirect signaling through microenvironmental modification, allowing for a permissive setting for cancer development.

The most commonly observed direct effect of the SASP on neighboring cells is the promotion of proliferation, exacerbating their potential to form tumours (Coppé, Christopher K. Patil, et al. 2010; Laberge et al. 2015; Nakamura et al. 2014; Kuilman et al. 2008; Bavik et al. 2006). The SASP has also been found to intensify other tumourigenic phenotypes such as epithelial-to-mesenchymal transition (EMT) (Coppé

et al. 2008b), chemotheraputic resistance (Canino et al. 2012) and tumour relapse (Demaria et al. 2017). Moreover, the SASP can also promote reprogramming and dedifferentiation of neighboring cells, which can lead to the formation of cancer stem cells (CSCs) (Parrinello et al. 2005; Cahu et al. 2012; Ohanna et al. 2013).

Evidence has also been found for the indirect involvement of the SASP on tumourigenesis through modulation of the tissue microenvironment. Numerous proangiogenic, but not angiostatic, factors are found in the SASP milieu (Campisi 2013), and evidence has shown that the SASP can induce the formation of tumour-supporting angiogenesis and the invasiveness of epithelial cells (Yu et al. 2013; Vital et al. 2014; Ancrile et al. 2007). Furthermore, the SASP can have profound impacts on the behavior of immune cells. An example of this is macrophages, which can be polarized towards a tumour-promoting phenotype (Lujambio et al. 2013). In addition, the SASP can drive the formation of immunosupressive microenvironments, which act as permissive setting for tumourigenesis and metastasis (Ruhland et al. 2016; Luo et al. 2016).

1.1.4 Biochemical mechanisms underlying cellular senescence

Traditionally, cellular senescence has been identified through the detection of senescence-associated β-galactosidase (SA-β-Gal). However, further research has uncovered that the complexity and heterogeneity of the senescent phenotype means that a combinatorial array of molecular markers are necessary to identify *bona fide* senescent cell populations (Sharpless & Sherr 2015; Campisi 2013; Manuel Collado & Serrano 2010; Hernandez-Segura et al. 2018). These markers represent the conserved molecular machinery necessary to maintain SASP production and the senescent phenotype across various cell type and senescent states. Examples include the activation of the DNA-damage response (DDR), SASP production, resistance to

apoptosis (mainly through upregulation of prosurvival pathways), loss of mitotic capacity and expansion of the lysosomal compartment.

1.1.4.1 Cellular senescence and cell cycle regulation

As mentioned previously, a hallmark of cellular senescence is the permanent arrest of the cell cycle. Therefore, when initially profiling a tissue for cellular senescence, negativity for proliferation indicators such as the cell-cycle marker Ki-67, the mitosis marker phosphorylated Histone H3 (Davalos et al. 2010) or genomic DNA uptake of thymidine analogues (EdU/BrdU) during S-phase is an initial indicator of senescence induction. Such analyses much be interpreted cautiously however, as quiescent cell populations will also show negativity for these markers but have the capacity to re-enter the cell cycle.

Mechanistically it is now known that the cell-cycle arrest experienced by senescent cells is predominantly due to $p16^{INK4A}$/Rb and the p53/$p21^{CIP1}$ pathways, however some exceptions to this have been reported. In some contexts either of these pathways can be abrogated while still maintaining the senescent phenotype, as they generally function cooperatively, however in some instances these pathways are indispensable (Kamijo et al. 1997; Zhu et al. 2015).

The tumour suppressor p53 (encoded by *TP53* in humans and *Trp53* in mice), known colloquially as 'the guardian of the genome' has crucial functions related to cancer prevention and cellular stress. Such stresses include: replicative stress, DNA damage, hyper proliferative signals due to oncogenic mutations, oxidative stress, hypoxia and nutrient deprivation, among others (Vousden & Ryan 2009; Bieging et al. 2014). *TP53* is also known to be one of the most commonly mutated genes in human cancers, with around 50% of sporadic cancers found to carry inactivating mutations

(Olivier et al. 2010). Furthermore, germ-line *TP53* mutations, known as Li-Fraumeni syndrome, results in an extremely high predisposition to the development of multiple cancers types (Nochols et al. 2001). Following the expression of p53, it activates pleiotropic responses, predominantly through its downstream effector $p21^{CIP1}$ (encoded by *CDKN1A*). These responses include: the arrest or slowing of the cell cycle, autophagy, promotion of DNA repair, apoptosis or senescence induction (Menendez et al. 2009; Meek 2009). Beyond stress responses, p53 also has reported roles in regulating stem cell self-renewal and differentiation (Spike & Wahl 2011). As many of these functions are intimately related to cancer progression and initiation, the profound interest in p53/$p21^{CIP1}$ signaling in the field of oncology is warranted.

One of the most critical mediators of senescent cell cycle repression is the $p16^{INK4A}$/Rb pathway. The tumour suppressor $p16^{INK4A}$ (encoded by the *CDKN2A* locus) is a negative regulator of the cell cycle (Serrano et al. 1993; Zhao et al. 2016) that is upregulated in response to stress, such as DNA damage. $p16^{INK4A}$ then acts to prevent the complexing of the cyclin-dependent kinases (CDK) CDK4 or CDK6 with cyclin D (Serrano et al. 1993; Zhao et al. 2016). The absence of this complex results in the retinoblastoma protein (Rb) maintaining a hypo-phosphorylated, growth suppressive state. Hypo-phosphorylated Rb is able to bind to and repress the activity of E2F transcription factors, preventing their transcriptional activation of their pro-growth target genes. $p16^{INK4A}$ has been demonstrated to be of significant importance in the induction and maintenance of the senescent state (Dai & Enders 2000; Ohtani & Hara 2013; Baker et al. 2011; Demaria et al. 2014; Burd et al. 2013; Sato et al. 2015). Therefore, $p16^{INK4A}$ is regarded as one of the most canonical markers of cellular senescence in various cellular contexts (Salama et al. 2014) and is also observed in senescent contexts, which are independent of p53/$p21^{CIP1}$ mediated arrest (Jacobs et al. 2004). Furthermore, $p16^{INK4A}$/Rb signaling is also observed to have a crucial role during OIS *in vivo* (Michaloglou et al. 2005; Serrano et al. 1996; Serrano et al. 1997; Sarkisian et al. 2007).

1.1.4.2 The DNA damage response and cellular senescence

Analysis of senescent cells has demonstrated that DNA damage is required for SASP activation (Rodier et al. 2009; Kang et al. 2015). Furthermore, oncogene-induced DNA damage appears to be necessary for the establishment and maintenance of OIS (Bartkova et al. 2006; Mallette, Ferbeyre, et al. 2007). Currently the mechanisms coupling oncogene expression with activation of the DDR are incompletely understood due to their complexity. It is known, however, that oncogene signaling can accelerate DNA replication, which can lead to sustained replicative stress, which ultimately results in DNA damage accumulation, such as double-stand breaks (DSBs) (Di Micco et al. 2006; Prieur et al. 2011; Halazonetis et al. 2008). Following the formation of DSBs, PARP-1 recruits the kinases ATM/ATR and DNA-PKcs, leading to the accumulation and phosphorylation of histone H2AX (yH2AX) at the sites of DSBs (Weaver & Yang 2013). A positive feedback loop initiated by yH2AX increases protein recruitment, such as ATM/ATR, at DSB sites to facilitate the activation of a signaling cascade which ends with the induction of DNA-checkpoint pathways, such as p53/p21^{CIP1} (Gaillard et al. 2015; Bonner et al. 2008).

1.1.4.3 The role of the NF$_\kappa$B signaling pathway

Nuclear factor kappa-light-chain-enhancer of activated B cells (NF$_\kappa$B) is an evolutionarily conserved transcription factor complex that plays major roles in the regulation of cellular stress and inflammation. Furthermore, this pathway has important functions during cancer and other diseases (Hayden et al. 2006; Lawrence 2009). Pathway activation is commonly due to inflammatory mediators such as Il1β, TGFβ and TNFα; DNA-damage pathway induction by PARP-1 activation of NEMO/ATM or oxidative stress signaling through p38MAPK (Weaver & Yang 2013). NF$_\kappa$B signaling is a critical pathway in cellular senescence that is required for the initiation and

maintenance of SASP production during OIS (Crescenzi et al. 2011; Ohanna et al. 2011; Freund et al. 2011; Salminen et al. 2012). Furthermore, this pathway has been shown to be involved in the reinforcement of the senescent phenotype in both a cell-autonomous and non-cell-autonomous manner (Acosta et al. 2008; Rovillain et al. 2011; Chien et al. 2011).

Molecularly, the $NF_{\kappa}B$ transcriptional complex is formed from heterodimers of class I (NFKB1 and NFKB2) and class II (REL, RELA, RELB) $NF_{\kappa}B$ subfamily members. During canonical signaling the $NF_{\kappa}B$ complex is sequestered in the cytoplam by inhibitory $I_{\kappa}B$ proteins. Upon pathway activation $I_{\kappa}B$ kinase (IKK) complexes, including NEMO/IKKy, target $I_{\kappa}B$ proteins for protosomal degradation through phosphorylation. This then allows for the translocation of $NF_{\kappa}B$ to the nucleus to activate the transcription of downstream target genes (Hayden & Ghosh 2012). $NF_{\kappa}B$ transcriptional targets include a plethora of chemokines and cytokines, stress response genes, immunoreceptors, growth factors and cell survival genes (Perkins 2007; Lawrence 2009).

1.1.4.4 The role of mTOR and autophagy pathways

The mechanistic target of rapamycin (mTOR) is a serine/threonine kinase that is a component of the mTORC1 signaling complex, which shows a high degree of evolutionary conservation. mTORC1 signaling is of significant importance in regulating proliferation and growth of cells in response to environmental factors such as the availability of nutrients. The predominant function of mTOR is to induce the activation of the protein synthesis machinery. Beyond this, signaling via mTOR has also been implicated in senescence initiation (Vousden & Ryan 2009; Castilho et al. 2009; Hasty et al. 2013) and SASP activation (Laberge et al. 2015; Herranz et al. 2015). Activated mTORC1 phosphorylates p70 ribosomal protein S6 kinase 1 (S6K1),

which results in the activation of protein translation and the eukaryotic initiation factor 4E-binding protein 1 (4E-BP1) through phosphorylation of ribosomal protein S6. Together these results in the activation of mRNA synthesis, ribosome biogenesis and protein translation.

mTOR also acts to inhibit autophagy, the process by which protein complexes and organelles are moved to vesicular autophagosomes before being degraded by lysosomes (Wirawan et al. 2012). However, the coupling between mTOR and autophagy appears to promote secretory phenotype in varied cellular contexts, including in OIS. Autophagy has varied functions but primarily provides energy during nutrient scarcity to support cell viability and also support cellular homeostasis by clearing potentially toxin misfolded proteins (Filomeni et al. 2015). The role that autophagy plays in cellular senescence is currently debated and it appears to have context dependent pro- and anti-senescence activities (White 2012; Kang & Elledge 2016).

1.1.4.5 The involvement of the lysosomal compartment in senescent cells

The current best practice for the identification of senescent cells is the use of the SA-β-Gal assay at pH 6.0 (Dimri et al. 1995; Debacq-Chainiaux et al. 2009). The increased activity of β-Galactosidase in senescent cells has been shown to be due to the overall increase in the lysosomal compartment of the cell (Kurz et al. 2000; Ivanov et al. 2013), which can also be assessed immunohistochemically using antibodies raised against GLB1, the protein responsible for the SA-β-Gal activity (Lee et al. 2006; Wagner et al. 2015). The expanded lysosomal compartment in senescent cells is thought to be a consequence of SASP productions, which is highly demanding on the cells protein production capabilities and leads to unfolded protein responses, endoplasmic reticulum stress and proteotoxicity (Dörr et al. 2013). However, high β-

Galactosidase activity is not a universal hallmark or specific marker of senescent cells as other cell types may show positivity for SA-β-Gal assays which are not senescent such as tissue macrophages (Hall et al. 2017).

1.1.5 Cellular senescence and cancer

The hypothesis that cellular senescence functions as a tumour-suppressive mechanism arises from comparisons of pre-malignant and malignant tumours, with the former showing features of senescence, while the latter do not. This phenomenon was initially described in the context of lung and pancreas tumourigenesis (Collado et al. 2005), lymphomagenesis (Braig et al. 2005), prostate tumourigenesis (Chen et al. 2005), the development of skin naevi (Michaloglou et al. 2005) and during pituitary tumourigenesis (Lazzerini Denchi et al. 2005).

During lung tumourigenesis, adenomas were found to display markers of cellular senescence; negativity for the proliferation marker Ki67 and expression of $p16^{INK4A}$, $p15^{INK4B}$, Dec1 and DcR2 as well as positive staining for SA-β-Gal. These senescence-associated markers were found to be absent in the more advanced adenocarcinomas. The same authors also observed similar differences between adenomas and adenocarcinomas in the pancreas (Collado et al. 2005). However, this may be an over-simplification as recently, sporadic senescent cells have been identified in several malignant tumours (Kim et al. 2017; Kim et al. 2014; Haugstetter et al. 2010; Reimann et al. 2010; te Poele et al. 2002; Vizioli et al. 2011; Roberson et al. 2005).

Further examples of the tumour-suppressive action of senescence preventing the acquisition of malignant features is found in Eμ-N-Ras transformed lymphocytes (Braig et al. 2005), Ras-driven, DMBA- and TPA-induced skin papillomas (Dhomen et al. 2009a), $Braf^{V600E}$-driven lung adenomas (Dankort et al. 2007; Michaloglou et al.

2005; Dhomen et al. 2009b), E2f3-driven pituitary hyperplasia (Denchi et al. 2005), Rheb-driven and Akt1-driven prostatic intraepithelial neoplasia (Majumder et al. 2008; C. Nardella et al. 2008) and β-Catenin-driven thymic tumours (Xu et al. 2008a). This list is by no means exhaustive and further research into various cancer types appears to show senescence as a common mechanism for preventing continued expansion. In addition to this, senescent features have also been observed in premalignant human tumours such as neurofibromas, melanocytic nevi, prostatic intraepithelial neoplasia and colon adenomas (Courtois-Cox et al. 2006; Gray-Schopfer et al. 2006; Z. Chen et al. 2005; Acosta et al. 2008; Bartkova et al. 2006; Kuilman et al. 2008).

1.1.5.1 Senescence bypass and escape

If cellular senescence is such an effective barrier to tumourigenesis then why do we develop cancer? To address this question, two non-mutually exclusive hypotheses have been proposed: (1) cells possessing oncogenic mutations never enter into senescence due to pre-existing mutations in genes necessary to reinforce the senescent phenotype (e.g. TP53, $p21^{CIP1}$, $p16^{INK4A}$, etc.), therefore allowing their unabated expansion and transformation to form malignant tumours; or (2) mutated cells, which have entered into cellular senescence, re-renter the cell cycle and proliferate due to either genetic, epigenetic or microenvironmental changes, which perturb the ability of the cell to maintain the senescent phenotype. These mechanisms have come to be termed senescence bypass and escape, respectively.

Evidence for senescence bypass has been gathered from an abundance of both *in vitro* and *in vivo* studies. It has been demonstrated that some mouse and human cells *in vitro* can evade the onset of senescence by disruption of either the p53 (Ferbeyre et al. 2000) or $p16^{INK4A}$/RB pathways (Narita et al. 2003) alone. However, in some contexts disruption of both pathways is necessary to abrogate the initiation of

senescence (Mallette, Gaumont-Leclerc, et al. 2007). Further to this, in a context dependent manner, senescence can be bypassed through disruption of the upstream DDR either on its own (Di Micco et al. 2006; Bartkova et al. 2006; Mallette, Ferbeyre, et al. 2007) or in combination with perturbation to the $p16^{INK4A}$/RB pathway (Di Micco et al. 2006; Bartkova et al. 2006; Mallette, Ferbeyre, et al. 2007). Genetic manipulation studies in mice have also provided *in vivo* evidence for senescence bypass in the context of oncogenic Braf-driven lung adenomas (Dankort et al. 2007), CyclinD1-driven pineoblastoma (Saab et al. 2009) and Ras-driven lymphomagenesis (Braig et al. 2005). These disparate oncogenic contexts normally display markers of cellular senescence, which acts to limit further growth, and this is abrogated through loss of p53 suggesting senescence escape as a potential tumourigenic mechanism *in vivo*.

While sufficient evidence has been gathered for senescence bypass to be appreciated as a *bona fide* biological phenomena *in vivo,* the evidence for senescence escape, however is significantly weaker. *In vitro* experiments has shown that reversion of senescent cells to a proliferative state is possible through disruption of the molecular factors involved in mitotic arrest. It has been shown that senescent mouse embryonic fibroblasts (MEFs) can be coaxed into dividing by reducing the levels of p53 by either micro-injection of anti-p53 antibodies or through stable shRNA-mediated suppression of p53 (Gire & Wynford-Thomas 1998; Dirac & Bernards 2003). The same result can also be achieved through ablation of RB in senescent MEFs (Sage et al. 2003). It appears as though the pathways that require dysregulating in order to escape senescence may be dependent on the cell type and senescence-inducing stimulus. This can be appreciated through experiments in which p53 is disrupted in either the human foreskin fibroblast cell line BJ or the human lung fibroblast cell line WI-38. p53 disruption in the foreskin fibroblasts resulted in senescence escape but has no effect in WI-38 cells (Beauséjour et al. 2003). Other components of the senescence machinery can be disrupted to allow for senescence escape, such as inactivation of DDR components in oncogenic Ras-induced

senescence (Di Micco et al. 2006) or through downregulation of inflammatory cytokine signaling that can act to reinforce senescence cell-autonomously (Kuilman et al. 2008). Furthermore, spontaneous senescence escape can be observed in senescent cell cultures, which is most likely due to increased mutational burden over time due to oxidative stress (Gosselin et al. 2009). While *in vitro* studies have shown that senescence escape is theoretically possible, confirming that this phenomenon occurs in an *in vivo* setting is technically challenging and to date remains unproven. Interestingly, a recent study from the laboratory of Clemens Schmitt artificially induced the escape of senescent B-cell lymphomas which lead to the acquisition of stem cell-like characteristics in the cells which had escaped senescence (Milanovic et al. 2017). While this study did not demonstrate the pathophysiological escape of cancer cells from a senescent state, it did provide interesting insight into the acquisition of aggressive features in cancer cells which may be important in normal carcinogenesis processes. Future studies in which senescent cell populations are permanently labeled *in vivo* are required in order to demonstrate that they are able to escape senescence and re-enter the cell cycle during the tumourigenesis process.

1.1.6 Novel tools for the study of cellular senescence *in vivo*

The *in vivo* identification and study of senescent cells has benefited considerably from the recent development of genetically engineered mouse models in which cells that activate the senescence program express a traceable marker. These "senescence-reporting mice" include *p16*-3MR (Demaria et al. 2014), *INK-ATTAC* (Darren J. Baker et al. 2011) and *p16*-LUC (Burd et al. 2013). All of these models are based on the expression of $p16^{INK4A}$ as a senescence biomarker and this should be taken into account as this gene can be expressed in non-senescent cells, such as macrophages (Hall et al. 2017). Furthermore, each model has intrinsic advantages and disadvantages that should be weighed according to the experimental

context. *p16*-LUC mice contain luciferase knocked-in downstream of the start codon of one endogenous $p16^{INK4A}$ allele. These mice allow for whole-body luciferase imaging, which permits the non-invasive global identification of senescent cells during aging. However, the luciferase knock-in results in disruption of one copy of $p16^{INK4A}$, which is a confounding variable that must be considered alongside appropriate controls (e.g. comparing with $p16^{+/-}$ animals).

Unlike *p16* -LUC, *p16*-3MR and *INK-ATTAC* mice not only allow the detection of senescent cells but also permit their specific ablation through the administration of certain drugs. However, the deleterious effects of continual drug administration must be taken into account for their use in longevity studies. As an advantage, *p16*-3MR and *INK-ATTAC* do not result in the disruption of one of the endogenous $p16^{INK4A}$ alleles, while *p16*-3MR can also be used to non-invasively identify bulk cellular senescence in tissues due to the expression of luciferase in senescent cells. Another consideration is that since both *p16*-3MR and *INK-ATTAC* use different promoter elements, it may be possible that their expression differs depending on cellular context and/or senescence inducing stimuli. The mechanism of cell ablation in both models also differs, meaning that each may be more efficient at inducing apoptosis depending on the context. As both *p16*-3MR and *INK-ATTAC* harbour fluorescent reporters, FACS isolation of senescent cell populations can be performed, which can be further investigated by qPCR and western blot for SASP expression. This can permit a more refined analysis of differences in the senescent state across varying age and tissue contexts. Furthermore, single cell RNA-sequencing can also be performed, allowing for data to be obtained on the transcriptomic heterogeneity of individual senescent cells.

New non-genetic tools for studying cellular senescence have also been generated. For example, mesoporous silica nanoparticles capped with galacto-oligosaccharides (GOS) have been used *in vitro* to label senescent cells with

rhodamine dye (Agostini et al. 2012). These nanoparticles take advantage of the increased β-galactosidase activity of senescent cells to remove the GOS cap, releasing their cargo. The nanoparticles can be filled with dyes to allow for identification of cellular senescence or genotoxic drugs to mediate their ablation. This tool is potentially advantageous, as it removes the need for breeding of senescence-reporters onto experimental genetic backgrounds and it possesses versatility as the nanoparticles can be filled with a variety of molecules for probing the location and function of senescent cell populations. Interestingly, a refined version of these nanoparticles were recently used to identify and eliminate senescent cells *in vivo,* through the delivery of fluorophores or cytotixic drugs, respectively. Furthermore, and of clinical relevance, the nanoparticles were also able to ameliorate the symptoms of pulmonary fibrosis and also promote tumour xenograft regression when used in combination with senescence-inducing drugs (Muñoz-Espín et al. 2018).

1.1.7 Therapeutic targeting of cellular senescence

The development of genetic and non-genetic tools to identify and ablate senescent cells *in vivo* has demonstrated that their removal is beneficial in ameliorating age-associated diseases. Examples of this include osteoarthritis, atherosclerosis, cataracts, cardiac hypertrophy, lipodystrophy, sarcopenia, renal dysfunction and tumourigenesis (Baker et al. 2016; Jeon et al. 2017; Baker et al. 2008; Darren J Baker et al. 2011; Childs et al. 2016). Furthermore, the ablation of senescent cells *in vivo* has remarkably been shown to lengthen both the ‘healthspan’ and median lifespan in mice (Baker et al. 2016). Therefore, the development of therapeutic strategies to safely remove senescent cells, or to disrupt the production of the SASP, are currently gaining significant scientific attention and the first human clinical trials appear to be on the horizon. Specifically, the main strategies currently being explored to tackle cellular senescence *in vivo* involve; (i) the selective ablation of these cells, referred to as

senolytics and (ii) the disruption of SASP production from senescent cells.

Currently there exist a number of technical hurdles that must be surpassed before senolytic therapy can be clinically translated. As previously mentioned, cellular senescence is not always detrimental to an organisms physiology and a variety of beneficial roles for cellular senescence have been identified such as tumour suppression, embryonic development, tissue regeneration and wound healing (see sections 1.1.2 and 1.1.5). Therefore, this knowledge must be taken into consideration when designing a senolytic therapy to prevent the ablation of physiologically beneficial senescent cells. The off-target effects of a developed senolytic must be ascertained to weigh the risk versus benefit of such a therapy. Indeed, some recently identified senolytic molecules, such as the widely used BCL-2 inhibitors, result in undesirable effects, such as the development of thrombocytopenia and neutropenia (Kaefer et al. 2014). Increased knowledge of the diversity of the cellular senescent state *in vivo* is required to allow for the effective development of senolytics that can either ubiquitously target all senescent cells or a subset in a particular organ or tissue system. Finally, the development of molecules that reduce or prevent the activation of the SASP in senescent cells would have to be rigorously tested for safety when used *in vivo*. As these molecules do not ablate the senescent cells they would require continuous dosing to be effective, which may exacerbate the chances of off-target effects. Indeed, the long-term use of certain SASP-blocking molecules, such as rapamycin, has been shown to be immunosuppressive (Baroja-Mazo et al. 2016). Moreover, as discussed previously in section 1.1.5.1, it is thought that some senescent cells may be capable of escaping the senescent state, allowing them to re-enter the cell cycle and contribute to malignant expansion. If this is found to be true *in vivo* then senolytic therapy, as opposed to disruption of the SASP, may be a more advantageous strategy as it removes senescent cells that may escape senescence later.

1.1.7.1 Senolytics

Senolytic drugs function by interfering with molecular pathways that are uniquely involved in maintaining the senescent state of a cell. Ideally these pathways are indispensable in senescent cells for maintaining their viability but are dispensable in non-senescent cells. Theoretically, this will allow for cells in a state of senescence to be specifically targeted for ablation while leaving neighboring non-senescent cells unperturbed. The first class of senolytic dugs identified exploit apoptotic-resistance, which is a feature of senescent cells, through targeting and inhibiting pro-survival pathways (Fuhrmann-Stroissnigg et al. 2017; Y. Zhu et al. 2016; Chang et al. 2016; Zhu et al. 2015; Yosef et al. 2016; Yosef et al. 2017). The evasion of apoptosis by senescent cells is achieved through a number of pro-survival mechanisms which include increased expression of B cell lymphoma 2 (BCL-2) family members (BCL-2, BCL-X_L and BCL-W), the p53/p21 pathway, PI3K/AKT signaling, activated receptor tyrosine kinases and the HIF-1α and HSP90 proteins, among others.

The majority of senolytic compounds currently used target BCL-2 family members due to the depth of knowledge currently available on these proteins at the molecular level, their attractiveness as drug targets and the observation that this protein family shows increased expression in different senescent cell types (Chang et al. 2016; Yosef et al. 2016). Excitingly, the utility of BCL-2 inhibitors in acting as senolytics has shown promise and these results have been confirmed by multiple laboratories (Childs et al. 2016; Chang et al. 2016; Yosef et al. 2016). One such senolytic BCL-2 inhibitor, navitoclax (also known as ABT-263), has resulted in promising therapeutic results when used in models of arteriosclerosis and was shown to result in the ablation of disease-associated senescent cells (Childs et al. 2016). Furthermore, navitoclax administration to sublethally irradiated mice has been shown to eliminate senescent muscle satellite cells (Y. Zhu et al. 2016) as well as senescent

cells in the bone marrow, resulting in improved hematopoietic function (Chang et al. 2016). Another pro-apoptotic senolytic is the molecule piperlongumine, which appears to show promising selectivity for ablating senescent cells *in vivo* (Chang et al. 2016). Intriguingly, piperlongumine activity appears to act in a synergistic manner when co-administered with navitoclax, suggesting alternative mechanisms of action. Further senolytic molecules identified include the proprietary molecule UBX0101 that demonstrated efficacy in clearing senescent cells and limiting disease progression in a mouse model of osteoarthritis (Jeon et al. 2017).

Further to this, a combination therapy consisting of the molecules dasatinib and quercetin has recently been employed in senolytic regimens. Dasatinib is a pan-tyrosine kinase inhibitor that is able to block ephrin-dependent receptor signaling (Baroja-Mazo et al. 2016) and quercetin is a plant-derived flavonoid that has pleiotropic biological effects, including the partial inhibition of serpin proteins (Boots et al. 2008; Chondrogianni et al. 2010). These molecules function as senolytics by also targeting anti-apoptotic signaling pathways in senescent cells, however they utilize less well-established targets than navitoclax. The rational for the use of the molecules was derived from observation of senescent pre-adipocytes in which the survival of these cells is dependent on six pro-survival signaling proteins: the serpin PAI1, BCL-X_L, p21, the kinase phosphatidylinositol 3-kinase-δ (PI3Kδ) and the ephrin's EFNB1 and EFNB3. Therefore, this warranted the use of dasatinib and quercetin combination therapy to inhibit these targets, which resulted in the clearance of senescent pre-adipocytes *in vitro* and senescent cells in the fat tissue of aged mice *in vivo* (Zhu et al. 2015). However, the combination of dasatinib and quercetin did not appear to elicit senolytic effects when used on senescent IMR90 cells suggesting that this combination therapy may only be useful in the ablation of specific senescent cell subpopulations that have unique exploitable properties (Baar et al. 2017). Furthermore, the combination of dasatinib and quercetin was unsuccessful in producing a therapeutic

response in a mouse model of atherogenesis, which has been previously achieved through naxitoclax administration or the use of genetically modified senescence ablating mouse models (Roos et al. 2016). Dasatinib and quercetin treatment has been shown to be effective in ablating profibrotic senescent primary human fibroblasts *in vitro* as well as clearing senescent cells in the widely utilized bleomycin-induced pulmonary fibrosis mouse model *in vivo* (Bai & Wang 2014). However, while this treatment regime improved the exercise capacity and lung compliance in pulmonary fibrosis mouse models it did not affect fibrosis, which is a pathological hallmark of human idiopathic pulmonary fibrosis (Schafer et al. 2017). Therefore, the fact that a dasatinib and quercetin combination inhibits a heterogeneous array of molecular targets coupled with the inability to clear senescent cells from different tissue contexts (pre-adipocytes versus IMR90 cells) makes this treatment regime an unattractive senolytic therapy.

Recently a new senolytic strategy has been discovered in which senescent cells can be ablated by interfering with the p53-forkhead box protein O4 (FOXO4) interaction (Baar et al. 2017). It has been shown that FOXO4 targets p53 to the cell nucleus in IMR90 cells following senescence induction after ionizing radiation exposure. Preventing the interaction between p53 and FOXO4 through a d-retro-inverso peptide (DRI-FOXO4), which is the reverse sequence of the FOXO4-p53 binding domain, results in nuclear exclusion of p53, facilitating the induction of apoptosis in targeted senescent cells. Intriguingly, short term DRI-FOXO4 treatment has been successful in alleviating age-associated defects (such as hair growth, running wheel activity and kidney function) in both progeroid and naturally aged mice. However, the mechanism by which these rejuvenatory effects were elicited remains to be established as earlier studies that pharmacogenetically eliminated senescent cells in progeroid mice with pre-established ageing phenotypes did not results in healthspan improvements (Darren J Baker et al. 2011; Baker et al. 2016).

1.1.7.2 Elimination of the SASP

The SASP produced by senescent cells are known to mediate a myriad to pleiotropic physiological responses in both an autocrine and paracrine manner. Therapies are currently being developed that aim to neutralise the production of SASP molecules from senescent cells to aid in the development of strategies that alleviate age-associated defects and/or aid in cancer treatment. There are three approaches currently being explored to reduce the SASP; (i) inhibition of the intracellular signaling cascades which promote SASP production in senescent cells, (ii) preventing the secretion of SASP molecules and (iii) blocking the functional activity of specific SASP components.

The complete suppression of SASP production, through interference with pro-SASP signaling pathway, is problematic due to the known anti-tumourigeneic effects of some SASP factors, such as the paracrine transmission or autocrine maintenance of the senescent state (Hoare et al. 2016; Eyman et al. 2009; Yang et al. 2006; Elzi et al. 2012). An example of this is the suppression of SASP production by NF-κB inhibition in a mouse lymphoma model, which retarded immune surveillance following therapy-induced senescence of the lymphoma cells. Furthermore, the blunted immune surveillance synergised with p53 insufficiency, promoting senescence escape and driving relapse and treatment resistance (Chien et al. 2011). A further example of this can be observed in prostate epithelial cells, induced to become senescent through PTEN loss. SASP inhibition in these cells through rapamycin treatment, which inhibits the mechanistic target of rapamycin complex 1 (mTORC1) that is important for SASP production (Laberge et al. 2015), resulted in a drastic reduction in cytostatic p53 translation and prevented the maintenance of the senescent state (Alimonti et al. 2010). Beyond these problems with maintaining the senescent state following SASP neutralization, rapamycin and its analogues have the side-effect of being

broad immunosuppressives, limiting their utility as being part of a chronic treatment regime (Baroja-Mazo et al. 2016). Counterintuitively, several studies have shown that epigenetic disruption of SASP production does not appear to impact the cell cycle inhibition of the affected senescent cells. Specifically, abolition of the epigenetic regulators mixed-lineage leukemia protein 1 (MLL1, also known as KMT2A) (Capell et al. 2016), bromodomain-containing protein 4 (BRD4) (Tasdemir et al. 2016) and HMGB2 (Aird et al. 2016) prevent the production of SASP while maintaining proliferative arrest. It is currently unknown why epigenetically interfering with SASP production spares the ability of senescent cells to arrest the cell cycle but why perturbation of pro-SASP signaling pathways does not.

Neutralization of the SASP can also be achieved through blocking the maturation or secretion of SASP components. However, unlike the well described signaling pathways which orchestrate the expression of SASP factors, much less is know about the myriad of mechanism which control their intracellular processing and export. Further work exploring this area may lead to novel therapeutic opportunities that allow for effective SASP blockade without stimulating re-entry of the cell cycle. Beyond this, the functional action of individual SASP components or their receptors, such as IL-6 or its receptor, can be inhibited. Generally, this can be achieved through the use of monoclonal antibodies that target either the ligand or receptors for defined SASP molecules. Examples of such antibodies include siltuximab (a monoclonal antibody targeting IL-6) and tocilizumab (a monoclonal antibody targeting the IL-6 receptor), which are approved drugs for treating inflammatory conditions (van Rhee et al. 2014; Emery et al. 2008). A benefit of this approach is that it represents a specific way to inhibit single SASP molecules with a low-risk of off-target effects using previously approved drugs. However, this approach would only allow for the blockade of only one out of a multitude of SASP components at one time, potentially limiting its efficacy.

1.2 The Pituitary

1.2.1 Anatomy, composition and function of the pituitary gland

The pituitary gland is considered to be the master regulator of organism homeostasis in vertebrates. It communicates signals from the hypothalamus and controls a plethora of vital physiological processes including metabolism, reproduction and sexual maturation, growth and stress responses (Melmed 2011). The hypothalamus integrates systemic signals from distant organs to maintain homeostatic balance of these various biological processes. These signals are then transmitted via hypothalamic factors to the pituitary gland through the hypophyseal portal blood vessel system, which regulate the systemic release of pituitary hormones. These hormones then act either systemically or on specific target organs such as the gonads, thyroid gland and adrenal glands. Following this, regulatory feedback loops are established from these target organs that signal back to either the pituitary or the hypothalamus (Perez-Castro et al. 2012). Together this system is termed the hypothalamic-pituitary (HP) axis , which is of significant clinical interest due to the severity of diseases or congenital defects affecting this system that generally results considerable morbidity (Denef 2008; Ward et al. 2006).

Anatomically the pituitary gland is comprised of anterior, intermediate and posterior lobes (AL, IL and PL respectively). Both the AL and the IL are derived from Rathke's pouch (RP), an embryonic invagination of the dorsal oral ectoderm at the rostral boundary of the pharyngeal endoderm. The PL is derived from the infundibulum, a diverticulum at the ventral midline of the diencephalon. Towards the end of mouse gestation at 18.5 days post coitum (dpc), the AL contains five hormone-producing cell types; lactotrophs, gonadotrophs, thyrotrophs, somatotrophs, and corticotrophs, which secrete prolactin (PRL), gonadotrophins (follicle stimulating

hormone (FSH) and luteinising hormone (LH)), thyroid-stimulating hormone (TSH), growth hormone (GH) and adenocorticotropin hormone (ACTH), respectively (Kelberman et al. 2009). Further to this, the AL contains the pituitary stem cells that persist into postnatal life, which are found in a sub-population of the SOX2/SOX9 expressing cell fraction (Castinetti et al. 2011; Cynthia Lilian Andoniadou et al. 2013; Rizzoti et al. 2013). These stem cells are mostly localised to the 'marginal zone', which comprises the dorsal AL and is mostly devoid of hormone-producing cells, and pituitary cleft in the IL (Fauquier et al. 2008; Garcia-Lavandeira et al. 2009; Pérez Millán et al. 2016; Goldsmith et al. 2016). Within the parenchyma of the AL scattered SOX2+/SOX9+ cells are also found in proximity to the hormone-producing cells (Mollard et al. 2012). The IL, which in humans is rudimentary, harbours the melanocyte-stimulating hormone (MSH) producing melanotrophs in mice and other vertebrates (Saland 2001). The PL does not contain hormone-producing cell types but is resident to glial cells known as pituicytes and axonal projections from hypothalamic neurons, which transport the neurohormones oxytocin (OXT) and vasopressin (VPN) (Markakis 2002) (Figure 1.2).

1.2.2 Embryonic development of the pituitary gland

Around 8.5 dpc a thickening of the dorsal oral ectoderm invaginates dorsally towards the prospective ventral diencephalon (VD) (Castinetti et al. 2011), which by 10.5 dpc has formed a lumen and is termed Rathke's pouch (RP). Following this, RP ascends further in close association with the VD, which itself thickens to form the future PL. RP has completely separated from the oral ectoderm by 12.5 dpc to form a closed pouch with the ventral side forming the future AL and the dorsal side forming the future IL, separated by a lumen known as the pituitary cleft, with the cells adjacent to this region being termed the 'marginal zone' (Hashimoto et al. 1998) (Figure 1.2).

Investigations over the past few decades had revealed many transcription factors and signaling pathways that orchestrate normal pituitary gland development. These signaling morphogens are derived from surrounding structures such as the oral ectoderm, the VD and the surrounding mesenchyme and they can direct the proliferation of unspecified progenitors, their commitment to differentiated endocrine cell populations (Kelberman et al. 2009) or restrict the activity of other signaling ligands (Zhu et al. 2007). An example of this if the developing hypothalamus which around 9.5 dpc, secretes factors including FGF8, FGF10, SHH and BMP4. These are necessary for RP induction and the expression of several transcription factors in RP progenitors such as *Sox2*, *Hesx1*, *Lhx3* and *Lhx4* (Ericson et al. 1998; Treier et al. 1998; Treier, O'Connell, a Gleiberman, et al. 2001). From 9.5 to 14.5 dpc RP progenitor cells are actively proliferative (Davis et al. 2011) and differentiate to form committed progenitors by expressing: (1) the T-box transcription factor Tpit, which activates expression of pro-opiomelanocortin (Pomc1) in corticotrophs and melanotrophs (Lamolet et al. 2001); (2) Sf1 (Nr5a1) in the cells of the gonadotroph lineage (Schimmer & White 2010) and (3) the POU class 1 homeobox (Pou1f1 or Pit1), which directs the differentiation of lactotrophs, thyrotrophs and somatotrophs (Dollé et al. 1990). These committed progenitors then give rise to all of the hormone-producing cells of AL between 13.5 and 16.5 dpc (Garcia-Lavandeira et al. 2009; Florio 2011), which is complete by 18.5 dpc (Bilodeau et al. 2009). The relevance of these transcription factors and signaling pathways for human pituitary development is demonstrated through the observation that mutations in the majority of these genes result in hypopituitarism (Fang et al. 2016).

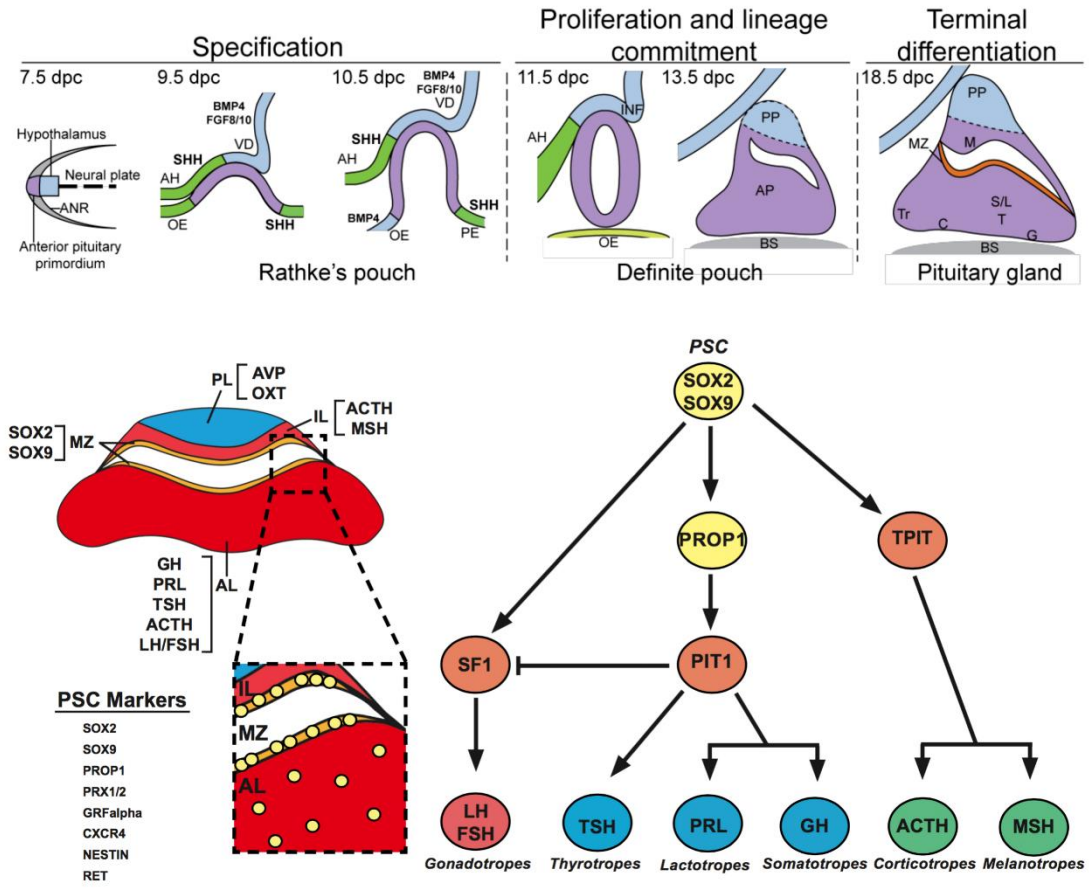

Figure 1.2. Schematic of pituitary developmental morphogenesis and cellular lineages. Rathke's pouch (RP) and the hypothalamus are derived from the anterior end of the anterior neural ridge (ANR) at 7.5 dpc. RP forms at 9.5 dpc from a thickening of the oral ectoderm (OE), which is in apposition to the ventral diencephalon (VD). The VD will give rise to the infundibulum (INF), the precursor of the posterior pituitary (PP) and by 12.5 dpc RP will have separated from the OE. RP progenitor cells then proliferate and migrate ventrally to form the anterior pituitary (AP) primordium. Differentiation of RP progenitors occurs between 13.5 and 18.5 dpc resulting in the formation of the mature pituitary, which contains all six of the hormone producing cell types. Lactotrophs (PRL/L), somatotrophs (GH/S) and *Pit1* dependent thyrotrophs (TSH/T) are located in the caudo-medial region of the pituitary. *Pit1*-independent thyrotrophs (rTSH/Tr) can be found in the AP rostral tip. Corticotrophs (ACTH/C) and gonadotrophs (FSH and LH/G) are located in the ventral region. The intermediate lobe (IL) contains the melanotroph (MSH/M) population. The marginal zone (MZ) is the location of the pituitary stem cell (PSC) niche. Figure adapted and modified from (Kelberman et al. 2009; Haston et al. 2018).

1.2.3 The role of stem/progenitor cells in embryonic and postnatal pituitary development

Stem cells are defined by their ability to both self-renew and differentiate into most, if not all, of a tissue-specialised cell types (Hsu et al. 2014). This ability to continually repopulate tissue-specific progenitors makes stem cells vital for embryonic growth, tissue homeostasis and regenration in adult life (Patel et al. 2013; van Es et al. 2012). Also, stem cells in many systems require the support of surrounding cells, which are collectively known as the niche (Gómez-Gaviro et al. 2012). Since stem cells reside atop the hierarchy of cellular differentiation, any impairment to their function has potentially disastrous consequences to their resident tissue such as age-associated functional decline of the organ or the development of cancer. The pituitary gland has demonstrated a tremendous capacity for adaptation in regulating the proportion and number of endocrine cell types in response to an organisms changing hormonal demands, such as pregnancy and puberty (Melmed 2003; Perez-Castro et al. 2012). As the AL is known to contain populations of stem/progenitor cells these cells may be of significant importance for responding to these various physiological demands.

1.2.3.1 The role of HESX1+ progenitor cells during pituitary development

As previously mentioned several transcription factors have been demonstrated to define the early progenitors of the pituitary gland (Ericson et al. 1998; Treier et al. 1998; Florio 2011; Vankelecom 2010; Rizzoti 2015), with a prominent example being the homeo-box transcription factor *Hesx1* (homeobox expressed in ES cells 1). *Hesx1* is known for its function in contributing to normal patterning of the forebrain (Andoniadou et al. 2011). However, it is also known to be essential in both mice and humans for pituitary development, with mutations resulting in the development hypopituitarism syndromes (Dattani et al. 1998; Kelberman et al. 2006; Jayakody et al.

2012; Sajedi et al. 2013; Gaston-massuet et al. 2011). Prior to pituitary development, *Hesx1* is initially expressed in the anterior-visceral endoderm (AVE) at 6.5 dpc and then at 7.5 dpc in anterior neural ectoderm, the prospective forebrain. Later *Hesx1* is found to be expressed in the oral ectoderm at 8.5 dpc. Involvement of *Hesx1* in pituitary development begins around 8.5 dpc where it is expressed in RP progenitors until13.5 dpc (Thomas & Beddington 1996; Hermesz et al. 1996). The importance of *Hesx1*-expressing RP progenitors can be appreciated by lineage tracing experiments, which show that these cells give rise to the vast majority of mature cell types by the end of gestation at 18.5 dpc (Gaston-massuet et al. 2011; Jayakody et al. 2012). Together these results demonstrate the importance of *Hesx1*-expressing RP progenitors in the development of the mature pituitary gland.

1.2.3.2 The role of SOX transcription factors in pituitary embryonic progenitors and post-natal stem cells

Studies over the past decade have provided convincing evidence for the existence of adult pituitary stem cells (PSCs). These cells have been identified by varying techniques including: (i) pituitary dissociation followed by either adherent or non-adherent culture in stem cell-promoting media (Lepore et al. 2005), and *in vitro* clonogenicity assays (Gleiberman et al. 2008; Garcia-Lavandeira et al. 2009; Nomura et al. 2009; Horiguchi et al. 2012; Higuchi et al. 2014); (ii) flow cytometric side population analysis (Chen et al. 2005) and (iii) genetic lineage tracing experiments (Cynthia Lilian Andoniadou et al. 2013). This work characterising the identity of PSCs has provided a potential set of markers defining their identity including PROP1, PRX1/2, GRFα, CXCR4, NESTIN, RET and the SOX transcription factors SOX2 and SOX9, among others (Carreno et al. 2016). However, genetic tracing experiments have been demonstrated differentiation potential in vivo only for Sox2 and Sox9 -expressing PSCs (Cynthia Lilian Andoniadou et al. 2013). In humans, it has been demonstrated

that pituitary cells exist that are capable of forming clonogenic floating spheres expressing PSC markers, including NESTIN, LHX3 and PITX2. These cells were also able to undergo hormonal commitment when cultured under differentiating conditions (Weiss et al. 2009).

SOX transcription factors are well known for the important role in regulating cell fate decisions during embryogenesis and in post-natal stem/progenitor cells from various organ system, especially the central nervous system (CNS). Of particular importance in respect to this is the SOXB1 group, which includes the transcription factors SOX1, SOX2 and SOX3 (Liu et al. 2013; Zhang & Cui 2014). During pituitary development SOX2 is the only SOXB1 factor found to be expressed. SOX2 expression is initially found in pituitary embryonic progenitors from 9.5 dpc (Rizzoti 2015). As these progenitors commit to more differentiated endocrine cell fates, SOX2 is found to be downregulated and at late developmental stages its expression is restricted to the pituitary marginal zone, which persists into adulthood. Lineage tracing experiments that follow the fate of SOX2-expressing pituitary cells revealed that following 9 months of tracing these cells differentiated into all of the hormone-producing cell lineages. Further to this, a subset of these traced cells retained SOX2 expression with the absence of differentiation markers suggesting self-renewal (Cynthia Lilian Andoniadou et al. 2013). The importance of SOX2 as a pituitary stem/progenitor factor can also be appreciated by experiments deleting its expression in *Hesx1*-expressing progenitors, which results in severely disrupted pituitary development and significant loss of pituitary progenitor cells (Jayakody et al. 2012).

Another important SOX transcription factor important for pituitary development is the SOXE group member SOX9. SOX9 has been demonstrated to be involved in mediating cell fate decisions in the skeleton, intestine, cardiac valves, developing CNS and the male gonads (Sun et al. 2013; Huang et al. 1999; Ikeda et al. 2004; Hattori et al. 2010; Akiyama et al. 2004; Moniot et al. 2004; Stolt et al. 2003; Kang et al. 2012).

Furthermore, SOX9 has been shown to be involved in establishing and maintaining the hair follicle stem cell niche (Adam et al. 2015), maintaining pancreatic progenitor cell identity (Seymour et al. 2007) and in mediating EMT and migration in delaminated neural crest (NC) cells (Cheung & Briscoe 2003; Theveneau & Mayor 2012). During pituitary development SOX9 is found to be co-expressed with SOX2 from 14.5 dpc and its expression has been postulated to correlate with the transition from a proliferative progenitor state to a more quiescent behavior (Castinetti et al. 2011). This co-expression of SOX2 and SOX9 is also preserved postnatally. Lineage tracing of SOX9-expressing cells in the pituitary also reveals that they give rise to hormone producing cells throughout life (Rizzoti et al. 2013). Together these results suggest that SOX2+/SOX9+ population in the pituitary function as stem cells developmentally and into adult life.

1.2.4 Pituitary tumours and disease

1.2.4.1 Pituitary developmental syndromes

The coordinated action of transcription factors (e.g. *Hesx1*, *Sox2*, *Lhx3/4*, *Prop1*, *Pitx1/2*) and signaling pathways (e.g. Shh, Bmp, Fgf, Wnt) is required for normal pituitary development, ensuring the correct balance of progenitor cell self-renewal and commitment as well as maturation of differentiated hormonal cell types. It should be of little surprise that dysregulation or mutations in these genes or signaling pathways give rise to various pituitary pathologies including; congenital hypopituitarism, septo-optic dysplasia and pituitary tumours (summarised in Table 1.1) (Davis et al. 2009). This information has been gathered from numerous human gene sequencing, expression and functional studies of patient biopsies and cell lines with disparate pituitary pathologies. However, *in vivo* experiments in genetically engineered mice have

provided the greatest insights into the role that these factors play during pituitary development and disease (Kelberman et al. 2009; Zhu et al. 2007).

Gene	Protein	Mouse loss of function phenotype	Human phenotype	Inheritance pattern mouse/human
HESX1	HESX1	Microopthalmia or anopthalmia, corpus callosum agenesis, lack of septum, dysgenesis or aplasia of the pituitary	Variable. Isolated growth hormone deficiency with ectopic posterior pituitary, combined pituitary hormone deficiency, septo-optic dysplasia	Recessive in mouse, dominant or recessive in human
OTX2	OTX2	Malformation of optic placode, forebrain or midbrain absence	Anterior pituitary hypoplasia, ectopic posterior pituitary, absent infundibulum, anopthalmia	Heterozygous: haploinsufficiency/ dominant negative in both mouse and human
SOX2	SOX2	Heterozygous or hemizygous: reduced fertility, abnormalities of the central nervous system, poor growth, anopthalmia, pituitary hypoplasia Homozygous: embryonic lethality	Anterior pituitary hypoplasia, hypogonadotrophic hypogonadism, abnormal hippocampus, abnormal corpus callosum, anopthalmia/micoopthalmia, learning difficulties, hearing loss, hypothalamic haratoma, esophageal atresia	Heterozygous mutation associated with haploinsufficiency in mouse, halpoinsufficiency in human
SOX3	SOX3	Craniofacial defects, poor growth, infundibular and hypothalamic abnormalities	Mental retardation, hypopituitarism, isolated growth hormone deficiency, infundibular hypoplasia, ectopic posterior pituitary, midline abnormalities	X-linked recessive in both mouse and human
GLI2	GLI2	Pituitary hypoplasia	Hypopituitarism, craniofacial defects, polydactily, partial agenesis of the corpus callosum, holoprosencephaly	Haploinsufficiency
LHX3	LHX3	Hypoplasia of RP	Pituitary hypoplasia (GH, TSH and	Recessive in both

			gonadotrophin deficiency), variable ACTH deficiency, short and rigid cervical spine, hearing loss	mouse and human
LHX4	LHX4	Mild anterior pituitary hypoplasia	TSH, GH and cortisol deficiency, abnormal cerebellar tonsils, persistent craniopharyngeal canal, anterior pituitary hypoplasia, ectopic posterior pituitary, absent infundibulum	Recessive in mouse, dominant in human
PROP1	PROP1	Anterior pituitary hypoplasia (GH, TSH, PRL, LH, FSH and ACTH affected)	Enlarged pituitary with involuted phenotype, TSH, GH, PRL and gonadotrophin deficiency (with evolving ACTH deficiency)	Recessive in both mouse and human
POU1F1	PIT1	Anterior pituitary hypoplasia (GH, TSH and PRL affected)	Variable posterior pituitary hypoplasia (GH, TSH and PRL deficiency)	Recessive in mouse, dominant/recessive in human

Table 1.1. Genes involved in developmental pituitary syndromes in both mouse and human (Adapted from Kelberman et al. 2009).

The vast majority of pituitary neoplasias are pituitary adenomas (PA), with a prevalence of 78-94 cases/100,000 people (Karavitaki 2012) and representing one of the most common intracranial neoplasms (Larkin & Ansorge 2000). These tumours are generally benign histologically, but are of clinical relevance as they can show infiltrative behaviour into surrounding neural structures and may cause endocrine disorders due to the over-production of one or more hormones. PAs are a heterogeneous class of tumours, which can be sporadic or familial. They can be subdivided based on their endocrinological activity (hormone-secreting or non-functional), driver mutations, histological features and clinical presentation (Larkin & Ansorge 2000; Di Ieva et al. 2014; Syro et al. 2015; Carreno et al. 2016).

Cell type	Hormone produced	Target		Regulator		Hypopituitarism phenotype	Pituitary tumour	Clinical features in tumour	Transcription factor expression in tumour
		Tissue	Response	Positive	Negative				
Posterior lobe									
Magnocellular	AVP	Kidney	Water reabsorption	Hypovolemia	Hyperosmolarity	Diabetes insipidus	-	-	-
Magnocellular	OT	Mammary gland, uterus	Milk-let down, contractions	Suckling	Progesterone	Hypogalactorrhea	-	-	-
Pituicyte (glial cells)	-	-	-	-	-	-	Pituicytoma	Diabetes insipidus, hypopituitarism, visual impairment	-
Intermediate lobe									
Melanotrophs	MSH	Pleiotropic functions	-	-	-	-	Not reported in humans	-	-
Anterior lobe									
Somatotrophs	GH	Liver, kidneys, most tissues	Growth	GHRH	SS	Dwarfism	Somatotropinomas	Acromegaly or gigantism	PIT1
Thyrotrophs	TSH	Thyroid gland	Thyroid hormone production (T3, T4)	TRH	Thyroid hormone (T3, T4)	Thyroid hypoplasia, dwarfism, cretinism, hypothyroidism	Thyrotropinomas	Hyperthyroidism	STF1, GATA2
Lactotrophs	PRL	Mammary gland	Milk production	Oestrogen, TRH	Dopamine	Hypogalactorrhea	Lactotropinomas	Hypogonadism and/or galactorrhea	PIT1

Corticotrophs	ACTH	Adrenal cortex	Glucorticoid production	CRH	Corticosteroids	Adrenal hypoplasia	Corticotropinomas	Cushings disease, hypopituitarism, pituitary hyperplasia	TPIT
Gonadotrophs	LH, FSH	Gonads	Spermatogenesis, ovulation	GnRH	Gonadal steroids	Sexual immaturity, infertility	Gonadotrophic adenomas and null cell adenomas	Silent or pituitary failure	PIT1

Table 1.2. Cell types found in the pituitary, their biological functions and pathological phenotypes. Adapted from Shlomo Melmed 2011.

Our understanding of pituitary tumours has also benefited enormously from the use of genetically engineered mouse models. These models have aided in the identification of pathways and genes involved in the pathogenesis of pituitary adenomas (Cano et al. 2014; Lines et al. 2016) and also the identification of cancer stem cells (CSCs) in pituitary tumours (Xu et al. 2009; Hosoyama et al. 2010; Chen et al. 2014; Donangelo et al. 2014; Mertens et al. 2015; Martinez-Barbera & Andoniadou 2016). The pathological consequences of pituitary hormone reduction and the types of pituitary adenoma arising from each of the differentiated cell types is summarised in Table 1.2.

1.2.4.2 Craniopharyngiomas

While pituitary adenomas make up the majority of diagnosed pituitary tumours in adults, adamantinomatous craniopharyngioma (ACP) represents the most common pituitary tumour in children (Barkhoudarian & Laws 2013). A different type of craniopharyngioma is the papillary form, which occurs in the elderly. Both types of craniopharyngioma are molecularly and histologically different.

1.3 Adamantinomatous craniopharyngioma (ACP)

1.3.1 Epidemiology and clinical features of ACP

Adamantinomatous craniopharyngioma (ACP) are epithelial tumours, which do not express hormones or pituitary differentiation markers and are non-malignant histologically. ACPs have a low incidence (2.14 cases/million per year for children and

1.6 cases/million for all ages) but are regarded as the most common non-neuroepithelial intracranial tumour found in children and form 11.5% of all paediatric tumours of the CNS (Bunin et al. 1998; Müller 2014a). Clinically the mean age of diagnosis shows a bimodal distribution with childhood onset ACP being diagnosed around 10 years of age and adult onset ACP being diagnosed around 74 years of age (Nielsen et al. 2011). However, adult and childhood ACP are currently not thought to be different disease entities and receive the same treatment regime. Furthermore, both ACP age groups show similar post-treatment survival, quality of life effects and recurrence incidence (Nielsen et al. 2011; Dekkers et al. 2006; Zoicas & Schöfl 2012). While the 5-year survival rate is high for ACP (95%), these tumours are considered to be highly aggressive and associated with significant morbidity because of invasion into surrounding structures such as the hypothalamus and optic tract (Müller 2013). Resection of these tumours is also complicated due to their tendency to invade the hypothalamus, optic tracts and pituitary gland, resulting in frequent detrimental clinical outcomes, for example hypothalamic obesity and type II diabetes, blindness, dysregulation of the metabolism, diabetes insipidus, resting/activity pattern disorders, and panhypopituitarism (Müller et al. 2004). There are no targeted therapies available against these tumours, and current treatments involve surgery and radiotherapy, which contribute further to the high morbidity. In summary, ACP is a chronic disease that is complex to manage clinically and associated with poor quality of life for the survivors and increase mortality rate in long-term follow up.

1.3.2 Histopathology and aetiology of human ACP

The cellular origins of ACP are currently unknown and are the subject of ongoing research. The persisting hypothesis regarding the aetiology of ACP postulates that they are derived from remnants of RP. This is due to the observation that certain cytokeratins share common expression in the oral epithelium and human ACP (Kato et al. 2004; Buslei et al. 2007b; Tateyama et al. 2001). Interestingly, recent RNA-sequencing studies have found analogous transcriptional profiles between human ACP and normal tooth development, supporting the notion of a possible origin in the embryonic oral ectoderm (Apps et al. 2018).

Intriguingly childhood ACP patients have a significant height reduction at around 1 year of age, before routine ACP diagnosis (Müller et al. 2004; Qi et al. 2013). This suggests that childhood ACP is a developmental disorder that originates during pituitary organogenesis. This is supported by the observation that several foetal cases of craniopharyngioma have been reported (Jurkiewicz et al. 2010; Joó et al. 2009; Scagliotti et al. 2016; Kostadinov et al. 2014) and furthered by a review of foetal CNS tumours, which observed an incidence of 11% for craniopharyngioma out of 154 cases (Isaacs 2009).

Histologically human ACP is very distinctive allowing for their differentiation from other pituitary tumours, including papillary craniopharyngioma (PCP). Characteristic histomorphological features include: 1) "palisading epithelium" comprised of closely associated columnar cells, which encapsulate the tumour; 2) "wet ketatin" which are areas formed by anucleated cell remnants, also known as "ghost cells", and are

eosinophilic, keratinous and can show calcifications; 3) areas of cells which are loosely connected and show evidence of microcystic morphology, termed "stellate reticulum" and is some cases 4) calcification and the presence of cholesterol-rich deposits (Figure 1.3).

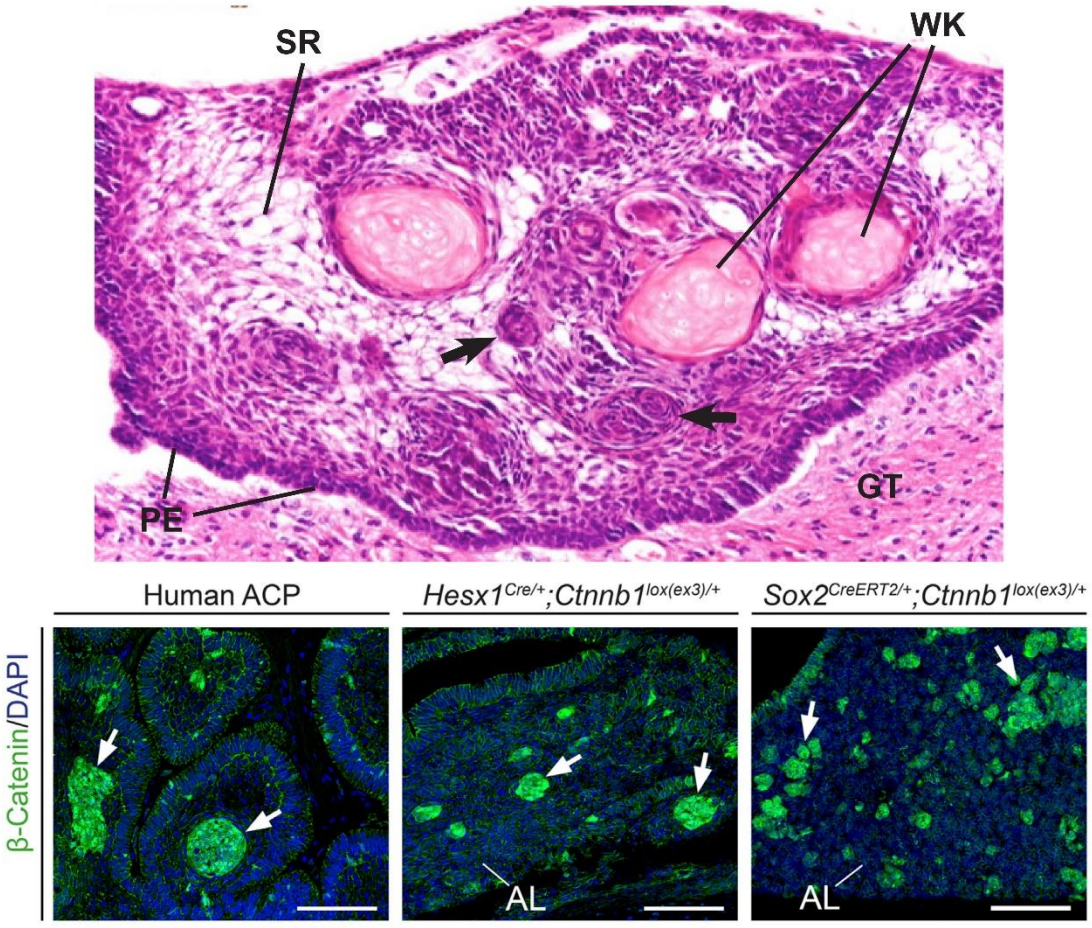

Figure 1.3. Histology of human adamantinomatous craniopharyngioma (ACP) and presence of nucleocytoplasmic accumulating β-catenin clusters in human tumours and mouse models. (Top) Haematoxylin & eosin staining of human ACP tumour showing characteristic features; palisaded epithelium (PE) separating tumour tissue from reactive glial tissue (GT), stellate reticulum (SR) and anucleated ghost cells termed wet keratin (WK). Whorl-like cell clusters are also present (arrows). (Bottom) Immunofluorescence images of human ACP (**a**) and two ACP mouse models (*Hesx1*$^{Cre/+}$*; Ctnnb1*$^{lox(ex3)/+}$ *and Sox2*$^{CreERT2/+}$*; Ctnnb1*$^{lox(ex3)/+}$) (**b**, **c**) for β-Catenin showing the presence of cell clusters accumulating the protein. *Hesx1*$^{Cre/+}$*; Ctnnb1*$^{lox(ex3)/+}$ image from an 18.5 dpc embryo, *Sox2*$^{CreERT2/+}$*; Ctnnb1*$^{lox(ex3)/+}$ image from a mouse 16-weeks post-tamoxifen induction. Scale bars: 100μm.

The presence of clusters of cells which accumulate nucleo-cytoplasmic β-Catenin are one of the most characteristic features of human ACP (Sekine et al. 2002; Kato et al. 2004; Gaston-massuet et al. 2011) (Figure 1.3). These cell clusters, while only forming a small fraction of the total tumour, represent a unique histological hallmark in ACP and are not found in PCP or other pituitary tumours. Furthermore, these cell clusters have also been observed in foetal ACP (Kostadinov et al. 2014; Scagliotti et al. 2016). Molecular studies have identified activating mutations in the β-Catenin gene (*CTNNB1*) in the vast majority of human ACP samples (Sekine et al. 2002; Kato et al. 2004; Buslei et al. 2005; Brastianos et al. 2014; Oikonomou et al. 2005). These somatic mutations are commonly located in the 3rd exon and prevent effective proteosomal degradation of the protein, leading to its accumulation and subsequent activation of the WNT signaling pathway. The reasons why only cluster cells and some other sporadic cells accumulate beta-catenin, rather than all the tumour cells carrying the *CTNNB1* mutations remain unknown.

1.3.3 Genetically engineered mouse models of ACP

1.3.3.1 Embryonic model of ACP: *Hesx1$^{Cre/+}$; Ctnnb1$^{lox(ex3)/+}$*

It has been previously shown that removal of the 3rd exon of mouse β-Catenin (*Ctnnb1*) also results in a degradation resistant form of the protein (also known as oncogenic β-Catenin), which is capable of nucleo-cytoplasmic accumulation and WNT pathway activation (Harada et al. 1999). Conditional expression of oncogenic β-Catenin in pituitary gland progenitor cells during development in *Hesx1$^{Cre/+}$; Ctnnb1$^{lox(ex3)/+}$* embryos results in the formation of pituitary tumours (Gaston-massuet et al. 2011).

Interestingly, driving oncogenic β-Catenin in committed progenitors or terminally differentiated pituitary cells does not result in tumour formation, indicating the important role that these embryonic progenitors play in the tumourigenesis process.

The pituitary tumours formed in *Hesx1*$^{Cre/+}$*; Ctnnb1*$^{lox(ex3)/+}$ mice show a partial recapitulation of human ACP histology. These murine tumours are negative for the expression of hormones, possess nodular "whorl-like" cell formations and microcystic changes, reminiscent of stellate reticulum, similar to human ACP. However, the murine tumours lack a generalised epithelial morphology, pallisading epithelium, calcifications and wet keratin. Importantly, the tumours in mice possess the hallmark of human ACP, nucleo-cytoplasmic β-Catenin accumulating cell clusters (Figure 1.3). Clusters are first observed from 9.5 dpc, persist throughout development and remain postnatally, prior to tumour formation. An interesting observation in mouse β-Catenin accumulating cell clusters is that they are non-proliferative, as evidenced by the lack of the proliferation marker Ki67. Furthermore, mouse cluster cells fail to incorporate bromo-deoxy-uridine (BrdU) and at 18.5 dpc express the cell cycle inhibitory proteins p27^{Kip1} and p57^{Kip2} (Gaston-massuet et al. 2011). This lack of proliferation, together with the observation that mouse clusters also express SOX2 led to the hypothesis that these cell possess stem/progenitor cell characteristics and may have entered into cellular senescence. Similar observations are also found in human ACP cluster cells, which express p21^{Cip1} and show absence of Ki67 in the clusters (Gaston-massuet et al. 2011; Stache et al. 2015). SOX2, however, is not found in human ACP clusters cells, indicating either the existence of species-specific differences or the timing of their analysis.

Gene expression profiling experiment comparing murine ACP cell clusters against non-cluster cells was conducted using a BAT-gal reporter, which expresses β-galactosidase in cells with activated WNT/β-Catenin pathway. Dissociation and flow sorting of BAT-gal positive (cell clusters) and negative (non-cluster cells) fractions from *Hesx1*$^{Cre/+}$; *Ctnnb1*$^{lox(ex3)/+}$; *BAT-gal* pituitaries was achieved using a β -galactosidase substrate that yield a fluorescent product. RNA isolation and microarray analysis revealed a significant increase in expression of members of several signaling pathways such as WNT, BMP, SHH, FGF and TGFβ in the cell clusters (Labeur et al. 2010; Wesche et al. 2011; Yauch et al. 2008). Interestingly, the expression of these factors is conserved in human ACP clusters as shown by *in situ* hybridisation (ISH), suggesting a potential role of these clusters as siganaling centers that may have paracrine interactions with the tumour tissue.

1.3.3.2 Inducible model of ACP: *Sox2*$^{CreERT2/+}$; *Ctnnb1*$^{lox(ex3)/+}$

As previously mentioned, it has been hypothesised that the cluster cells possess a signature of "stemness" due to their quiescent nature and expression of the pituitary progenitor/stem cell marker SOX2. The observation that targeting oncogenic β-catenin to more differentiated cell types is unable to drive tumour formation lends support to this hypothesis. Expression of oncogenic β-catenin in Sox2-expressing cells either embryonically or postnatally in *Sox2*$^{CreERT2/+}$; *Ctnnb1*$^{lox(ex3)/+}$ generates tumours resembling human ACP. Similar to the tumours formed in the *Hesx1*$^{Cre/+}$; *Ctnnb1*$^{lox(ex3)/+}$ model, *Sox2*$^{CreERT2/+}$; *Ctnnb1*$^{lox(ex3)/+}$ tumours were negative for hormone expression and the tumour bearing pituitaries also harboured clusters of cells, which accumulated nucleo-cytoplasmic β-Catenin and were negative for markers of proliferation (Figure

1.3). Further to this the clusters upregulated expression of the signaling factors previously observed in the *Hesx1*$^{Cre/+}$*; Ctnnb1*$^{lox(ex3)/+}$ model and human ACP (e.g. WNT, BMP, SHH, FGF) (Cynthia L. Andoniadou et al. 2012). This study demonstrated that the cell of origin for the clusters are found in the SOX2+ stem cell compartment.

Fascinatingly, lineage tracing experiments following the fate of SOX2+ pituitary stem cells targeted with oncogenic β-catenin in *Sox2*$^{CreERT2/+}$*; Ctnnb1*$^{lox(ex3)/+}$*; Rosa26*$^{YFP/+}$ revealed that the tumours were not derived from the cluster cells, as the tumours did not express the yellow fluorescent protein (YFP) reporter. This result was confirmed through laser capture microdissection (LCM) of tumour cells, followed by PCR, revealing that the tumours did not show recombination of either the *Rosa26* (which carries the YFP reporter) or the *Ctnnb1* loci (Cynthia L. Andoniadou et al. 2012). In addition, lineage tracing in the *Hesx1*$^{Cre/+}$*; Ctnnb1*$^{lox(ex3)/+}$*; Rosa26*$^{YFP/+}$ mouse model also revealed that the majority of the tumours form non-cell autonomously (Gonzalez-Meljem et al. 2017a). Together these results suggest that the tumour does not cell-autonomously derive from the mutation-sustaining cells. Therefore, *Sox2*$^{CreERT2/+}$*; Ctnnb1*$^{lox(ex3)/+}$ and *Hesx1*$^{Cre/+}$*; Ctnnb1*$^{lox(ex3)/+}$ mice develop tumours in a paracrine manner through the action of the oncogenic β-catenin targeted cell clusters (Figure 1.4). Currently the identity of the cell(s), which is responding to the paracrine influence of the clusters cells and derives the tumour proper is unknown, as is the specific mechanism by which the cluster cells drive transformation of neighbouring cells.

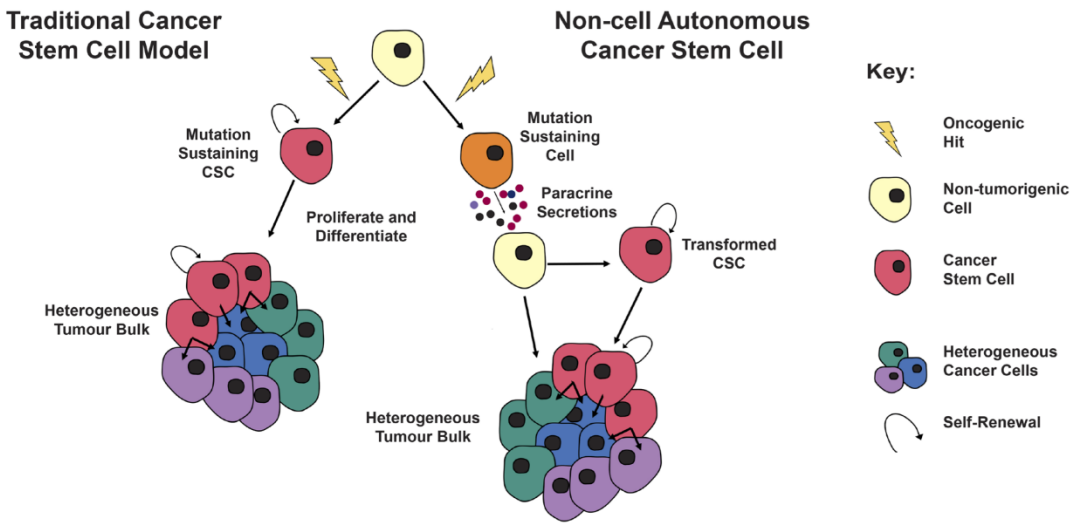

Figure 1.4. Comparison of the canonical cancer stem cell (CSC) model with non-cell autonomous tumourigenesis observed in the pituitary gland. *(*Left) The canonical CSC paradigm postulates that following neoplastic transformation of an existing resident tissue stem cell, restricted progenitor or differentiated cell, that this cell transitions to a stem-like state (red cells) and is responsible for cell-autonomously "differentiating" into the cells which comprise the tumour bulk (blue, green and purple cells), similar to normal tissue homeostasis. (Right) Non-cell autonomous tumourigenesis in pituitary gland differs from this model as the mutation-sustaining cell (orange cell) induces the transformation of a neighboring cell (yellow cell) that then cell-autonomously generates the tumour.

1.4 Papillary craniopharyngioma (PCP)

1.4.1 Epidemiology and clinical features of PCP

Like ACPs, PCPs are rare tumours, with an calculated incidence of 0.14 cases per million persons per year (Tariq et al. 2017). PCPs like ACPs are histologically benign epithelial tumours of the sellar region with absence of hormonal and pituitary differentiation marker expression. Due to the shared location, PCP patients show a high degree of morbidity arising from tumour invasion of

surrounding neural structures (Müller 2014b). Traditionally PCP, like ACP is managed by surgical resection followed by postoperative radiotherapy to retard the chances of recurrence. However, their anatomical location and propensity to recur result in PCP being surgically extremely difficult to manage (Müller 2014b). Furthermore, unlike ACP, PCP develops almost exclusively in adults, with a peak incidence between 50 to 75 years (Tariq et al. 2017).

1.4.2 Histopathology and aetiology of human PCP

PCP histology differs from that of ACP significantly. PCP tumours are solid and rarely show cystic characteristics, unlike ACP. Furthermore, features of ACP tumours, such as calcification, the presence of wet keratin, and cholesterol-rich deposits are absent in PCP. PCP tumours are histologically simpler than APC and are characterised by fibrovascular cores, which are lined with a non-keratinising epithelium (Figure 1.5).

Recently, molecular studies have shown that PCP, like ACP, appears to be driven by mutations of a single gene, which in the context of PCP is *BRAF*. Specifically *BRAF-V600E* mutations, which lead to constitutive activation of MAPK/ERK pathway, appear to be found almost exclusively in analysis of PCP tumour cohorts (Brastianos et al. 2014). The discovery of the *BRAF-V600E* as the genetic driver of PCP has resulted in clinical testing of the BRAF inhibitors vemurafenib and debrafenib on their own or in combination with the MEK inhibitor trametinib, to dampen MAPK/ERK signaling. Excitingly, these molecularly targeted clinical studies against PCP have shown great early promise. Treatment of a 38 year-old male, who suffered from multiple recurrent

PCP tumours with *BRAF-V600E* mutations, with debrafenib and trametinib resulted in shrinkage of the tumour by 85% after 35 days. Furthermore, common mutations that mediate MAPK pathway inhibition resistance were not found following treatment (Brastianos et al. 2016). These promising clinical results have also been recapitulated in other patients using the same treatment regime (Rostami et al. 2017; Roque & Odia 2017). Furthermore, another BRAF inhibitor, vemurafenib, has also been used successfully in a PCP patient to promote tumour regression (Aylwin et al. 2016). Despite the advances in targeted therapy of PCP, little is known about the aetiology of the disease. Such investigations are limited by the absence of genetically engineered mouse models of the disease.

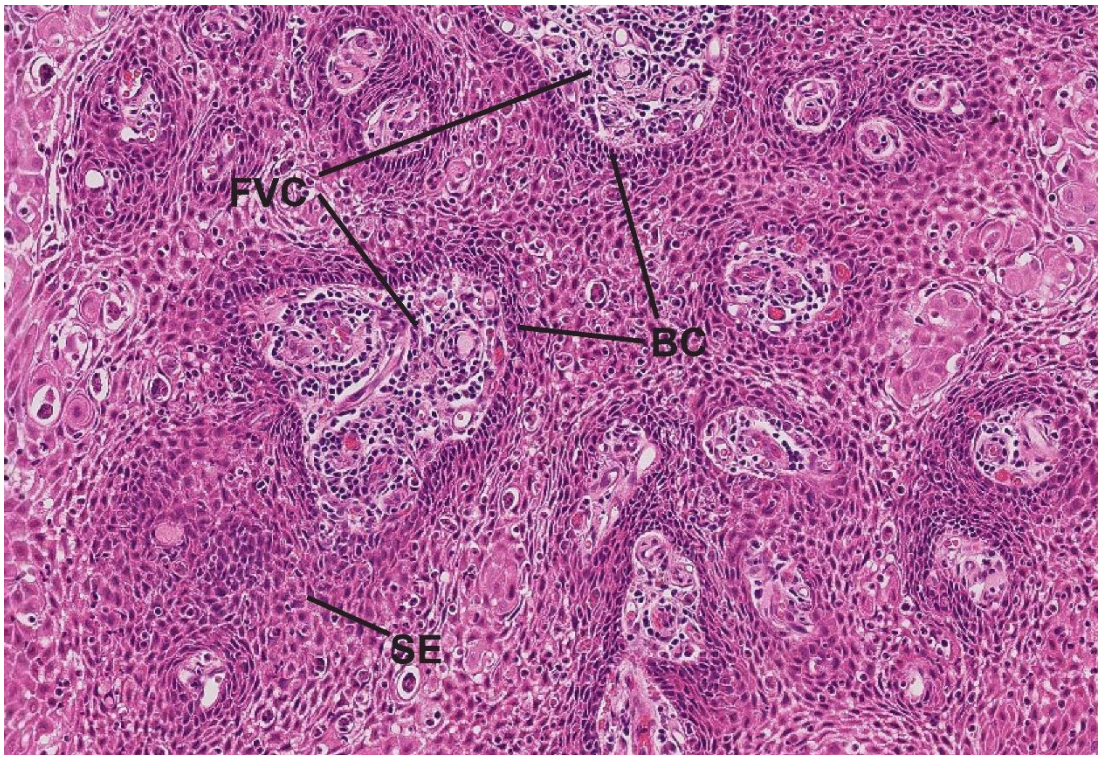

Figure 1.5. Histology of human papillary craniopharyngioma (PCP). Haematoxylin & eosin staining of human PCP showing the presence of fibrovascular cores (FVC) surrounded by a basal cell layer (BC). The remainder of the tumour is primarily composed of a squamous epithelium.

1.5 The lung

1.5.1 Anatomy, composition and function of the lung

The lung is a tremendously complex and fragile organ that facilitates oxygen and carbon dioxide gas exchange between the blood and the atmosphere. Following inhalation, air passes down the trachea, which branches to form two bronchi that supply each lung. The bronchus then narrows and branches extensively to give rise to bronchioles, which are lined with a ciliated cuboidal epithelium and a smooth muscle layer. Together these extraordinarily branched conducting airways constitute around two million meters of overall length. The predominant cell types in the bronchioles are neuroendocrine cells, basal cells, serous cells, ciliated cells, goblet cells and clara cells. Clara cells are cuboidal or columnar in appearance and fulfil a secretory function and are the main progenitors, which respond to injury of the bronchioles. They project beyond the ciliated cells into the lumen of the airway (Effros 2006) (Figure 1.6).

The bronchioles finally terminate into alveoli, sac-like structures, which are the primary site of gas exchange in the lung and are greater than 500 million in number, with a cumulative surface area of over 50 m2. The alveoli are separated from one another by a layer of continuous epithelial cells, which overlays the small capillaries necessary for gas exchange, and are lined by two distinct cell types: type I and type II alveolar cells. Alongside this, alveolar macrophages sit on the inner surface of the alveoli and are important for immune surveillance of this vital tissue (Effros 2006).

Type I alveolar cells are the predominant alveolar cell type and comprise 95% of the alveolar surface area. These cells are usually quiescent but are responsible for mediating gas exchange between the blood and the external atmosphere and also form a strong barrier, through tight junctions, to prevent the direct interaction of internal and external environments. Type II alveolar cells are generally found at the intersections between adjacent alveoli. The predominant function of these cells is to produce surfactant which is important for controlling alveolar surface tension. Further to this, a subset of type II alveolar cells, which function in a stem cell-like manner, are able to undergo proliferation and can differentiate into type I alveolar cells (Desai et al. 2014; Nabhan et al. 2018). Type II alveolar cells are also thought to be important for enhancing alveolar macrophage function (Effros 2006).

The lung fulfils its gas exchange function while contending with exposure to copious foreign matter such as infectious agents, fine and large particulate debris and toxic gases (Gridelli et al. 2015). The interaction between these exogenous threats and the diverse array of cell types, which populate the lung, make for the ideal environment for mutation acquisition that can lead to neoplastic change and cancer development.

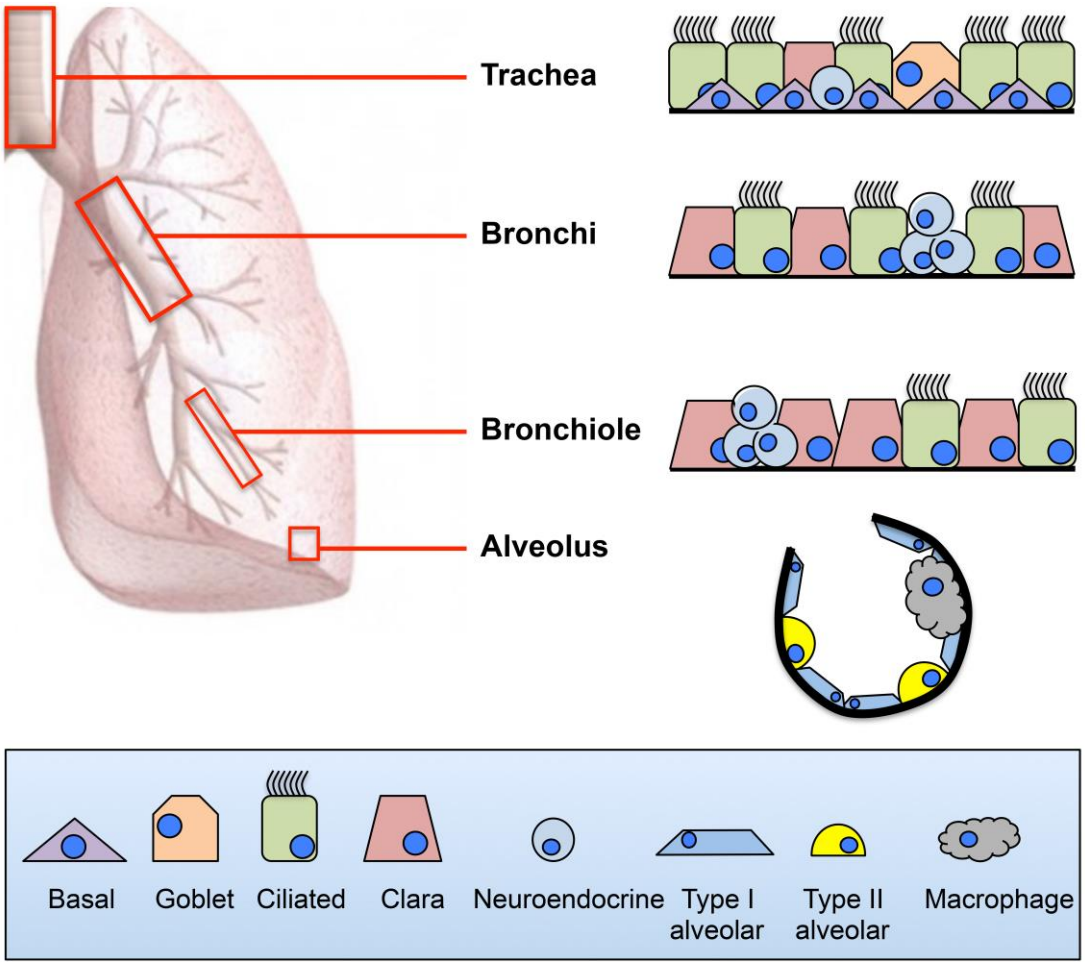

Figure 1.6. Schematic of the anatomy of the lung and its associated cell types. The human respiratory system is divided into two lungs with the left being comprised of two lobes (upper and lower) and the right being comprised of 3 lobes (upper, middle and lower). Inhaled air enters the respiratory system via the trachea which bifurcates into two bronchi with each supply one lung. Each bronchi then extensively branches to form bronchioles which terminate in alveoli, the site of gas exchange between air and blood. The trachea is predominantly comprised of ciliated cells overlaying basal cells. Interspersed in the trachea there are also occasional neuroendocrine cells and the mucin producing goblet cells. The bonchi and bronchioles have a similar cellular composition comprising clara cells, which secrete glycosaminoglycans to protect the respiratory epithelium, ciliated cells and neuroendocrine cells. Distal parts of the conducting airways have an increased proportion of clara cells to ciliated cells, relative to more proximal regions. Alveoli are primarily comprised of type I and type II alveolar cells which facilitate gas exchange and secrete pulmonary surfactants, respectively. Furthermore, alveolar macrophages can be found surveying the alveolar environment to aid in the elimination of inhaled pathogens.

1.5.2 Non-small-cell lung cancer (NSCLC)

1.5.2.1 Epidemiology and clinical features

Lung cancer is one of the most commonly diagnosed cancer types in humans, contributing to 13% of total new cancer cases, and remains as the leading cause of cancer deaths worldwide, making up 19.4% of total cancer deaths (Ferlay et al. 2015). Non-small-cell lung cancer (NSCLC) forms approximately 85% of all newly diagnosed lung cancer cases and represents a heterogeneous class of tumour entities. The remaining 15% is accounted for by small-cell lung cancer (SCLC) (Govindan et al. 2006; Travis et al. 2013). The leading cause of lung cancers remains as tobacco smoking with environmental air pollution and radon exposure also contributing to disease development (Ferlay et al. 2015). Currently the predicted 5-year survival rate is around 16% for NSCLC and has barely improved of the last few decades owing to a lack of effective therapeutic strategies (Z. Chen et al. 2014) (Figure 1.7).

Diagnostic approaches for NSCLC include X-rays, PET and CT imaging as well as histological assessment of tumour biopsies. Furthemore, the most recent guidelines by the World Health Organisation also place significant importance on molecular testing of patient biopsies by immunohistochemistry and genomic sequencing to improve diagnosis (Travis et al. 2015). Staging of NSCLC tumours is performed using the Tumour-Node-Metastasis (TNM) classification system (Goldstraw et al. 2007; Shepherd et al. 2007). Staging of the disease accurately is important to inform prognosis and facilitate appropriate treatment regimes, which commonly involve one or more of the following interventions: surgery, radio- and chemo-therapy, immunotherapy, anti-

angiogenic monoclonal antibody therapy and tyrosine kinase inhibitors (depending on the results of mutational profiling on the patients tumour) (Gridelli et al. 2015).

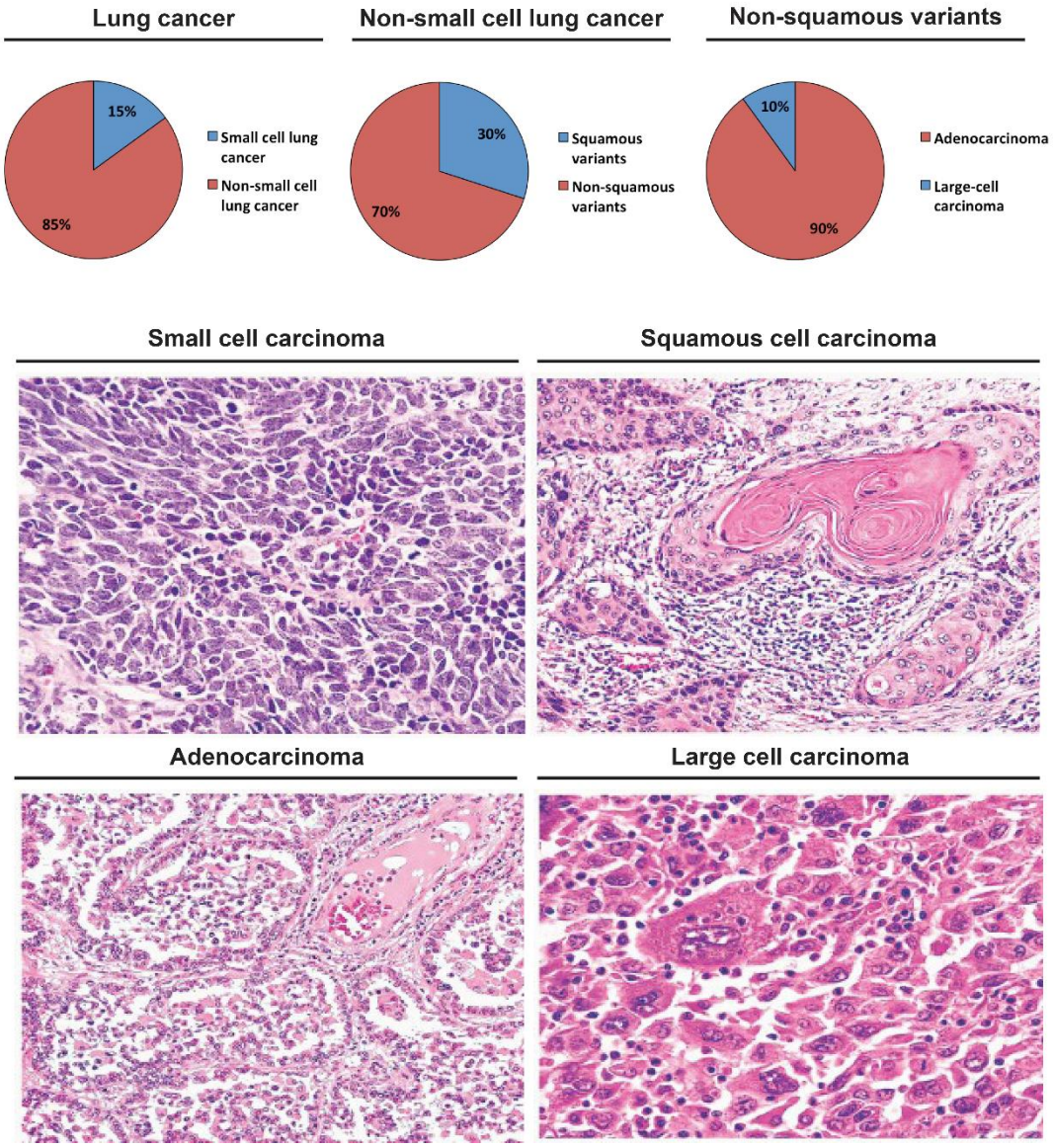

Figure 1.7. Lung cancer subtypes and histology. (Top) The proportions of small (SCLC) and non-small cell lung (NSCLC) cancers, followed by the proportions of squamous and non-squamous NSCLC variants. Non-squamous NSCLCs can be further divided into adenocarcinomas and large cell carcinomas. (Bottom) Haematoxylin & eosin images showing the histology of various human lung cancer tumours.

Histologically NSCLC can be subdivided into squamous and non-squamous variants, which comprise 30% and 70% of NSCLC cases, respectively. Further to this, non-squamous NSCLC can be further compartmentalised into adenocarcinoma and large-cell carcinoma, with respective incidences of 90% and 10%.

1.5.3 Genetic alterations in NSCLC

Detailed sequencing studies have been performed, which have elucidated the heterogeneous mutational landscape of lung cancer (Collisson et al. 2014; J. Gao et al. 2013) (Table 1.3). Such studies are important for not only identifying driver mutations, which may be therapeutically targetable, but for understanding intra-tumour heterogeneity and the clonal evolution of the disease.

Lung tumours found in individuals who smoke possess the greatest number of somatic mutations, approximately ten mutations per megabase, with non-smokers possessing a mutational burden that is 90% lower. The most common oncogenic genomic alteration associated with NSCLC include activating mutations in *EGFR* and translocations of the anaplastic lymphoma kinase (*ALK*) gene, which are found in 10-60% of adenocarcinomas. Variations in the frequency are believed to be due to factors such as patient smoking habits, with the highest incidence found in never smokers (Pao & Miller 2005) and geographical region (~10% in patients of European descent and ~60% in patients of Asian descent). The most frequent mutations in *EGFR* are deletions in exon 19 (E746-A750) and substitutions in exon 21 (L858R) and exon 18 (G719C, G719S, G719A) (Pao & Miller 2005). The *ALK* translocations result in the gene coming in under the regulatory control of promoter elements from various other genes, with echinoderm microtubule-associated protein-like 4 (*EMAL4*) and kinesin 1

heavy chain (*KIF5B*) being the most common (Shaw & Engelman 2013). Mutations in MAPK componentsare also particularly common in lung adenocarcinomas, with activating mutations in *KRAS* (25-32%), *BRAF* (4-8%), and receptor tyrosine kinases (24%) as well as loss of *NF1* (11%), a negative regulator of MAPK signaling (Herbst et al. 2008; Ding et al. 2008; Collisson et al. 2014; Imielinski et al. 2012; Devarakonda et al. 2015; Lemjabbar-Alaoui et al. 2015; Vicent et al. 2004; Wistuba & Gazdar 2006; Shigematsu & Gazdar 2006). Thus demonstrating the significant importance of this pathway in NSCLC progression.

More infrequent genetic abnormalities in lung cancer include translocations of *ROS1* and *RET* as well as mutations in *HER2* and *MET.* Oncogenic amplifications in *HER2* , *MET* and *FGFR1* have also been reported. Further to this, mutations are commonly found in the tumour-suppressors *RB1* and *TP53* and are not restricted to a particular subtype of lung cancer, although they show a slightly higher tendency to be found in SCLC rather than NSCLC (Collisson et al. 2014). Functional loss of the tumour-suppressor p53 is particularly common in lung adenocarcinomas and is observed in around 70% of patients, either through direct mutations in *TP53* or alterations in the p53 regulators ATM or HDM2 (Ding et al. 2008; Collisson et al. 2014; Lemjabbar-Alaoui et al. 2015).

1.5.4 Lung cancer cell-of-origin

The identify of the cell or cells-of-origin for NSCLC currently remain poorly understood. However, work using genetically engineered mouse models has begun to provide some clarity. This issue is confounded by the significant heterogeneity of the

histological subtypes and genetic alterations that are found in NSCLC tumours (Z. Chen et al. 2014). Therefore, it is currently unknown whether there is one cell type that has the capacity to give rise to all of the varied NSCLC tumour entities (i.e. adenocarcinoma, large cell carcinoma and squamous cell carcinoma) or if there are multiple cells-of-origin that each give rise to a specific NSCLC tumour subtype due to their intrinsic properties or microenvironmental location.

Biological Process	Gene	Lung adenocarcinoma	Lung squamous cell carcinoma	Mutation effect
Proliferation, cell survival, translation	*EGFR*	27%	<9%	Activating
	ERBB2/3	3%	2-4%	Activating
	MET	7%	-	Activating
	FGFR1, 2, 3	-	7%, 3%, 2%	Activating
	ALK	<8%	-	Activating
	RET	1%	-	Activating
	ROS	2%	-	Activating
	KRAS	32%	3%	Activating
	NRAS	<1%	<1%	Activating
	RASA	-	4%	Inactivating
	HRAS	<1%	3%	Activating
	RIT1	2%	-	Activating
	NF1	11%	11%	Inactivating
	BRAF	7%	4%	Activating
	MAP2K1	<1%	<1%	Activating
	PTEN	3%	15%	Inactivating
	PIK3R1	<1%	-	Inactivating
	PI3CA	4%	16%	Activating

	STK11	17%	2%	Activating
	AKT1	1%	<1%	Activating
	AKT2	-	4%	Activating
	AKT3	-	16%	Activating
	TSC1/2	3%	3%	Inactivating
	MDM2	8%	-	Activating
	ATM	9%	-	Inactivating
	TP53	46%	90%	Inactivating
Cell cycle progression	*CDKN2A*	43%	70%	Inactivating
	CCND1	4%	-	Activating
	CDK4	7%	-	Activating
	CCNE4	3%	-	Activating
	RB1	7%	7%	Inactivating
Oxidative stress response	*KEAP1*	19%	12%	Inactivating
	CUL3	<1%	7%	Inactivating
	NFE2L2	3%	19%	Activating

Table 1.3. Common mutations found in human lung adenocarcinoma and squamous cell carcinoma. Adapted and modified from Herbst et al. 2018

Lung adenocarcinomas have historically been thought to arise from Clara cells or Type II alveolar cells due to a similar imunohistochemical staining profiles between these cell types and the tumour (Davidson et al. 2013; Langer et al. 2010). However, such correlation can not be taken as definitive proof of the identify of the cell-of-origin for these tumours as their immunohistochemical staining profile is a snapshot in time and not necessarily indicative of their cellular beginning. Studies of NSCLC using genetically engineered mouse models have provided much greater insight into the cell(s)-of-origin of NSCLC tumours. Initially this was through the observations of which

cell types first show hyper-poliferative phenotypes following non-specific activation of oncogenes (e.g. *Kras*^{G12D}) or loss of tumour supressors (e.g. *Pten*), following intra-nasal infection of pulmonary epithelial cells with adenoviruses carrying Cre-recombinase. Such studies identified bronchioalveolar stem cells (BASCs) as potential candidates for adenocarcinoma cell-of-origin (Kim et al. 2005; Tiozzo et al. 2009; Ventura et al. 2007). However, targeted expression of oncogenic *Kras* to club cell secretory protein (CCSP) (which is expressed by BASCs and Clara cells) or surfactant protein C (SPC) (which is expressed by BASCs and type II alveolar cells) expressing cells found that adenocarcinomas could only be generated from SPC-expressing type II alveolar cells. Targeting of oncogenic Kras to BASCs produced only bronchiolar hyperplasia, but not adenocarcinoma during the same experimental time frame (Xu et al. 2012). Furthermore, independent studies have found that targeting oncogenic *Kras*^{G12D} to mature type II alveolar cells, using a Cre-recombinase under the regulatory control of the LysozymeM promoter (LysM-Cre), was sufficient to induce the development of lung adenocarcinomas that expressed type II alveolar cell markers (Nkx2.1 and SftpD) and lacked expression of Clara cells markers (CCSP) (Desai et al. 2014). In agreement with previous studies, these authors also failed to produce lung adenocarcinoma through driving oncogenic *Kras*^{G12D} expression in Clara cells/BASCs using an inducible CCSP-driven Cre-recombinase (CCSP-Cre-ER) (Desai et al. 2014). These observations are consistant with reports from other laboratories which also found that alveolar type II cells are the predomiant cell type capable of undergoing malignant transformation to form lung adenocarcinomas following oncogenic Kras^{G12D} expression, whearas targeted Clara cells or BASCs only produce bronchiolar and bronchioalveolar hyperplasias and rarely, lung adenomas (Mainardi et al. 2014; Sutherland et al. 2014). Therefore, while the current evidence suggests that alveolar type II cells appear to be the cell of origin for lung adenocarcinomas, It should be noted however, that these results are all

obtained through the activation of a single, specific oncogene, $Kras^{G12D}$. Therefore, it is entirely feasible that other oncogenic mutations in other cell types, such as BASCs or Clara cells may be capable of inducing lung adenocarcinoma.

Further work using other cell-type restricted Cre-drivers and oncogenic mutations is required to expand our understanding of the cell(s)-of-origin of the heterogeneous NSCLC tumour subtypes. Such experiments will potentially facilitate a more complete understanding of NSCLC cell(s)-of-origin and may be beneficial for clinical practice as the knowledge of the cell-of-origin could provide information that is useful for predicting treatment responses.

1.5.5 Mouse models of lung cancer

Currently a wide variety of different mechanisms have been employed to model lung cancer (NSCLC and SCLC) initiation and development in mice and has been extensively reviewed (Safari & Meuwissen 2015). These strategies include the study of strains of mice, which are susceptible to spontaneous lung tumourigenesis, lung tumour models induced by chemical carcinogen exposure, xenotransplantation and orthotopic transplantation of human lung cancer into immunocompromised mice and genetically engineered mouse models. Each of these model systems posses advantages and disadvantages that must be taken into account during experimental design. Table 1.3 summarises an array of lung caner mouse models, their method of initiation, phenotype and relevance to human lung cancers.

1.5.5.1 Genetically modified mouse models of lung cancer

Recent work has provided a range of genetically engineered mouse models, which show greater recapitulation of the genotype-phenotype correlations that exist in human lung cancers and are the most commonly used mouse models of lung cancer. Generally these models rely on genetic recombination technology (Cre/lox, FLP/frt or DRE/rox) or a tetracycline-inducible bi-transgenic system to allow for spacial-temporal control of oncogene activation/tumour-suppressor loss (Safari & Meuwissen 2015). The most commonly employed strategy using Cre/lox recombination allows for the conditional expression of an oncogene through the deletion of an upstream *LoxP-Stop-LoxP* sequence (*LSL*, a transcriptional stop sequence flanked by two *LoxP* sites) by a Cre recombinase either under the control of a cell-type specific promoter or by intranasal/intratracheal administration of a Cre-carrying virus. Somatic mutation in *Braf*, *Kras*, *Egfr*, *Lkb1*, *Rac1* and *Tp53* have all been generated in this manner and have been useful for studying lung cancer initiation and progression (Kwon & Berns 2013). See table 1.4 for details on commonly employed mouse models of lung cancer.

Numerous promoters have been utilised to drive the expression of Cre-recombinase in different lung epithelial cell populations to induce lung cancer. The most successful of these include; Clara cell secretory protein (CCSP) specific promoter (*CC10*) for Clara cells, lung surfactant protein C (*SPC*) promoter for type II pneumocytes and the lung neuroendocrine cell promoter *CGRP* (Safari & Meuwissen 2015). A potential problem that arises from the use of tissue-specific promoters is that the continual expression of Cre-recombinase may result in significant *in vivo* genotoxicity (Hameyer et al. 2007).

Cre delivery using adenoviral or lentiviral vectors is advantageous as the multiplicity of tumours formed can be controlled by the number of viral particles administered to the mouse. The use of either an adenoviral or lentiviral vector will have significantly different outcomes in inducing lung tumourigensis. Lentiviral vectors allow for the stable integration of Cre into the genome of both dividing and non-dividing cells (Singer & Verma 2008), whereas adenoviral vectors allow for only transient expression of Cre due to their non-integrating nature (Breyer et al. 2001). The infection efficiency is known to be significantly greater with adenoviral vectors than lentiviral vectors. Lentiviral vectors have an added advantage, however, over adenoviruses as the stable integration of their DNA allows it to act as a permanentsmarker for tracing the lineage of infected cells (Winslow et al. 2011). The issue of continuous Cre expression found in tissue-specific Cre-drivers is also true for lentiviral vectors, however this can be circumvented through the use of lentiviruses carrying a floxed Cre-recombinase to delete its own expression (Pfeifer et al. 2001).

Mouse model	**Used method**	**Phenotype**	**Relevance and relation to human lung cancer**	**Reference**
SpC-IgEGF, SpC-cMyc;SpCIgEGF, Sp-C-cMyc	Transgene expression controlled by the human SpC promoter in alveolar type II pneumocytes	SpC-Myc mouse developed multifocal bronchioloalveolar hyperplasia, adenomas, and adenocarcinomas whereas SpC-IgEGF developed hyperplasia of the alveolar epithelium	These transgenic mice are useful models for lung bronchioloalveolar adenocarcinomas (BACs) since *C-MYC* and *TGFα* are frequently overexpressed in human lung bronchioloalveolar adenocarcinomas	Ehrhardt et al. 2001
Conditional activatable	Intranasal administration of	Adenomas and adenocarcinomas after a long latency.	Confirms the role of spontaneous *KRAS* mutations in lung	Jackson et al. 2001

Kras^{G12D} allele	Ad-Cre to induce *Kras*^{G12D} expression	Lesions arose from alveolar type II cells or their precursors	cancer formation in which proliferating type II cells were found in early lesions within the bronchial epithelium	
CCSP-rtTA TetO-Kras G12D	CCSP-rtTA transgene; induction with doxycycline for 7 days. Removal of doxycycline after tumour development can lead to complete regression of tumour growth	Adenomas and adenocarcinomas developed after 2 months Dox induction, followed by focal invasion of the pleura at later stages. Removal of doxycycline led to rapid fall in levels of mutant *Kras* RNA, causing complete tumour relapse	Show Kras as driving oncogene for adenocarcinoma formation, as well as dependence on Kras expression for tumour maintenance	Fisher et al. 2001
CCSP-rtTA TetO-Kras^{G12D} in *Trp53*$^{-/-}$ and *Ink4A/Arf* $^{-/-}$ background	Identical to *CCSPrtTA* *Kras*^{G12D} mice	Tumours arose more quickly (within 1 month of Dox administration) and displayed more malignancy as compared to single *CCSP-rtTA Kras*^{G12D} mice. Complete tumour regression even in Trp53 $^{-/-}$ or *Ink4A/Arf* $^{-/-}$	10–35 % of human lung carcinoma contains *Trp53* somatic mutations, whereas 5–14 % harbours *Ink4A/Arf* somatic mutations Results confirmed important role of *Trp53* or *Ink4A/Arf* loss during NSCLCs progression. NSCLC growth dependence on Kras is even maintained in *Trp53*$^{-/-}$ or *Ink4A/Arf*$^{-/-}$ background	Fisher et al. 2001
Kras$^{LSL-G12D/+}$; *Tr*p53$^{flox/flox}$	Lentiviral-mediated somatic activation of oncogenic *Kras* and deletion of *Trp53* in lung epithelial cells	Accelerated Lung adenocarcinoma spectrum with sporadic metastases to lymph nodes, kidney, and liver	Unique lentiviral integration site tags enable to distinguish metastatic from non-metastatic tumors and determine gene expression alterations that distinguish these	Winslow et al. 2011

			tumour types. Progressed tumours can be used for therapeutics testing	
Pten$^{\Delta5/\Delta5}$; *CCSP*$^{Cre/+}$, *Pten*$^{\Delta5/\Delta5}$; *Kras*$^{LSL-G12D/+}$; *CCSP*$^{Cre/+}$ and *Kras*$^{LSL-G12D/+}$; *CCSP*$^{Cre/+}$	*Kras*$^{LSL-G12D/+}$, *Pten*^{flox}, and *CCSP-Cre* knock-in strains were interbred	PTEN inactivation alone had no visible effect on bronchial epithelial histology. However, initiation of lung tumourigenesis was faster and showed more vascularity and inflammation than that induced by Kras alone	About 3 % of human lung carcinoma harbor *PTEN* somatic mutations. Somatic inactivation of PTEN accelerates Kras-initiated lung tumourigenesis	Iwanaga et al. 2008
Kras$^{LSL-G12D/+}$; *Lkb1*$^{flox/flox}$ and *Kras*$^{LSL-G12D/+}$; *Lkb1*$^{flox/+}$	Ad-Cre infection regulates *Kras*^{G12D} expression and inactivation of *Lkb1*	Compared to tumors lacking *Trp53* or *Ink4a/Arf*, *Lkb1*-deficient tumours showed shorter latency, an expanded histological spectrum (adeno-, squamous, and large-cell carcinoma), and more frequent metastasis to regional lymph nodes and axial skeleton	Inactivating somatic mutations of *LKB1* have been reported in 10–25 % of primary human lung adenocarcinomas and squamous cell carcinoma derived cell lines. Lkb1 influences lung cancer differentiation and metastasis. Useful for testing therapeutics	Ji et al. 2007
SP-C-rtTA; *TetO-cRaf*, *CCSP–rtTA*; *TetO-cRaf*	Doxycycline diet at 5 weeks of age for a period of 4 to 6 months	*SP-C-rtTA* mice developed limited number of adenocarcinomas with no invasive and metastatic malignancy. *CCSP-rtTA* mice only produced less progressed adenomas. Tumours completely regress after DOX withdrawal via autophagy but not apoptosis	*cRAF* somatic mutations are rarely found in human lung carcinomas (≤1 %)	Ceteci et al. 2011
CreER;Kras$^{LSL-G12D/+}$	Induction of tamoxifen to introduce mutation in *Kras* in CC10 + epithelial cells and	Only type II cells progressed to adenocarcinoma-putative bronchoalveolar stem cells as cells of	The mouse lines used in this study will be useful in identifying initiating cells in future models	Xu et al. 2012

	Sftpc+ type II alveolar cells of the adult mouse lung	origin for KRas-induced lung hyperplasia		
TetO-PI3KCA ^{H1047R}; CCSP-rtTA	Systemic doxycycline Administration (food pellet)	Mice developed adenocarcinomas after 14 weeks doxycycline administration	Some 4 % of human NSCLC contains mutations in *PI3KCA*. Results from models indicate the important function of *PI3K* mutations in driving NSCLC development	Engelman et al. 2008
$Rb^{flox/flox}$; $Trp53^{flox/flox}$; $p130^{-/-}$	Viral Cre intratracheal Administration causing somatic inactivation of both *Rb1* and *Trp53* Use of adenovirus with tissue-specific promoters enabled targeting of specific cell types in the lung; Ad-CGRP-Cre: neuroendocrine cells, Ad-SP-C-Cre: mainly alveolar type 2 cells, Ad-CCSP-Cre: mainly Clara cells	Nuroendocrine cell hyperplastic lesions progressing to aggressive tumours with SCLC histology; rapid metastases formation into bone, brain, adrenal, ovary, liver; sporadic large cell neuroendocrine tumours and rare adenocarcinomas. Additional loss of *p130* accelerates tumour development with similar histology Ad-CGRP-Cre and to a far lesser extent, Ad-SP-C-Cre-induced SCLC Infected Clara cells did almost never produce any SCLC	Over 90 % of human SCLC contains somatic mutations of both *RB1* and *Trp53*. Loss of *p130* is rarely found in human SCLC but lower p130 protein levels are linked with more severe histopathological grade and poorer prognosis. Genome-wide comparison between mouse and human SCLC revealed a high similarity and conserved amplifications of *NFIB* and *LMYC*. Pulmonary neuroendocrine cells are the likely cells of origin for SCLC	Meuwissen et al. 2003; Sutherland & Berns 2010
$Braf^{LSL-V600E}$; $Braf^{LSL-V600E}$; $Ink4a/Arf^{flox/flox}$ and $Braf^{LSL-V600E}$; $Trp53^{flox/flox}$	Viral infection with Ad-Cre	*$Braf^{LSL-V600E}$* mice displayed benign lung adenomas with rare adenocarcinomas. *$Braf^{LSL-V600E}$; $Ink4a/Arf^{flox/flox}$ and $Braf^{LSLV600E}$; $Trp53^{flox/flox}$* resulted in more penetrant adenocarcinoma phenotype	Mutationally activated BRAF p.V600E has been identified in about 3 % of human NSCLC and results in continuous activation of MEK1/2–ERK1/2 cascade	Dankort et al. 2007

CCSP-rtTA/TetOhEGFR *L858R -Luc* and *CCSP-rtTA/TetOhEGFR* *Del19 -Luc*	Dox-inducible human EGFR with exon19 in-frame deletion or L858R mutation	Broad spectrum of adenocarcinomas are being formed, from early precancerous atypical adenomatous hyperplasia (AAH) lesions to invasive adenocarcinomas. Latency of L858R is shorter than exon 19 deletion. No metastases were detected	23 % of all human lung adenocarcinomas harbour EGFR somatic mutations These models will be useful for the testing of EGFR inhibitors as well as other novel therapeutics	Ji et al. 2006; Politi et al. 2006
Rac1$^{flox/flox}$*, Kras*$^{LSL-G12D/+}$ and *Kras*$^{LSL-G12D/+}$*; Rac1*$^{flox/flox}$	Viral infection with Ad-Cre	The *Kras*$^{LSL-G12D/+}$*; Rac1*$^{flox/+}$ mice displayed hyperplasia and adenomas. Tumor progression was similar to *Kras*$^{LSL-G12D/+}$ mice. Contrarily, tumour numbers were significantly reduced in *Kras*$^{LSL-G12D/+}$*; Rac1*$^{flox/flox}$ mice due to complete loss of *Rac1*	Loss of *Rac1* reduces proliferative activity and thereby dramatically delays tumour formation by oncogenic *Kras*	Kissil et al. 2007
Kras$^{LSL-G12D/+}$, *Kras*$^{LSL-G12D/+}$*; Rosa26*^{LSLRac1b}	Viral infection with Ad-Cre	*Kras*$^{LSL-G12D/+}$*; Rosa26*^{LSLRac1b} and *Kras*$^{LSL-G12D/+}$ mice produced a similar number of tumours. The tumour to lung volume ratio (T/L ratio) was significantly higher in *Kras*$^{LSL-G12D/+}$*; Rosa26*^{LSLRac1b} compared to *Kras*$^{LSL-G12D/+}$ mice at 24 weeks post-tumour initiation	These findings point out that *Rac1b* synergizes with oncogenic *Kras* to increase proliferation and tumour progression	Zhou et al. 2013
Kras$^{LSL-G12V/+}$	CMV-Cre$^{+/T}$	Constitutive activation of oncogenic *Kras*$^{LSL-G12V/+}$ allele results in the development of multifocal lung	Similar findings to that reported by Jackson et al. 2001	Guerra et al. 2003

		lesions		
Kras$^{LSL-G12V/+}$; *Braf*$^{flox/flox}$, *Kras*$^{LSL-G12V/+}$; *cRaf*$^{flox/flox}$	Viral Ad-Cre infection	Conditional ablation of *Braf* alleles in *Kras*-driven NSCLC did not increase survival. *Kras*$^{LSL-G12V/+}$; cRaf$^{flox/flox}$ mice survived significantly longer than the *Kras*$^{LSL-G12V/+}$ control cohort	These results suggest that *c-Raf* plays a unique role in mediating Kras signalling and makes it a suitable target for therapeutic intervention	Blasco et al. 2011
Kras$^{LSL-G12V/+}$, *Kras*$^{LSL-G12V/+}$; *Erk1*$^{-/-}$, *Kras*$^{LSL-G12V/+}$; *Erk2*$^{flox/flox}$, *Kras*$^{LSLG12V/+}$; *Erk1*$^{-/-}$; *Erk2*$^{flox/flox}$, *Erk1*$^{-/-}$; *Erk2*$^{flox/flox}$; *RERT*$^{ert/ert}$, *Erk2*$^{flox/flox}$; *RERT*$^{ert/ert}$	Viral Ad-Cre infection to inactivate either *Erk1* or *Erk2* or both *RERT*^{ert} mice, expressing Cre^{ERT2} were fed *ad libitum* with a tamoxifen containing diet to systemically excise the *Erk2*^{flox} alleles	Absence of either *Erk1* or *Erk2* only led to limited increase in life span but tumour burden was similar to those of control animals. All of the *Erk1*$^{-/-}$;*Erk2*$^{flox/flox}$; *RERT*$^{ert/ert}$ mice died within 3 weeks due to multiple organ failure	These observations indicate that a single *Erk*, either *Erk1* or *Erk2*, is enough to process *KrasG12V* oncogenic signalling to initiate NSCLC development. Ablation of both *Erk1* and *Erk2* activity completely blocks NSCLC formation. Additionally, loss of *Erk* proteins is discordant with life in adult mice	Blasco et al. 2011
Kras$^{LSL-G12V/+}$; *Mek1*$^{flox/flox}$, *Kras*$^{LSL-G12V/+}$; *Mek 2*$^{-/-}$ *mice, Kras*$^{LSL-G12V/+}$; *Mek1*$^{flox/flox}$; *Mek2*$^{-/-}$ and *Mek1*$^{flox/flox}$; *Mek2*$^{-/-}$; *RERT*$^{ert/ert}$	Viral Ad-Cre infection and, if applicable for *Mek1*$^{flox/flox}$; *Mek2*$^{-/-}$; *RERT*$^{ert/ert}$ mice, exposure to tamoxifen diet	*Kras*$^{LSL-G12V/+}$; *Mek1*$^{flox/flox}$ and *Kras*$^{LSL-G12V/+}$; *Mek2*$^{-/-}$ mice showed a slight increase in life span with the similar tumour burden like *Kras*$^{LSL-G12V/+}$ control animals *Kras*$^{LSLG12V/+}$; *Mek1*$^{flox/flox}$; *Mek2*$^{-/-}$ mice displayed significant lower tumour burden and increased survival *Mek1*$^{flox/flox}$; *Mek2*$^{-/-}$; *RERT*$^{ert/ert}$ mice showed a rapid impairment of their health	These results show that both Mek1/2 kinases are essential for *Kras*-driven lung tumour development. Systemic loss of Mek1/2 is incompatible with adult survival	Blasco et al. 2011
Braf$^{V600E/+}$; *Kras*$^{G12D/+}$	Viral Ad-Cre infection	Benign lung adenomas	Demonstrated that oncogene induced senescence, arresting the development of benign lung adenomas, underlies	Cisowski et al. 2016

			the mutual exclusivity of oncogenic BRAF and KRAS in lung cancer.	
Braf$^{CA/+}$; *Trp53*$^{flox/flox}$, *Braf*$^{FA/+}$; *Trp53*$^{flox/flox}$;	Viral Ad-Cre (*Braf*$^{CA/+}$) or Ad-FLP (*Braf*$^{FA/+}$) infection and *CAG::CreER* to mediate recombination of *Trp53*$^{flox/flox}$ alleles in *Braf*$^{FA/+}$; *Trp53*$^{flox/flox}$ mice	Benign lung adenomas and adenocarcinomas	Provided evidence that *Trp53* loss is not sufficient to promote senescence escape of arrested lung adenomas	Garnett et al. 2017
Orthotopic transplantation	Direct tumour cell injection directly into the main bronchi or pulmonary parenchyma	Human lung squamous cell carcinoma and adenocarcinoma cell	This model may provide the proper microenvironment for transplanted (human) lung tumour cells	Kang et al. 2010

Table 1.4. Commonly used mouse models for studying lung cancer and their relevance to human lung cancer. Adapted and modified from Safari & Meuwissen 2015

1.5.5.2 Inducible model of NSCLC: *Kras*$^{LSL\text{-}G12D/+}$

It is known that the lung epithelium is susceptible to transformation when experiencing sustained MAPK signaling. Activating mutations in *Kras*, *Craf* or *Braf* in mouse lungs results in the formation of lung tumours that are dependent on MEK1/2 (Dankort et al. 2007; Johnson et al. 2001; Jackson et al. 2001; Guerra et al. 2003; Kramer et al. 2004; Trejo et al. 2012). One of the most successful and widely used method for generating NSCLC in mice is the use of the *Kras*$^{LSL\text{-}G12D/+}$ conditional allele activated through adenoviruses carrying Cre (Ad-Cre), hereafter referred to as K-AdCre model (Meuwissen et al. 2001; Jackson et al. 2001; Guerra et al. 2003). This system can be used in isolation to study NSCLC initiation and progression or it can be combined with homozygous floxed alleles of *Tp53* (KP-AdCre model) to accelerate the tumourigenesis process (DuPage et al. 2009; Jackson et al. 2005).

The K-AdCre system can generate upwards of 200 tumours per mouse that bear histological resemblance to human NSCLC and the number of the tumours can be controlled through viral titration to lower levels. The median survival of K-AdCre mice is 185 days, falling to 75 days if combined with *Trp53* loss due to the increased growth of the tumours generated (Jackson et al. 2005). Histologically these lung tumours can be graded into four stages according to the severity of their cellular dysplasia (DuPage et al. 2009). The first lesions to form, termed grade I, are small adenomas or atypical adenomatous hyperplasias (AAH) that show uniform nuclei. These lesions are observed in the K-AdCre model from around two to three weeks post infection. Grade II lesions, which are the first to appear visibly on the surface of the lung, are adenomas of a larger size, which possess nuclei that are slightly larger than normal and can be observed around six to eight weeks after infection. Grade III tumours are classified as adenocarcinomas and show a significant degree of pleiomorphic cells with atypical nuclei and form around 16 weeks after Ad-Cre infection. Grade IV adenocarcinomas are invasive, have a similar morphology to grade III adenocarcinomas but with a greater proliferative index. These adenocarcinomas also show a distinctive desmoplastic stromal reaction at the invasive front and invasive edges that border the lung pleura as well as blood and lymphatic vessels. These invasive grade IV adenocarcinomas are seen around 18 weeks after viral infection in KP-AdCre animals but are generally absent in K-AdCre mice. In around half of infected KP-AdCre mice local metastasis can be observed to the pleural cavity and mediastinal lymph nodes, and to a lesser extent in the kidneys or liver, from 18 weeks onwards. It is important to note that not all tumour advance at a similar rate, resulting in a considerable degree of tumour heterogeneity within the lung. As an example of this, in K-AdCre mice, six weeks after viral induction the distribution of tumour grades can be seen to be around

90% grade I lesion and 10% grade two lesions. At 26 weeks this changes to 30% of grade I, 40% grade II, 30% grade III (Jackson et al. 2005).

1.5.6 Lung cancer and cellular senescence

As previously discussed, cellular senescence is thought to act canonically as a tumour-suppressive mechanism to limit the expansion of neoplastic cells. Such a mechanism is believed to act during lung tumourigenesis to prevent the transition from benign adenomas to malignant adenocarcinomas. This can be observed in work from several groups where activation of oncogenic *Braf* or *Kras* expression in the lung epithelium results in the formation of predominantly benign lung adenomas, with very few adenocarinomas being generated, especially in the oncogenic *Braf* context (Collado et al. 2005a; Dankort et al. 2007; Michaloglou et al. 2005; Dhomen et al. 2009a). Some studies have also reported that these adenomas show canonical markers of cellular senescence including $p16^{INK4A}$, $p21^{CIP1}$ and p53 as well as negativity for proliferation markers. Controversially, however, some groups have failed to find evidence for a senescent arrest of murine lung adenomas (Tuveson et al. 2004), therefore, further work is required to explain these discrepancies. The concept of cellular senescence acting as a barrier to more advanced stages of tumourigenesis has resulted in the origin of malignant lung adenocarcinomas being regarded as a consequence of senescence escape of arrested lung adenomas (Collado et al. 2005a). Evidence for this hypothesis is currently inferential and is derived from both mouse genetics studies and from sequencing of malignant human lung adenocarcinomas.

Murine experiments in which a critical mediator of cellular senescence is abrogated (i.e. *p16*^{INK4A} or *Trp53*) concomitantly with oncogene induction show a significantly higher incidence of adenocarcinomas compared with activation of the oncogene alone. This has been observed in the context of *Kras*^{G12D}-driven lung tumourigenesis with either *Trp53* (DuPage et al. 2009; Winslow et al. 2011; Muzumdar et al. 2016; Fisher et al. 2001), *p16*^{INK4A} (Fisher et al. 2001; Konstantinidou et al. 2013; Schuster et al. 2014; Ding et al. 2008) or *p21*^{CIP1} loss (Chen et al. 2015). Similar results have also been obtained with oncogenic *Braf*-driven lung tumourigenesis combined with the loss of either *Trp53* or *p16*^{INK4A} (Dankort et al. 2007). As previously mentioned, sequencing studies have shown the enormous genetic heterogeneity of human NSCLC (Collisson et al. 2014; J. Gao et al. 2013). Consistent with the idea that disruption of cellular senescence allows for the formation of adenocarcinomas, it is observed that the tumour suppressor and senescence mediator *TP53* is mutated by either gene loss or impairment of function, in around 70% of patients (Ding et al. 2008; Collisson et al. 2014; Lemjabbar-Alaoui et al. 2015). Moreover, somatic mutations in the *CDKN2A* locus, which encodes *p16*^{INK4A}, are found in around 5% of patient cohorts (Greulich 2010). However, hypermethylation of the promoter region of the *p16*^{INK4A} gene, which greatly impairs its ability to be expressed, are found in around 53% of human NSCLC cohorts (Liu et al. 2006). These results are consistent with the hypothesis that cellular senescence limits the neoplastic expansion of lung adenomas and prevents their transition into malignant adenocarcinomas. However, these results do not differentiate between senescence bypass or escape mechanisms as it is not known whether the senescence program needs to be disrupted before or after oncogene activation.

Interestingly, a recent study examined whether escape of cellular senescence was a mechanism of adenocarcinoma development. This was performed by inducing the expression of oncogenic *Braf*^{V600E} in the mouse lung epithelium, which resulted in the formation of benign adenomas with arrested proliferation due to the onset of OIS. The authors found, as previously reported, that simultaneous activation of the oncogene and loss of *Tp53* resulted in bypass of cellular senescence and the formation of adenocarcinomas. However, by temporally decoupling the activation of oncogenic *Braf* expression and loss of *Trp53* through Cre and Flp recombinases the authors found that loss of *Trp53* in tumours with an established senescence program failed to escape, instead maintaining their mitotic arrest (Garnett et al. 2017b). Therefore, this study was the first to demonstrate *in vivo* that *Braf*^{V600E} mediated OIS appears irreversible. This research also implies that the observation from human and mouse studies showing the correlation between the loss of components of the senescence pathway and progression to malignant adenocarcinomas may not be due to the escape of senescence. Rather, "pre-neoplastic" cells, which have compromised senescence-promoting genes when transformed through oncogene activation are likely to be the cell-of-origin for malignant adenocarcinomas. Whereas normal (non-pre-neoplastic) cells enter cellular senescence following an oncogenic insult, leading to the formation of benign adenomas. Further work is required to explore whether OIS is irreversible in lung adenomas when induced with other oncogenic hits (i.e *Kras*^{G12D}), or whether the loss of further senescence mediators (i.e p16^{INK4A}) is required to permit senescence escape.

1.6 β-Catenin/WNT Signaling

1.6.1 β-Catenin/WNT pathway overview

WNTs are a class of secreted cystine-rich glycoproteins which fulfil important functions in stem cell biology, developmental biology, cancer and other diseases. Currently 19 WNT genes have been described in humans with context dependent distinct and overlapping functions (Mikels & Nusse 2006). During development WNT are best known for their role in stem cell and niche regulation (Clevers et al. 2014) as well as being morphogens, which act to direct cell fate specification based on their tissue concentration gradient (Hüsken & Carl 2013). As the functions of WNT signaling have been shown to be highly conserved during evolution (Klaus & Birchmeier 2008) this has resulted in their study being of tremendous value in understanding both normal development and physiology as well as disease and potential treatment in humans.

Depending on the organism or developmental context WNT signaling occurs in either a canonical (β-Catenin dependent) or non-canonical (β-Catenin independent) manner (Reya & Clevers 2005). For the purposes of this introduction only canonical WNT signaling will be discussed. Mechanistically, canonical WNT signaling begins with the interaction of the WNT ligand with its receptor Frizzled (Fz) and a single-transmembrane low-density lipoprotein receptor-related protein (LRP5 or LRP6) (Reya & Clevers 2005). In the absence of WNT ligand a cytoplasmic 'destruction complex' forms, which is comprised of Axin, adenomatous polyposis coli (APC), casein kinase I (CKI) and glycogen synthase kinase 3-β (GSK3β). GSK3β and CK1 phosphorylate β-

Catenin at its N-terminus, allowing for polyubiquitination by the E3-ubiquitin ligase betaTRCP and subsequent proteosomal degradation (Figure 1.8).

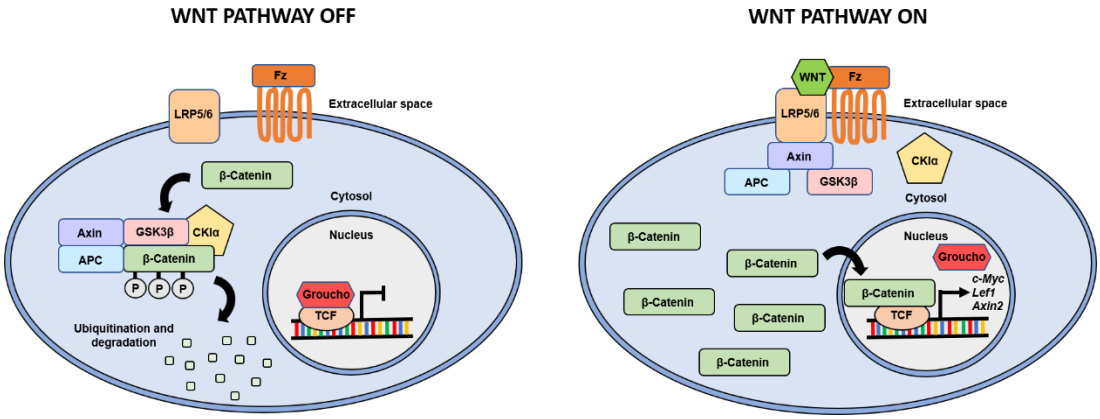

Figure 1.8. Schematic of the WNT/β-Catenin signalling pathway. In the absence of WNT ligant, β-Catenin levels are kept low through proteosomal degradation following phosphorylation by a "destruction complex" composed of Axin, GSK3β, APC and CDIα. Activation of the pathway by WNT ligand, interacting with its receptor Frizzled (Fz), results in the stabilisation of β-Catenin, by inhibiting the action of the destruction complex components. This then allows β-Catenin to translocate to the nucleus where it can activate TCF mediated transcription of WNT pathway target genes.

However, activation of the Fz receptor by WNT results in translocation of Dishevelled (Dvl) to the plasma membrane which prevents the action of the destruction complex resulting the stabilisation and increase in levels of β-Catenin protein. β-Catenin is then free to translocate to the nucleus where is can displace TLE repressing factors, which inhibit the transcription factor T cell factor/lymphoid enhancer factor (TCF/LEF) to allow for the transcriptional activation of WNT pathway downstream targets (Reya & Clevers 2005) (Figure 1.8). β-Catenin further promotes the activation of TCF/LEF factors through the recruitment of coactivators such as BCL9 and CBP/p300. Target genes activated have important roles in promoting cell survival, proliferation and differentiation. Further to this, activated WNT signaling induces the expression of

negative regulators of the pathway, such as Axin2, to prevent continual pathway activation (Stamos & Weis 2013).

1.6.2 β-Catenin/WNT Signaling and carcinogenesis

The discovery of Wnt proteins has its origin in the field of cancer research, during a screen for genes that were activated in response to viruses that induce the formation of mammary tumours in mice (Nusse & Varmus 1982). This experiment resulted in the discovery of the proto-oncogene *Int1* (integration 1), which is a homologue of the *Drosophila melanogaster* gene *Wg* (*Wingless*). This work let to the amalgamation of the *Wg* and *Int1* genes into what is now known as *Wnt* (Klaus & Birchmeier 2008). Following over a decade of research the link between human carcinogenesis and WNT signaling was found following the discovery that β-Catenin interacts with the tumour-suppressor ACP (Rubinfeld et al. 1993; Su et al. 1993).

Familial adenomatous polyposis is a condition characterised by the growth in the colon of several thousand benign polyps, which eventually progresses to malignant cancer (Bodmer et al. 1987; Leppert et al. 1987). Mutations in the APC gene are strongly associated with this condition and are present in around 85% of colorectal cancers (Kinzler & Vogelstein 1996). Furthermore, whole exome sequencing performed on human colorectal cancers has shown that loss-of-function *APC* mutations are likely driver mutations (Wood et al. 2007). This view is bolstered by the observations that the frequency of *APC* mutations appear to be consistent, irrespective of the stage of the tumour progression (i.e. late tumours vs early tumours) and are even found in microscopic adenomas (Fearon 2011). Further to this, accumulation of nuclear β-catenin is considered as a defining feature of this malignancy (Inomata et al. 1996).

Modelling these human genetic lesions in mice has also been met with success in recapitulating adenomatous polyposis-like tumours. Mice, which carry a truncated form of ACP (termed *Min* (Multiple Intestinal Neoplasia)) generate intestinal polyps (Su et al. 1992). Moreover, a conditional activating mutation in the 3rd exon of β-Catenin in mice also results in intestinal tumourigenesis (Harada et al. 1999). These studies provided the first experimental evidence that over activation of WNT signaling can promote tumour formation. This has led to our current understanding that mutations in WNT pathway components (APC, β-Catenin etc.) results in the nuclear accumulation of β-catenin that leads to excessive downstream target transcriptions, which can promote the survival and proliferation of tumour cells (Polakis 2012).

As discussed, there exists significant evidence for the role that activated Wnt signaling plays in the development of colorectal cancer, however, its function in other malignancies is less well understood. Activating mutations in *CTNNB1* have been described in a range of cancers (Polakis 2012), with higher levels of nuclear β-Catenin correlating with a poorer prognosis (Anastas & Moon 2013). In regard to paediatric malignancies, the role of oncogenic β-catenin has only been addresses in a few conditions, such as ACP, hepatoblastoma, WNT-driven medulloblastoma and Wilms' tumours (Gaston-massuet et al. 2011; Brastianos et al. 2014; Polakis 2007; Koesters et al. 1999; Huff 2011). Furthermore, in regard to lung physiology, WNT-signaling in type II alveolar cells has recently been identified as a mechanism by which these cells self-renew to maintain the size of their population. Blocking WNT-signaling results in the depletion of alveolar type II cells by promoting their transdifferentiation into alveolar type I cells (Nabhan et al. 2018). Moreover, the authors also identified that lung injury results in autocrine WNT-signaling within alveolar type II cells which acts to expand their population to act as a stem cell compartment to aid in the regeneration process

(Nabhan et al. 2018). Beyond normal lung physiology, recent analysis of lung adenocarcinomas in both humans and mouse models has revealed that these tumours demonstrate populations of WNT-signaling and WNT-reponding cells. Interestingly, WNT-reponding cells show increased tumour propagating abilities, suggesting that they may posess stem cell-like properties. Furthermore, perturbation of WNT-signaling, either genetically or pharmacologically, was able to retard tumour growth, limit the proliferative potential of the tumour cells and expand the survival of treated mice (Tammela et al. 2017). Together these results suggest that further research into the role that oncogenic WNT-signaling plays could provide novel therapeutic insights as well as information regarding the aetiology and pathogenesis of many cancer types.

1.7 Mitogen activated protein kinase (MAPK) signaling

1.7.1 Mitogen activated protein kinase (MAPK) pathway overview

The mitogen activated protein kinase (MAPK) pathway is an ancient and highly evolutionarily conserved signaling pathway, comprised of Serine/Threonine kinases, that is found in all eukaryotic cells and converts extracellular signaling into a variety of cellular responses. The pathway has many pleiotropic functions, which include the regulation of growth, proliferation, cell survival, cell motility, apoptosis and metabolism, among others (Widmann et al. 1999). The MAPK pathway is critical during development for orchestrating correct embryogenesis and it also plays important physiological and pathological functions in post-natal life.

In mammals, 14 MAPKs have been described and divided into seven groups. The conventional MAPK proteins characterised are the extracellular signal-related kinases 1/2 (ERK1/2), p38 isoforms (alpha, beta, gamma and delta), ERK5 and c-Jun amino (N)-terminal kinases 1/2/3 (JNK1/2/3) (Cheng et al. 1996; Kyriakis & Avruch 2012; Pearson et al. 2001). Non-conventional MAPKs such as Nemo-like kinase (NLK), ERK3/4 and ERK7 have also been described which possess certain peculiarities (Coulombe & Meloche 2007).

The MAPK signaling cascade is comprised of three sets of kinases that acts sequentially: a MAPK, a MAPK kinase (MAPKK) and a MAPKK kinase (MAPKKK). The upstream Serine/Threonine kinase MAPKKK is generally activated in response to an extracellular stimulus by either phosphorylation or through interaction with a small GTP-binding proteins, belonging to the Ras/Rho family (clinically relevant members include HRAS, KRAS and NRAS). Upstream activators of the MAPK pathway include signaling molecules such as FGF and EGF and PDGF, among others. The activation of MAPKKK results in a cascade of phosphorylation events, which phosphorylates and activates MAPKKs that then results in the activation of MAPK proteins through dual phosphorylation of threonine and tyrosine residues (Cargnello & Roux 2011). The canonical MAPK pathway comprises three MAPKKK kinases: A-RAF, B-RAF and RAF-1 (or C-RAF), with *BRAF* being the most frequently mutated kinase at this level of regulation in human malignancies. Beneath these is MEK1 and MEK2, the canonical MAPKKs, and the MAPKs ERK1 and ERK2, which are the terminal effectors of the signaling cascade (Robinson & Cobb 1997) (Figure 1.9). Activated MAPKs regulate their pleiotropic functions by phosphorylation of an array of substrates, which includes a family of proteins known as MAPK-activated protein kinases (MAPKAPKs). Members of this family include mitogen- and stress activated kinases (MSKs) (Arthur 2008), p90

ribosomal S6 kinases (RSKs) (Carriere et al. 2008), MAPK-interacting kinases (MNKs) (Buxade et al. 2008) and MAPK-activated protein kinases2/3 (MK2/3) (Ronkina et al. 2008).

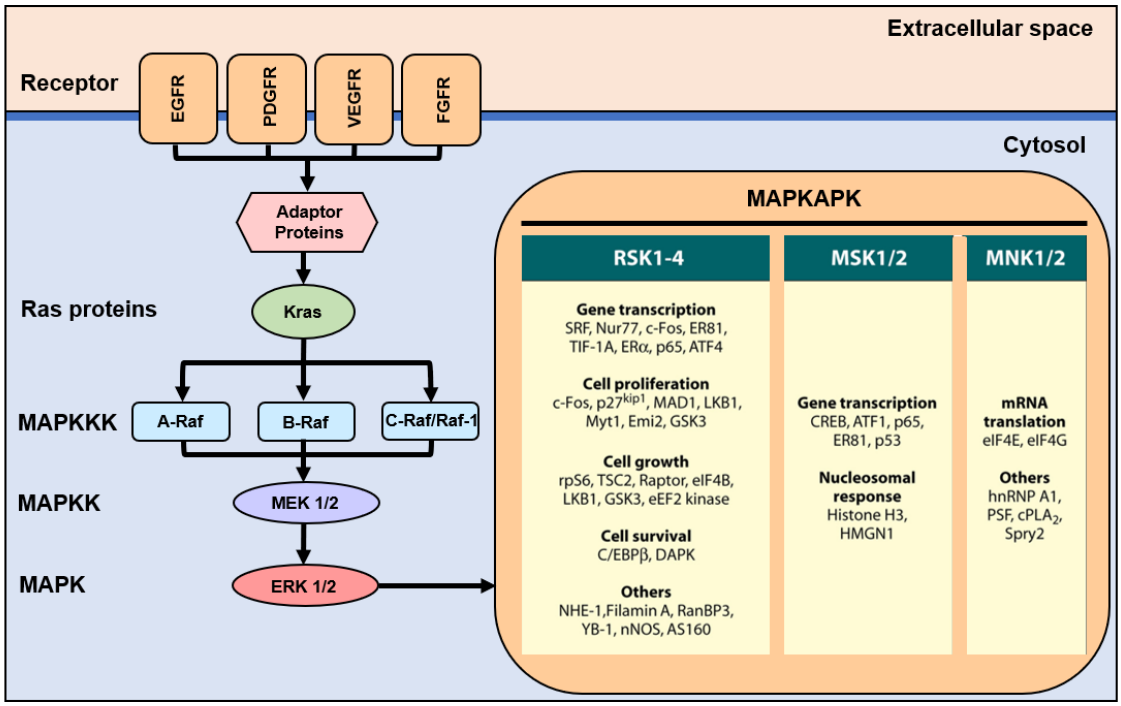

Figure 1.9. Schematic of the mitogen activated protein kinase (MAPK) signalling pathway. Following stimulation of upstream receptors, Ras small GTPases are activated which in turn activate MAPKKK proteins such as Braf. Activated MAPKKK then initiate a cascade of phosphorylation events through MAPKK and MAPK kinases. Ultimately, this leads to the activation of MAPKAPK protein which mediate changes in cell physiology such as modulation of cell growth, cell survival, proliferation, gene transcripton and translation.

1.7.2 Mitogen activated protein kinase (MAPK) signaling and carcinogenesis

The consensus view in the field of cancer biology is that for a cell to be considered cancerous it must posses profound dysregulation of at least six cellular behaviors leading to the acquisition of the following properties; independence from the

requirement of proliferative signals to undergo growth, apoptosis evasion, resistance to anti-proliferative signals, unlimited potential to replicate, sustained angiogenesis to maintain nutrient supply and the ability to invade surrounding tissue and metastasize (Hanahan & Weinberg 2011; Hanahan & Weinberg 2000). As the MAPK signaling pathway's varied repertoire of functions overlaps with many of these hallmarks of cancer it should be of little surprise that this pathway plays critical roles during carcinogenesis.

Mutations in genes encoding MAPK signaling components, or upstream receptors, have been found across many human cancer types, including but not limited to: melanoma, NSCLC, colorectal cancer, thyroid cancer, breast cancer, glioma, ovarian cancer, hepatocellular carcinoma and papillary craniopharyngioma of the pituitary (Burotto et al. 2014). Generally these mutations dysregulate kinase activity in the MAPK signaling cascade, or result in constitutively activated receptors, which ultimately leads to hyperactivated MAPK signaling. Common examples of such mutations include: *EGFR* exon 21 mutations or *del19EGFR*, *KRAS* mutations and *BRAF* mutations (such as *BRAF-V600E*) (Burotto et al. 2014). Interestingly, mutations found in MAPK signaling components in human malignancies are generally seen as single independent events. Two or more mutations in MAPK pathway components in the same tumour are appreciated as infrequent events (Burotto et al. 2014). However, mutation detection will depend on the proportion of tumour cells carrying a genetic lesion and, rare, but potentially biologically significant, mutational events, representing intra-tumour heterogeneity, may be missed when analysing a bulk tumour sample.

Aside from the well-studied oncogenic properties of MAPK signaling, the MAPK pathway can also have tumour suppressive functions. Abnormal MAPK pathway activation can result in the induction of cellular senescence, which can acts to cell-autonomously prevent neoplastic cell expansion and therefore, tumour-suppression. This is achieved through activated MAPK signaling promoting the degradation of proteins necessary for cell cycle progression (Serrano et al. 1997). Such tumour-suppressive functions of MAPK signaling through senescence induction has been observed in normal human fibroblasts, benign prostate tumours and lung adenomas (Deschenes-Simard et al. 2013; Cisowski et al. 2016; Garnett et al. 2017b). Furthermore, silencing of *MEK1* promoted lymphamogenesis in MYC-expressing lymphoid cells, indicating a tumour-suppressive role for this MAPKK (Bric et al. 2009).

1.8 Thesis aims and rationale

Cellular senescence is no longer simply regarded as a cell-autonomous mechanism whereby expansion of damaged cells is prevented to restrict tumour formation. Instead senescence is now appreciated to have much more profound and pleiotropic roles that can be both beneficial or detrimental depending on the cellular context. Senescence is now considered to be physiologically beneficial during embryonic development and wound regeneration in addition to its canonical role as a tumour-suppressive mechanism. However, senescent cells also have a sinister side, as they appear to promote organismal aging and development of age-associated diseases as well as, paradoxically, tumour growth and progression to malignancy.

Furthermore, as cellular senescence is now appreciated to be a complex phenotype that differs depending on the cell type undergoing senescence, the nature of the senescence-inducing stimuli and the duration in which the cell has experienced senescence means that a comparative understanding of the roles that senescence plays in disparate tumourigenic systems is warranted. To this end, this thesis explores the role of cellular senescence in the context of tumour development in two mouse organ systems; the pituitary gland and the lungs.

The recently described phenomenon of non-cell autonomous ACP-like tumourigenesis in the pituitary gland coupled with the observation that non-proliferative clusters of mutated stem cells are found in close association with the developing tumours raises the possibility that cellular senescence and the SASP may be inducing cellular transformation. During lung tumourigenesis the role of cellular senescence

have been poorly elucidated and there exits controversy surrounding whether senescence acts in a tumour-suppressive manner or whether it plays a role in promoting the disease.

Currently we are in the early stages of our understanding of what the many varied function of cellular senescence are, particularly in respect to their paradoxical relationship with tumour initiation and evolution. Therefore, the study of cellular senescence during the process of tumourigenesis is of significant importance not only for furthering our basic knowledge of the interactions between these populations, but potentially for advancing strategies to prevent cancer formation.

The specific questions that this thesis aims to address are the following:

1) Does cellular senescence play a role in mediating paracrine tumourigenesis in the pituitary gland in the context of craniopharyngioma?

2) What is the cell-of-origin from which non-cell autonomously derived pituitary tumours originate?

3) Is activation of the cellular senescence program sufficient to drive paracrine tumourigenesis of the pituitary gland?

4) What is the functional role of cellular senescence during lung tumourigenesis in a mouse model of NSCLC?

My central hypotheses are that in the tumoural pituitary gland, in the ACP mouse models, the cluster cells have entered into cellular senescence, which through the activities of the SASP induces transformation in neighbouring cells, leading to non-cell autonomous tumour formation. In the lung, benign adenomas have entered into cellular senescence to prevent their growth into malignant adenocarcinomas and ablation of these senescent adenoma cells will lead to a reduction in the tumour burden.

CHAPTER 2: MATERIALS AND METHODS

2.1 Mouse and human samples

2.1.1 Maintenance of mouse colonies

All animal procedures were carried out under the Animals (Scientific Procedures) Act 1986 and in accordance with the Medical Research Council guidelines, which are fully compliant with the current Home Office legislation.

2.1.2 Mouse strains and genetic crosses

2.1.2.1 *Hesx1-Cre* mouse line

The *Hesx1-Cre* mouse line was generated previously by the host lab (Andoniadou et al. 2007). The *Hesx1* coding region was replaced with a cassette containing Cre recombinase and the line has been maintained on a C57B16 background for over 50 generations. Heterozygous animals were used for genetic crosses to obtain embryos at various stages. Specifically, this line was crossed with $Braf^{V600E/+}$ and $Kras^{G12D/+}$ heterozygotes to generate $Hesx1^{Cre/+}$; $Braf^{V600E/+}$ and $Hesx1^{Cre/+}$; $Kras^{G12D/+}$ double-heterozygote embryos for analysis.

2.1.2.2 *Sox2-CreERT2* mouse line

The *Sox2-CreERT2* mouse line was generated previously by the host lab (Cynthia Lilian Andoniadou et al. 2013). Embryonic stem cells (ESCs) were electroporated and targeted clones were injected into C57BL16 blastocysts. The neo-

cassette was removed by crossing these mice with ACTB:FLIPe mice. *Sox2-CreERT2* mice were then maintained on a C57BL16 background for over 20 generations. Heterozygous animals were used for genetic crosses to obtain post-natal mice for experimentation. Specifically, this line was crossed with *Rosa26*$^{YFP/+}$ and *Ctnnb1*$^{lox(ex3)/+}$ mice to generate *Sox2*$^{CreERT2/+}$; *Ctnnb1*$^{lox(ex3)/+}$ *Rosa26*$^{YFP/+}$ triple-heterozygotes.

2.1.2.3 *Braf-V600E* and *Kras-G12D* mouse line

The *Braf-V600E* and *Kras-G12D* mouse lines have been previously described (Mercer et al. 2005.; Tuveson et al. 2004). In both cases the expression of the oncogenic protein is activated following Cre-mediated recombination. These lines were crossed with *Hesx1*$^{Cre/+}$ heterozygotes to obtain *Hesx1*$^{Cre/+}$; *Braf*$^{V600E/+}$ and *Hesx1*$^{Cre/+}$; *Kras*$^{G12D/+}$ double heterozygotes for analysis of pituitary phenotypes. For generating lung tumours *Kras*$^{G12D/+}$ animals were crossed with *Rosa26*$^{YFP/+}$ and *p16*$^{FDR/+}$ mice to generate *Kras*$^{G12D/+}$*; p16*$^{FDR/+}$*; Rosa26*$^{YFP/+}$ *and Kras*$^{G12D/+}$*; Rosa26*$^{YFP/+}$ animals.

2.1.2.4 *Rosa26-YFP* mouse line

The *Rosa26-YFP* mosue line contains a *YFP* gene inserted into the ubiquitously transcriptionally active *Rosa26* locus. Expression of *YFP* is inhibited by the presence of an upstream transcriptional STOP cassette comprised of 3 polyadenylation sequences, which is flanked by two *loxP* sites (Soriano 1999). Crossing of *Rosa26*$^{YFP/+}$ mice with a Cre-driver line allows for the removal of the stop cassette, permitting the

irreversible activation of *YFP* expression in a targeted cell populations and all of it cellular descendants. This strategy is known as cellular lineage tracing (Sauer & Henderson 1988). These reporter mice were bread onto a *Sox2*$^{CreERT2/+}$ and *Kras*$^{G12D/+}$ background to allow for lineage tracing of mutation sustaining cells in the pituitary and lung, respectively.

2.1.2.5 *Rosa26-mTmG* mouse line

Rosa26-mTmG mouse line has been previously described (Muzumdar et al. 2007). These mice express a membrane-tethered tdTomato ubiquitously which is replaced with a membrane-tethered GFP following Cre-mediated recombination. The embryos from these mice were used in proof-of-principle morula aggregation experiments.

2.1.2.6 *Ctnnb1-lox(ex3)* mouse line

The *Ctnnb1-lox(ex3)* mouse line was acquired from Professor Taketo (Harada et al. 1999). This recombinase-conditional line contains *loxP* sites flanking the 3rd exon of the *Ctnnb1* gene, alongside a neo-casette. Cre-mediated recombination results in the removal of the 3rd exon and the in-frame connection of exons 2 and 4, which produces a degradation resistant but transcriptionally functional β-catenin protein. These mice were bred onto a *Sox2*$^{CreERT2/+}$ background to enable the generation of pituitary tumours.

2.1.2.7 *p16-FDR* mouse line

The *p16-FDR* mouse line was generated as part of this thesis. For details on the generation of this mouse line see section 2.7. These mice allow for the direct visualisation, pharmacogenetic ablation (through diptheria toxin administration) and lineage tracing of *p16*-expressing cell populations. Specifically, a mammalian optimized FLP-recombinase and a diptheria toxin receptor-mCherry fusion construct were inserted into the 3' end of the *p16* gene to permit their expression under the control of the *p16* promoter. The mice were backcrossed for 5 generations onto a C57BL16 background before *in vivo* analysis. These mice were used to analyse the involvement of cellular senescence during lung tumourigenesis by crossing this line with the *Kras-G12D* inducible oncogene line and the *Rosa26-YFP* reporter line.

2.1.3 Murine lung tumour induction using intranasal Ad5CMVCre adenovirus administration

Ad5CMVCre adenoviral particles (University of Iowa, Viral Vector Core) were diluted in DMEM to reach a concentration of $5x10^5$ particles/µl and $CaCl_2$ was added to reach a final concentration of 4mM. This solution was incubated at room temperature to allow for the formation of viral precipitates. This solution was then used within 45 minutes of its generation. 4 to 6 weeks old mice (from the following genotypes: $Kras^{G12D/+}$, $Kras^{G12D/+}$; $Rosa26^{YFP/+}$ and $Kras^{G12D/+}$; $p16^{FDR/+}$; $Rosa26^{YFP/+}$) were initially anesthetized by a single intra-peritoneal injection of a Domitor/Ketamine solution (0.3mg/kg Domitor (Vetoquinol) and 60mg/kg Ketamine (Dechra) in 0.9%

NaCl). Once anesthetized, 25 µl of the Ad5CMVCre solution was delivered under each nostril per mouse (i.e 50 µl of the solution used in total per mouse), which the mice passively inhaled. Following intranasal delivery of the Ad5CMVCre adenovirus mice were given an intra-peritoneal injection of 1 mg/kg of Antisedan (Zoetis) in 0.9% NaCl to reverse the sedative and analgesic effects. Mice were then allowed to recover on a heated mat.

2.1.4 Sample collection and processing

2.1.4.1 Mouse embryos

Experimental embryos for this research was obtained through timed matings. Female mice were crossed with male mice and the females were inspected for vaginal plugs the following day and embryos were designated 0.5 dpc at noon of this day. Dissection of embryos took place on specific days depending on the developmental stage needed. Pregnant dams were humanely culled by cervical dislocation and the uterus was removed. Embryos were removed from the muscular wall of the uterus, Reichert's membrane and the yolk sac using forceps. Embryos were dissected in ice cold Dulbecco's Modified Eagle's Medium (DMEM) containing 10% fetal calf serum (FCS) under a dissecting microscope. Embryonic pituitaries were then isolated is a similar manner to adult pituitaries (see below).

2.1.4.2 Adult mouse pituitaries

Adult mice at the appropriate age were humanely culled by cervical dislocation. The head was then decapitated using scissors and the scalp and skull were removed with scissors and forceps. Using forceps the brain was reflected posteriorly out of the cranial cavity and the cranial nerves were severed to facilitate visualisation of the pituitary gland. Forceps were then used to carefully remove the membranes surrounding the pituitary allowing it to be removed from the skull for analysis.

2.1.4.3 Adult mouse lungs

Following humane culling, the skin on the thorax was reflected back to expose the rib cage, which was then removed using scissors. The heart was then removed to permit manipulations of the lungs. The lungs were isolated by severing of both the oesophagus and trachea and removal or surrounding membranes between the lungs and the rib cage.

2.1.4.4 Tissue processing

Processing of embryos and pituitaries (embryonic and adult) was conducted first by washing the tissue in 1x phosphate-buffered saline (PBS) followed by fixation in 4% paraformaldehyde (PFA) overnight at 4 degrees rolling. Following this the tissue

was washed three times in 1x PBS for 1 hour per wash and the dehydrated through a graded ethanol series to 70% ethanol in double distilled MiliQ water, with each wash lasting 1 hour. Embryos and pituitaries were stored at this stage and/or genotyped. Embryos and pituitaries to be embedded were then further dehydrated in 80%, 90%, 95% and 100% ethanol, with 1 hour per wash. Dehydrated tissues in 100% ethanol were incubated at 4 degree while rolling overnight.

2.1.4.5 Paraffin embedding

Following complete dehydration tissues were equilibrated to room temperature for 5 minutes in fresh 100% ethanol. Paraffin embedding of embryos between 10.5 and 16.5 dpc was initiated by two washes in HistoClear (National Diagnostics) with the length of the wash depending on the embryonic stage of the embryo (10.5 dpc - 20 minutes, 12.5 dpc - 35 minutes, 14.5 and 16.5 dpc - 45 minutes). For 18.5 dpc embryos two washes in Xylene (Sigma) were performed for a length of 1 hour each. Following this embryos were washed for varying lengths of time in a mix of 50% solvent (HistoClear for 10.5, 12.5 14.5 and 16.5 dpc embryos or Xylene for 18.5 dpc embryos) and 50% paraffin wax at 60°C degrees (10.5 dpc - 30 minutes, 12.5 dpc - 40 minutes, 14.5 and 16.5 - 50 minutes and 18.5 dpc - 1 hour). After this all embryos are washed three times in paraffin wax for 1 hour each before orienting the embryos and allowing the wax to solidify at room temperature. 10.5, 12.5, 14.5 and 16.5 dpc Embryos were oriented sagittally and 18.5 dpc embryos were oriented frontally. Adult mouse pituitaries were incubated twice in HistoClear for 10 minutes, one wash at room temperature and one wash at 60°C degree. Following this pituitaries were incubated for 15 minutes at 60°C degrees in 50% HistoClear, 50% paraffin wax. Wax washed were then performed

for 1 hour each at 60°C degrees. Following wax washed adult pituitaries were oriented on their posterior side to maintain the ventro-dorsal axis when sectioning. Adult mouse lung tissue was processed in an identical manner for 18.5 dpc embryos. Lungs were oriented on their flat ventral side and sectioned in a ventral to dorsal manner. Paraffin embedded tissues were sectioned with a microtome. Sections were cut at 7um for all experiments. Sections were mounted serially onto SuperFrost Plus slides (VWR International). Slides were dried overnight in a 37°C degree incubator and used for histological staining.

2.1.5 Administration of substances

2.1.5.1 Tamoxifen inductions

Cre induction was performed in *Sox2*$^{CreERT2/+}$*; Rosa26*$^{YFP/+}$ and *Sox2*$^{CreERT2/+}$*; Ctnnb1*$^{lox(ex3)/+}$; *Rosa26*$^{YFP/+}$ mice at 4 weeks or 6 months of age by a single intra-peritoneal injection of tamoxifen (Sigma) at a dose of 0.15mg per gram of body weight.

2.1.5.2 EdU DNA uptake experiments

For EdU labelling of embryonic pituitaries, pregnant females at 14.5 dpc were subjected to a single intra-peritoneal injection of EdU at a dose of 100 mg/kg and embryos dissected either 2 hours later for short-term tracing experiments or 48 h later at 16.5 dpc for longer term tracing. Visualisation of EdU was conducted using the Click-It EdU imaging kit (Invitrogen) according to manufacturer's instructions.

2.1.5.3 Diphtheria Toxin

For *p16*-expressing cell ablation experiments in $p16^{FDR/+}$ animals, mice were injected subcutaneously with 10 ng/g of diphtheria toxin (Sigma) twice a week.

2.1.6 Human samples

Anonymised archival frozen and FFPE specimens of human PCP were accessed through Brain UK (University of Southampton, UK). Human foetal pituitary tissue was accessed through the Human Developmental Biology Resource (HDBR, Newcastle and London, UK). Anonymised post-mortem human adult pituitary was accessed from the Medical Research Council Edinburgh Brain and Tissue bank and Royal Victoria Infirmary (Newcastle, UK) (Ethical approval 14/LO/2265).

2.1.7 Haematoxylin and eosin staining

Staining of histological sections was performed using Harris' haematoxylin for morphology and Mayer's haematoxylin for counter-stain following immunohistochemistry (IHC). For morphological analysis slides were dewaxed twice in HistoClear for 5 minutes, then serially re-hydrated from 100% ethanol to running tap, with each wash lasting 2 minutes. Slides were then dipped into Harris' haematoxylin for 2 minutes and then incubated in running tap water for 5 minutes. Following this, slides were incubated in eosin for 1 minute before being allowed to sit under a running tap

water wash for 5 minutes. The slides were then dehydrated in a graded ethanol series and then mounted on coper slips using hard set VectaMount (Vector Laboratories).

Counter staining after IHC was performed with Mayer's haematoxylin. Slides were dipped into Mayer's solution for 30 seconds following IHC staining and checked under a microscope. Slides were then dehydrated in the same graded ethanol seried and mounted in hard set VectaMount (Vector Laboratories).

2.2 Fluorescence activated cell sorting (FACS)

2.2.1 Lung and pituitary tissue dissociation

Following extraction of either lung or pituitary tissue, the tissue was dissected into pieces around $1mm^3$ in size. These tissue fragments were then incubated in an enzymatic dissociation mix (0.5% w/v Collagenase type 2 (Lorne Laboratories Ltd.), 0.1x Trypsin (Gibco) and 50 µg/ml DNaseI (Worthington) with 2.5 µg/ml Fungizone (Gibco) in Hank's Balanced Salt Solution (HBSS (Gibco) for 3 hours at 37°C. Following enzymatic treatment the tissue fragments were dissociated into single cells through mechanical tituration using a pipette before being passed through a 70 µm filter. Single cells were then washed in HBSS and suspended in PBS supplemented with 1% Foetal Calf Serum (PAA), 25 mM HEPES and 1 ng/µl of propidium iodide (PI, BD Pharmigen) for live/dead cell discrimination before being analysed using a Flow Cytometer.

2.2.2 Isolation of pituitary stem/progenitor cells

To isolate pituitary stem/progenitor cells, dissociated single cells from either *Sox2*$^{CreERT2/+}$*; Ctnnb1*$^{lox(ex3)/+}$*; Rosa26*$^{YFP/+}$ or *Sox2*$^{CreERT2/+}$*; Rosa26*$^{YFP/+}$ pituitaries were flow sorted for YFP (pituitary stem/progenitor and cellular progeny fraction) and PI (dead cell fraction) fluorescence using a MoFlo XPD (Beckman Coulter, Fullerton, CA, USA) Flow Cytometer. Fluorescence was detected using a 530/540 filter, where PI positive cells were excluded and the YFP positive and negative fractions collected directly into RLT buffer (Qiagen) supplemented with 1% 2-mercaptoethanol (Sigma) for subsequent RNA isolation.

2.2.3 Isolation of lung tumour cells and senescent cells

To isolate lung tumour cells and senescent cells, dissociated single cells from *Kras*$^{G12D/+}$*; p16*$^{FDR/+}$*; Rosa26*$^{YFP/+}$ lungs were flow sorted for YFP (lung tumour cell compartment), DAPI (dead cell fraction) and mCherry (senescent cell fraction) fluorescence using a BD FACSAriaIII (Becton Dickinson, UK) Flow Cytometer. Fluorescence was detected using a DAPI 450/50 filter, YFP 530/30 filter and mCherry 610/20 filter, where DAPI positive cells were excluded and the mCherry positive and YFP positive and negative fractions were collected directly into RLT buffer (Qiagen) supplemented with 1% 2-mercaptoethanol (Sigma) for subsequent RNA isolation.

2.3 DNA methods

2.3.1 Genotyping of mice and embryos by PCR of genomic DNA

Adult mice were genotypes using an ear biopsy and for embryos a tail biopsy was used. Genomic DNA was extracted using a 25 µl solution, consisting of 5 µl of DNAreleasy (Anachem) and 20 µl of water, according to the manufacturer's instructions. Following lysis, this solution was used for genotyping.

Genotyping of mice and embryos were performed using specific primer sets, which are detailed in table 2.1. Genotyping was performed using polymerase chain reaction (PCR) amplification. PCR sequences were amplified using Taq polymerase (Bioline) or JD buffer (3X JD buffer: 60 mM K-glutamate, 24 mM Hepes, 90 mM Tris, 15 mM $MgCl_2$, 6 mM DTT, 180 mM NH4Ac, 3% DMSO, 24% glycerol). Reactions were made up to the volumes described in table 2.2**.** 1 µl of DNA template was used for each reaction. Two negative controls were always used: lysis buffer without biopsied tissue (T-) and the PCR reaction mix only without genomic DNA (C-). A positive control was also always used which contained genomic DNA that had been previously analysed to contain the correct PCR product following amplification (C+). Generally, initial strand denaturation was performed at 94°C for 2 minutes. Further denaturation steps were conducted at 94°C for 30 seconds followed by a primer-dependent annealing step and polymerisation extension at 72°C for 1 minute. The final extension step was conducted at 72°C for 5 minutes. PCR products from each PCR were resolved by gel electrophoresis.

Mouse Line	Primer Sequences (5'-3')	Annealing Temperature and Cycle Numbers	Reaction Buffer Conditions	Expected Products
Braf-V600E	**137 BRAF:** GCTTGGCTGGACGTAAACTC **125 BRAF:** GCCCAGGCTCTTTATGAGAA **143 BRAF:** AGTCAATCATCCACAGAGACCT	65 for 1 minute (30 cycles)	Taq Pol. Buffer	**WT:** 460 bp **MUT:** 140 bp
Ctnnb1-lox(ex3)	**Fwd:** AGAATCACGGTGACCTGGGTTAAA **Rev:** CATTCATAAAGGACTTGGGAGGTGT	62 for 20 sec (40 cycles)	Taq Pol. Buffer	**WT:** 600 bp **MUT:** 700 bp
Hesx1-Cre	**OL89:** GGAGACAATTCTTTTGTGAAACCCTG **OL91**: CCAGAGTGTCTGGCTTCTGTC **CreT:** CAGAAGCATTTTCCAGGTATGCTC **OL39:** TCAGCAAAGCTACAAGGTGAACTG	58 for 30 sec (35 cycles)	JD	**WT:** 500 bp **MUT:** 300 bp
Kras-G12D	**KRas-G12D 1:** GTCTTTCCCCAGCACAGTGC **KRas-G12D 2:** CTCTTGCCTACGCCACCAGCTC **KRas-G12D 3:** AGCTAGCCACCATGGCTTGAGTAAGTC TGCA	61 for 30 sec (35 cycles)	JD	**WT:** 622 bp **MUT:** 500 bp
p16-FDR	**p16FDR1:** CCAAGCACAAGCGGCTATC **p16FDR2:** CGTTGTAAGGGATGATGGTG **p16FDR3:** TAAAGCCACATGCTAGACACGC	58 for 30 sec (30 cycles)	JD	**WT:** 342 bp **MUT:** 621 bp

Rosa26-mTmG	**mTmG1:** CTCTGCTGCCTCCTGGCTTCT **mTmG2:** CGAGGCGGATCACAAGCAATA **mTmG3:** TCAATGGGCGGGGGTCGT T	58 for 25 sec (32 cycles)	Taq Pol. Buffer	**WT:** 330 bp **MUT:** 250bp
Rosa26-YFP	**R26R1:** AAAGTCGCTCTGAGTTGTTAT **R26R2:** GCGAAGAGTTTGTCCTCAACC **R26R3:** GGAGCGGGAGAAATGGATATG	60 for 1 min (35 cycles)	Taq Pol. Buffer	**WT:** 250 bp **MUT:** 600 bp
Sox2-CreERT2	**Fwd:** GATGCAACGAGTGATGAGGTTCGC **Rev:** ACCCTGATCCTGGCAATTTCGGC	63 for 30 sec (30 cycles)	Taq Pol. Buffer	**MUT:** 500 bp
Vav1-Cre	**Vav1-Cre Fwd:** ATCAGCCACACCAGACACAGAGATC **Vav1-Cre Rev:** AGATGCCAGGACATCAGGAACCTG	65 for 1 minute (30 cycles)	Taq Pol. Buffer	**MUT:** 250bp

Table 2.1. Primers used for PCR genotyping of mice and embryos

Component	**DNA Mix (µl)**		**Enzyme Mix (µl)**	
	Taq Buffer	**JD Buffer**	**Taq Buffer**	**JD Buffer**
H_2O	7.08	1.7	6.4	1.55
Taq Pol. Buffer (10x)	1.2	-	0.8	-
$MgCl_2$ (25 mM)	0.72	-	0.48	-
JD Buffer (3x)	-	2.5	-	0.83
Primer 1	1 (25 µM)	0.5 (10 µM)	-	-
Primer 2	1 (25 µM)	0.5 (10 µM)	-	-
dNTPs (25 mM)	-	0.3	0.16	-
Taq Pol (5 U/µl)	-	-	0.16	0.12

Table 2.2. Reaction mixes for PCR genotyping

2.3.2 DNA restriction enzyme digestion

Digestion of DNA by restriction enzymes was performed for either in vitro transcription of RNA probes, molecular cloning or diagnostic reactions. Enzyme mix was scaled up to 100 µl, 50 µl or 15 µl respectively. Restriction digests were performed according to the manufacturer's instructions (Promega, Roche or New England BioLabs). Reactions contain 1x restriction enzyme digest buffer and a proportional amount of restriction enzyme according to the concentration of the DNA used. The reaction solution was then incubated at 37°C for 2 hours.

2.3.3 Extraction of DNA from PCR products and agarose gels

DNA from PCR products between 100 bp and 10 kb was extracted using the QIAquick PCR Purification Kit (Qiagen), according to the manufacturer's instructions. In a similar way, PCR product bands ranging from 70 bp to 10 kB, were excised from agarose gels using a scalpel under UV light and DNA was extracted with the Qiagen Gel Extraction Kit (Qiagen), according to the manufacturer's instructions.

2.3.4 Molecular cloning

2.3.4.1 Vector and insert preparation

Plasmid vectors were digested with the appropriate restriction enzyme/s and restriction buffer/s in a total volume of 50 µl (in water) for 1-2 hours at 37°C. Efficient

digestion was usually confirmed by running 2ul of restriction product on a 1% agarose gel. Linearised vectors were treated with 1ul of Alkaline Phosphatase (AP, 20 U/µl) and 10 µl of AP buffer in water for a total reaction volume of 100 µl to prevent self-ligation of the cut plasmid. Following this, the digestion product was purified by QIAquick PCR Purification (Qiagen) according to the manufacturer's instructions.

Two different approaches were used to prepare cloning inserts: 1) Cloning inserts were liberated from host vectors through enzymatic digestion (as described above, except using no AP) and the whole digestion reaction was ran on a 1% agarose gel and the insert isolated by gel extraction, 2) a PCR reaction was ran using primers flanking the region of interest (i.e. the insert) with restriction sites added at their 5' ends. Approximately 25% of the PCR product was then digested for 4 hours to ensure complete digestion. The restriction product was the purified by QIAquick PCR Purification (Qiagen).

2.3.4.2 Ligation

For each experiment two ligation reactions were carried out, one containing both vector and insert and one with only the vector as a negative control for the experiment. In general, a total reaction volume of 15 µl was used containing the linearised vector (between 50-100 ng), the insert (1:3 molar ratio of vector:insert), 1 µl of T4 ligase (3 U/µl, Promega), 1.5 µl of 10x ligation buffer (Promega) and the remainder comprising water. The reaction was carried out at 15-16°C for 3 hours. The final ligation product was then transformed into competent bacterial cells.

2.3.4.3 Bacterial transformation and plasmid isolation

Transformation of plasmid DNA was performed through heat-shock in competent *E.Coli* DH5α cells (ThermoFisher). Specifically, 5 µl of DNA was added to 50 µl of DH5α cells (the amount of DNA never exceeded 10% of the total volume of the cells), which were then incubated on ice for 20 minutes. Bacterial cells were then heat-shocked at 37°C for 5 minutes before the addition of antibiotic-free L-broth for 45-60 minutes to allow transformed cells to express the antibiotic resistance gene. Following brief centrifugation, cell pellets were resuspended in a drop of L-broth and then plated onto agar bacterial plates containing the appropriate antibiotic for selection. Bacterial plates were then incubated at 37°C overnight and bacterial colonies were picked the following day. Single bacterial colonies picked following transformation were then inoculated in a larger volume of antibiotic-containing L-broth (1.5 ml for Miniprep extraction and 100 ml for Maxiprep extraction). These inoculation were incubated overnight at 37°C with vigorous shaking. Isolation of plasmid DNA was the achieved using QIAgen Mini spin columns or Maxiprep columns (Qiagen), following the manufacturer's instructions.

2.3.5 DNA quantification, quality control and sequencing

Isolated plasmid DNA was quality controlled by using the NanoDrop N-1000 (NanoDrop Technologies) spectrophotometer for absorbance-based nucleic acid quantification as well as gel electrophoresis, and restriction enzyme digestion. Specific primers were generated and used to perform Sanger DNA sequencing. This was

performed by Source BioScience. Sequencing analysis was performed using Snap Gene software. Sequences were manually checked against a reference sequence.

2.3.5.1 Detection of BRAF p.V600E mutations in papillary craniopharyngioma tumours

DNA was diluted fivefold with nuclease-free water (Ambion). Each digital PCR reaction was made up to 20 µl with 2 µl diluted DNA, 10 µl ddPCR Supermix for Probes (No dUTP; Bio-Rad), forward and reverse primers, dual-labelled probes for wild-type and mutant templates, and nuclease-free water. Sequences for the BRAF-V600E assay oligonucleotides are from (Hindson et al. 2011), and were used at the concentrations stated. Reactions were partitioned into ~23,000 droplets with Droplet Generation Oil for Probes (Bio-Rad) using the QX200 Droplet Generator (Bio-Rad). All samples were tested in duplicate, with no-template controls included in all columns. Standard cycling conditions, as recommended by the manufacturer were used with a annealing temperature of 60°C. Results were analysed with QuantaSoft software, v1.7. A mean of 19,080 droplets were successfully read in each well, including controls. Two droplets positive for wild-type template were seen in the negative controls, indicating a negligible degree of contamination.

2.4 RNA methods

2.4.1 RNA isolation, cDNA preparation and quantitative real-time PCR (qRT-PCR)

Samples from lung tumours (*Kras*$^{G12D/+}$;*Rosa26*$^{YFP/+}$;*p16*$^{FDR/+}$) and *Sox2*$^{CreERT2/+}$;*Ctnnb1*$^{lox(ex3)/+}$;*Rosa26*$^{YFP/+}$ flow sorted pituitary cell fractions were processed for total RNA extraction using the RNeasy Micro kit (Qiagen). In total, 5 µl of eluted RNA was then amplified using the Ovation Pico WTA V2 kit (NuGEN), followed by purification of the resultant cDNA using the QIAquick PCR purification kit (Qiagen).

Pituitaries from *Hesx1*$^{Cre/+}$;*Braf*$^{V600E/+}$, *Hesx1*$^{Cre/+}$;*Kras*$^{G12D/+}$ and control littermates were dissected at 18.5 dpc. The posterior lobe of the pituitary was discarded and the intermediate and anterior lobes were processed for total RNA extraction using the RNeasy Micro kit (Qiagen). Approximately 1 µg of total RNA was reverse transcribed to cDNA using the iScript Reverse Transcription Kit and random hexamers (BIORAD).

Total RNA was extracted from MEFs using the RNeasy Micro kit (Qiagen) and approximately 1 µg of total RNA was reverse transcribed to cDNA using the iScript Reverse Transcription Kit and random hexamers (BIORAD).

Quantitative real-time PCR reactions were run in triplicate using the iTaq SYBR Green (BIORAD) and replicated using a minimum of four independent samples for each

genotype. Thermocycling conditions were performed according to the manufacturer's instructions. Primer sequences are included in table 2.3 (For *Shh*, the Qiagen QuantiTect Primer Assay (Cat. no. 249900) was used). Glyceraldehyde 3-phosphate dehydrogenease (*GAPDH*) was used as the house keeping gene. Results were manually analysed using the ΔΔCt method.

Gene	Forward (5'-3')	Reverse (5'-3')
Axin2	CATCAAGAAGCAACAGATCG	AGTCCCCCGTTACTCATGTA
Bmp4	TTCCTGGTAACCGAATGCTGA	CCTGAATCTCGGCGACTTTTT
Ccl20	AGCAACTACGACTGTTGCCT	TGACTCTTAGGCTGAGGAGGT
Cdkn1a	CAGATCCACAGCGATATCCA	ACGGGACCGAAGAGACAAC
Cdkn2a	CGTGAACATGTTGTTGAGGC	GCAGAAGAGCTGCTACGTGA
Cxcl1	CTGGGATTCACCTCAAGAACATC	CAGGGTCAAGGCAAGCCTC
Cxcl2	CCAACCACCAGGCTACAGG	GCGTCACACTCAAGCTCTG
FDR	TCTTTGTGTACCGCTGGGAA	GGATTCTCCTCGACGTCACC
Fgf20	TCTTCGGTATCCTGGAATTCAT	GTACAGGCCACTGTCCACAC
Gapdh	ATGACATCAAGAAGGTGGTG	CATACCAGGAAATGAGCTTG
Gh	ACCTCGGACCCGTGTCTATGAGA	CATCTTCCAGCTCCTGCATCA
Il1α	CGCTTGAGTCGGCAAAGAAAT	TGGCAGAACTGTAGTCTTCGT
Il1β	TGCCACCTTTTGACAGTGATG	TGATGTGCTGCTGCGAGATT
Il6	CAAGAAAGACAAAGCCAGAGTC	GAAATTGGGGTAGGAAGGAC
Lef1	AAATCATCCCAGCCAGCAAC	CGCTGTTCATATTGGGCATC
Sox2	TCGGTGATGCCGACTAGAAAA	GCGCCTAACGTACCACTAGAACTT
Sox9	CGGAGGAAGTCGGTGAAGA	GTCGGTTTTGGGAGTGGTG
Tgfβ1	CTGAACCAAGGAGACGGAAT	TTGCTGTCACAAGAGCAGTG
Trp53	GCGTAAACGCTTCGAGATGTT	TTTTTATGGCGGGAAGTAGACTG
Tshα	GCCCAGAACACATCCCTCAA	ACCAGAATGACAGCTGCATATTTTC

Table 2.3. Primers used for qRT-PCR

The quantification of the absolute number of mRNA copies was determined for each sample by comparison of obtained Cq values with that of a standard of known copy number for each transcript investigated. Variations in input cDNA used for each reaction were accounted for by normalising differences in Gapdh expression between samples and genotypes, and applying this normalisation factor to absolute copy numbers obtained for each mRNA species of interest. 3 µl of the amplified product and 3 µl of loading buffer were ran on gel electrophoresis to visualise the amplification of a product of the expected size.

2.4.2 RNA *in situ* hybridisation (ISH) on paraffin sections

2.4.2.1 Preparation of antisense riboprobes

Linearised plasmid was purified using a QIAquick PCR purification kit (Qiagen). The purified product was re-suspended in 40 µl RNase-free water (Sigma) for *in vitro* transcription. 1 ug of purified linear plasmid DNA was used for transcription. RNase inhibitor, transcription buffer, nucleotide 10x DIG-labelling mix (Digoxigenin-11-2'-deoxy-uridine-5'-triphosphate) and either SP6/T3/T7 RNA polymerase (Roche, New England Biolabs or Promega) was used in a total volume of 20 µl and incubated at 37°C for 2 hours. 1 µl of the product was ran by gel electrophoresis to determine the presence of a band corresponding to the generated riboprobe. The transcribed product was then re-suspended in 40 µl RNase free water and 1 µl 0.5M ethylenediaminetetraacetic acid (EDTA) to stop the reaction. The resulting product was cleaned using the CHROMA SPIN 100 columns (Clontech), according to he manufacturer's instructions.

2.4.2.2 *In situ* hybridisation on paraffin sections

In situ hybridisation was performed as previously described (Cynthia L. Andoniadou et al. 2012). All solutions were treated with 0.1% v/v diethylpyrocarbonate (DEPC) in double distilled MiliQ water and autoclaved. Histological slides were de-waxed in HistoClear and re-hydrated in a graded ethanol series. The slides were then fixed for 20 minutes in fresh 4% PFA, treated with Protinase K (20 µg/ml) for 8 minutes and re-fixed in 4% PFA. Slides were then treated with 0.1M triethalolamine and 0.25% acetic anhydride. Slides are then de-hydrated in the same ethanol series and left to dry for 1 hour. Specific probes were hybridised overnight at 65°C in 50:50 Formamide: 0.3M sodium chloride, 20 mM Tris-hydrochloric acid, 5 mM EDTA, 10% Dextran sulphate, 1x Denhardt's reagent and RNAse inhibitor with the relevant DIG-labelled probe at 1:100 dilution. Following overnight incubation slides were subjected to stringent washes in formamide and saline sodium citrate washes at the hybridisation temperature. Slides are then blocked in Buffer 1 and Buffer 2 (0.1M Tris-hydrochloric acid pH 9.5, 0.15M sodium chloride, 0.05M magnesium chloride). Staining was achieved with addition of nitro-blue tetrazolium chloride (4.5 µl/ml) and 5-bromo-4-chloro-3-indolyl phosphate (3.5 µl/ml) in 10% polyvinyl alcohol. After efficient staining slides were stopped in running tap water, dehydrated and washed in HistoClear and mounted in hard set VectaMount. The antisense riboprobes used (*Fgf10, Shh, Bmp4* and *Lh*x3) have been described (Gaston-Massuet et al. 2008; Sajedi et al. 2008; Jayakody et al. 2012; Trowe et al. 2013). Full-length *Braf* and *Kras* antisense riboprobes were obtained from Source Bioscience (PX00999A07 and IRAVp968D072D, respectively).

2.4.3 RNA sequencing and analysis

For RNA-Seq of *Sox2*$^{CreERT2/+}$;*Ctnnb1*$^{lox(ex3)/+}$;*Rosa26*$^{YFP/+}$ and *Sox2*$^{CreERT2/+}$;*Rosa26*$^{YFP/+}$ flow-sorted YFP+ cells, isolated RNA was initially checked for the integrity of the mRNA using Tapestation 4200 (Agilent Genomics). RNA was then processed by the SMARTer V4 low input assay kit (Clontech) to generate amplified cDNA using the strand-switching protocol. Library preparation was performed with 200 pg of amplified cDNA using the Nextera XT preparation kit with 12 cycles of PCR. Sequencing was then performed on an Illumina NextSeq 500 with 43 bp paired end reads. Sequencing data was then aligned in BaseSpace. FASTQ and BAM files are available on Array Express (E-MTAB-5538), Differential expression was performed using DESeq267. For GSEA, genes were ranked by the Wald statistic and GSEA performed using the pre-ranked tool in GSEA v2.2 (Broad Institute) (Subramanian et al. 2005). Significantly enriched gene sets were determined if the normalised enrichment score was >1 and the false discovery rate was <0.25 (Subramanian et al. 2005). The GSEA gene sets were obtained from the hallmark molecular signatures database v5.2 (Broad Institute). The OIS and SASP GSEA datasets were derived from human IMR90 ER:RAS fibroblasts that possess a steroid receptor-KrasG12V fusion protein (Acosta et al. 2013). GO analysis was performed on differentially expressed gene sets derived from the RNA-seq experiment using the GOSeq package in R (Young et al. 2010). Human ACP tumour cell compartment RNA-Seq datasets have been previously described (Gonzalez-Meljem et al. 2017b).

2.5 Protein methods

2.5.1 Immunohistochemistry (IHC) and immunofluorescence (IF) on paraffin sections

Immunofluorescence (IF) staining of histological sections was performed as previously described (Cynthia Lilian Andoniadou et al. 2013). Briefly, slides were de-waxed in HostoClear, re-hydratedfrom 100% elthanol to double distilled MiliQ water and underwent antigen retrieval in an antigen retrieval unit (BioCare Medial Decloaking chamber NXGEN) for 2 minutes at 110°C. Slides were then washed in 1x PBT which consists of 1x PBS and 0.1% Triton X-100. Histological slides were then blocked for 1 hour at room temperature in blocking buffer and 10% heat inactivated sheep serum (HISS), blocking buffer contains 0.1% Triton X-100, 0.15% glycine, 2mg/ml BSA in 1x PBS. See tables 3.4 and 3.5 for antigen retrieval conditions, antibody concentrations and amplification of each antibody used. Primary and secondary antibodies were diluted in blocking buffer and 1% HISS. Sections were counter stained with 4',6-Diamidino-2-Phenylindole (DAPI) for 5 minutes (1:10,000, Sigma) and mounted onto coverslips with VectaMount (Vector Laboratories). For immunohistochemical (IHC) staining, slides were first incubated with an Avidin-Biotinylated Peroxidase Complex (Vector). Chromogenic detection was then performed through the addition of 3,3'-diaminodenzidine (DAB, Vector) for 2-5 minutes and then counterstained with Myer's hematoxylin (Sigma).

Antibody Application	Target	Host Species	Clonality	Clone	Company	Catalogue Number	Dilution	Antigen Retrieval Method
Primary	GFP/YFP	Chicken	Polyclonal	N/A	Abcam	ab13970	1:300	Tris-EDTA pH9.0
Primary	β-Catenin	Mouse	Monoclonal	6F9	Sigma	C7082	1:300	Tris-EDTA pH9.0
Primary	β-Catenin	Rabbit	Polyclonal	N/A	Thermo	RB-9035-P1	1:300	Tris-EDTA pH9.0
Primary	Synaptophysin	Mouse	Monoclonal	27G12	Leica	RTU-SYNAP-299	Ready-to-use	Tris-EDTA pH9.0
Primary	Ki67	Rabbit	Monoclonal	SP6	Abcam	ab16667	1:100	Tris-EDTA pH9.0
Primary	p21	Rabbit	Polyclonal	M-19	Santa Cruz	sc-471	1:400	Tris-EDTA pH9.0
Primary	DNA-PKcs	Mouse	Monoclonal	10B1	Abcam	ab18356	1:200	Tris-EDTA pH9.0
Primary	tdTomato	Rabbit	Polyclonal	N/A	Abcam	Ab28664	1:300	Tris-EDTA pH9.0
Primary	mCherry	Chicken	Polyclonal	N/A	Abcam	ab205402	1:300	Tris-EDTA pH9.0
Primary	p16	Rabbit	Polyclonal	N/A	Rockland	100-401-170	1:100	Tris-EDTA pH9.0
Primary	BRAF p.V600E	Mouse	Monoclonal	VE1	Spring Bioscience	E19290	1:50	Tris-EDTA pH9.0
Primary	pERK1/2	Rabbit	Polyclonal	N/A	Cell Signaling	9101	1:250	Tris-EDTA pH9.0
Primary	PIT1	Rabbit	Monoclonal	N/A	S. Rhodes, Indiana University School of Medicine, Indianapolis	N/A	1:1000	Tris-EDTA pH9.0
Primary	SF1	Rabbit	Monoclonal	N/A	Thermo	434200	1:200	Tris-EDTA pH9.0
Primary	TPIT	Rabbit	Monoclonal	N/A	J. Drouin, Montreal Clinical Research Institute, Montreal	N/A	1:1000	Tris-EDTA pH9.0

Primary	GH	Rabbit	Polyclonal	N/A	NHPP	AFP-5641801	1:1000	Tris-EDTA pH9.0
Primary	PRL	Rabbit	Polyclonal	N/A	NHPP	AFP-425-10-91	1:1000	Tris-EDTA pH9.0
Primary	TSH	Rabbit	Polyclonal	N/A	NHPP	AFP-1274789	1:1000	Tris-EDTA pH9.0
Primary	FSH	Rabbit	Polyclonal	N/A	NHPP	AFP-7798-1289	1:1000	Tris-EDTA pH9.0
Primary	LH	Rabbit	Polyclonal	N/A	NHPP	AFP-C697071P	1:1000	Tris-EDTA pH9.0
Primary	ACTH	Mouse	Monoclonal	N/A	NHPP	10C-CR1096M1	1:1000	Tris-EDTA pH9.0
Primary	Cga (αGSU)	Rabbit	Polyclonal	N/A	NHPP	AFP-66P9986	1:1000	Tris-EDTA pH9.0
Primary	CyclinD2	Rabbit	Polyclonal	M-20	Santa Cruz	SC-593	1:200	Tris-EDTA pH9.0
Primary	Sox2	Goat	Polyclonal	N/A	Immune Systems	GT15098	1:500	Tris-EDTA pH9.0
Primary	Sox9	Rabbit	Polyclonal	N/A	Millipore	AB5535	1:400	Tris-EDTA pH9.0
Primary	Pan-Cytokeratin	Mouse	Monoclonal	DMNF116	Dako	M0821	1:300	Tris-EDTA pH9.0
Primary	Cytokeratin19	Mouse	Monoclonal	RCK108	Dako	M088	1:300	Tris-EDTA pH9.0

Table 2.4. Primary antibodies, dilutions and antigen retrieval conditions for IHC

Antibody Application	Target Species	Host Species	Clonality	Company	Catalogue Number	Dilution	Conjugate
Secondary	Mouse	Goat	Polyclonal	Thermo Fisher	A11001	1:250	Alexa Fluor® 488
Secondary	Mouse	Goat	Polyclonal	Thermo Fisher	A11004	1:250	Alexa Fluor® 568
Secondary	Rabbit	Goat	Polyclonal	Thermo Fisher	A11008	1:250	Alexa Fluor® 488
Secondary	Rabbit	Goat	Polyclonal	Thermo Fisher	A11036	1:250	Alexa Fluor® 568
Secondary	Goat	Chicken	Polyclonal	Thermo Fisher	A21467	1:250	Alexa Fluor® 488
Secondary	Mouse	Goat	Polyclonal	Dako	E0433	1:250	Biotin
Secondary	Rabbit	Goat	Polyclonal	Dako	E0432	1:250	Biotin
Secondary	Mouse	Goat	Polyclonal	Dako	P0447	1:250	Horseradish peroxidase (HRP)

Table 2.5. Secondary antibodies and dilutions for IHC

2.6 Cell Culture Methods

2.6.1 Cell culture reagents

2.6.1.1 Feeder cells

Feeder cells were obtained by Mitomycin C treatment of SNH cells (Kindly provided by Prof. Liz Robertson). SNH cells are immortalised cells clonally derived from the STO line; they have been modified to stably express the neomycin (Thomas & Capecchi 1988) and the LIF (Williams et al. 1988) genes. SNH were propagated in the absence of gelatine in complete DMEM. To generate feeder cells, SNH were treated with 10 µg/ml mytomicin C to inhibit nuclear division. After 2.5 to 3 hours of treatment, SNH cells were dissociated and plated onto gelatinised tissue-culture plates at the required density.

2.6.1.2 Mouse embryonic stem cells (ESCs)

ESCs were routinely cultured either in feeder-dependent conditions in ESC medium, or in feeder-free conditions in ESC medium supplemented with LIF (1000 U/mL, Millipore ESG1107). In the absence of feeders, ESC were plated onto gelatinised tissue-culture plates. Serum-free culture was performed in N2B27.

2.6.1.3 HEK-293T cells

HEK (Human Embryonic Kidney)-293T were maintained in DMEM supplemented with 10% foetal bovine serum, 50U/ml penicillin and 50 µg/mL streptomycin. No coating was required for cell plating.

2.6.1.4 Reagents and medium composition

Gelatine (0.1% in PBS)

PBS (Gibco, 14190169)

Trypsin-EDTA (0.025% in PBS, Gibco 15400054)

Puromycin (Sigma, P9620)

Mitomycin C (Sigma, M4287)

Complete DMEM

Dulbecco's Modified Eagle's Medium (Gibco, 11960085)

10% Fetal Calf serum (PAA, A15-151)

1mM Sodium Pyruvate (Gibco, 11360-039)

2mM L-glutamine (Gibco, 25030-024)

Non-essential amino acids (Gibco, 11140-035)

50mM 2-mercaptoethanol (Gibco, 31350010)

ESC medium

Knockout-DMEM (Gibco, 10829018)

15% Fetal calf serum (PAA, A15-151)

2mM L-glutamine (Gibco, 25030-024)

Non-essential amino acids (Gibco, 11140-035)

50mM 2-mercaptoethanol (Gibco, 31350010)

2i + LIF

N2B27 supplemented with:

LIF 100U/ml (Millipore ESG1107)

PD0325901 1 μM (Axon MedChem, Axon1408)

CHIR99021 3 μM (Axon MedChem, Axon1386)

2.6.2 Mouse embryonic fibroblast isolation and culture

Mouse embryonic fibroblasts (MEFs) were isolated from 13.5 dpc embryos. Pregnant females were humanely culled by cervical dislocation and the uterus was removed and briefly rinsed in 70% ethanol to partially sterilize it. Embryos were removed from the uterus with sterile dissecting equipment and each embryo was transferred to single well of a 6-well cell culture plate. The heart and liver were then removed and the head was transferred to an eppendorph for later genotyping. The remainder of the body was covered in sterile PBS and triturated with a scalpel to form a homogenous paste. The PBS was then removed and the triturated body was resuspended in 1 ml of 0.025% trypsin (v/v in PBS) for 5 minutes at 37°C. Following incubation the tissue was triturated again with a pipette and returned to the incubator for a further 5 minutes. This process was repeated 2 to 3 times to obtain a single cell suspension. The trypsin was then inactivated with 2 ml of fibroblast culture medium (DMEM supplemented with 10% fetal calf serum, 50U/mL penicillin and 50 µg/mL streptomycin). Cells were never allowed to incubate for more than 20 to 30 minutes in undiluted trypsin. Cell suspensions were then pelleted by centrifugation at 1000 rpm for 5 minutes, resuspended in 1 ml of fibroblast culture medium and then passed through a 100 µm cell strainer. Isolated MEFs were then plated in a 10 cm cell culture dish, with the medium being changed every 2 days, until cells grew to confluency, at which point each plate was frozen down into 2 cryovials.

2.6.2.1 *In vitro* senescence induction

To induce cellular senescence in MEFs *in vitro* they were serially passaged until they were no longer proliferative. It has been shown that MEFs cultured in the presence of atmospheric concentrations of oxygen (20%) suffer from significant oxidative stress over time which induces DNA damage and the induction of the cellular senescence program (Parrinello et al. 2003). Specifically, $1.5x10^6$ cells were plated in a 10 cm plate and they were passaged and counted by haemocytometer every 4 days. The medium was changed ever 2 days to ensure adequate nutrition of the cells. By passage 6 the majority of the wild type and $p16^{FDR/+}$ cells had stopped dividing, therefore this passage was used at the senescent passage. Proliferating passage 2 cells were used as a non-senescent control passage for the majority of experiments.

2.6.2.2 Diphtheria toxin ablation experiment

Diphtheria toxin ablation experiment on wild type, $p16^{FDR/+}$ and $p16^{FDR/FDR}$ MEFs was performed at passages 2 and 6. Specifically, 5000 cells were plated per well in 96-well plates and diphtheria toxin (Sigma) was added at concentrations of 1, 10 and 100 ng/ml the following day. 3 days after the addition of diphtheria toxin the cells were fixed in 4% PFA for 10 minutes on ice and the cells were counted using a haemocytometer.

2.6.2.3 SA-β-Gal staining

SA-β-Gal staining of MEFs was performed using the senescent cell histochemical staining kit (Sigma), according to manufacturers instructions.

2.6.2.4 Crystal violet staining

For crystal violet staining of MEFs, 20,000 cells were plated per well in 6-well plates. Cells were passaged ever 4 days and the medium was changed ever 2 days. Prior to staining cells were washed twice with ice-cold PBS and then fixed for 10 minutes in ice-cold 100% methanol. The methanol was then aspirated and the cells were covered with a room temperature solution of 0.5% crystal violet and 25% ethanol in water for 10 minutes. Cells were then washed in water until the crystal violet staining stops coming off of the cells at which point they were allowed to dry at room temperature before imaging.

2.6.3 General cell culture methods

2.6.3.1 Cell passaging

Cells were generally passaged when they reached 70-80% confluency. First, media was aspirated and cells were washed with 1x PBS to eliminate any residual serum. Following this 0.025% trypsin (v/v in PBS) was added to the plate, which was then incubated at 37°C for 5 minutes to allow for cell detachment. Subsequently, 5

volumes of complete DMEM were added to neutralise the trypsin and the cells were collected in a 15 ml falcon tube. Following this the cells were centrifuged at 1000 rpm for 5 minutes and cell pellets were resuspended in the required volume of medium and plated at the desired density. For routine passaging cells were split on a 1:3-1:10 ratio.

2.6.3.2 Cell freezing

For freezing, cell pellets were collected as described in the cell passaging paragraph. A minimum of 2 freezing aliquots was generated per 80% confluent plate/flask. Briefly, celllpellets were resuspended in freezing medium (90% FCS-10% DMSO). 1 ml of cell suspension was then stored in cryogenic vials (Nunc®, 377224) and quickly transferred to -80°C. The following day, frozen aliquots were transferred to a N_2(lq) tank for long-term storage. For 96-well plates freezing, 150 µl of freezing medium (80% EmbyoMax FBS (Millipore ES-009) / 20% DMSO) was added to cell suspension, and the whole 96-well plate was wrapped in paper and stored at -80°C.

2.6.3.3 Cell thawing

Cryogenic vials were quickly thawed in a 37°C water bath until a small frozen residue was visible. Cell suspensions were then transferred to 10 ml of pre-warmed cell culture medium and spun at 1000 rpm for 5 minutes. Cell pellets were then resuspended in the required medium and plated onto appropriately sizes flasks/plates.

2.6.4 Cell culture procedures

2.6.4.1 Embryonic stem cell colony picking

Generally, the remaining embryonic stem cell colonies after 7 to 8 days of antibiotics selection were picked for future expansion and integration confirmation. Colonies were picked from 10 cm tissue culture plates into single wells of a 96-wells U-bottom plates filled with 20 µl of PBS. Single colonies were picked by suction with a 20 µl pipette set at 5 µl. Following transfer to the 96-wells plate, 25 µl of 0.025% Trypsin-EDTA was added and plates were transferred to a 37°C incubator for 5 minutes. Trypsin was quenched with 150 µl of ESC medium, and after mechanical dissociation, cells were plated onto a 96-well plate (flat bottom) where a layer of feeder cells was previously placed. The following day medium was not changed to allow proper adhesion. Once cells reached 80% confluency, they were passaged 1:3 onto 3X 96-well plates: one for DNA extraction, one for expansion and one for freezing.

2.6.4.2 Transient transfection of plasmid DNA into 293T cells using Lipofectamine 2000

HEK-293T (350,000 cells per well) cells were seeded onto non-coated tissue-culture 12-well plates in DMEM supplemented with 10% foetal bovine serum, 50 U/ml penicillin and 50 µg/ml streptomycin one day before transfection. Transfection was carried out 24 hours after plating using Lipofectamine 2000® according to manufacturer instructions. The specific amount of Lipofectamine 2000 reagent was optimized according to the experimental procedure. Briefly, the transfection reagent was diluted in

reduced serum medium (Opti-MEM, Gibco 31905062) and incubated at room temperature for 5 minutes. Following incubation, 1 µg of DNA (per well to be transfected) were mixed with the Lipofectamine reagents and DNA-Lipofectamine complexes were allowed to form by incubation at room temperature for 20 minutes. Finally, DNA-Lipofectamine complexes were added to each well in a drop-wise manner and plates were gently swirled to guarantee homogeneous distribution of the reagents. Transfected cells were returned to the incubator and medium was changed after 12 to 24 hours.

For ESC transient transfection, a similar procedure was followed, with the exception of performing the transfection in suspension instead of onto pre-seeded plates. To this aim, DNA-Lipofectamine complexes were added into 15 ml falcon tubes containing desired cell suspension and left at room temperature for 10 minutes before plating.

2.6.4.3 Mouse pituitary stem/progenitor cell adherent culture and clonogenicity assay

Pituitaries from *Hesx1*$^{Cre/+}$*;Braf*$^{V600E/+}$, *Hesx1*$^{Cre/+}$*;Kras*$^{G12D/+}$ and control littermates were dissected at 18.5 dpc and the posterior lobe was removed. Anterior pituitaries were dissociated into a single cell suspension (as described in section 2.2.1). Dissociated single cells were suspended in pituitary stem cell medium (DMEM supplemented with 5% fetal calf serum, 20 ng/ml bFGF (R&D systems, 233-FB-025), 50 ng/ml cholera toxin (Sigma, C8052), 50 U/ml penicillin and 50 µg/ml streptomycin)

and seeded at densities of 2000, 4000 and 8000 cells per well of a six-well plate for adherent culture. Cells were cultured for 3 days at which point they were fixed with 4% PFA and colonies were stained with Haematoxylin (as described in section 2.1.7). The proportion of colonies observed after 3 days of culture relative to seeded cells was used to estimate total clonogenic cells in 18.5 dpc pituitaries by multiplying this value by the total number of cells quantified following dissociation of the pituitary.

2.7 CRISPR/Cas9 targeting of the *Cdkn2a* locus to generate the *p16FDR* mouse line

To lineage trace, direct visualise and pharmacogenetic ablate $p16^{INK4A}$-expressing cells, a multicistronic targeting vector was generated that contained a mammalian optimised FLP recombinase along with a diphtheria toxin receptor (DTR) that is fused with an mCherry fluorescent reporter. The cassette was termed *FDR* (Flipase, Diphtheria toxin receptor and Reporter) and was synthesised by GenScript into a pcDNA3.1(+) plasmid backbone. Both upstream and downstream of the FLP-recombinase, P2A sequences were added to facilitate ribosomal "skipping" over these regions during translation of the mRNA to produce multiple protein products (i.e p16, FLP and DTR-mCherry). This cassette was flanked by two sequences homologous to regions 2.5 kb upstream an 1.9 kb downstream of the $p16^{INK4A}$ protospacer adjacent motif (PAM) site (Figure 2.1). The sequence for the DTR (human membrane-anchored heparin-binding EGF-like growth factor with I117V and L148V mutations to repress the growth factor activities) was kindly provided by Kenji Kohno.

Initially, two fragments of 2.5 kb (5'-p16 homology arm) and 1.9 kb (3'-p16 homology arm) were generated by high-fidelity PCR amplification (Phusion™, TermoFisher F553). The sense and antisense primers used for the generation of the 5' homology arm contained a NotI restriction site at their 5' end, preceded by a TTAAT cap sequence to guarantee the digestion process (Table 2.6). The sense and antisense primers used for the generation of the 3' homology arm contained a XbaI restriction site at their 5' end, preceded by a GCG cap sequence to guarantee the digestion process (Table 2.6). Subsequently, the two homology arms were cloned, respectively, upstream and downstream the *FDR* cassette in the pcDNA3.1(+)_FDR plasmid through the NotI and XbaI restriction sites. The final donor plasmid (pcDNA3.1(+)_FDR_HA) was subjected to diagnostic digestion to confirm insert orientation and purified for transfection.

For targeting of the *Cdkn2a* locus, a guide RNA (gRNA) (Table 2.6) targeting a region 12nt upstream the $p16^{INK4A}$ stop codon was designed and cloned into the px330-U6-Chimeric_BB-CBh-hSpCas9 (Addgene, plasmid #42230) to generate the px330-p16-gRNA vector. Briefly, two oligos corresponding to the sense and antisense gRNA in which a BbsI restriction site was added at the 5' end were synthetized and cloned into the backbone vector (px330, linearized with BbsI). To validate insertion in the gRNA scaffold and to ensure disruption of the BbsI restriction site, the modified px330 plasmid was sent for Sanger sequencing (Table 2.6).

Primer Name	Sequence (5'-3')	Use
gRNA-p16-S	CACCGCCGGATTTAGCTCTGCTCTT	Sense gRNA (BbsI)
gRNA-p16-AS	AAACAAGAGCAGAGCTAAATCCGGC	Antisense gRNA (BbsI)
pX330-FWD	CATATGCTTACCGTAACTTG	pX330 sequencing
pX330-REV	AGTTGATAACGGACTAGCCT	pX330 sequencing
p16-5'HA-FWD	TTAATGCGGCCGCACCACACAATCCCAGTTCGG	5' Homology arm generation (NotI)
p16-5'HA-REV	TTAATGCGGCCGCTAGATTGGCCGCGAAGTTCCA	5' Homology arm generation (NotI)
p16-3'HA-FWD	GCGTCTAGACAAGAGCAGAGCTAAATCCG	3' Homology arm generation (XbaI)
p16-3'HA-REV	GCGTCTAGACTGTTTGCTATTTGAGGTACAAGA	3' Homology arm generation (XbaI)
p16-5'HA-EXT-FWD	TGGTAGTCCAGAGTGGATG	Integration of FDR cassette
p16-5'HA-INT-REV	GATGTCGAACTGGCTCAT	Integration of FDR cassette
p16-WT-SEQ-FWD	CCAAGCACAAGCGGCTATC	*p16* wild type allele sequencing
p16-WT-SEQ-REV	TAAAGCCACATGCTAGACACGC	*p16* wild type allele sequencing

Table 2.6. gRNA and primers used for the cloning and screening of *p16^{FDR}* mouse line

Genome editing of wild type CCE ESC line was then carried out by stable transfection with Lipofectamine 2000 (described in section 2.6.4). 1x10^6 ESC were co-transfected with 1 µg of purified px330-p16-gRNA vector, 1 µg of purified pcDNA3.1(+)_FDR_HA targeting vector and 125 ng (1:8) of a *KO-Puro* Puromycin resistance plasmid. Following transfection, ESCs were plated at clonal densities (100,000/50,000/25,000 cells) in 10 cm tissue-culture plates on a layer of mitotically inactivated SNH cells in ESC medium. In parallel, a mock transfection in which the same amount of ESCs were transfected with only the px330-p16-gRNA

vector was performed as a selection control. On the next day, puromycin selection at 2 µg/mL was performed for the following 48 hours. At the end of the selection process, no colonies were detected in the control plate, confirming selection efficacy. The rest of the plates were left to expand for a further 5 to 6 days in normal ESC medium. Good sized colonies were picked and DNA was extracted.

Insertion of the FDR cassette into the 3' end of the *p16*^{INK4A} gene was screened through PCR using primers which generated a 2915 bp fragment which spans the 5' homology arm (i.e a pair of primers which are external to the 5' homology region and inside the FDR cassette) (Figure 2.1). Positive clones were sent for Sanger sequencing to confirm integration of the *FDR* cassette into the *Cdkn2a* locus. To determine if only one or both of the *p16*^{INK4A} alleles were targeted, amplification of a 312 bp PCR product using the p16-WT-SEQ-FWD and p16-WT-SEQ-REV primers was performed (Figure 2.1). With this experimental approach, amplification of the allele containing the *FDR* cassette (targeted allele) was not achievable by PCR amplification due to its large size, generating only one product corresponding to the second allele, which was sent for Sanger sequencing to check for alteration in the proximity of the PAM region.

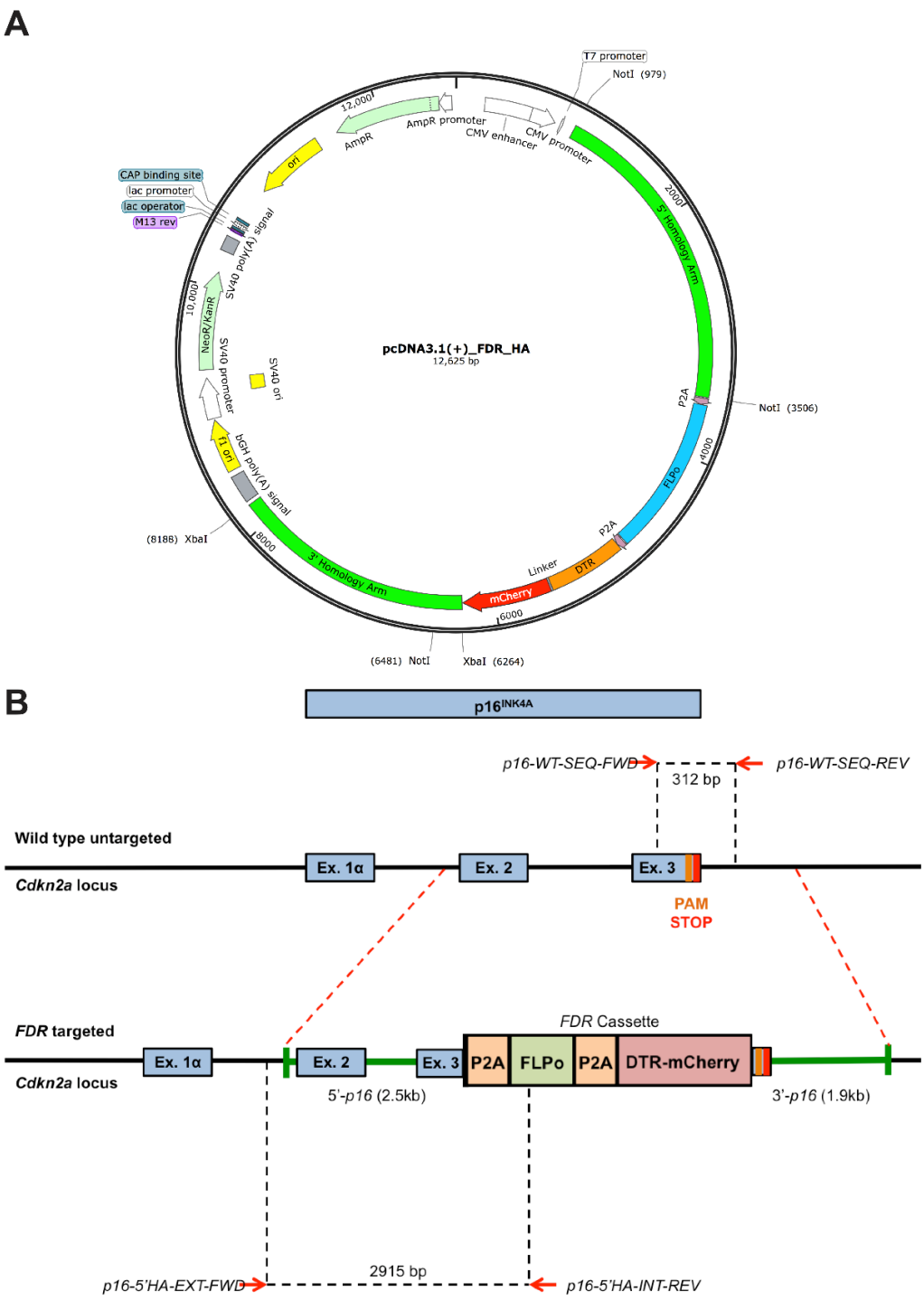

Figure 2.1. Screening strategy for the insertion of the *FDR* cassette into the *Cdkn2a* locus by homologus recombination. (**A**) Plasmid map of the *pcDNA3.1(+)_FDR_HA* targeting vector. (**B**) Schematic of the insertion of the *FDR* cassette into the *Cdkn2a* locus showing PCR strategy for confirming integration.

2.8 Generation of chimeras

The sandwich aggregation technique was used to generate chimeric mice through the aggregation of two morulae from different genotypes. Briefly, a microdrop culture was established in a 6 cm culture dish using KSOM medium (Sigma) and the drops were covered with mineral oil. A sterile needle was then used to create 6 indentations in the plastic of the dish, within each microdrop before being warmed to 37°C in a cell culture incubator. 8-cell stage to morula stage embryos from the genotypes to be aggregated were collected through oviduct flushing at 2.5 dpc. Collected embryos were washed in three drops of fresh FHM medium (Sigma) to remove any debris. The flushed embryos were then incubated at 37°C in KSOM medium in a center-well organ culture dish. To remove the zona pellucida embryos were washed through 1 drop of FHM medium, 3 drops of Tyrode's acid solution. Once the zona pellucida has dissolved the embryos were transferred through 2 drops of FHM medium. Following zona pellucida removal, 1 embryo from each of the two genotypes was placed was placed in the same indentation in the aggregation plate, with care being taken to ensure that the two embryos are physically attached to one another. The aggregation plate is then returned to the incubator and allowed to aggregate overnight. The following day the embryos have aggregated to form a single embryo that is at the late morula/blastocyst stage. These aggregated embryos are then transferred to a pseudo-pregnant recipient female mouse to allow development to continue to generate chimeric mice.

2.9 Microscopy, imaging, cell quantification and statistical analysis

2.9.1 Microscopy and image analysis

Whole-mount imaging was conducted in a Leica MZ FLIII stereomicroscope connected to a Leica DC500 camera. Imaging of freshly dissected lungs were conducted at 0.8x magnification. For endogenous fluorescence imaging, the exposure was set to 9.0 seconds. The scale of the image was then calculated from graticuled images at the same magnification and Fiji/ImageJ software (Schindelin et al. 2012) was used to measure tissue sizes.

Immunofluorescent stainings on paraffin sections were visualized with a Leica DMLM widefield microscope and imaged with a CoolSnap monochrome camera. Visualization of immunohistochemical, ISH and H&E staining was conducted in a Zeiss Axioplan2 microscope and captured with a Zeiss Axiocam HRc colour camera.

Image processing was conducted using Photoshop CC 2015 (Adobe), which included brightness/contrast enhancement and merging of fluorescence channels to produce composite images. Cell counting from microscope images was conducted manually using Fiji/ImageJ and the cell counter plugin.

2.9.2 Cell quantification

All cell counting analysis were performed in three to five non-consecutive histological sections immunostained using the relevant antibodies. PIT1, SF1, TPIT, KI67, SOX2 and CyclinD2 expressing populations were determined by taking the proportion of positive cells relative to total DAPI positive nuclei. Around 4000 to 7000 DAPI-positive cells and 300 to 1000 marker-positive (PIT1+, SF1+, TPIT+, KI67+, SOX2+ and CyclinD2+) cells were counted for each genotype. For analysis of EdU-tracing experiments, the proportions of SOX2-, PIT1- or KI67-positive cells were determined relative to the EdU-positive cell population. Around 500 to 1500 EdU-positive cells and 200 to 600 marker-positive cells were counted for each genotype. Analysis of hormone-producing cell populations (GH +, PRL +,TSH+, FSH+, LH+, ACTH + and αGSU +) was assessed through determining the relative proportion of hormone-positive population to total DAPI+ nuclei in a section. These proportions were then applied to average cell counts of dissociated pituitaries to determine an approximation of the absolute numbers of these populations in the pituitary. Around 5500 to 8500 DAPI+ cells and 200 to 2500 marker-positive cells were counted for each genotype.

2.9.3 Statistical analysis

Statistical analysis was conducted using SPSS Statistics software (IBM). Statistical significance level was set as 0.05. Mendelian ratios were evaluated using the chi-squared test. Clonogenic potential of control, *Hesx1*$^{Cre/+}$*; Kras*$^{G12D/+}$ and *Hesx1* $^{Cre/+}$*;*

Braf$^{V600E/+}$ pituitaries was evaluated using a paired t-test. Total cell counts of control, *Hesx1*$^{Cre/+}$*; Kras*$^{G12D/+}$ and *Hesx1*$^{Cre/+}$*; Braf*$^{V600E/+}$ pituitaries and quantitative real-time PCR data were analysed by unpaired t-test.

CHAPTER 3: THE ROLE OF PITUITARY STEM CELL SENESCENCE IN THE NON-CELL AUTONOMOUS INDUCTION OF MURINE ACP

3.1 INTRODUCTION

It is known that gain-of-function mutations in β-Catenin (*Ctnnb1*) result in Wnt pathway activation and that this can lead to neoplastic transformation and ultimately the development of cancer (Reya & Clevers 2005). In genetically-engineered mouse model of ACP, targeting of oncogenic β-Catenin to either pituitary precursor cells (*Hesx1*$^{Cre/+}$*; Ctnnb1*$^{lox(ex3)/+}$*; Rosa26*$^{YFP/+}$ mice) or to the stem/progenitor cell compartment (*Sox2*$^{CreERT2/+}$*; Ctnnb1*$^{lox(ex3)/+}$*; Rosa26*$^{YFP/+}$ mice) results in the formation of cell clusters, derived from the stem/progenitor cells that are non-proliferative (Cynthia L. Andoniadou et al. 2012). A similar situation is observed in cluster cells found in human ACP, which are also known to not divide (Buslei et al. 2007b; Gaston-massuet et al. 2011) or apoptose (Zhu & You 2015). Therefore, this raises the question: why do the cluster cells persist in association with the developing tumor?

Intriguingly, the cluster cells in mouse and human ACP are known to be highly secretory, producing many signaling ligands and other molecules that have established role in promoting cancer, such as: FGFs, BMPs, SHH and WNT ligands, suggesting that the clusters may have an active role in promoting the development of ACP (Cynthia L. Andoniadou et al. 2012). Lineage tracing has been performed on the oncogenic β-Catenin mutation sustaining pituitary stem cell clusters (*Sox2*$^{CreERT2/+}$*; Ctnnb1*$^{lox(ex3)/+}$*; Rosa26*$^{YFP/+}$ mice) and demonstrated that, remarkably, the tumours formed non-cell autonomously (Cynthia L. Andoniadou et al. 2012). This study proposed that the mutated stem cell clusters had activated the cellular senescence program, to prevent their further expansion, concomitantly with a

SASP, which could be the mediator of the observed paracrine tumourigenesis. This hypothesis was tested by examining the *Sox2*$^{CreERT2/+}$*; Ctnnb1*$^{lox(ex3)/+}$*; Rosa26*$^{YFP/+}$ model for canonical markers of cellular senescence and SASP activation in the oncogenic β-Catenin targeted pituitary stem cell clusters. Further to this, analysis of the effect of modulating the intensity of the SASP by targeting pituitary stem cells with oncogenic β-Catenin in older animals was investigated.

3.2 RESULTS

3.2.1 Tumourigenic pituitary stem cells targeted with oncogenic β-Catenin have entered into cellular senescence with activation of the SASP

From previous studies it is appreciated that expression of oncogenic β-Catenin in Sox2+ pituitary stem cells (*Sox2*$^{CreERT2/+}$*; Ctnnb1*$^{lox(ex3)/+}$*; Rosa26*$^{YFP/+}$ mice) at 4–6 weeks of age results in the formation of cell clusters that accumulate nucleo-cytoplasmic β-Catenin and later the non-cell autonomous induction of pituitary tumours (Cynthia Lilian Andoniadou et al. 2013) (Figure 3.1). To test the hypothesis that these cluster cells have entered into cellular senescence they were characterised by IF and transcriptomic analyses for the absence of proliferation and the expression of SASP and canonical cellular senescence markers.

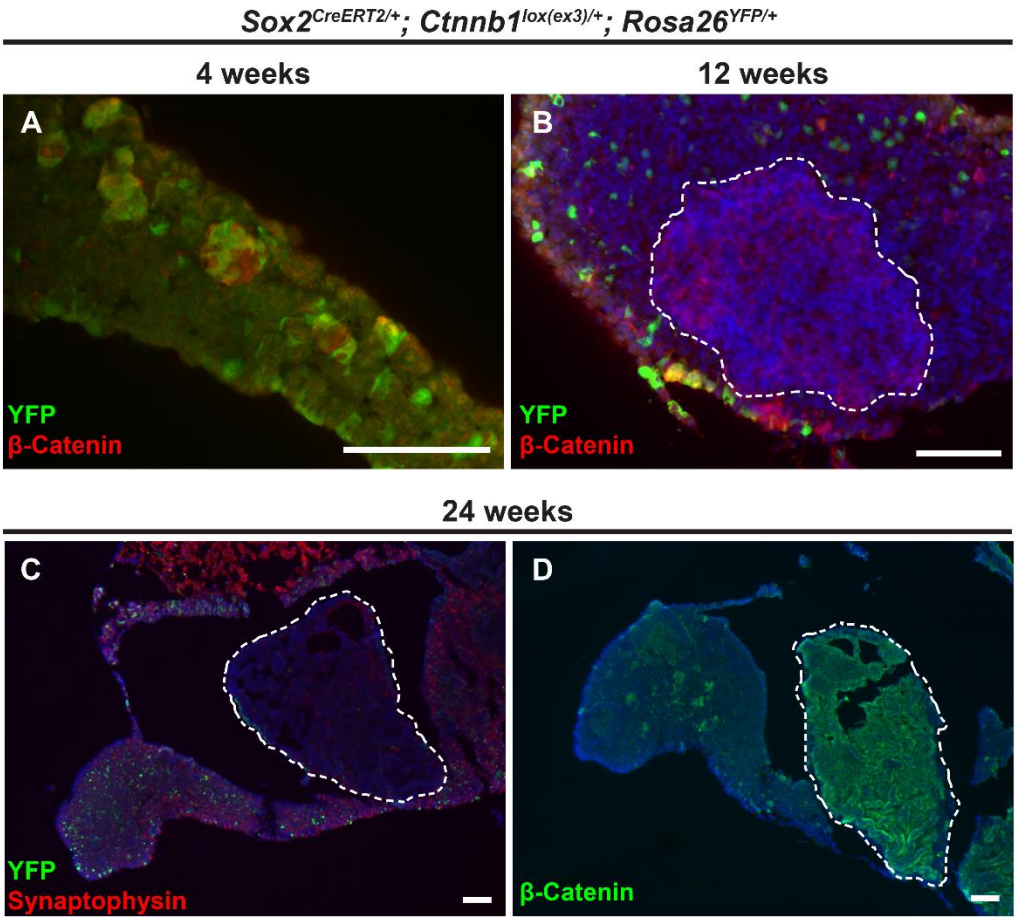

Figure 3.1. *Sox2*$^{CreERT2/+}$*; Ctnnb1*$^{lox(ex3)/+}$*; Rosa26*$^{YFP/+}$ mice show non-cell autonomous pituitary tumour formation. (**A**-**D**) Sections of the anterior lobe of the pituitary from *Sox2*$^{CreERT2/+}$*; Ctnnb1*$^{lox(ex3)/+}$*; Rosa26*$^{YFP/+}$ mice induced with tamoxifen at 4 weeks of age and collected at the indicated timepoints. (**A**) 4 weeks post induction pituitary showing the presence of nucleocytoplasmic β-catenin-accumulating cluster cells that are derived from the Sox2 lineage resulting in them being YFP+. (**B**) 12 weeks post induction pituitary with a small developing tumour lesion that is negative for the YFP lineage reporter indicating paracrine induction. Note the presence of neighboring cluster cells that accumulate β-catenin and are YFP+. (**C**-**D**) 24 weeks post induction pituitary with advanced tumours present that are negative for the YFP lineage reporter and synaptophysin, a marker of endocrine cells (**C**) and accumulate β-catenin (**D**). Pituitary tumours indicated by dashed line. Scale bars; 200 μm.

3.2.1.1 Cluster cells are non-proliferative, express cell cycle inhibitor p21 and possess DNA damage

Initially, *Sox2$^{CreERT2/+}$; Ctnnb1$^{lox(ex3)/+}$; Rosa26$^{YFP/+}$* mice were induced with tamoxifen at 4 weeks of age and their pituitaries were collected 4 weeks later, a time point at which YFP+ nucleocytoplasmic β-Catenin cell clusters are present, but tumourigenesis has not initiated. As a control, *Sox2$^{CreERT2/+}$; Rosa26$^{YFP/+}$* mice were induced similarly so as to compare the cluster cells with lineage traced Sox2+ pituitary stem/progenitor cells. This analysis revealed that at 4 weeks post tamoxifen administration in *Sox2$^{CreERT2/+}$; Ctnnb1$^{lox(ex3)/+}$; Rosa26$^{YFP/+}$* mice β-Catenin accumulating cluster cells are negative for the proliferation marker Ki67 (Figure 3.2 B). Furthermore, the cluster cells show nuclear expression of the cyclin dependent kinase inhibitor p21, an effector of the cell cycle arrest phenotype of senescent cells, and the DNA-damage marker DNA-PKcs (Figure 3.2 D, F). In control *Sox2$^{CreERT2/+}$; Rosa26$^{YFP/+}$* mice a few scattered Ki67+ cells were observed, which is consistent with the known quiescent nature of the pituitary gland at postnatal time points (Levy 2002) (Figure 3.2 A). Control mice also showed low levels of physiological p21 in scattered cells throughout the anterior lobe but were negative for DNA-PKcs (Figure 3.2 C,E). Together these IF staining studies show that the cluster cells in the inducible ACP mouse model are non-proliferative, possess DNA damage and express the senescence marker p21, a situation consistent with the induction of cellular senescence.

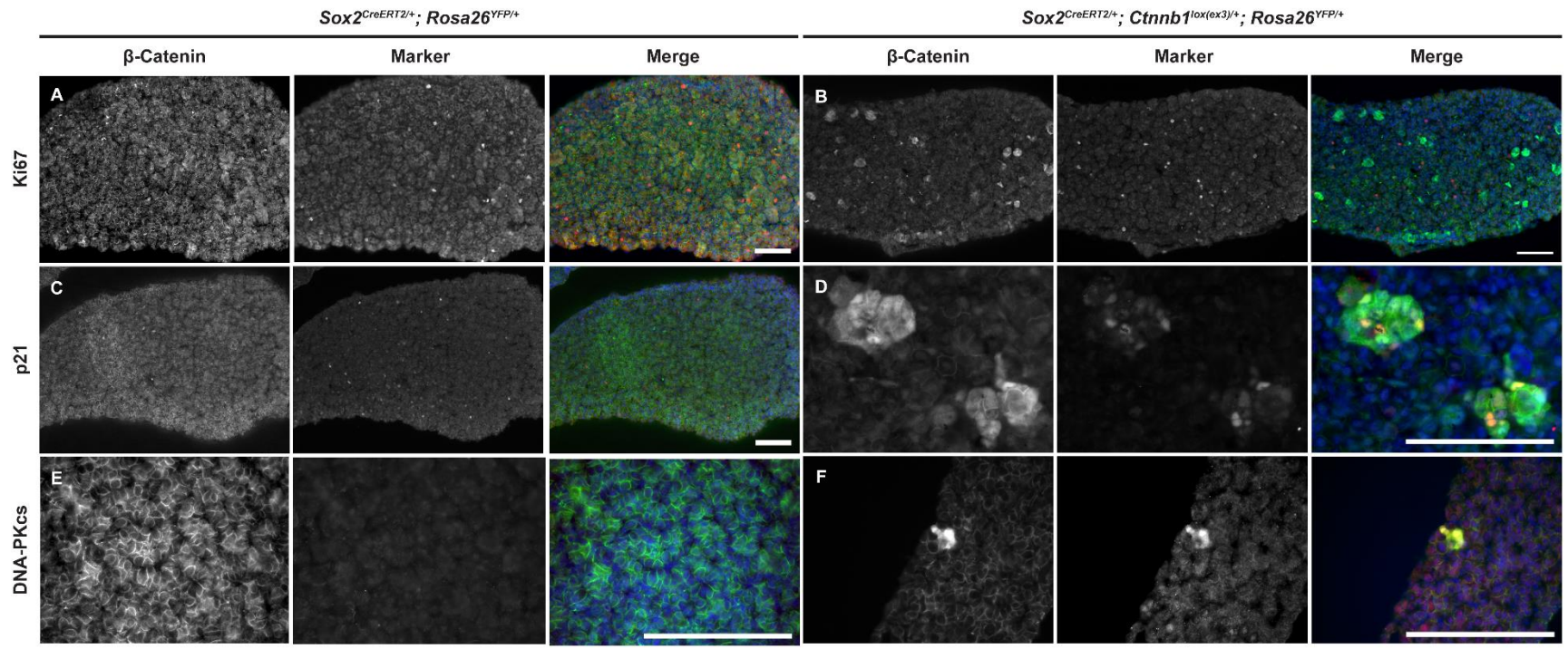

Figure 3.2. *Sox2$^{CreERT2/+}$; Ctnnb1$^{lox(ex3)/+}$; Rosa26$^{YFP/+}$* pituitary cluster cells show markers of cellular senescence. (**A**-**F**) Control, *Sox2$^{CreERT2/+}$; Rosa26$^{YFP/+}$* mice do not possess β-Catenin-accumulating cells clusters while mutant *Sox2$^{CreERT2/+}$; Ctnnb1$^{lox(ex3)/+}$; Rosa26$^{YFP/+}$* mice do. (**A**-**B**) The clusters in mutant pituitaries are negative for the proliferation marker Ki67. (**C**-**D**) Cluster cells are also positive for the senescence effector p21 (**D**), while the control pituitaries only show scattered p21 expression in a few cells of the anterior lobe (**C**). Expression of DNA-PKcs is also found in the cluster cells of mutant mice indicating the presence of DNA damage (**F**), a situation not observed in control mice which do not show any considerable levels of DNA damage (**E**). Scale bars; 200 μm. Representative immunofluorescence images shown from *Sox2$^{CreERT2/+}$; Ctnnb1$^{lox(ex3)/+}$; Rosa26$^{YFP/+}$* (n=6) and *Sox2$^{CreERT2/+}$; Rosa26$^{YFP/+}$* (n=4) genotypes.

3.2.1.2 Oncogenic β-Catenin targeted pituitary stem cell clusters can be isolated by flow cytometry

Previously, a transcriptomic profile of cluster cells has been obtained. This was achieved through microarray comparison of FACS isolated, WNT-activated (nucleocytoplasmic β-Catenin accumulating cluster cells) and WNT-non-activated (the remainder of the pituitary) cells derived from *Hesx1*$^{Cre/+}$*; Ctnnb1*$^{lox(ex3)/+}$ mice that carried a *BAT-gal* reporter of WNT/β-Catenin signaling (*Hesx1*$^{Cre/+}$*; Ctnnb1*$^{lox(ex3)/+}$*; BAT-gal*) (Cynthia L. Andoniadou et al. 2012; Maretto et al. 2003).

However, the molecular signature of the cluster cells in *Sox2*$^{CreERT2/+}$*;Ctnnb1*$^{lox(ex3)/+}$*;R26*$^{YFP/+}$ mice has not yet been revealed, which would be advantageous in exploring the hypothesis that they have entered into cellular senescence. Therefore, in an attempt to determine if isolation of oncogenic β-Catenin expressing cell clusters was possible, *Sox2*$^{CreERT2/+}$*;Ctnnb1*$^{lox(ex3)/+}$;*R26*$^{YFP/+}$ mice were induced with tamoxifen at 4 weeks of age and the pituitaries were analysed 4 weeks later, when clusters are present (Figure 3.3 B). These pituitaries were dissociated into single-cell suspensions and YFP+ (pituitary stem cells and β-Catenin accumulating cell clusters) and YFP− (the remainder of the pituitary) cell fractions were isolated by flow sorting and subjected to qRT-PCR analysis (Figure 3.3 A). This analysis revealed that the YFP+ fraction contained a higher abundance of *Sox2* and *Sox9* mRNA transcripts, markers of pituitary stem/progenitor cells, as well as the WNT-pathway target *Lef1* (Figure 3.3 C). Furthermore, significantly lower of *Gh* and *Tsh* (markers of terminally differentiated somatotrophs and thyrotrophs, respectively) was

also observed in the YFP+ cell fraction (Figure 3.3 C). Together this gene expression profile is consistent with the presence of non-differentiated β-catenin-accumulating cluster cells that are derived from the Sox2+ stem cell compartment in the YFP+ population.

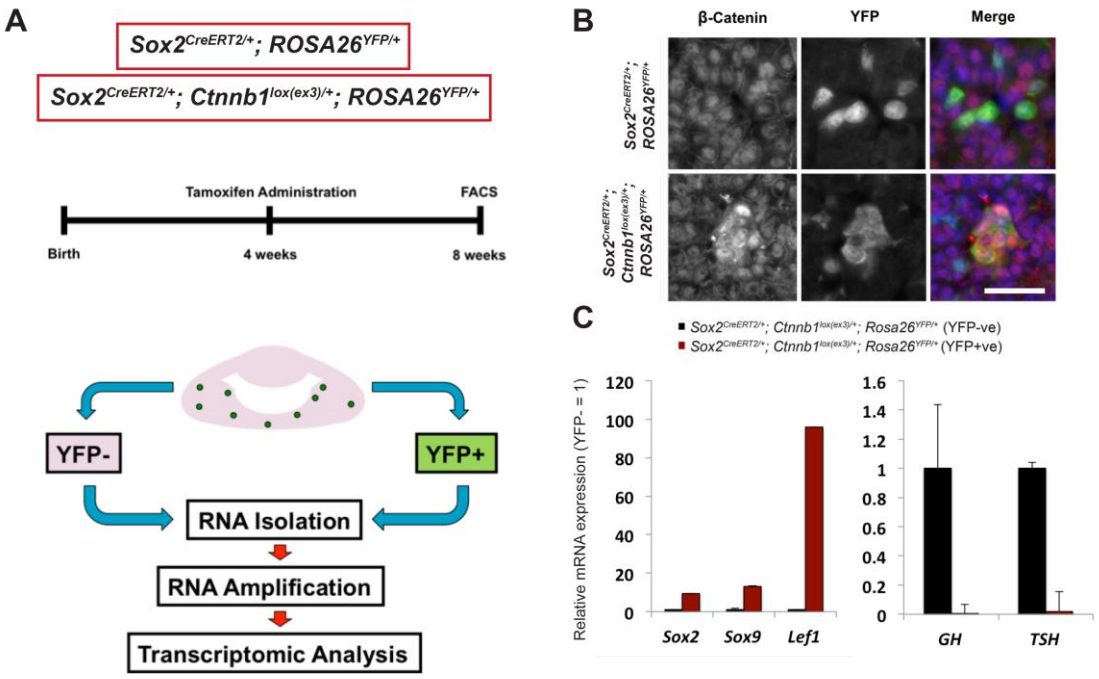

Figure 3.3. Cluster cells from *Sox2*$^{CreERT2/+}$; *Ctnnb1*$^{lox(ex3)/+}$; *Rosa26*$^{YFP/+}$ mice can be isolated by flow cytometry. (**A**) Schematic representation of the strategy to enrich mutant cluster cells and control cells from *Sox2*$^{CreERT2/+}$; *Ctnnb1*$^{lox(ex3)/+}$; *Rosa26*$^{YFP/+}$ and *Sox2*$^{CreERT2/+}$; *Rosa26*$^{YFP/+}$ mice, respectively. Mutant and control mice are induced with tamoxifen at 4 weeks of age and the pituitaries are harvested and dissociated for flow cytometric analysis 4 weeks later. The YFP+ and YFP- cell fraction are isolated by FACS and the RNA is extracted, amplified and used for downstream transcriptomic analysis. (**B**) IF showing histological sections from control and mutant mice where the cluster cells are observed to be YFP+ in the mutant mice. (**C**) qRT-PCR analysis comparing the YFP+ and YFP- cell fractions from *Sox2*$^{CreERT2/+}$; *Ctnnb1*$^{lox(ex3)/+}$; *Rosa26*$^{YFP/+}$ mice that demonstrate a significant increase in abundance of the pituitary stemness factors *Sox2* and *Sox9* as well as the WNT-pathway target *Lef1* in YFP+ cells. A decreased abundance of *Gh* and *Tsh*, markers of differentiated pituitary cell types, was also observed in the YFP+ fraction (*P≤0.05, **P≤0.01, ***P≤0.001 Student's t-test). n=4 per group for qRT-PCR analysis. Representative immunofluorescence images shown from *Sox2*$^{CreERT2/+}$; *Ctnnb1*$^{lox(ex3)/+}$; *Rosa26*$^{YFP/+}$ (n=3) and *Sox2*$^{CreERT2/+}$; *Rosa26*$^{YFP/+}$ (n=3) genotypes. Data are mean±s.e.m. Scale bar: 50 μm.

3.2.1.3 Transcriptomic profiling of cluster cells reveals a signature of senescence and SASP

In order to expand upon the previous microarray analysis and gain a more detailed understanding of the molecular differences that oncogenic β-Catenin expression in pituitary stem/progenitor cells produces, RNA-seq was performed on pituitary stem cells harboring either wild type or oncogenic β-Catenin. Specifically, *Sox2*$^{CreERT2/+}$*; Ctnnb1*$^{lox(ex3)/+}$*; Rosa26*$^{YFP/+}$ mutant and *Sox2*$^{CreERT2/+}$*; Rosa26*$^{YFP/+}$ control mice were induced with tamoxifen at 4 weeks of age and 4 weeks later the pituitaries were dissociated, the YFP+ cell fraction was isolated by flow cytometry and the RNA was subjected to sequencing. Initially, gene expression values for each mutant and control sample were plotted using principle component analysis (PCA) (Figure 3.4 A). PCA is used to convert a set of observations (gene expression values) of possibly correlated variables into a set of linearly un-correlated principle components, which allows for variation and patterns in the data to be emphasized. Control samples (*Sox2*$^{CreERT2/+}$*; Rosa26*$^{YFP/+}$*)* demonstrated the highest degree of variability between individual samples when compared with the mutant samples (*Sox2*$^{CreERT2/+}$*; Ctnnb1*$^{lox(ex3)/+}$*; Rosa26*$^{YFP/+}$), which clustered closely together. PCA confirmed that control and mutant genotypes grouped separately (Figure 3.4 A). Further to this, generation of a heatmap detailing all of the 1465 significantly differentially expressed genes in each samples grouped the mutants separately from controls, confirming that the oncogenic β-Catenin targeted pituitary stem cells are transcriptionally divergent from control pituitary stem cells (Figure 3.4 B).

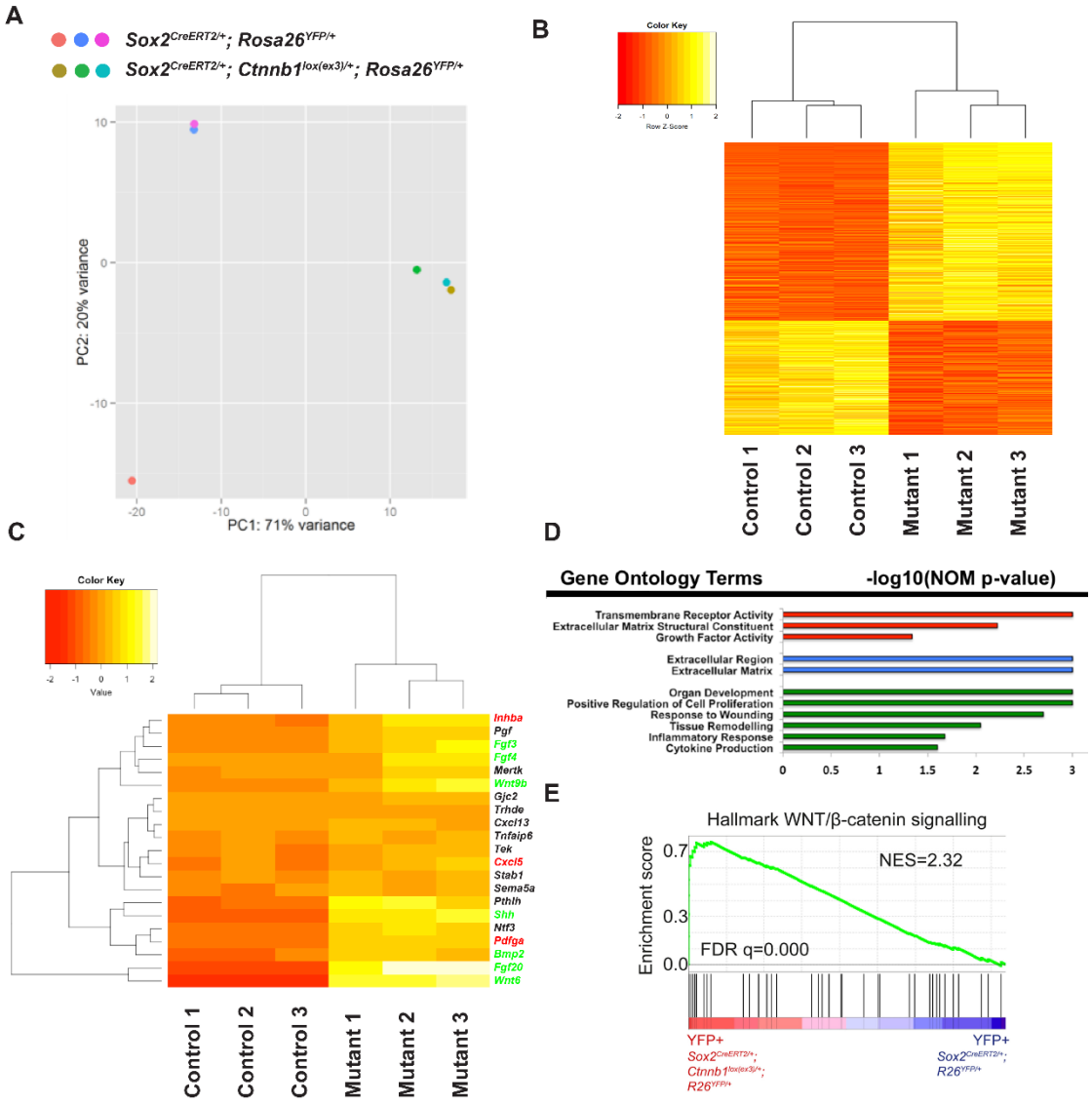

Figure 3.4. Unbiased trasncriptomic analysis reveals that cluster cells are actively involved in cell-cell signaling. (**A**) Principle component analysis plot showing separate clustering of mutant (*Sox2*$^{CreERT2/+}$*; Ctnnb1*$^{lox(ex3)/+}$*; Rosa26*$^{YFP/+}$) and control (*Sox2*$^{CreERT2/+}$*; Rosa26*$^{YFP/+}$) YFP+ cell fractions following RNA-sequencing (n=3 per group). (**B**) Heatmap of all significantly differentially expressed genes between control and mutant showing large transcriptomic difference between the samples. (**C**) Heatmap showing a subset of significantly differentially expressed genes that fall under the cell-cell signaling gene ontology term (GO:0007267). Note the presence of both canonical SASP (red) and ACP cell cluster factors (green). (**D**) Gene ontology analysis showing statistically significantly enriched molecular functions (red), cellular components (blue) and biological processes (green) in cluster cells, which are predominantly involved in cellular signaling and extracellular matrix modification. (**E**)

Gene set enrichment analysis plot showing a significant enrichment of the WNT/β-Catenin pawthay in cluster cells. NES = Normalised enrichment score. FDR: False discovery rate.

As an indicator of confidence in the dataset, analysis of differentially expressed genes also confirmed the upregulation of genes in YFP+ *Sox2*$^{CreERT2/+}$*; Ctnnb1*$^{lox(ex3)/+}$*; Rosa26*$^{YFP/+}$ samples that previously have been found to be enriched in both the cluster cells of an embryonic mouse model of ACP (*Hesx1*$^{Cre/+}$*; Ctnnb1*$^{lox(ex3)/+}$) and in human ACP cluster cells (Figure 3.4 C). These genes included members of the fibroblast growth factor (FGF), wingless-related integration site (WNT), hedgehog (HH) and bone morphogenetic protein (BMP) families. The up regulation of these genes was also confirmed by qRT-PCR analysis (Figure 3.5 A).

In order to interrogate the biological consequences of oncogenic β-Catenin expression in pituitary stem cells, the differentially expressed genes were analysed by gene set enrichment analysis (GSEA) and gene ontology (GO) analysis. Both of these bioinformatic techniques allow for the degree of enrichment of experimentally derived gene sets against gene sets derived from known biological processes, such as activated signaling pathways or other molecular functions to be ascertained. GO analysis reveled that statistically significantly enriched molecular functions include; transmembrane receptor activity, extracellular matrix structural constituent and growth factor activity. Enriched cellular components included the extracellular region and extracellular matrix. Biological processes that showed enrichment by GO analysis included organ development, positive regulation of cell proliferation, response to wounding, tissue remodeling, inflammatory response and cytokine production (Figure 3.4 D). GSEA demonstrated positive enrichment for WNT/β-Catenin signaling,

providing further validation that the YFP+ fraction from *Sox2*$^{CreERT2/+}$*; Ctnnb1*$^{lox(ex3)/+}$*; Rosa26*$^{YFP/+}$ pituitaries are enriched for WNT-signaling active cells (Figure 3.4 E). Significant enrichment in these cells was also found for signaling via Il6, Il2, TGFβ, TNFα, and p53 in the cluster cells, which are molecular signatures compatible with the hypothesis that the cluster cells have entered into cellular senescence. Furthermore, glycolysis also showed a trend towards positive enrichment in the cluster cells by GSEA with a concomitant significant negative enrichment for oxidative phosphorylation, potentially suggesting a Warburg-shift in the cellular respiration of the cluster cells (Figure 3.5 B).

To determine in an unbiased manner whether the oncogenic β-Catenin targeted pituitary stem cells activate the cellular senescence program and SASP, the differentially expressed gene list derived from RNA-Sequencing was compared to gene sets derived from established transcriptomic signatures of OIS and SASP. These gene sets were obtained from human IMR90 ER:RAS fibroblasts that possess a steroid receptor-KrasG12V fusion protein, which can be used to trigger growth arrest, senescence induction and SASP expression (Acosta et al. 2013). GSEA of oncogenic pituitary stem cells reveled significant enrichment for both OIS induction and SASP expression (Figure 3.5 B). This result was confirmed by qRT-PCR, which demonstrated a significantly increased mRNA abundance for the cyclin-dependent kinase inhibitors; *Cdkn1a* and *Cdkn2a*. Furthermore, significantly increased expression of the SASP factors *Il1a*, *Il1b*, *Cxcl1*, *Ccl20* and *Tgfβ1* was also observed in oncogenic cluster cells (Figure 3.5 A).

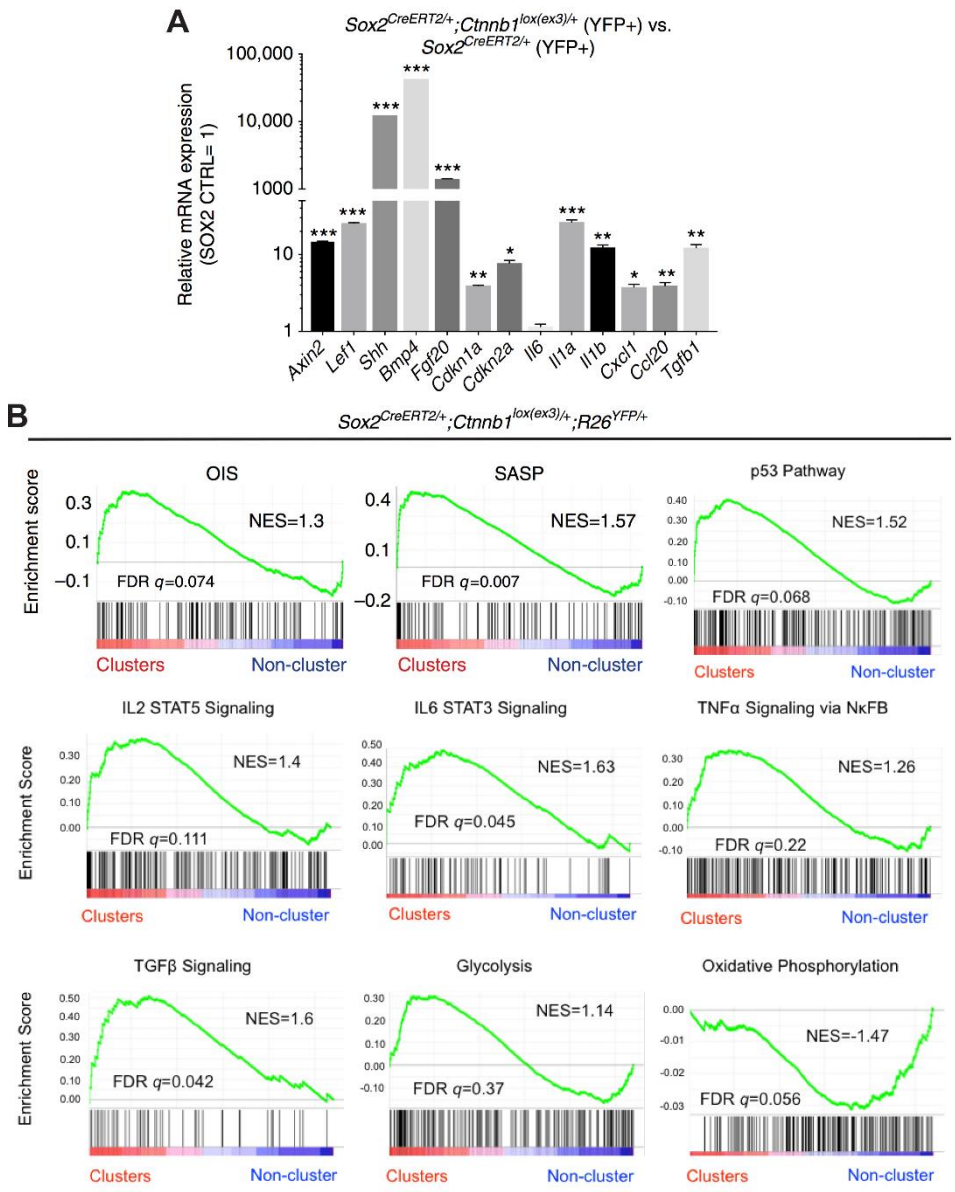

Figure 3.5. Cluster cells possess a transcriptomic signature of cellular senescence and SASP. (**A**) qRT-PCR analysis comparing the YFP+ cell fractions from mutant (*Sox2*$^{CreERT2/+}$*; Ctnnb1*$^{lox(ex3)/+}$*; Rosa26*$^{YFP/+}$) and control (*Sox2*$^{CreERT2/+}$*; Rosa26*$^{YFP/+}$) pituitaries demonstrating the statistically significant upregulation of WNT pathway targets (*Axin2* and *Lef1*), previously identified ACP developmental signaling ligands (*Shh*, *Bmp4* and *Fgf20*) and senescence and SASP factors (*Cdkn1a*, *Cdkn2a*, *Il1α*, *Il1β*, *Cxcl1*, *Ccl20* and *Tgfβ1*). (**B**) Gene set enrichment analysis plots showing enrichment for OIS and SASP as well as senescence related (p53, Il2, Il6, Tnfα and Tgfβ) and respiration pathway (Glycolysis and Oxidative phosphorylation). (*P≤0.05, **P≤0.01, ***P≤0.001 Student's t-test). n=4 per group for qRT-PCR analysis. Data are mean±s.e.m. NES = Normalised enrichment score. FDR: False discovery rate.

Together these results suggest that oncogenic β-Catenin targeted pituitary stem cells have an active role in intercellular signaling and modification of the extracellular space, which is consistent with the potential of these cells to modify the behavior of neighboring cells in a paracrine manner. Moreover, transcriptomic analysis provides evidence that these cluster cells have entered into OIS with an activated SASP.

3.2.1.4 A conserved transcriptomic signature is observed between human and mouse cluster cells

Recently, the transcriptomic profile specific human ACP tumour cell compartments were elucidated through a combination of laser-capture microdissection of tumour compartments followed by RNA-sequencing (Apps et al. 2018, Array Express accession code: E-MTAB-5266). To determine whether the signature of senescence and SASP was conserved between the clusters of mouse and human ACP, the degree of transcriptomic equivalence was ascertained by bioinformatic hierarchical clustering. This analysis revealed a grouping between the clusters found in *Sox2*$^{CreERT2/+}$*; Ctnnb1*$^{lox(ex3)/+}$*; Rosa26*$^{YFP/+}$ pituitaries and human ACP, suggesting analogous transcriptomic profiles (Figure 3.6 A). Furthermore, comparing either the top 100 or 500 most upregulated genes in human ACP clusters against the previously described cluster gene expression profile from *Sox2*$^{CreERT2/+}$*; Ctnnb1*$^{lox(ex3)/+}$*; Rosa26*$^{YFP/+}$ mice by GSEA revealed a significant positive enrichment (Figure 3.6 B). These analyses suggest that mouse and human ACP cluster cells are equivalent cellular structures that share a transcriptomic signature of cellular senescence and SASP.

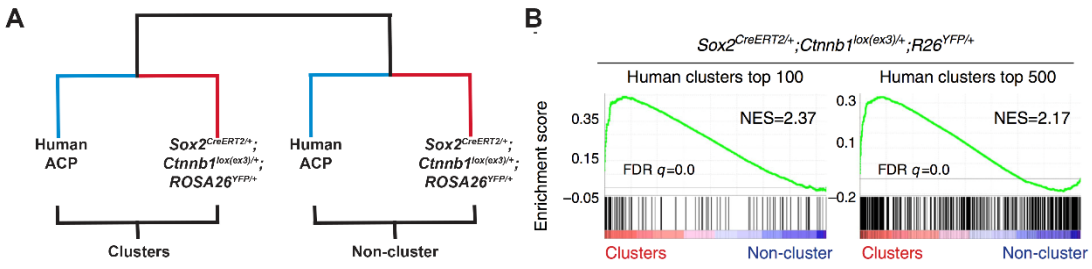

Figure 3.6. The cluster cells from mouse and human ACP are molecularly analogous. (**A**) Hierarchical clustering analysis of RNA-data sets from human and *Sox2*$^{CreERT2/+}$*; Ctnnb1*$^{lox(ex3)/+}$*; Rosa26*$^{YFP/+}$ cluster and non-cluster cell populations indicating coherent grouping between specific cell compartments. (**B**) GSEA of the top 100 or 500 most upregulated genes in human clusters and the whole transcriptome of *Sox2*$^{CreERT2/+}$*; Ctnnb1*$^{lox(ex3)/+}$*; Rosa26*$^{YFP/+}$ mouse clusters demonstrating a common molecular signature. NES = Normalised enrichment score. FDR: False discovery rate.

3.2.2 Aged pituitary stem cells targeted with oncogenic β-Catenin have reduced SASP and show decreased tumour-inducing potential

In cancer biology it is now appreciated that the cellular context in which an oncogene is activated or tumour-supressor is lost plays a significant role in whether or not the cell will undergo neoplastic transformation. This has been elegantly shown in a recent study by the Gilbertson group, where various oncogenic insults were induced in tissues at varying ages, resulting in drastically different tumourigenic incidences. In essence, some cell types may be competent to undergo transformation at one stage of life but not at another (L. Zhu et al. 2016).

3.2.2.1 Targeting of Sox2+ pituitary stem cells later in life results in greatly impaired tumourigenic potential

Therefore, the effect of organismal age was explored in the development of paracrine tumourigeneis in the pituitary using the *Sox2*$^{CreERT2/+}$*; Ctnnb1*$^{lox(ex3)/+}$*; Rosa26*$^{YFP/+}$ model. To achieve this *Sox2*$^{CreERT2/+}$*; Ctnnb1*$^{lox(ex3)/+}$*; Rosa26*$^{YFP/+}$ mice were induced with tamoxifen at either 1 month or 6-9 months of age. At 1 month of age the pituitary stem cells are still actively engaging in organ growth, while at 6-9 months of age the Sox2+ pituitary stem cell compartments contribution to organ homeostasis is significantly lower (Levy 2002). Pituitaries from these tamoxifen-induced mice were analysed histologically for tumour formation 3 months post-induction. This analysis revealed that 100% of mice (n = 15/15) induced at 3 months had developed pituitary tumours, with 48 individual lesions found in total (average of 2-4 tumours per pituitary). Strikingly, mice induced at 6-9 months of age showed that less than 20% of the cohort (n = 3/17) developed pituitary tumours, with only 5 individual lesions being observed (p<0.0001) (Table 3.1).

***Sox2*$^{CreERT2/+}$*; Ctnnb1*$^{lox(ex3)+}$*; Rosa26*$^{YFP/+}$**		
Age at tamoxifen induction	**Tumour incidence[a]**	**Number of mice**
1 month	15 (48 lesions)	15
6-9 months*	3 (5 lesions)	17

Table 3.1. Reduced tumour-inducing potential in older vs. young Sox2+ pituitary stem cells.

[a] Tumour incidence was assessed histologically at 3 months post-tamoxifen induction

* Unpaired *t*-test showed a statistically significant difference in tumour formation between age groups (*p*=<0.0001)

3.2.2.2 Sox2+ pituitary stem cells targeted later in life enter into cellular senescence with SASP activation

To understand the significantly reduced tumour burden in *Sox2*$^{CreERT2/+}$*; Ctnnb1*$^{lox(ex3)/+}$*; Rosa26*$^{YFP/+}$ mice induced at 6-9 months of age, their pituitaries were analsyed for the presence of cell clusters, senescence and SASP. IF analysis was performed on pituitaries from *Sox2*$^{CreERT2/+}$*; Ctnnb1*$^{lox(ex3)/+}$*; Rosa26*$^{YFP/+}$ mice induced at 6 months and collected 1 month later, a latency period which produced cluster cells from *Sox2*$^{CreERT2/+}$*; Ctnnb1*$^{lox(ex3)/+}$*; Rosa26*$^{YFP/+}$ mice induced at 1 month of age (Figure 3.7 A). Staining for β-Catenin in these aged animals revealed clusters of cells with nucleocytoplasmic accumulation of the protein, similar to what is observed when these mice are induced at 1 month of age (Figure 3.7 B). Comparison of the number of cells comprising the cell clusters from mice induced at either 1 or 6 months of age revealed that clusters contained fewer cells in aged *Sox2*$^{CreERT2/+}$*; Ctnnb1*$^{lox(ex3)/+}$*; Rosa26*$^{YFP/+}$ mice. The average number of cluster cells in 1 month induced *Sox2*$^{CreERT2/+}$*; Ctnnb1*$^{lox(ex3)/+}$*; Rosa26*$^{YFP/+}$ mice was 3.16 +/-1.57 which fell to 1.95 +/-1.12 in mice induced at 6 months of age ($p<0.0001$) (Figure 3.7 C).

To investigate whether these cluster cells formed in older mice are capable of activating the senescence and SASP program they were interrogated by a combination of IF and qRT-PCR analysis. Staining of the cluster cells from older mice revealed that they were negative for the proliferation marker Ki67 and positive for the senescence effector p21, which is analogous to the cluster cells in younger mice and consistent with a senescent phenotype (Figure 3.7 B). To explore the gene expression profile of the cluster cells formed in older mice, flow cytometry was performed in which the YFP+

fraction was isolated for qRT-PCR analysis from *Sox2*$^{CreERT2/+}$*; Ctnnb1*$^{lox(ex3)/+}$*; Rosa26*$^{YFP/+}$ mutant and *Sox2*$^{CreERT2/+}$*; Rosa26*$^{YFP/+}$ control pituitaries induced with tamoxifen at 6 months of age and collected 1 month later. This analysis showed a significant increase in the abundance of *Lef1* and *Axin2* transcripts in the YFP+ fraction of late induced *Sox2*$^{CreERT2/+}$*; Ctnnb1*$^{lox(ex3)/+}$*; Rosa26*$^{YFP/+}$ mutants, relative to YFP+ control cells from *Sox2*$^{CreERT2/+}$*; Rosa26*$^{YFP/+}$ pituitaries. Moreover, a significant increase in expression of *Shh*, *Bmp4* and *Fgf20* was also observed in older cluster cells when compared to age matched control stem cells (Figure 3.7 D). These finding are comparable to the ones obtained when analysing cluster cells generated from *Sox2*$^{CreERT2/+}$*; Ctnnb1*$^{lox(ex3)/+}$*; Rosa26*$^{YFP/+}$ mice induced at 1 month of age (see Figure 3.5 A). Examination of senescence and SASP markers in these older cluster cells revealed a significant increase in the expression of the senescence effectors *Cdkn1a* and *Cdkn2a* as well as the SASP factor *Il1b* (Figure 3.7 D).

Together these results suggest that *Sox2*$^{CreERT2/+}$*; Ctnnb1*$^{lox(ex3)/+}$*; Rosa26*$^{YFP/+}$ mice induced at older ages are capable of forming β-Catenin accumulating cluster cells, albeit of a smaller size. These cluster cells also posses the previously identified hallmarks of ACP clusters, including WNT pathway activation and expression of developmental signaling ligands. The clusters formed at older ages also showed indications of senescence pathway and SASP activation.

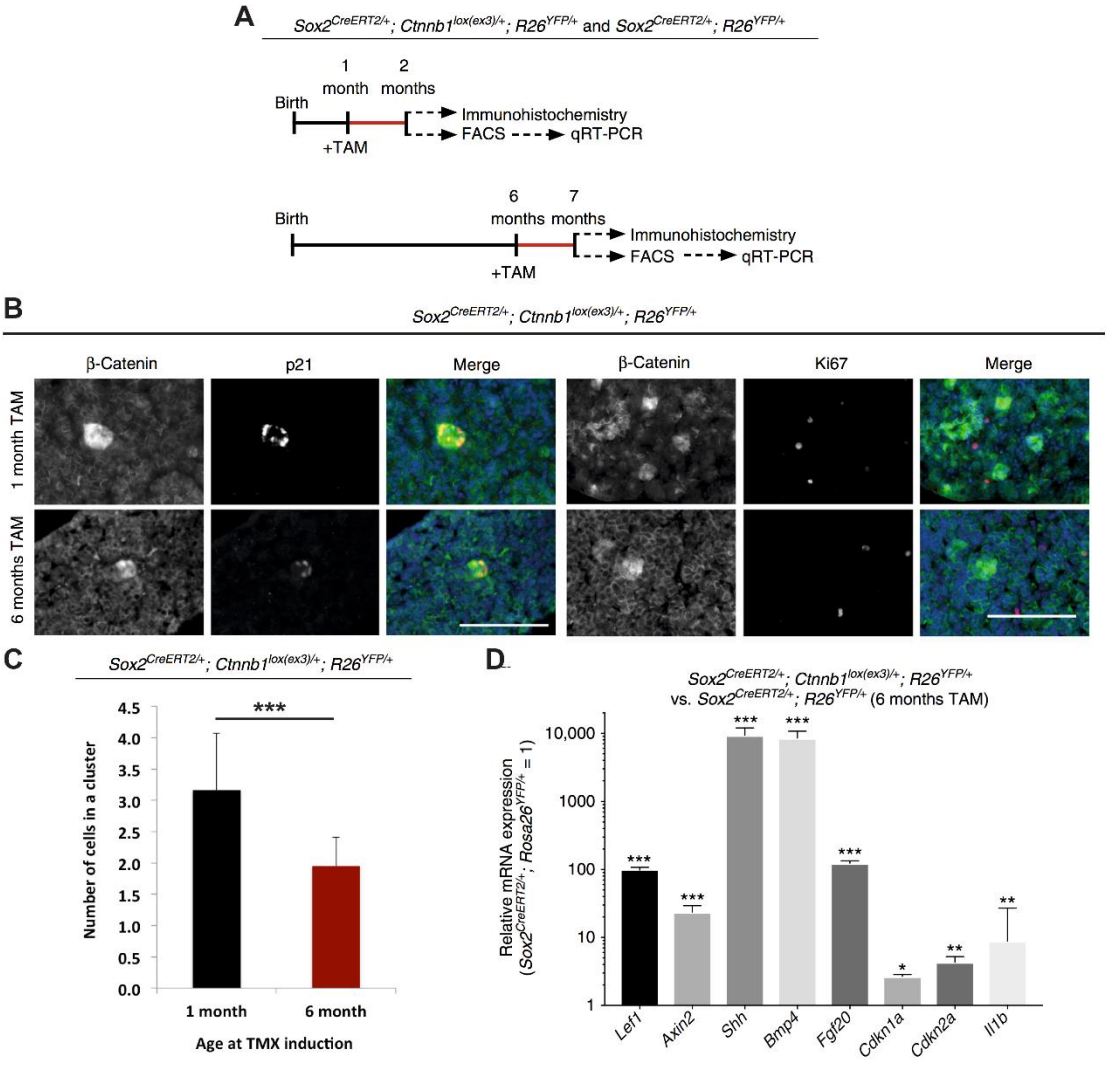

Figure 3.7. *Sox2*$^{CreERT2/+}$*; Ctnnb1*$^{lox(ex3)/+}$*; Rosa26*$^{YFP/+}$ mice induced at older ages possess β-Catenin-accumulating senescent cell clusters. (**A**) Schematic representation of the experimental design. Mutant (*Sox2*$^{CreERT2/+}$*; Ctnnb1*$^{lox(ex3)/+}$*; Rosa26*$^{YFP/+}$) and control (*Sox2*$^{CreERT2/+}$*; Rosa26*$^{YFP/+}$) mice were induced with tamoxifen at either 1 month or 6 months of age and the pituitaries collected 1 months later for analysis by IF and qRT-PCR. (**B**) IF of mutant mice induced at either 1 or 6 months of age showing the presence of β-Catenin-accumulating cell clusters, which express the senescence marker p21 and are negative for the proliferation marker Ki67. (**C**) Quantification of the number of cells that comprise clusters shows that clusters induced in *Sox2*$^{CreERT2/+}$*; Ctnnb1*$^{lox(ex3)/+}$*; Rosa26*$^{YFP/+}$ mice from 6 months of age are significantly smaller. (**D**) qRT-PCR analysis comparing mutant and control mice induced at 6 months of age. Significant upregulation of WNT pawaths targets (*Lef1* and *Axin2*), ACP cluster developmental signaling ligands (*Shh*, *Bmp4* and *Fgf20*) and senescence and SASP factors (*Cdkn1a*, *Cdkn2a* and *Il1b*) are observed. (*P≤0.05, **P≤0.01, ***P≤0.001 Student's t-test). n=4 per group for qRT-

PCR analysis, n=3 per group for the quantification of number of cells in a cluster. Representative immunofluorescence images shown from *Sox2*$^{CreERT2/+}$*; Ctnnb1*$^{lox(ex3)/+}$*; Rosa26*$^{YFP/+}$ (n=3) and *Sox2*$^{CreERT2/+}$*; Rosa26*$^{YFP/+}$ (n=3) genotypes. Data are mean±s.e.m. Scale bars: 100 μm.

3.2.2.3 Cluster cells formed in older animals demonstrate a reduced intensity in the SASP with a lower mitogenic potential

In order to further examine the similarities and potential differences between the cluster cells induced to form at older or younger ages, qRT-PCR analysis was performed comparing the cluster cells from older and young mice. Specifically, comparison of the YFP+ cell fractions isolated from *Sox2*$^{CreERT2/+}$*; Ctnnb1*$^{lox(ex3)/+}$*; Rosa26*$^{YFP/+}$ mice induced at either 1 or 6 months of age and collected 1 month later was performed. This analysis showed a non-significant reduction in *Lef1* expression in older clusters, potentially suggesting comparable levels of WNT-pathway activation between the cluster cells induced at different ages (Figure 3.8 A). However, significantly reduced expression of developmental signaling ligands (*Shh*, *Bmp4* and *Fgf20*), senescence proliferative arrest mediators (*Trp53*, *Cdkn1a* and *Cdkn2a*) and SASP factors (*Il6* and *Cxcl2*) was observed (Figure 3.8 A). Interestingly, not all measured SASP factors were reduced as both *Il1b* and *Tgfb1* expression were found to be unchanged between older and younger cluster contexts (Figure 3.8 A).

Generally the pituitary is relatively quiescent in post-natal life, with only around 1% of cells showing expression of the proliferation marker Ki67 at 2 months of age. Interestingly, analysis of the proliferative index of non-cluster cells in *Sox2*$^{CreERT2/+}$*;*

Ctnnb1$^{lox(ex3)/+}$*; Rosa26*$^{YFP/+}$ pituitaries induced at 1 month of age and analysed 1 month later revealed an almost a 4-fold increase in dividing cells, suggesting a potential mitogenic response to the clusters. However, *Sox2*$^{CreERT2/+}$*; Ctnnb1*$^{lox(ex3)/+}$*; Rosa26*$^{YFP/+}$ mice induced at 6 month of age and analysed 1 month later did not show this increase in non-cluster cell proliferation, but instead had a proliferative index that was comparable to age-matched *Sox2*$^{CreERT2/+}$; *Rosa26*$^{YFP/+}$ control mice (Figure 3.8 B).

In an attempt to examine why the cluster formed in older animals have reduced expression of senescence and SASP components when compared to their younger counterparts, gene expression analysis was performed comparing non-mutated pituitary stem cells isolated from either younger (2 months of age) or older (7 months of age) mice. Specifically, the YFP+ fraction isolated from *Sox2*$^{CreERT2/+}$*; Rosa26*$^{YFP/+}$ control mice induced at either 1 or 6 months of age and collected 1 month later were compared by qRT-PCR. This analysis showed a trend towards an age-dependent increase in the expression of the senescence-associated markers *Cdkn2a* and *Trp53*, which may underlie the attenuated senescence and SASP response of older pituitary stem cells targeted with oncogenic β-Catenin (Figure 3.8 C).

Therefore, cluster cells formed in older *Sox2*$^{CreERT2/+}$*; Ctnnb1*$^{lox(ex3)/+}$*; Rosa26*$^{YFP/+}$ mice express lower levels of senescence and SASP-related transcripts than clusters form in younger animals. This decrease in the intensity of the senescence and SASP phenotype correlates with an age-associated increase in the expression of senescence/quiescence factors in the wild type pituitary stem cell compartment, which may explain the reduced response to oncogenic β-Catenin expression, as quiescent

cell populations show a reduced ability to enter cellular senescence following DNA-damaging insults (Leontieva & Blagosklonny 2010). Furthermore, a mitogenic response to the presence of the cluster cells was found in younger animals which was ameliorated in an aged context.

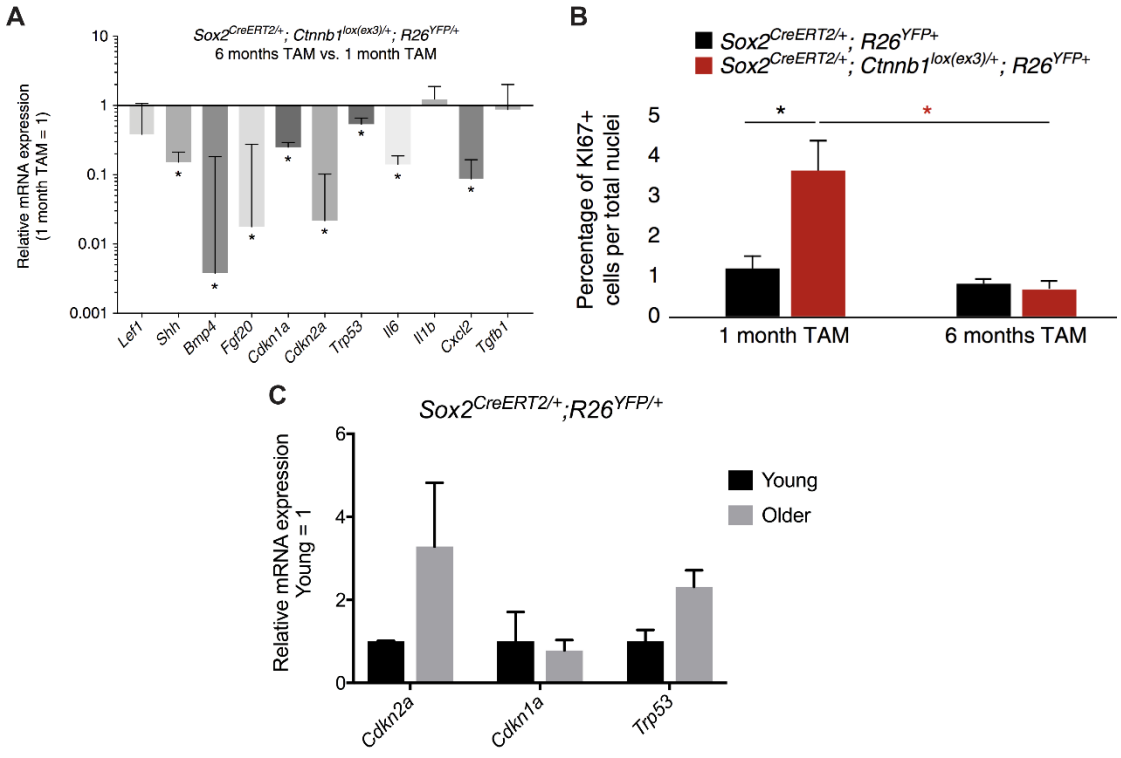

Figure 3.8. The cluster cells from older *Sox2$^{CreERT2/+}$; Ctnnb1$^{lox(ex3)/+}$; Rosa26$^{YFP/+}$* mice have a reduced mitogenic potential and have lower levels of SASP expression than clusters from younger animals. (**A**) qRT-PCR analysis comparing the YFP+ cluster cell fractions from *Sox2$^{CreERT2/+}$; Ctnnb1$^{lox(ex3)/+}$; Rosa26$^{YFP/+}$* mice induced at 1 or 6 months of age showing a reduction in the expression of developmental signaling ligands (*Shh*, *Bmp4* and *Fgf20*) and senescence and SASP related transcripts (*Cdkn1a*, *Cdkn2a*, *Trp53*, *Il6* and *Cxcl2*). (**B**) Quantification of the number of non-cluster cells that are proliferating in control (*Sox2$^{CreERT2/+}$; Rosa26$^{YFP/+}$*) and mutant (*Sox2$^{CreERT2/+}$; Ctnnb1$^{lox(ex3)/+}$; Rosa26$^{YFP/+}$*) mice induced at either 1 or 6 months of age. Note the reduced mitogenic response of the non-cluster cells in mutant mice induced at 6 months of age. (**C**) qRT-PCR analysis of the YFP+ fraction from control mice induced at either 1 or 6 months of age which shows a trend towards increased expression of the senescence-related factors *Cdkn2a* and *Trp53* in the stem cell compartment of older animals.

(*P≤0.05, Student's t-test). n=4 per group for qRT-PCR analysis, n=5 per group for the quantification of non-cluster proliferation. Data are mean±s.e.m.

3.2.4 Towards an understanding the lineage of origin from which non-cell autonomously derived pituitary tumours originate

The non-cell autonomous induction of pituitary tumours observed in the *Sox2*$^{CreERT2/+}$*; Ctnnb1*$^{lox(ex3)/+}$*; Rosa26*$^{YFP/+}$ model indicated that the oncogenic β-Catenin mutation sustaining cell and the tumour cell-of-origin is distinct. From lineage tracing experiments, following the fate of the Sox2+ pituitary cells demonstrated that the tumour cell of origin is not derived from the pituitary stem cell compartment (Cynthia Lilian Andoniadou et al. 2013) (see Figure 3.1). Interestingly, recent lineage tracing studies have been conducted in which *Hesx1*+ embryonic pituitary progenitors have been traced, following activation of oncogenic β-Catenin (*Hesx1*$^{Cre/+}$; *Ctnnb1*$^{lox(ex3)/+}$*; Rosa26*$^{YFP/+}$) (Gonzalez-Meljem et al. 2017a). This study revealed that the tumour does not arise from these progenitors. Together this indicated that the tumour cell of origin is not derived from the pituitary lineage at all. Knowledge of the tumour cell of origin is an important question, as it will facilitate the generation of more refined experimental paradigms for exploring the mechanisms behind non-cell autonomous tumourigenesis, such as exploring the role of different SASP components in cell culture models. As the tumour cell of origin is not derived from the pituitary lineage, likely candidates are cells that reside in the pituitary or circulate through the vasculature, but are not derived from the Hesx1 lineage. Such candidates include; endothelial cells, pericytes and other neural crest derivatives or hematopoietic/bone marrow derived cells.

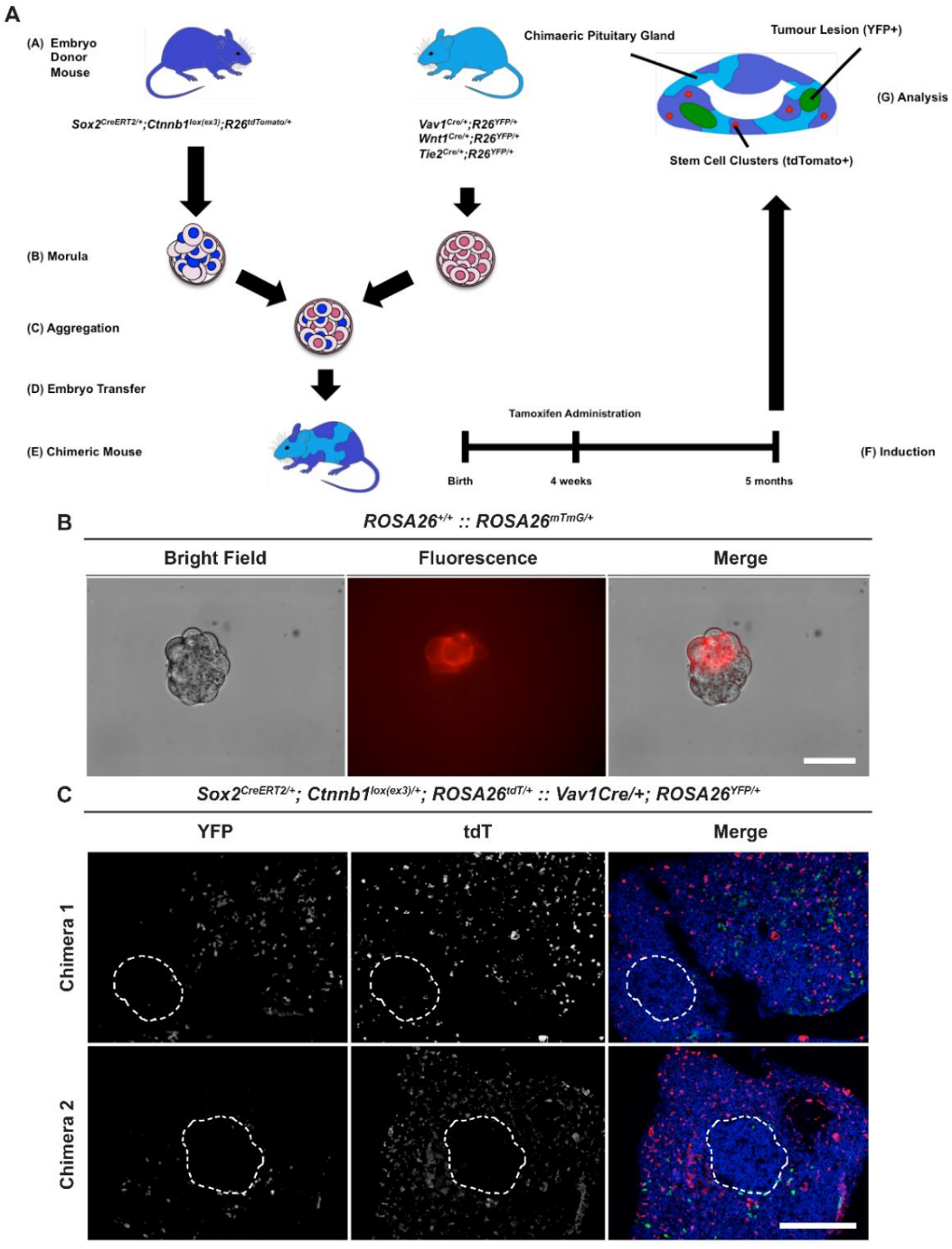

Figure 3.9. Analysis of *Sox2*$^{CreERT2/+}$; *Ctnnb1*$^{lox(ex3)/+}$; *Rosa26*$^{tdT/+}$::*Vav1*$^{Cre/+}$; *Rosa26*$^{YFP/+}$chimaeric mice demonstrated that the tumour cell or origin is not derived from the haematopoietic lineage. (**A**) Schematic representation of the experimental design for generating chimeric mice. Chimeric mice generated were induced with tamoxifen at 4 weeks of age and the pituitaries were analysed between 3 to 5 months later. (**B**) Proof of principle

experiment generating chimeric morula from wild type and *Rosa26*$^{mTmG/+}$ embryos. Red fluorescence indicates the contribution from *Rosa26*$^{mTmG/+}$ embryos. (**C**) Analysis of the pituitaries from two *Sox2*$^{CreERT2/+}$; *Ctnnb1*$^{lox(ex3)/+}$; *Rosa26*$^{tdT/+}$::*Vav1*$^{Cre/+}$; *Rosa26*$^{YFP/+}$chimeric mice which show pituitary tumour formation (dashed line). Note that the tumours are negative for tdTomato expression, indicating that they are non-cell autonomously derived from the mutation sustaining cluster cells. The tumour are also negative for the YFP lineage trace reporter indicating that the tumour cells are not derived from the Vav1 haematopoietic lineage.

To investigate if any of these lineage give rise to the paracrine tumours, chimeric mice were generated which possessed two distinct genomes. One which could give rise to lineage traced cluster cells, which initiate tumourigenesis following tamoxifen administration (*Sox2*$^{CreERT2/+}$; *Ctnnb1*$^{lox(ex3)/+}$; *Rosa26*$^{tdT/+}$) and one which would allow for the lineage tracing of the candidate tumour cell of origin lineage (Figure 3.9 A). As a proof of concept for this approach, chimeric morulae were generated from wild type and ubiquitously membrane-targeted tandem dimer Tomato-expressing embryos (Figure 3.9 B). This resulted in the successful generation of chimeric morulae.

3.2.4.1 The tumour cell of origin is not derived from the Vav1+ haematopoietic lineage

(Morula aggregation experiments were performed by Massimo Signore at the Institute of Child Health, Unniversity College London)

To assess if the haematopoietic lineage is capable of being transformed by the paracrine influence of the oncogene-targeted pituitary cluster cells, 8-cell stage

embryos belonging to either *Sox2*$^{CreERT2/+}$*; Ctnnb1*$^{lox(ex3)/+}$*; Rosa26*$^{tdT/+}$ *or Vav1*$^{Cre/+}$*; Rosa26*$^{YFP/+}$ were aggregated, transferred to a pseudo-pregnant female and allowed to develop into chimeric mice (Figure 3.9 A). PCR genotyping confirmed *Sox2*$^{CreERT2/+}$*;Ctnnb1*$^{lox(ex3)/+}$*;Rosa26*$^{tdT/+}$*::Vav1*$^{Cre/+}$*;Rosa26*$^{YFP/+}$ chimerism in 2 animals which were subsequently induced with tamoxifen at 1 month of age to stimulate cluster and tumour formation. These mice were the culled and the pituitaries analysed 4 to 6 months later when symptoms of tumourigenesis were evident. Analysis of the pituitaries by IF for tdT (oncogenic β-Catenin targeted Sox2+ cells) and YFP (Vav1 haematopoietic derivatives) expression revealed a great number of both of these lineage-traced populations in the pituitaries of both mice. As expected, cluster cells were lineage-traced by tdT expression and the number of cell clusters was qualitatively no different than when analysing non-chimeric *Sox2*$^{CreERT2/+}$*; Ctnnb1*$^{lox(ex3)/+}$*; Rosa26*$^{YFP/+}$ mice. One or two small tumour lesions were detectable in each of the chimeric pituitaries, consistent with previous reports of tumourigenic incidence in the *Sox2*$^{CreERT2/+}$*; Ctnnb1*$^{lox(ex3)/+}$*; Rosa26*$^{YFP/+}$ model and as expected they were negative for the tdT lineage-trace. However, no expression of YFP was found in any of the tumour lesions analysed, indicating that the haematopoietic lineage is unlikely to be the paracrine tumour cell of origin (Figure 3.9 C).

3.3 CONCLUSIONS

In summary, these results show that β-catenin clusters cells, which precede non-cell autonomous tumour formation in *Sox2*$^{CreERT2/+}$*; Ctnnb1*$^{lox(ex3)/+}$*; Rosa26*$^{YFP/+}$ mice are non-proliferative, express the senescence marker p21 and possess DNA-damage.

These cluster cells can be enriched by flow cytometry and analysis of their gene expression profile demonstrated the expression of several canonical markers of ACP cell clusters (*Shh*, *Bmp4*, *Fgf20*) as well as expression of common SASP factors (*Il1a*, *Il1b*, *Cxcl1*, *Ccl20* and *Tgfb1*). Unbiased transcriptomic analysis also furthered confidence that the cluster cells had entered senescence through comparison with OIS and SASP gene sets derived from external sources. Furthermore, analogous gene expression signatures were observed in cluster cells from human ACP samples.

Intriguingly, in *Sox2*$^{CreERT2/+}$*; Ctnnb1*$^{lox(ex3)/+}$*; Rosa26*$^{YFP/+}$ mice induced at later ages, a dramatic reduction in tumourigenic capacity was observed. These older *Sox2*$^{CreERT2/+}$*; Ctnnb1*$^{lox(ex3)/+}$*; Rosa26*$^{YFP/+}$ mice also possessed cell clusters which had hallmarks of cellular senescence but had a significantly reduced intensity of the SASP. These results are consistent with the initial hypothesis that the cluster cells have entered into senescence and through the action of the SASP are able to transform neighboring cells to give rise to tumours as reduction of the SASP, by oncogenically targeting animals later in life, correlated with a reduction in tumourigenic incidence.

CHAPTER 4: UNDERSTANDING THE CONSEQUENCES OF MAPK DYSREGULATION IN EMBRYONIC PITUITARY PRECURSORS AND POSTNATAL STEM CELLS

4.1 INTRODUCTION

In the previous chapter, it was shown that targeting oncogenic β-Catenin to pituitary stem cells results in the formation of ACP-like tumours in the pituitary. The targeted pituitary stem cells formed clusters and demonstrated non-cell autonomous tumour-inducing potential, concomitantly with a cell-autonomous activation of the cellular senescence program and SASP. Furthermore, it was shown that a reduction in the intensity of the SASP correlated with a profound decrease in the incidence of tumour formation. Therefore, this led to the question: can induction of cellular senescence in the context of wild type β-Catenin drive tumourigenesis in the pituitary?

To achieve this a transgenic approach was adopted, where cellular senescence can be activated though the conditional expression of Cre-recombination activated oncogenic *Braf* (*Braf*$^{V600E/+}$) or *Kras* (*Kras*$^{G12D/+}$), either in the adult pituitary stem cell compartment (*Sox2*$^{CreERT2/+}$ driven) or in the embryonic precursors of the pituitary gland (*Hesx1*$^{Cre/+}$ driven). As previously mentioned, *Braf* and *Kras* are downstream members of the MAPK signaling pathway and fulfill kinase and GTPase functions, respectively. Their oncogenic variants, *Braf*$^{V600E/+}$ and *KRas*$^{G12D/+}$, have been demonstrated to act as potent inducers of cellular senescence in both *in vitro* and *in vivo* contexts (Dhomen et al. 2009; Mercer et al. 2005.; Tuveson et al. 2004; Jackson et al. 2001). Furthermore, activating mutations in *BRAF* are thought to be drivers of human PCP through patient sequencing studies (Brastianos et al. 2014). Currently very little is known regarding the role of MAPK signaling during development of the pituitary or of the relationship between oncogenic *Braf* and PCP development in humans.

Therefore, this chapter focuses on investigating the role that oncogenic MAPK pathway components play during pituitary organogenesis and their potential role in stimulating tumourigenesis.

4.2 RESULTS

4.2.1 The MAPK pathway influences pituitary stem cell proliferation and differentiation during pituitary development

Previously it has been shown that the *Hesx1-Cre* mouse line can drive Cre-recombinase expression robustly during pituitary development from 9.0 dpc (Andoniadou et al. 2007; Gaston-massuet et al. 2011; Jayakody et al. 2012). Therefore, this genetic tool was used to assess the role that the MAPK signaling pathways plays during pituitary development and its ability to induce cellular senescence by crossing it with either *Braf*$^{V600E/+}$ or *Kras*$^{G12D/+}$ animals (Jackson et al. 2001; Mercer et al. 2005).

4.2.1.1 Severe anterior lobe hyperplasia, neonatal lethality and absence of cellular senescence markers in *Hesx1*$^{Cre/+}$*;Braf*$^{V600E/+}$ and *Hesx1*$^{Cre/+}$*;Kras*$^{G12D/+}$ mutants

Analysis of the genotypes of *Hesx1*$^{Cre/+}$*; Braf*$^{V600E/+}$*, Hesx1*$^{Cre/+}$*; Kras*$^{G12D/+}$ and control embryos obtained between 10.5-18.5 dpc revealed no statistically significant

difference from the expected Mendelian ratios (Table 4.1). However, no viable postnatal mice from the mutant genotypes were found, indicating neonatal lethality (Table 4.1). Examination of mutant mice from both genotypes found dead at birth showed expanded airway structures, indicating abnormal lung development, which could be the cause of the observed perinatal death (Figure 4.1) (Tang et al. 2011).

	Genotypes (% Expected)[a]									
	Hesx1$^{Cre/+}$ *Kras*$^{G12D/+}$ (25%)	*Hesx1*$^{Cre/+}$ *Kras*$^{+/+}$ (25%)	*Hesx1*$^{+/+}$ *Kras*$^{G12D/+}$ (25%)	*Hesx1*$^{+/+}$ *Kras*$^{+/+}$ (25%)		*Hesx1*$^{Cre/+}$ *Braf*$^{V600E/+}$ (25%)	*Hesx1*$^{Cre/+}$ *Braf*$^{+/+}$ (25%)	*Hesx1*$^{+/+}$ *Braf*$^{V600E/+}$ (25%)	*Hesx1*$^{+/+}$ *Braf*$^{+/+}$ (25%)	
Stage					Total					Total
10.5 dpc	8	7	8	10	33	6	5	5	8	24
12.5 dpc	10	5	8	3	26	12	10	3	4	29
14.5 dpc	9	5	7	11	32	10	7	8	6	31
18.5 dpc	7	9	3	7	26	10	9	6	7	32
Embryos[†] (% Observed)	34 (29%)	26 (22%)	26 (22%)	31 (26%)	117	38 (33%)	31 (27%)	22 (19%)	25 (21%)	116
Pups[‡] (% Observed)	0 (0%)	10 (36%)	15 (53%)	3 (11%)	28	0 (0%)	7 (32%)	10 (45%)	5 (23%)	22

[a]Derived from expected Mendelian ratios

[†]Chi-square test showed no signifiant deviation from the expected Mendelian ratio in both *Hesx1*$^{Cre/+}$ *x Kras*$^{G12D/+}$ (p=0.6598) and *Hesx1*$^{Cre/+}$ *x Braf*$^{V600E/+}$ (p=0.1596).

[‡]Chi-square test showed a statistically significant deviation from the expected 25% ratio in both *Hesx1*$^{Cre/+}$ *x Kras*$^{G12D/+}$ (p=0.0033) and *Hesx1*$^{Cre/+}$ *x Braf*$^{V600E/+}$ (p=0.0219).

Table 4.1. Genotypes obtained from *Hesx1*$^{Cre/+}$ x *Kras*$^{G12D/+}$ and *Hesx1*$^{Cre/+}$ x *Braf*$^{V600E/+}$ intercrosses

Staining of *Hesx1*$^{Cre/+}$*; Braf*$^{V600E/+}$ and *Hesx1*$^{Cre/+}$*; Kras*$^{G12D/+}$ mutants with Haematoxylin and Eosin at 10.5 dpc revealed no morphological differences in RP, relative to control littermates (Figure 4.2 A-C). However, evidence for morphological defects were initially apparent at 12.5 dpc where anterior lobe

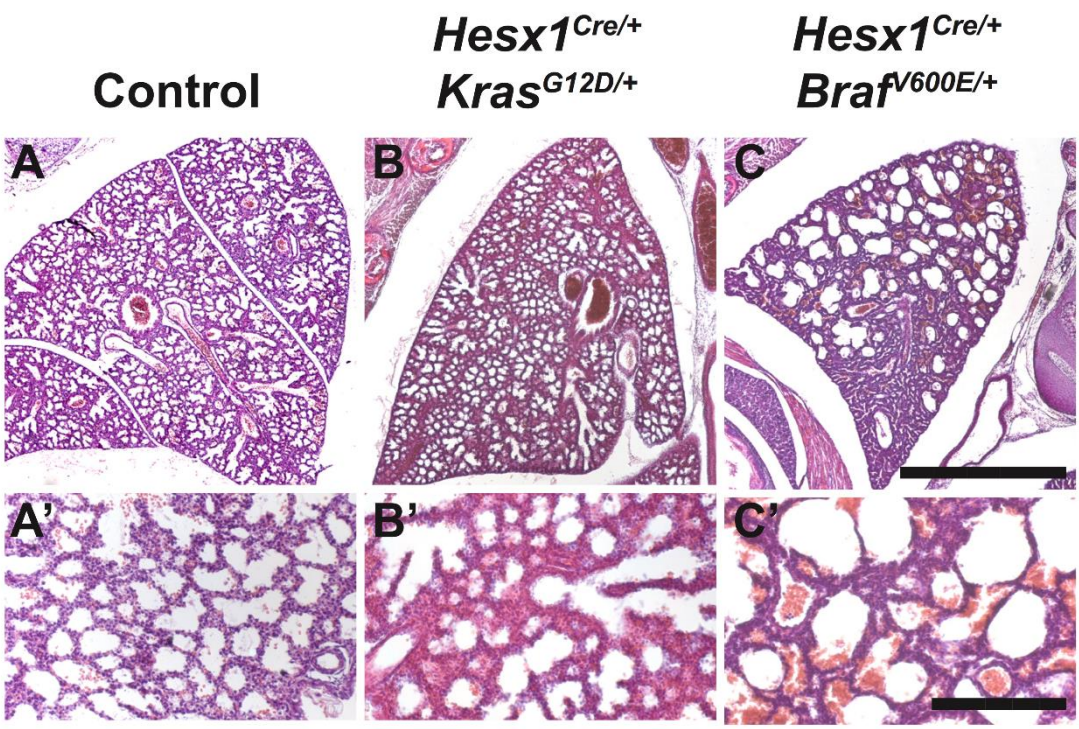

Figure 4.1. Abnormal morphogenesis is observed in the lungs in *Hesx1$^{Cre/+}$; Braf$^{V600E/+}$* and *Hesx1$^{Cre/+}$; Kras$^{G12D/+}$* mutants. (**A**-**C**) Haematoxylin and eosin staining of lung tissue at 18.5 dpc in *Hesx1$^{Cre/+}$; Braf$^{V600E/+}$* (n=3), *Hesx1$^{Cre/+}$; Kras$^{G12D/+}$* (n=3) and control embryos (n=2) showing expansion of the airway structures. Note that they are especially evident in *Hesx1$^{Cre/+}$; Braf$^{V600E/+}$* mutants. Scale bar is 200μm (**A'**-**C'**) Inserts show higher magnification of terminal airways and alveoli. Scale bar is 100μm.

hyperplasia was observed and this was accentuated by 14.5 dpc (Figure 4.2 D-I). By 18.5 dpc this phenotype was much more pronounced and a fully penetrant phenotype consisting of server hyperplasia of the anterior lobe with branched pituitary cleft was seen in all analysed embryos (Figure 4.2 J-L). By analysing cellcounts of pituitaries dissociated at 18.5 dpc it was observed that there were a total of 96,000±2.7% cells in the *Hesx1$^{Cre/+}$; Braf$^{V600E/+}$* mutant ($p \leq 0.01$), 101,666±4.3% cells in the *Hesx1$^{Cre/+}$;Kras$^{G12D/+}$* mutant ($p \leq 0.01$) and 67,200±3.5% cells in control wild-type mice (Figure 4.2 M). The hyperplasic phenotype observed appeared to be restricted tothe anterior lobe

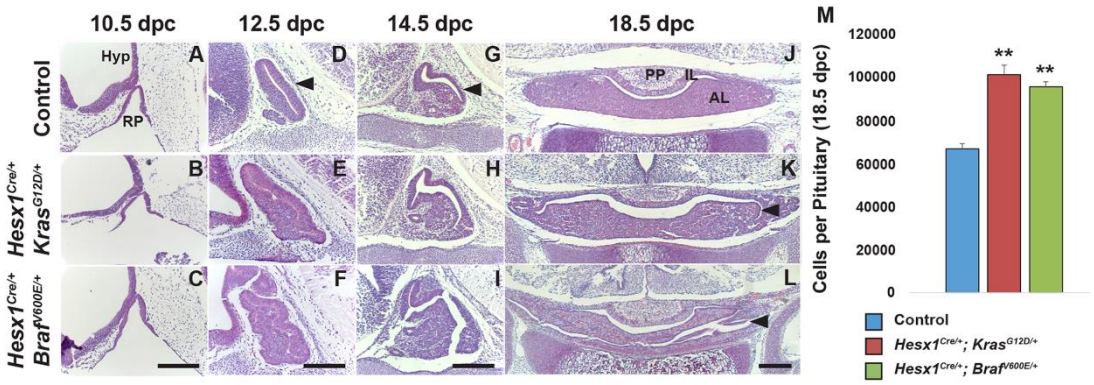

Figure 4.2. Abnormal pituitary morphogenesis in *Hesx1$^{Cre/+}$; Kras$^{G12D/+}$* and *Hesx1$^{Cre/+}$; Braf$^{V600E/+}$* mutants. Haematoxylin and Eosin staining of sagittal (**A**-**I**) or transverse (**J**-**L**) histological sections of the embryonic pituitary gland during development in control and mutant embryos; genotypes and stages are indicated. (**A**-**C**) At 10.5 dpc, Rathke's pouch (RP) is comparable morphologically between genotypes. (**D**-**I**) The embryonic pituitary is larger and dysmorphic in the mutant compared with the control pituitary at 12.5 and 14.5 dpc (arrowheads). (**J**-**L**) At 18.5 dpc, the pituitary cleft is expanded and tortuous in the mutant pituitaries (arrowheads in **K**,**L**) compared with the control (**J**). The posterior pituitary (PP) is comparable between genotypes. AL, anterior lobe; IL, intermediate lobe. (**M**) Quantification of total numbers of cells in the control, *Hesx1$^{Cre/+}$; Kras$^{G12D/+}$* and *Hesx1$^{Cre/+}$; Braf$^{V600E/+}$* pituitaries at 18.5 dpc, showing a significant increase in the mutants (**P≤0.01, Student's t-test). Representative H&E images shown from 3 mice per genotype per timepoint. Quantitifcation of number of cell per pituitary performed on 4 mice from each of the indicated genotypes. Data are mean±s.e.m. Scale bars: 200 μm.

and the posterior lobe for morphologically normal in both mutant genotypes (Figure 4.2 J-L). The induction of cellular senescence was investigated in 18.5 dpc *Hesx1$^{Cre/+}$; Braf$^{V600E/+}$* and *Hesx1$^{Cre/+}$; Kras$^{G12D/+}$* mutants by IF analysis for the senescence effectors p16 and p21. Unexpectedly, there was no difference in the levels of these markers between mutant or control genotypes (Figure 4.3).

Together, these data suggest that the induction of RP is normal in *Hesx1*$^{Cre/+}$; *Braf*$^{V600E/+}$ and *Hesx1*$^{Cre/+}$; *Kras*$^{G12D/+}$ mutants. However, there appears to be an increase in proliferation that leads to anterior pituitary hyperplasia by the end of gestation but absence of canonical markers of cellular senescence.

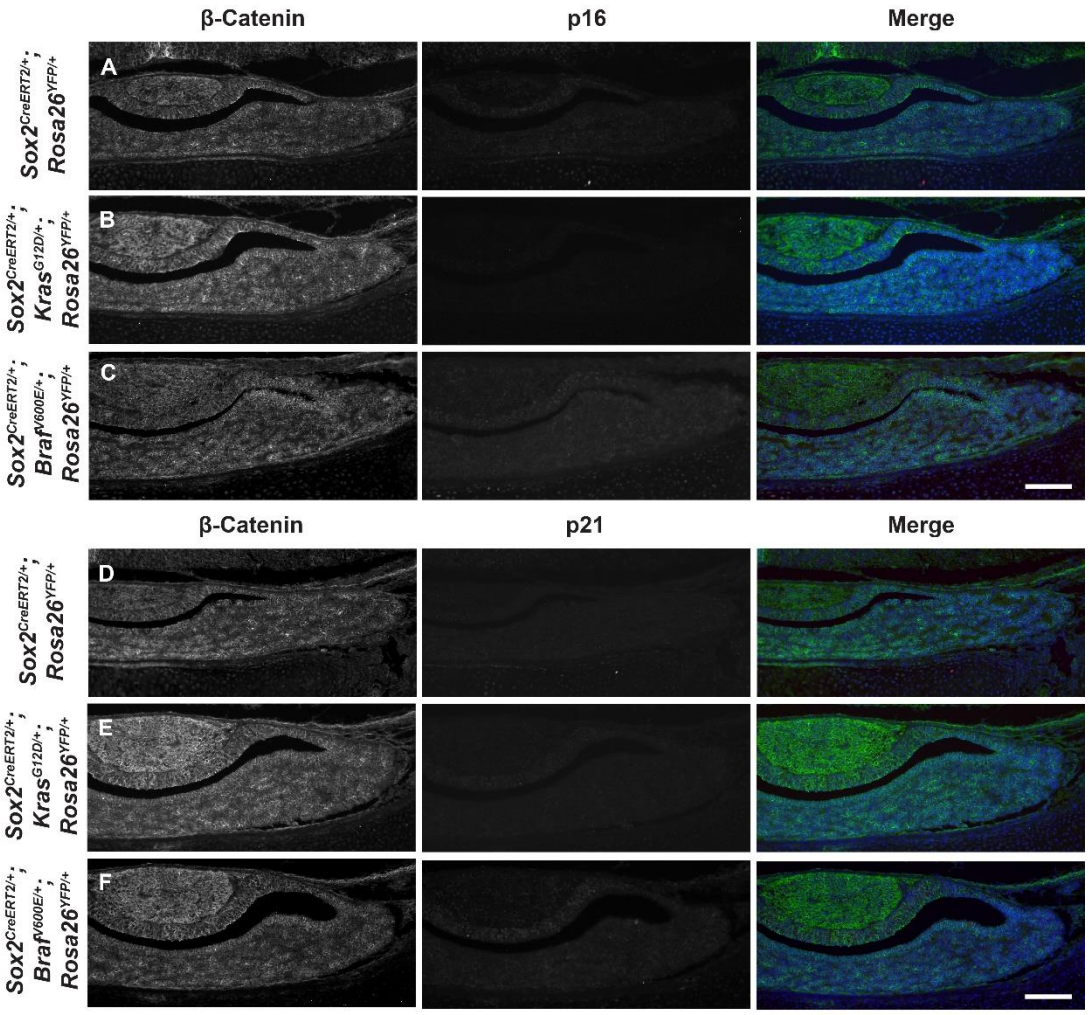

Figure 4.3. Absence of senescence-associated markers in *Hesx1*$^{Cre/+}$; *Braf*$^{V600E/+}$ and *Hesx1*$^{Cre/+}$; *Kras*$^{G12D/+}$ mutants. IF staining against the cellular senescence effectors p21 and p16 on histological sections of control and mutant pituitaries at 18.5 dpc. **(A-F)** p21 and p16 are not expressed in control or mutant pituitaries. Scale bars; 200μm. Representative immunofluorescence images from *Hesx1*$^{Cre/+}$; *Braf*$^{V600E/+}$ (n=4), *Hesx1*$^{Cre/+}$; *Kras*$^{G12D/+}$ (n=4) and control pituitaries (n=3).

4.2.1.2 The MAPK/ERK pathway is regulated in both a temporal and spatial manner during normal pituitary development

In order to examine the expression of *Braf* and *Kras* mRNA as well as the protein expression of pERK1/2, to determine activated MAPK signaling, *in situ* hybridisation and IF was performed on histological sections of wild type and mutant embryos. *Braf* and *Kras* mRNA were observed in the prospective hypothalamus, including the posterior diencephalon and pre-optic area, in addition to the developing RP at 10.5 dpc in wild type embryos (Figure 4.4 A, D). Later in development, at 14.5 dpc these transcripts were detected throughout the developing pituitary, including the infundibulum, periluminal epithelium and anterior lobe (Figure 4.4 B, E). Later still, *Braf* and *Kras* expression was restricted to the periluminal area, including the intermediatelobe and marginal zone, with scattered cells dispersed throughout the anterior lobe at 18.5 dpc (Figure 4.4 C, F).

Examination of *Braf* transcripts in *Hesx1*$^{Cre/+}$*; Braf*$^{V600E/+}$ (Figure 4.5) and *Kras* transcripts in *Hesx1*$^{Cre/+}$*; Kras*$^{G12D/+}$ (data not shown) mutants demonstrated that they were comparable to those in wild-type embryos. Interestingly, the expression patterns of these transcripts did not correlate with pERK1/2 expression at all analysed embryonic stages. pERK1/2 expression was very similar between control and mutant genotypes at 10.5 dpc, both in the developing hypothalamus and in RP (Figure 4.6 A, E, I), which overlaps with the expression of *Braf* and *Kras* mRNA (Figure 4.2 A-C). However, mutant and wild type embryos at 12.5 and 14.5 dpc showed very few pERK1/2 cells, in contrast to the broad expression of *Braf* and *Kras* mRNA (Figure 4.6

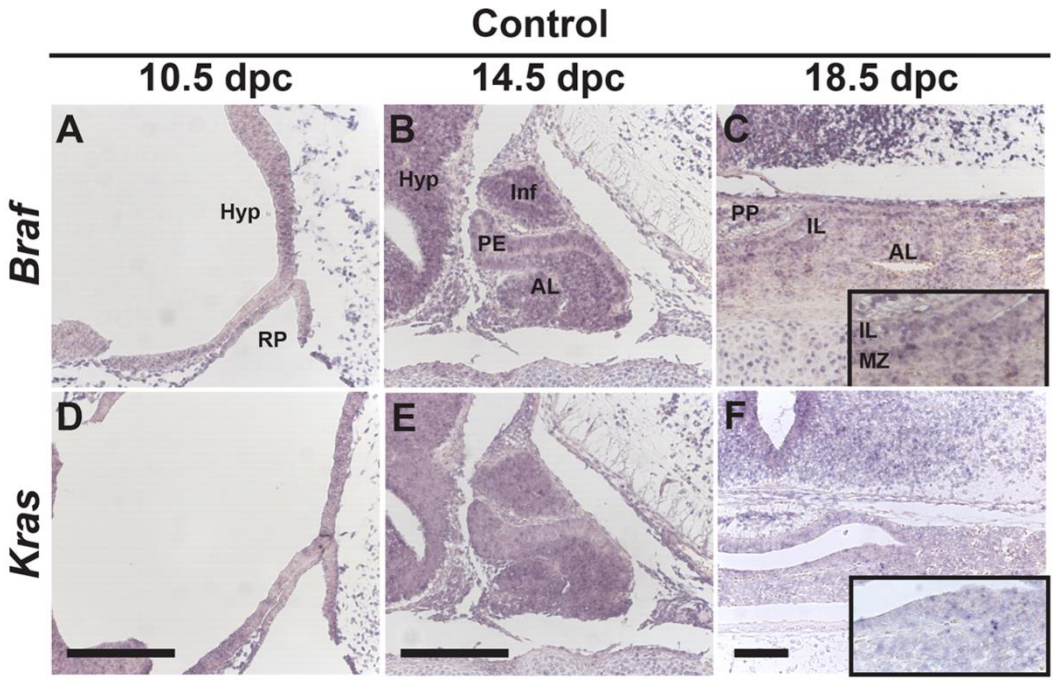

Figure 4.4. *Braf* and *Kras* mRNA is detected in the developing hypothalamus and pituitary gland. *In situ* hybridisation using antisense riboprobes against *Braf* and *Kras* mRNA on histological sections of developing wild-type pituitaries (3 embryos were analysed for each probe per embryonic stage). (**A**,**D**) At 10.5 dpc, overall expression of *Braf* and *Kras* is weakly detected in the prospective hypothalamus (Hyp) and Rathke's pouch (RP). (**B**,**E**) At 14.5 dpc, strong expression is detected in the infundibulum (Inf), hypothalamus (Hyp), periluminal epithelium (PE) and developing anterior lobe (AL). (**C**,**F**) At 18.5 dpc, expression is detected in specific cells within the posterior pituitary (PP), intermediate lobe (IL) and the parenchyma of the anterior lobe (AL), including the marginal zone (MZ). Insets in C,F show the IZ and MZ at higher magnification. Scale bars: 200 μm.

B, C, F, G, J, K), as well as BrafV600E mutant protein throughout the *Hesx1*$^{Cre/+}$*; Braf*$^{V600E/+}$ pituitary (Figure 4.5 D-F). pERK1/2 expression was noticeably increased at 18.5 dpc in both *Hesx1*$^{Cre/+}$*; Braf*$^{V600E/+}$ and *Hesx1*$^{Cre/+}$*; Kras*$^{G12D/+}$ mutants relative to control pituitaries (Figure 4.6 D, H, L), which correlated with the previous *in situ* hybridisation observations (Figures 4.4 and 4.5).

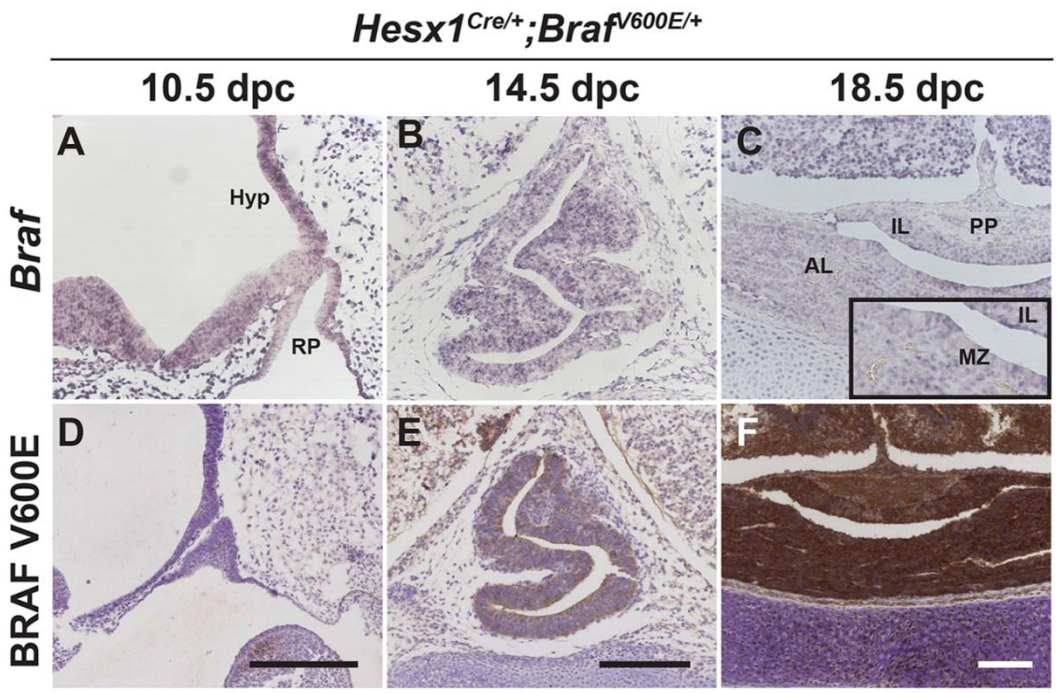

Figure 4.5. *Braf* mRNA and BRAF-V600E protein are expressed in the developing pituitary in *Hesx1*$^{Cre/+}$; *Braf*$^{V600E/+}$ mutants. *In situ* hybridisation using *Braf* antisense riboprobes (**A**-**C**) and immunohistochemistry against BRAF-V600E mutant protein (**D**-**F**) on histological sections of *Hesx1*$^{Cre/+}$; *Braf*$^{V600E/+}$ embryos at the indicated stages. (**A**-**C**) *Braf* mRNA expression is detected in the hypothalamic neuroepithelium (Hyp) and developing pituitary at all stages analysed, with a similar expression pattern to the wild-type embryos (Fig. 4.4 A-C). (**D**-**F**) At 10.5 dpc, only a few cells express the BRAF-V600E protein in the developing Rathke's pouch (RP), but numbers increased between 12.5 and 18.5 dpc. Inset in C shows the IL and MZ at higher magnification. 3 *Hesx1*$^{Cre/+}$; *Braf*$^{V600E/+}$ embryos were analysed at each indicated timepoint. Scale bars: 200 μm.

These expression studies demonstrate that the MAPK pathway is regulated in a temporal fashion, with the greatest levels observed at 10.5 and 18.5 dpc. Furthermore, the majority of the cells which have activated the pathway are found in the marginal zone, an area enriched for Sox2+ pituitary stem/progenitor cells (Cynthia Lilian Andoniadou et al. 2013).

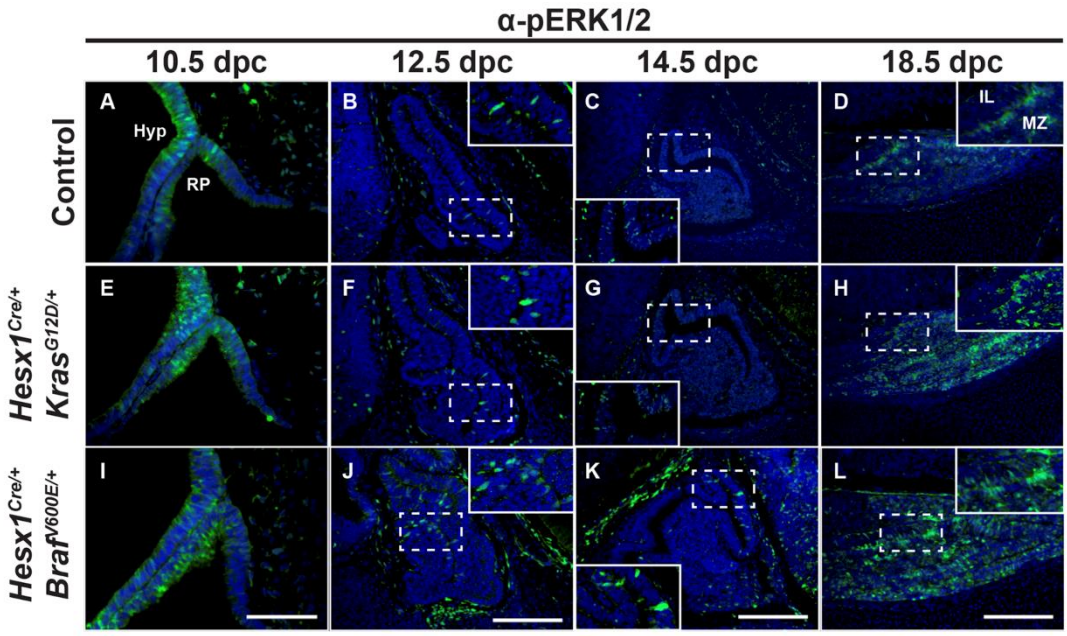

Figure 4.6. Temporal and spatial regulation of pERK1/2 expression developing pituitary. IHC staining against pERK1/2 on histological sections of control and mutant pituitaries; genotypes and stages are indicated. (**A**-**D**) Abundant pERK1/2^{+} cells are detected in the hypothalamus (Hyp) and Rathke's pouch (RP) at 10.5 dpc, but only very few cells express pERK1/2 at 12.5 and 14.5 dpc. At 18.5 dpc, most of the signal is restricted to the intermediate lobe (IL) and marginal zone (MZ) of the anterior lobe. (**E**-**L**) A similar expression pattern is observed in both *Hesx1$^{Cre/+}$; Kras$^{G12D/+}$* (**E**-**H**) and *Hesx1$^{Cre/+}$; Braf$^{V600E/+}$* (**I**-**L**) mutant pituitaries. However, the pERK1/2 signal is markedly increased in 18.5 dpc pituitaries (**H**,**L**) relative to the control (**D**). Insets show the outlined areas at higher magnification. Representative immunofluorescence images from *Hesx1$^{Cre/+}$; Braf$^{V600E/+}$* (n=4), *Hesx1$^{Cre/+}$; Kras$^{G12D/+}$* (n=4) and control pituitaries (n=3). Scale bars: 200 μm.

4.2.1.3 Over-activation of the MAPK/ERK pathway results in abnormal terminal differentiation of specific hormone-producing cells

In order to ascertain the effects that overactivation of the MAPK pathway has on RP induction and pituitary cell lineage commitment and differentiation, an expression

analysis was performed at 10.5, 14.5 and 18.5 in both mutant and control genotypes.

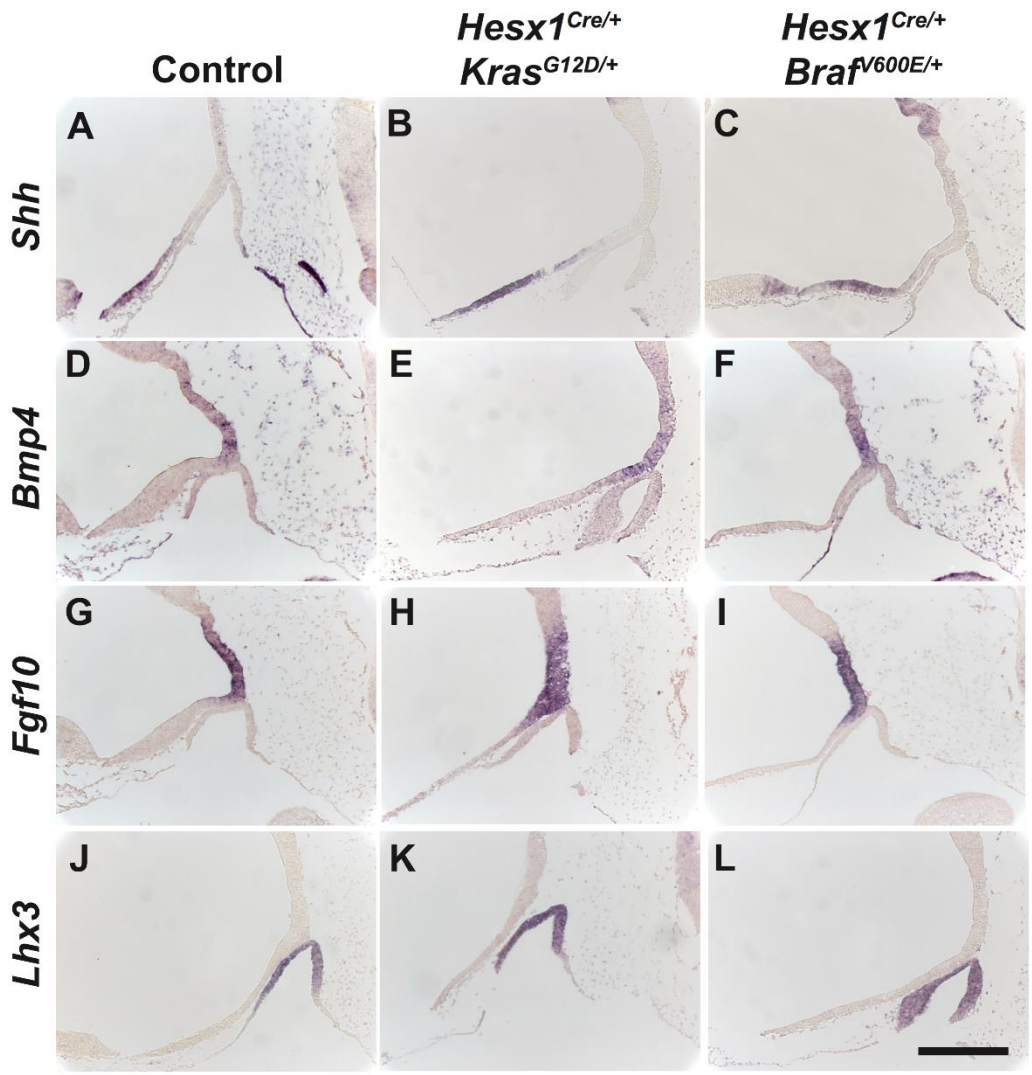

Figure 4.7. Normal Rathke's pounch specification in *Hesx1*$^{Cre/+}$; *Braf*$^{V600E/+}$ and *Hesx1*$^{Cre/+}$; *Kras*$^{G12D/+}$ mutants. *In situ* hybridisation on sagittal histological sections of 10.5 dpc embryos; probes and genotypes are indicated. Note the comparable expression of *Shh*, *Fgf10* and *Bmp4* in the prospective hypothalamus and *Lhx3* in Rathke's pouch, between mutant and control embryos. 4 embryos were analysed for each of the genotypes per probe. Scale bar is 200μm.

RP induction was examined through the expression of *Fgf10*, *Bmp4* and *Shh* in the hypothalamus, as they are required for the activation of *Lhx3* in the progenitors of

RP (Ericson et al. 1998; Treier et al. 1998; Treier, O'Connell, a Gleiberman, et al. 2001). The expression domain of these markers was not distinguishable between mutant and control genotypes at 10.5 dpc. Therefore, suggesting that early RP induction is normal in embryos *Hesx1*$^{Cre/+}$*; Braf*$^{V600E/+}$ and *Hesx1*$^{Cre/+}$*; Kras*$^{G12D/+}$ (Figure 4.7)

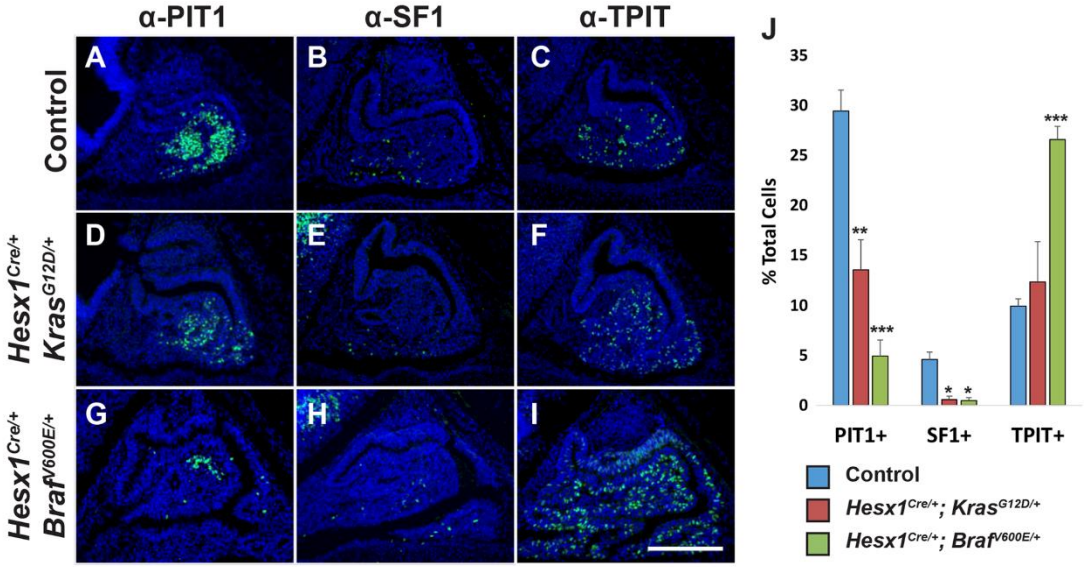

Figure 4.8. **Cell-lineage commitment is disrupted in *Hesx1*$^{Cre/+}$*; Kras*$^{G12D/+}$ and *Hesx1*$^{Cre/+}$*; Braf*$^{V600E/+}$ mutants**. IHC (green) against the commitment markers PIT1, SF1 and TPIT on sagittal histological sections of mutant and control embryos at 14.5 dpc. (**A**-**I**) The expression of TPIT (**A**,**D**,**G**) and SF1 (**B**,**E**,**H**) are markedly reduced in the mutant pituitary, especially in the *Hesx1*$^{Cre/+}$*; Braf*$^{V600E/+}$ mutant, relative to the control. In contrast, TPIT expression is elevated in the mutant pituitary, more apparently in the *Hesx1*$^{Cre/+}$*; Braf*$^{V600E/+}$ genotype (**C**,**F**,**I**). Blue staining is DAPI. (**J**) Quantification analyses demonstrate the significant reduction of PIT1+ and SF1+ cells in both mutants relative to the control pituitary, but the increase of TPIT+ cells is significant only in the *Braf* mutants (*P≤0.05, **P≤0.01, ***P≤0.001, Student's t-test). Data are mean±s.e.m. Representative immunofluorescence images from *Hesx1*$^{Cre/+}$*; Braf*$^{V600E/+}$ (n=6), *Hesx1*$^{Cre/+}$*; Kras*$^{G12D/+}$ (n=5) and control pituitaries (n=5). Cell count quantification performed on *Hesx1*$^{Cre/+}$*; Braf*$^{V600E/+}$ (n=6), *Hesx1*$^{Cre/+}$*; Kras*$^{G12D/+}$ (n=5) and control pituitaries (n=5). Scale bar: 200 μm.

Pituitary cell lineage commitment was examined at 14.5 dpc through IF for POU1F1 (PIT1), NR5A1 (SF1) and TPIT, which are markers of anterior pituitary cell-lineage committed precursors. Such an analysis revealed defects that were evident in both mutant genotypes, relative to control embryos. In *Hesx1*$^{Cre/+}$*; Braf*$^{V600E/+}$ mutants the proportion of PIT1+ cells was reduced significantly relative to total cells (control, 29%; *Braf* mutant, 4%; *p*=0.001), SF1 + cells were almost undetectable (control, 4%; *Braf* mutant, 0.5%; *p* ≤0.05) and the number of TPIT + cells were expanded (control, 10%; *Braf* mutant, 26%; *p*=0.001) (Figure 4.8). *Hesx1*$^{Cre/+}$*; Kras*$^{G12D/+}$ mutants showed significant reduction of both PIT1 + and SF1 + cell lineage precursors (PIT1 +: control, 29%; *Kras* mutant, 13%; p ≤0.01; SF1 +: control, 4.5%; *Kras* mutant, 0.6%; p≤0.05). However this was less pronounced than in *Hesx1*$^{Cre/+}$*; Braf*$^{V600E/+}$ mutants. Quantification of the number of TPIT + cells found that they were similar between mutants and controls (control, 10%; *Kras* mutant, 12%; p=0.6156) (Figure 4.8).

Terminal differentiation into hormone producing cells was also determined by IHC. Staining for hormonal cell markers was performed and the total number of these cells per pituitary were calculated by adjusting the proportion of each cell types to the total number of cells in a pituitary gland of either *Hesx1*$^{Cre/+}$*; Braf*$^{V600E/+}$, *Hesx1*$^{Cre/+}$*;Kras*$^{G12D/+}$ or control genotype at 18.5 dpc (See section 2.9.2). The purpose of this approach was to avoid bias in the quantitative analysis of the cell type proportions due to the observed pituitary hyperplasia in mutant genotypes (e.g. the total cell numbers of a particular hormonal cell type could be the same in both mutant and controls genotypes but due to the hyperplasia they could be distributed in more histological sections in the mutant pituitary, and therefore seem proportionally reduced). This analysis revealed that abnormal hormonal terminal differentiation was found in

both mutant genotypes, however *Hesx1*$^{Cre/+}$*; Braf*$^{V600E/+}$ mutant pituitary were more severely affected (Figure 4.9 A-R). Analysis of the *Hesx1*$^{Cre/+}$*; Braf*$^{V600E/+}$ mutant pituitaries showed that numbers of somatotrophs (GH+) (wild type, 23560; *Braf* mutant, 3185), lactotrophs (PRL+) (wild type, 17604; *Braf* mutant, 3233) and thyrotrophs (TSH+) (wild type, 4043; *Braf* mutant, 664) (i.e. the Pit1 cell lineage) were significantly reduced, and gonadotrophs (FSH +) (wild type, 6134; *Braf* mutant, 1686) and (LH+) (wild type, 1564; *Braf* mutant, 23) were almost completely absent, relative to controls (Figure 4.9 S). ISH against αGSU (wild type, 6861; *Braf* mutant, 2977) also confirmed the reduction of thyrotrophs and gonadotrophs in *Braf* mutant pituitaries (Figure 4.10). Interestingly, the numbers of corticotrophs (ACTH +) (wild type, 15958; *Braf* mutant, 28778) appeared to be elevated significantly in *Hesx1*$^{Cre/+}$*; Braf*$^{V600E/+}$ mutants (Figure 4.9 P, R, S). Abnormalities in terminal differentiation were also evident in Hesx1$^{Cre/+}$; Kras$^{G12D/+}$ mutant pituitaries, albeit to a lesser extent than in Hesx1Cre/+;BrafV600E/+ mutants (Figure 4.9 A- R). Specifically, a reduction in the numbers of thyrotrophs (wild type, 4043; Kras mutant, 1371), gonadotrophs (FSH +) (wild type, 6134; *Kras* mutant, 4044) and lactotrophs (wild type, 17604; *Kras* mutant, 6710) were observed (Figure 4.9 S). Analogously to the *Hesx1*$^{Cre/+}$*;Braf*$^{V600E/+}$ mutants, increased corticotroph counts were also seen in *Hesx1*$^{Cre/+}$*;Kras*$^{G12D/+}$ mutant pituitaries (wild type, 15958; *Kras* mutant, 21370) (Figure 4.9 P,Q,S). Moreover, by using qRT-PCR to perform absolute quantification of mRNA transcripts in *Hesx1*$^{Cre/+}$*; Braf*$^{V600E/+}$, *Hesx1*$^{Cre/+}$*; Kras*$^{G12D/+}$ and control pituitaries isolated at 18.5 dpc, it was observed that a significant reduction in Gh and a trend towards increased Acth expression was observed in both of the mutant genotypes (Figure 4.9 T), which was in agreement with the cell quantifications.

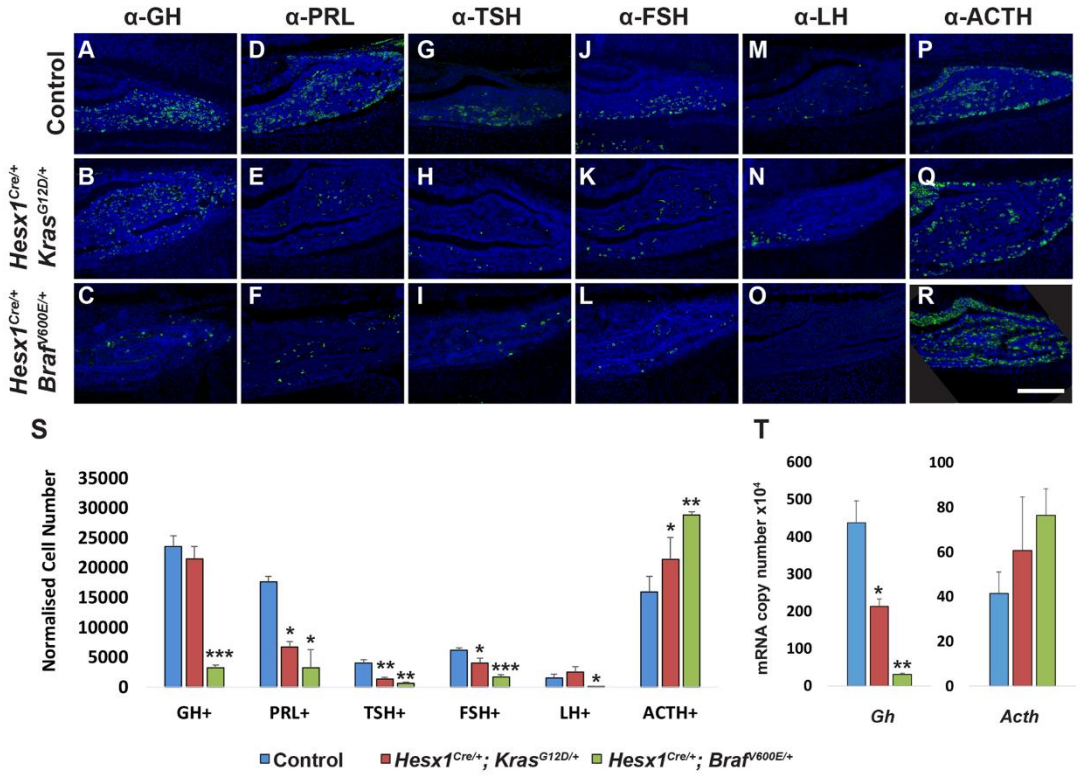

Figure 4.9. Terminal differentiation of hormone-producing cells is impaired in *Hesx1$^{Cre/+}$; Kras$^{G12D/+}$* and *Hesx1$^{Cre/+}$; Braf$^{V600E/+}$* mutants. IHC against pituitary hormones (green) on transverse histological sections of mutant and control embryos at 18.5 dpc. (**A**-**R**) Numbers of GH+ (somatotrophs) (**A**-**C**), PRL+ (lactotrophs) (**D**-**F**), TSH+ (thyrotrophs) (**G**-**I**), as well as FSH+ and LH^{+} (gonadotrophs) cells (**J**-**O**) appear reduced in the *Braf* and *Kras* mutants relative to the control pituitary. Blue staining is DAPI. (**P**-**R**) ACTH^{+} cell numbers (corticotrophs and melanotrophs) look increased in the mutant pituitaries compared with the control. (**S**) Quantitative analyses demonstrate a significant reduction of all of the hormone-producing cells in the *Hesx1$^{Cre/+}$; Braf$^{V600E/+}$* mutant pituitary, except for ACTH+ cells, which are markedly increased relative to controls. *Hesx1$^{Cre/+}$; Kras$^{G12D/+}$* mutant pituitaries show a significant decrease in the number of only PRL+, TSH+ and FSH+ cells, and ACTH+ cell number is also increased. (**T**) Absolute quantitative RT-PCR analysis of *Gh* and *Acth* mRNA expression in mutant and control pituitaries at 18.5 dpc. Significance is only reached for *Gh* expression, but there is a trend towards an increase in *Acth* expression (*P≤0.05, **P≤0.01, ***P≤0.001, Student's t-test). Representative immunofluorescence images from *Hesx1$^{Cre/+}$; Braf$^{V600E/+}$* (n=6), *Hesx1$^{Cre/+}$; Kras$^{G12D/+}$* (n=6) and control pituitaries (n=6). Cell count quantification performed on *Hesx1$^{Cre/+}$; Braf$^{V600E/+}$* (n=6), *Hesx1$^{Cre/+}$; Kras$^{G12D/+}$* (n=6) and control pituitaries (n=6). Absolute quantitative PCR performed on 3 embryonic pituitaries per genotype. Data are mean±s.e.m. Scale bar: 200 μm.

These analyses show that the cell-lineage commitment at 14.5 dpc and terminal differentiation at 18.5 dpc were significantly disrupted following activation of the MAPK pathway in pituitary progenitor cells, with a global reduction in hormone-producing cells by the end of development.

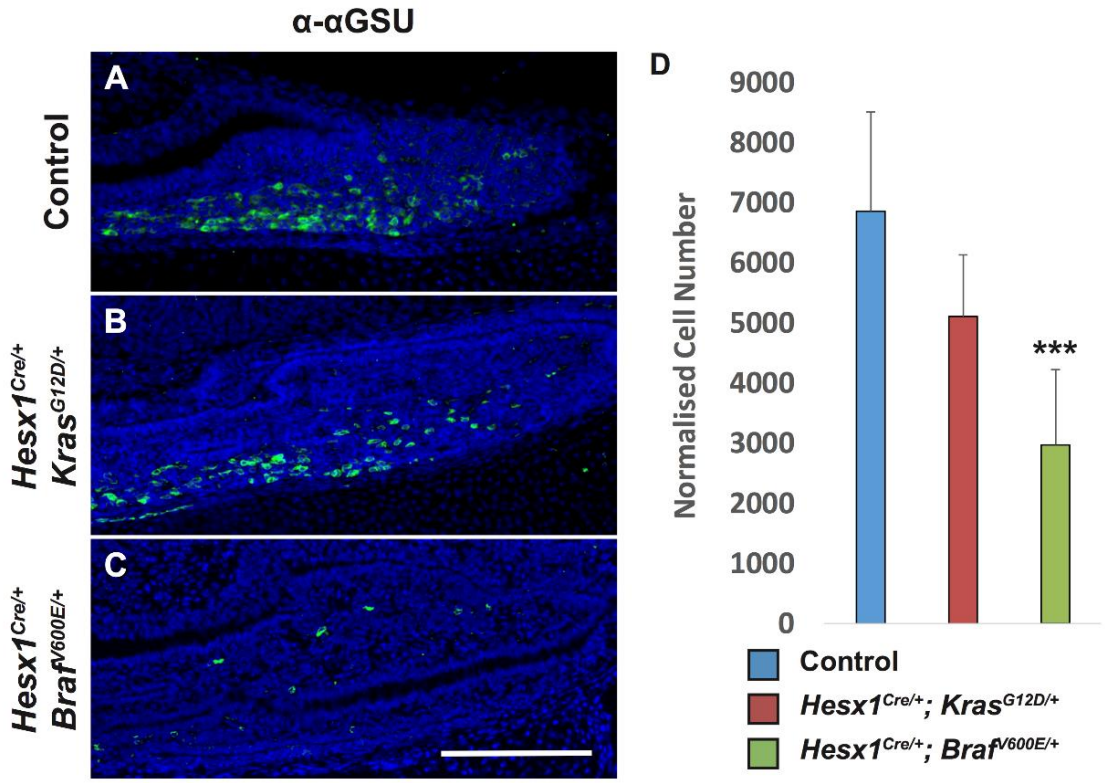

Figure 4.10. Reduced αGSU expression in *Hesx1*$^{Cre/+}$; *Braf*$^{V600E/+}$ and *Hesx1*$^{Cre/+}$; *Kras*$^{G12D/+}$ mutants. (**A**) IHC on transverse histological sections revealing the expression of αGSU in mutants and a control embryo. (**B**) Quantitative analysis of αGSU+ cells in mutant and control pituitaries revealing a reduction in total numbers of αGSU+ cells, which reaches statistical significance for the *Braf*-deficient mutant. Representative immunofluorescence images from *Hesx1*$^{Cre/+}$; *Braf*$^{V600E/+}$ (n=6), *Hesx1*$^{Cre/+}$; *Kras*$^{G12D/+}$ (n=6) and control pituitaries (n=6). Cell count quantification performed on *Hesx1*$^{Cre/+}$; *Braf*$^{V600E/+}$ (n=6), *Hesx1*$^{Cre/+}$; *Kras*$^{G12D/+}$ (n=6) and control pituitaries (n=6). Scale bar is 200μm.

4.2.1.4 Increased proliferation is observed in the developing pituitaries of *Hesx1$^{Cre/+}$;Braf$^{V600E/+}$* and *Hesx1$^{Cre/+}$;Kras $^{G12D/+}$* embryos

The effects of MAPK pathway activation on the RP progenitor proliferation was ascertained at 12.5, 14.5 and 18.5 dpc in both of the mutant genotypes and control pituitaries. This was achieved by performing IF against Ki67, which marks cells in the cell cycle, to obtain a quantitative analysis of the proliferative index. This demonstrated that there was no difference at 12.5 dpc, with around 70% of pituitary cells being Ki67+ (Figure 4.11 A-C,J). Analysis of later stage embryos (14.5 and 18.5 dpc), however, did result in a significant difference in proliferation in both Hesx1Cre/+; BrafV600E/+ and Hesx1Cre/+; KrasG12D/+ pituitaries, when compared to control pituitaries (Figure 4.11 D-J).

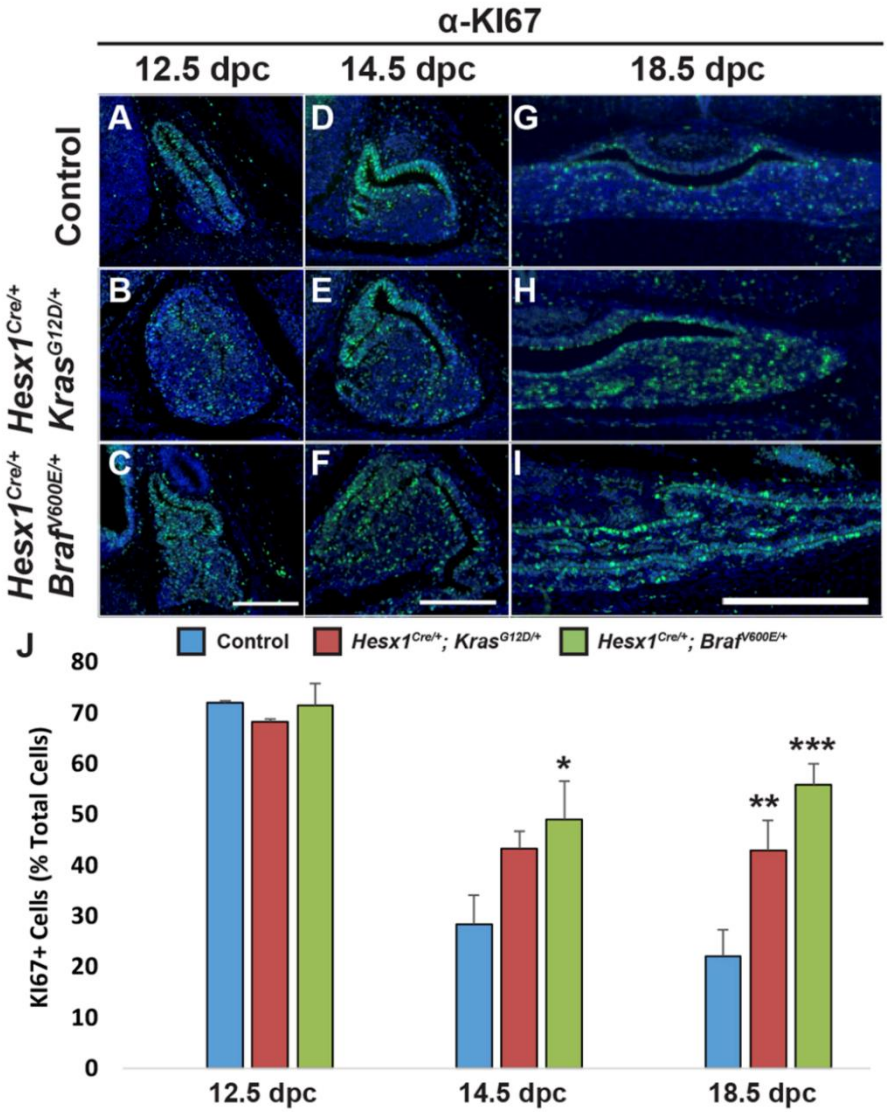

Figure. 4.11. Increased proliferation in the *Hesx1$^{Cre/+}$; Kras$^{G12D/+}$* and *Hesx1$^{Cre/+}$; Braf$^{V600E/+}$* mutant pituitaries. (**A**-**I**) IHC staining against Ki67 (green) on histological sections of mutant and control embryos; genotypes and stages are indicated. (**J**) Quantitative analyses of the number of Ki67+ cells out of the total DAPI+ cells (blue) demonstrate a significant increase in the proliferation index in the *Hesx1$^{Cre/+}$; Kras$^{G12D/+}$* at 18.5 dpc and *Hesx1$^{Cre/+}$; Braf$^{V600E/+}$* at 14.5 and 18.5 dpc (*P≤0.05, **P≤0.01, ***P≤0.001, Student's t-test). Representative immunofluorescence images from *Hesx1$^{Cre/+}$; Braf$^{V600E/+}$* (12.5 dpc n=3, 14.5 dpc n=5, 18.5 dpc n=6), *Hesx1$^{Cre/+}$; Kras$^{G12D/+}$* (12.5 dpc n=3, 14.5 dpc n=4, 18.5 dpc n=6) and control pituitaries (12.5 dpc n=3, 14.5 dpc n=4, 18.5 dpc n=5). Cell count quantification performed on *Hesx1$^{Cre/+}$; Braf$^{V600E/+}$* (12.5 dpc n=3, 14.5 dpc n=5, 18.5 dpc n=6), *Hesx1$^{Cre/+}$; Kras$^{G12D/+}$* (12.5 dpc n=3, 14.5 dpc n=4, 18.5 dpc n=6) and control pituitaries (12.5 dpc n=3, 14.5 dpc n=4, 18.5 dpc n=5). Data are mean±s.e.m. Scale bars: 200 μm.

Interestingly, while the proliferative index fell gradually in the control embryos from 72% at 12.5 dpc to 22% at 18.5 dpc, this was not seen to the same magnitude in either of the mutant genotypes. Towards the end of gestation, at 18.5 dpc, the proliferative index was reduced to only 42% and 55% in the *Hesx1*$^{Cre/+}$*; Kras*$^{G12D/+}$ and *Hesx1*$^{Cre/+}$*; Braf*$^{V600E/+}$ mutant genotypes, respectively (Figure 4.11 J). This increased proliferation was confirmed by also performing IF against CyclinD2, a protein important for controlling G1/S progression, that is known to be expressed in the progenitors of RP which are found in the periluminal epithelium (Bilodeau et al. 2009) (Figure 4.12 A-C). The proportion of CyclinD2-expressing cells were quantified, revealing a trend toward increased numbers in both of the mutant genotypes, relative to controls (Figure 4.12 D).

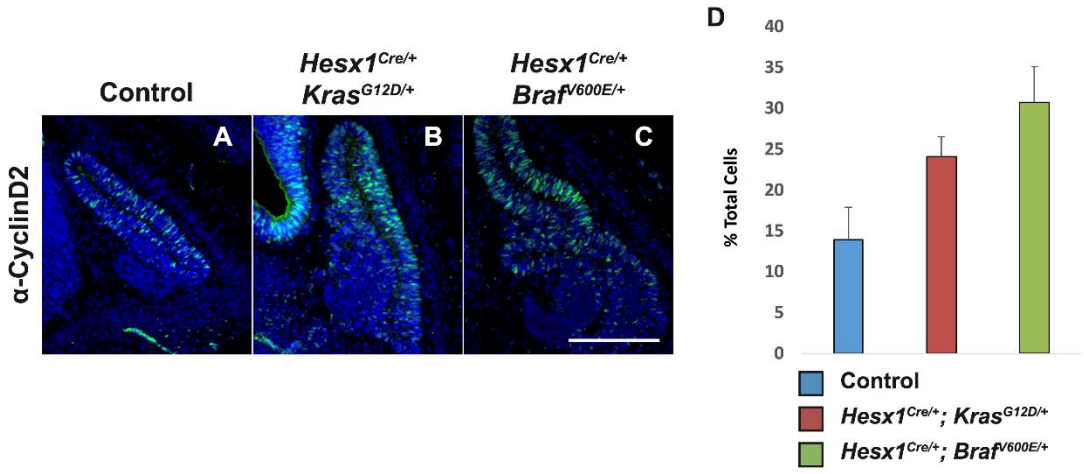

Figure 4.12. Increased cyclin D2 expression in *Hesx1*$^{Cre/+}$*; Braf*$^{V600E/+}$ and *Hesx1*$^{Cre/+}$*; Kras*$^{G12D/+}$ mutants. (**A**) immunostaining on sagittal histological sections revealing the elevated expression of cyclin D2 in the periluminal epithelium of Rathke's pouch in the mutants relative to the control embryo. (**B**) Quantification of cyclin D2+ cells as a proportion of the total DAPI+ nuclei of the perilumal epithelium showing a higher proportion of expressing cells in the mutant embryos relative to the controls. Representative immunofluorescence images from *Hesx1*$^{Cre/+}$*; Braf*$^{V600E/+}$ (n=3), *Hesx1*$^{Cre/+}$*; Kras*$^{G12D/+}$ (n=3) and control pituitaries (n=3). Cell count quantification performed on *Hesx1*$^{Cre/+}$*; Braf*$^{V600E/+}$ (n=3), *Hesx1*$^{Cre/+}$*; Kras*$^{G12D/+}$ (n=3) and control pituitaries (n=3) Scale bar is 200μm.

4.2.1.5 MAPK pathway activation results in expansion of the pituitary stem cell compartment and alters the balance between self-renewal and differentiation

As the expression of pERK1/2 was concentrated in the periluminal epithelium, where an increase in proliferation markers was also observed, the Sox2+ pituitary stem/progenitor population was assessed to determine if they were behaving aberrantly in response to activated MAPK signaling. To achieve this, pituitaries from control, *Hesx1*$^{Cre/+}$*; Braf*$^{V600E/+}$ and *Hesx1*$^{Cre/+}$*; Kras*$^{G12D/+}$ embryos were analysed by IF for Sox2 expression at the previously analysed developmental stages. Quantification of Sox2+ cells at 12.5 dpc revealed that their proportion was similar between control and mutant genotypes, with around 80% of pituitary cells expressing Sox2 (Figure 4.13 A-C, J). As development progressed the number of Sox2+ cells in control pituitaries reduced to around 21% by the end of gestation at 18.5 dpc (p=0.0004) **(**Figure 4.13 G, J). However, in the mutant pituitaries, high proportions of Sox2+ cells were maintained and fell to around 53% (p=0.0519) and 72% (p=0.068) in *Hesx1*$^{Cre/+}$*; Kras*$^{G12D/+}$ and *Hesx1*$^{Cre/+}$*; Braf*$^{V600E/+}$ pituitaries, respectively, suggesting a non-significant trend towards decreased Sox2+ cell numbers with time (Figure 4.13 H-J). Furthermore, the transcription of *Sox2* mRNA had a trend toward increased abundance in *Hesx1*$^{Cre/+}$*; Kras*$^{G12D/+}$ pituitaries and was significantly increased *Hesx1*$^{Cre/+}$*; Braf*$^{V600E/+}$ in mutants, as assessed by qRT-PCR (Figure 4.13 K).

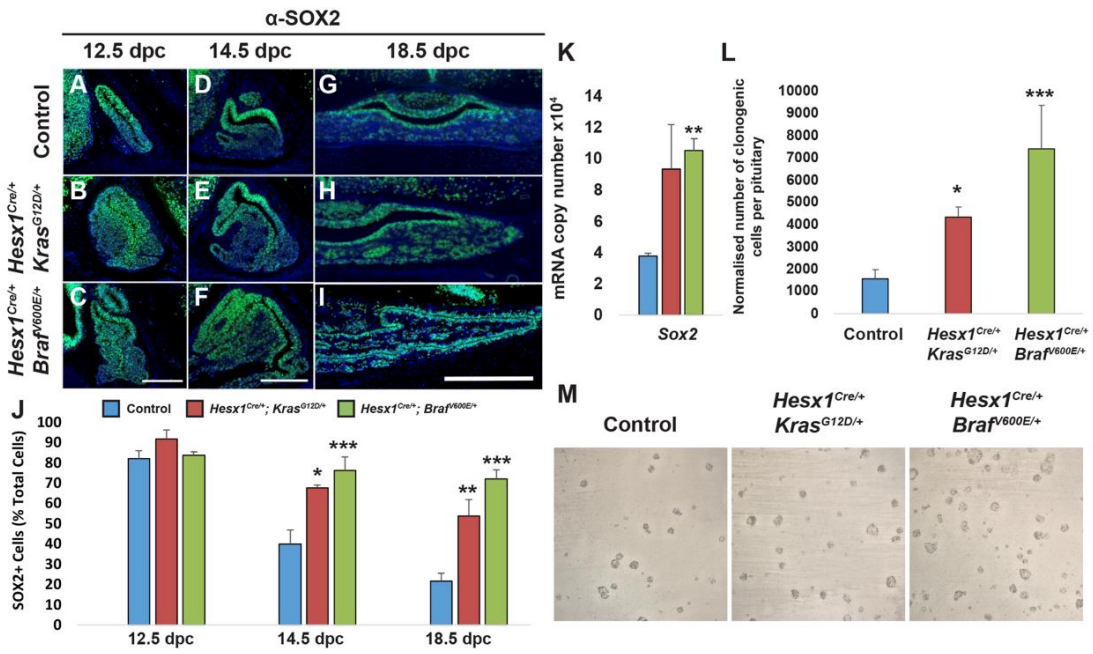

Figure 4.13. The Sox2^{+} stem cell compartment is increased in *Hesx1$^{Cre/+}$; Kras$^{G12D/+}$* and *Hesx1$^{Cre/+}$; Braf$^{V600E/+}$* mutant pituitaries. (**A**-**I**) Immunofluorescence staining revealing the presence of SOX2+ cells (green) in the developing pituitary; genotypes and stages are indicated. The overall numbers appear elevated in the mutant pituitary relative to the controls at all stages analysed. Blue staining is DAPI. (**J**) Quantitative analyses demonstrate that the number of SOX2+ cells is significantly increased in the mutant pituitaries compared with controls at 14.5 and 18.5 dpc. (**K**) Absolute quantitative RT-PCR analysis of *Sox2* mRNA expression in mutant and control pituitaries at 18.5 dpc, n=4 per genotype. (**L**, **M**) Culture of dissociated cells reveals a significantly higher clonogenic potential of the mutant pituitaries relative to the controls (*P≤0.05, **P≤0.01, ***P≤0.001, Student's t-test, n=4 per genotype). Data are mean±s.e.m. Representative immunofluorescence images from *Hesx1$^{Cre/+}$; Braf$^{V600E/+}$* (12.5 dpc n=3, 14.5 dpc n=5, 18.5 dpc n=6), *Hesx1$^{Cre/+}$; Kras$^{G12D/+}$* (12.5 dpc n=3, 14.5 dpc n=4, 18.5 dpc n=6) and control pituitaries (12.5 dpc n=3, 14.5 dpc n=4, 18.5 dpc n=5). Cell count quantification performed on *Hesx1$^{Cre/+}$; Braf$^{V600E/+}$* (12.5 dpc n=3, 14.5 dpc n=5, 18.5 dpc n=6), *Hesx1$^{Cre/+}$; Kras$^{G12D/+}$* (12.5 dpc n=3, 14.5 dpc n=4, 18.5 dpc n=6) and control pituitaries (12.5 dpc n=3, 14.5 dpc n=4, 18.5 dpc n=5). Scale bars: 200 μm.

To corroborate these histological observations, the clonogenic capacity of *Hesx1$^{Cre/+}$; Kras$^{G12D/+}$* and *Hesx1$^{Cre/+}$; Braf$^{V600E/+}$* pituitaries in stem-cell promoting medium was assessed at 18.5 dpc and was found to be almost three and five times higher, respectively, when compared to control pituitaries (Figure 4.13 L,M).

Together these results suggest MAPK signaling may be regulating the balance of differentiation and self-renewal of the pituitary stem cell compartment during development.

To explore this hypothesis further, pulse-chase experiments were performed using the nucleotide analogue EdU, which allows for visualisation of cells in the S-phase of the cell cycle due to its ability to be incorporated into genomic DNA during DNA synthesis. EdU was injected at 14.5 dpc, a time point where the majority of the Sox2+ stem/progenitor cells are dividing, and pituitaries were analysed at 16.5 dpc, at which point the progenitors have stopped proliferating and begin cell-lineage commitment (Fauquier et al. 2008; Bilodeau et al. 2009). Due to the increased severity of the phenotype in *Hesx1*$^{Cre/+}$*; Braf*$^{V600E/+}$ mice, this genotype, along with wild type mice were used for this analysis. Control animals demonstrated that around 25% of the EdU labeled cells expressed the commitment marker PIT1 and 21% expressed Sox2 (Figure 4.14 A, C, D, F). However, in mutants the proportion of EdU+/PIT1+ co-localised cells fell to 3% with the proportion of EdU+/Sox2+ cells increasing to 40% (Figure 4.14 B, C, E, F). In contrast to the previously observed expansion of the ACTH+ corticotroph population in the mutant pituitaries at 18.5 dpc, the numbers of cells co-expressing EdU+/TPIT+ were similar between control and mutant genotypes (8% in controls, 9% in mutants) (Figure 4.14 H, I). Furthermore, this pulse-chase experiments showed that a higher percentage of EdU+ cells were Ki67+ in the mutant genotype (25%) relative to controls (18%) (Figure 4.14 J-L).

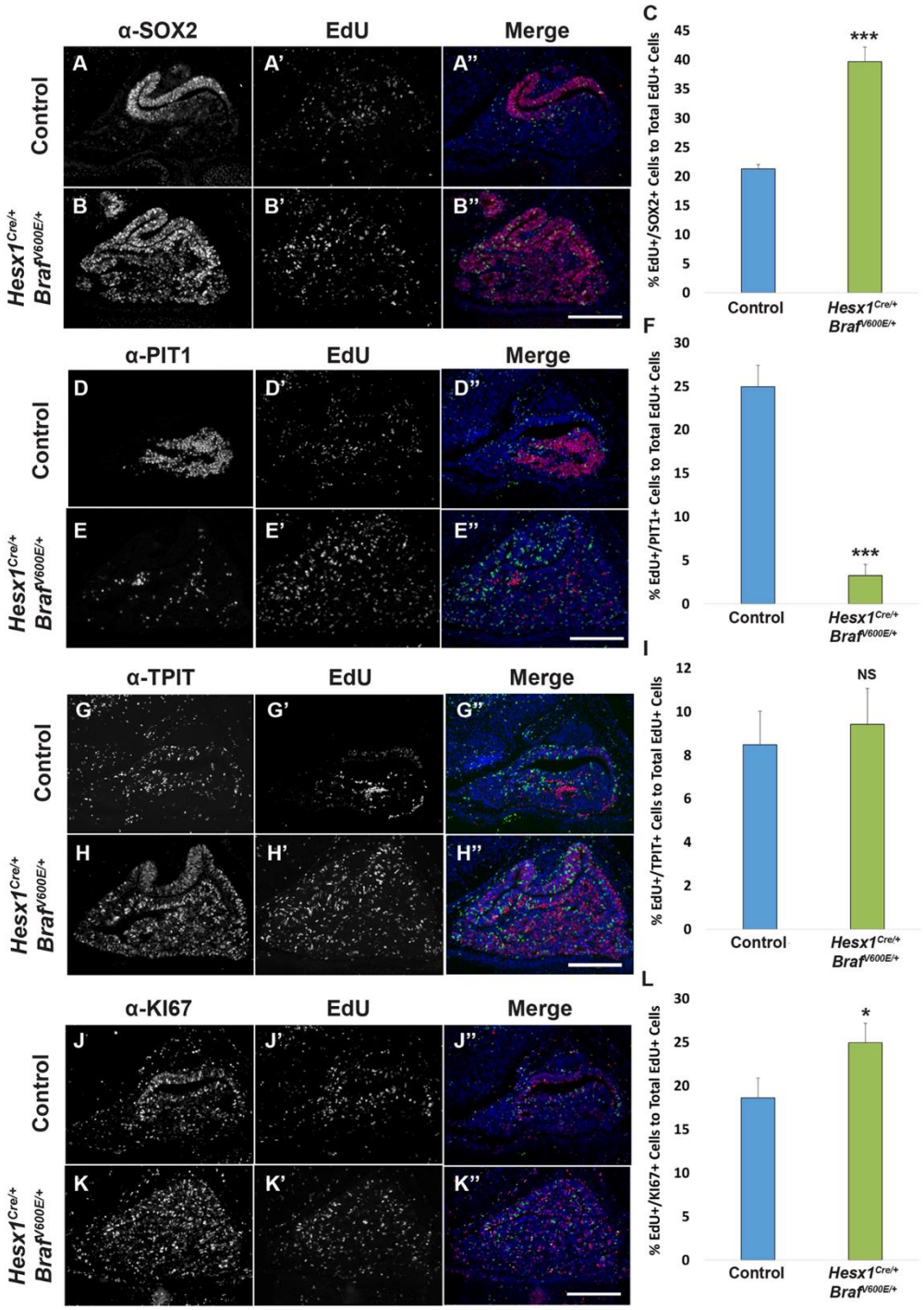

Figure 4.14. Abnormal balance between self-renewal and differentiation in the *Hesx1$^{Cre/+}$; Braf$^{V600E/+}$* mutant pituitaries. The nucleotide analogue EdU was administered once to pregnant females at 14.5 dpc and embryos were analysed at 16.5 dpc. (**A**-**C**) Numbers of SOX2;EdU double-positive cells are increased in the mutant pituitary relative to the control. (**D**-**F**) In contrast, the proportion of PIT1;EdU double-positive cells is dramatically reduced in the mutant gland. (**G**-**I**) The proportion of TPIT;EdU double-positive cells remained constant between genotypes. (**J**-**L**) The percentage of cycling cells within the initially EdU-labelled population is significantly higher in the *Hesx1$^{Cre/+}$; Braf$^{V600E/+}$* mutants

compared with controls (*P≤0.05, ***P≤0.001; NS, not significant; Student's t-test). Data are mean±s.e.m. Representative immunofluorescence images from *Hesx1*$^{Cre/+}$*; Braf*$^{V600E/+}$ (n=5) and control pituitaries (n=4). Cell count quantification performed on *Hesx1*$^{Cre/+}$*; Braf*$^{V600E/+}$ (n=5) and control pituitaries (n=4). Scale bars: 200 μm.

In order to understand what cells were initially labeled with EdU at 14.5 dpc a shorter pulse-chase experiment was performed in which cells were labeled with EdU at 14.5 dpc and collected 2 hours later. The results from the experiment showed that most of the EdU+ cells co-localised with Sox2, with 74% of Edu+ cells expressing Sox2 in control embryos and 87% in the *Hesx1*$^{Cre/+}$*; Braf*$^{V600E/+}$ mutants, suggesting a trend towards increased co-localisation (p=0.1599) (Figure 4.15 A-C). Control pituitaries also showed that 6% of EdU+ cells co-expressed PIT1 and 1.4% co-express TPIT. In *Hesx1*$^{Cre/+}$*;Braf*$^{V600E/+}$ mutant pituitaries, 0.1% of EdU+ cells expressed PIT1 and 3.7% expressed TPIT, which are both statistically significantly different from control (p=0.0246, PIT1 and p=0.0490, TPIT) (Figure 4.15 D-I).

Together these results suggest that MAPK pathway activation promotes the self-renewal of Sox2+ pituitary stem/progenitor cells and that these cells are impaired in their capacity to differentiate into PIT1+ progenitors. Furthermore, it appears as if there is no bias in the ability of the Sox2+ cells to differentiate into TPIT+ progenitors, however, these cells seem to cell-autonomously increase their proliferation in response to activated MAPK signaling.

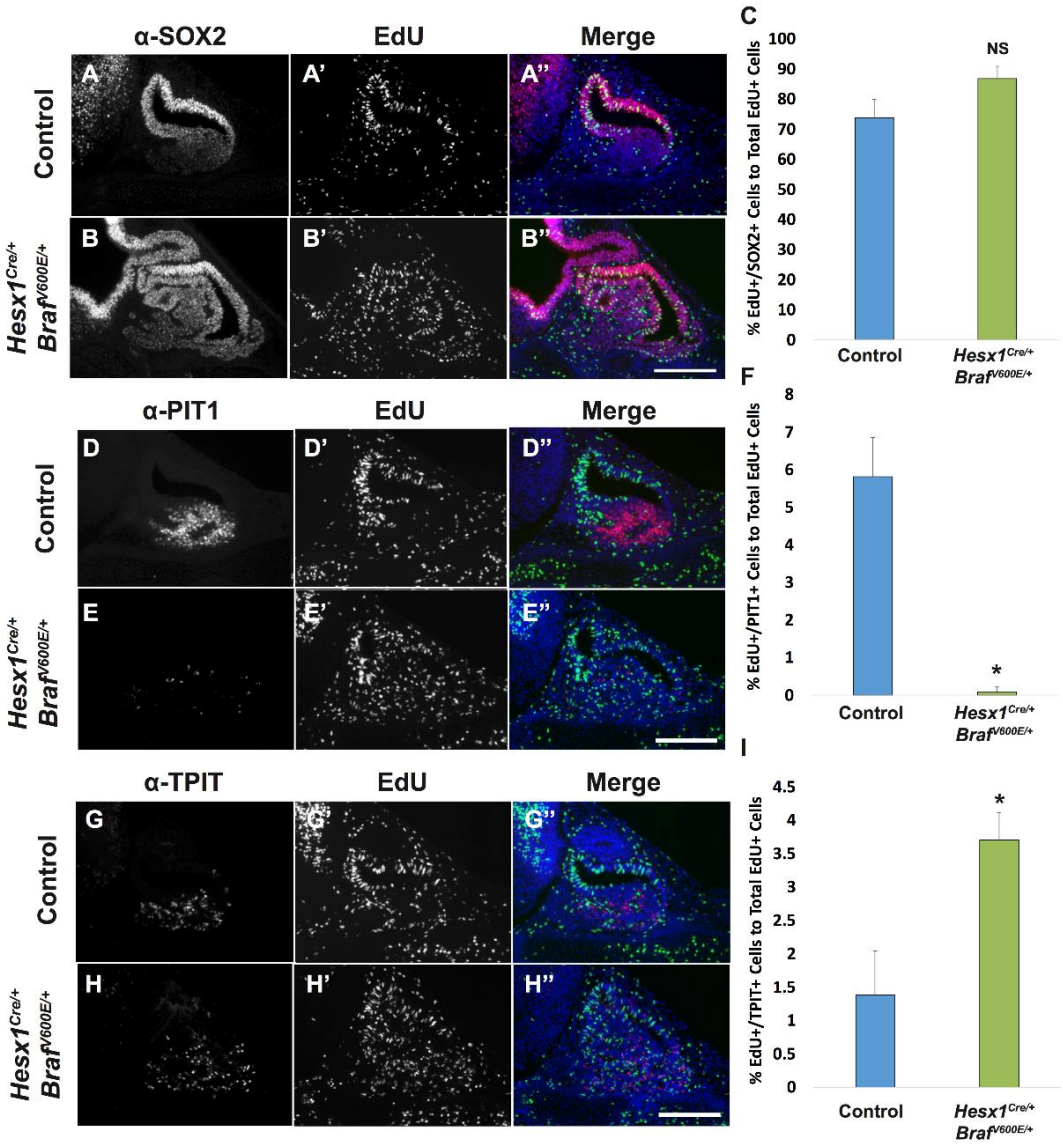

Figure 4.15. Proliferation of TPIT+ and PIT1+ progenitor populations are affected in *Hesx1$^{Cre/+}$; Braf$^{V600E/+}$* mutant pituitaries at 14.5 dpc. EdU was administered once to pregnant females at 14.5 dpc and embryos were analysed 2 hours later. (**A**-**C**) Most of the labels cells are SOX2+ with a trend towards increased numbers in the mutant pituitaries relative to controls (controls 74%, mutants 87%; p=0.1599). (**D**-**I**) In the control pituitaries, 6% of the EDU+ cells expressed PIT1 and 1.4% TPIT, whilst in the mutant developing glands, only 0.1% of the EDU+ cells express PIT1 and 3.7% TPIT. Both, the increase in TPIT and decrease in PIT1 progenitor proliferation are statistically significant (p=0.0246, PIT1 and p=0.0490, TPIT). Representative immunofluorescence images from *Hesx1$^{Cre/+}$; Braf$^{V600E/+}$* (n=4) and control pituitaries (n=3). Cell count quantification performed on *Hesx1$^{Cre/+}$; Braf$^{V600E/+}$* (n=4) and control pituitaries (n=3). Scale bar is 200μm.

4.2.1.6 Sox2+ve cells represent the majority of proliferating cells in human papillary craniopharyngioma

It is known that expanded numbers of a tissues stem cell compartment with impaired differentiation potential can result in tumour formation in many organ system, including the pituitary (Gaston-massuet et al. 2011). Studies of human papillary craniopharyngioma (PCP) have identified BRAF p.V600E mutations as the sole genetic event associated with the disease. As previously mentioned in the general introduction (see section 1.4) PCP are histologically benign tumours that are characterised by the presence of fibrovascular cores that are lined with basal cells and also a suprabasal layer of well-differentiated non-keratinised squamous epithelium (Figure 4.16 A). PCP tumours are also known to be non-functional and do not express any pituitary hormones (Louis et al. 2016). Therefore, it was examined whether activated MAPK signaling in human PCP tumours recapitulates the cellular alteration observed in the *Hesx1*$^{Cre/+}$*;Braf*$^{V600E/+}$ mutant pituitary (i.e. expansion of the Sox2+ pituitary stem cell compartment with impaired differentiation potential).

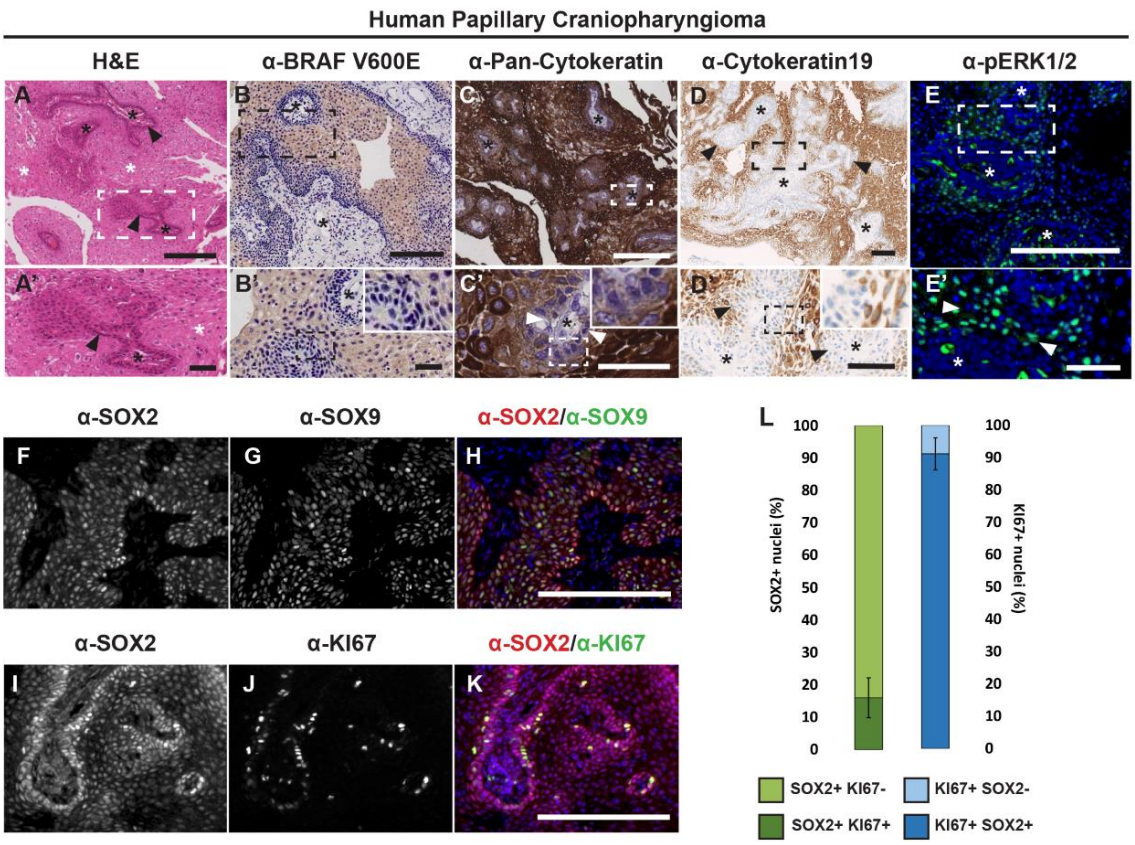

Figure 4.16. Human PCP tumours contain a population of cycling SOX2$^+$ cells. Analysis of histological sections of human PCP tumours. (**A**, **A'**) Haematoxylin and Eosin staining showing the presence of fibrovascular cores (black asterisks) lined by a layer of basal cells (arrowheads) and large areas of suprabasal squamous epithelium (white asterisks). (**B**, **B'**) IHC revealing the expression of BRAF-V600E in a PCP tumour. Staining is present (light brown) in the vast majority of tumour cells. Black asterisks indicate the presence of fibrovascular cores. (**C**, **C'**) Immunohistochemical detection using a pan-cytokeratin antibody. Most of the tumour cells show positive staining (dark brown) with the exception of the basal cell layer (arrowheads) surrounding the fibrovascular cores (black asterisks). (D,D′) Specific staining (light brown) against cytokeratin 19 showing absent staining in the basal layer cells (arrowheads) surrounding fibrovascular cores (asterisks). The difference in the staining, from light to dark brown, is due to technical reasons (e.g. antibody used, manual or automatized immunohistochemistry). (**E**, **E'**) Immunofluorescence staining of pERK1/2 showing expression restricted to the cells surrounding the fibrovascular cores (white arrowheads), with some positive cells within the fibrovascular cores (white asterisk). Outlined areas in A-E are shown in A′-E′. Outlined areas in A′-E′ are shown in the insets in A′-E′. (**F**-**H**) Double immunofluorescent staining shows the co-expression of SOX2 and SOX9 in cells surrounding the fibrovascular cores, with stronger signal in the basal cells. (**I**-**K**) Double immunofluorescence staining reveals the co-expression of SOX2 and Ki67 in

basal cells. (**L**) Quantification of SOX2:Ki67 double-positive cells as a proportion of either the SOX2+ or Ki67+ populations in human PCP. Data are mean±s.e.m. of SOX2+ KI67+ and KI67+ SOX2+ cell quantifications. Scale bars: 200 μm; 100 μm in insets.

This was achieved by utilising a series of formalin-fixed paraffin embedded (FFPE) PCP samples (n=5), in which the presence of BRAF p.V600E mutations were confirmed by sequencing (see section 2.3.5 and Table 4.2) and assessing the presence of the mutation in all cells of the tumour by IHC (Figure 4.16 B). Analysis of pERK1/2 expression revealed that it showed restriction in its expression to the areas surrounding the fibrovascular cores (Figure 4.16 E). Furthermore, the majority of the tumour cells, with the exception of basal cell layer, were found to be positive for cytokeratins using a pan-cytokeratin antibody (Figure 4.16 D). Double IF staining demonstrated that the basal cells also expressed Sox2 and Sox9 in a graded manner, with higher levels of expression observed in cells closest to fibrovascular cores, with loss of intensity in the signal in cells further away (Figure 4.16 F-H). Quantification of the relationship between Sox2 and Ki67 revealed that around 16% of Sox2+ cells expressed Ki67 (Figure 4.16 I-L). However that vast majority of dividing cells in the tumour (around 91%) were positive for Sox2, suggesting that the Sox2+ population may be the main drivers of tumour growth (Figure 4.16 L). This was compared against the physiological proliferation observed in Sox2+ cells, both in adulthood and during normal pituitary development in humans. Analysis of human pituitary at CS20 (Carnegie stage 20; gestational day 49), analogous to 14.5 dpc in the mouse, showed that the tissue was predominantly Sox2+/Sox9 double positive and that the majority of these cells were proliferating, as evidenced by Ki67 positivity (Figure 4.17 A-C, J-L). However, adult human pituitaries possessed very little Sox2+ cells in the anterior lobe (Figure 4.17 D-I) and these cells rarely expressed Ki67 (Figure 4.17 M-R).

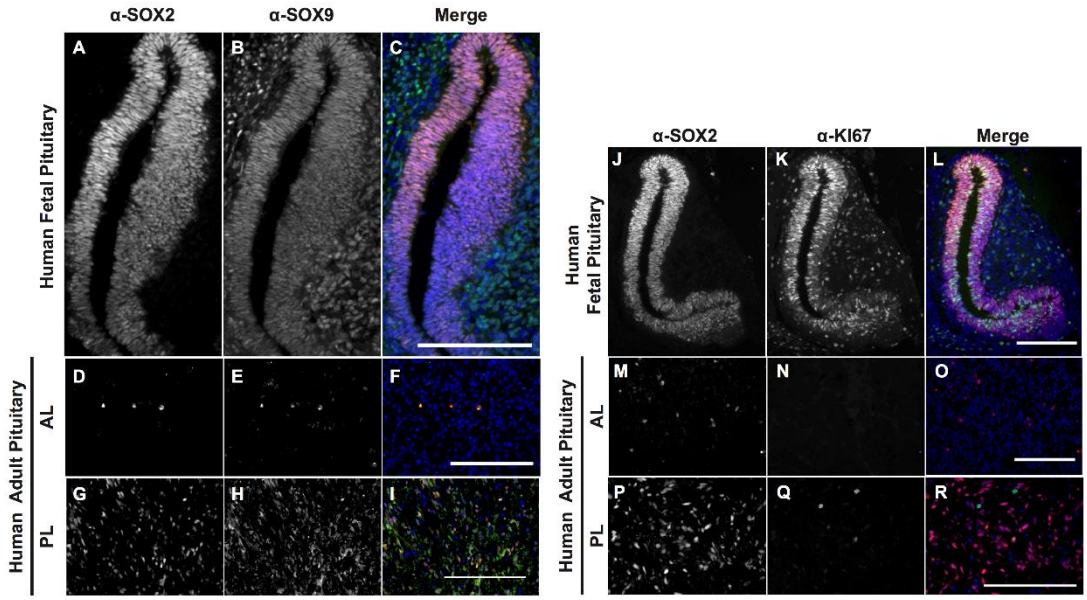

Figure 4.17. Expression of SOX2, SOX9 and Ki67 in human fetal and adult pituitaries. IHC on histological sections of human pituitaries, stages and markers are indicated. (**A**-**I**) At embryonic stage CS20 (n=3) (**A**-**C**), SOX2 and SOX9 are co-expressed in the vast majority of the embryonic progenitors of the developing Rathke's pouch. In contrast, expression of SOX2 and SOX9 is not observed in the adult anterior pituitary (n=2) (**D**-**F**), but there are expressing cells in the posterior pituitary (**G**-**I**). (**J**-**R**) At embryonic stage CS20 (**J**-**L**), double immunostaining reveals the co-expression of SOX2 and the cycling marker Ki67 in the periluminal progenitors of Rathke's pouch. However, in the adult pituitary, Ki67+ cells are rare and do not co-localise with SOX2+ cells in the anterior (**M**-**O**) or posterior (**P**-**R**) pituitary, where they are more abundant (**P**). Scale bar is 200μm.

Together, these observations suggest that, similar to the *Hesx1Cre/+; Braf*$^{V600E/+}$ mouse model, activated MAPK signaling in human PCP results in an increase in the proliferative capacity and reduction in differentiation potential of the Sox2+ cells.

Case Number	DIgnosis	DNA (copies/µl)	BRAF-V600E Digital PCR		
			Mean mutant copies/µl	Mean wild type copies/µl	Mean % mutant
87	PCP	2087	252.5	655	27.60%
91	PCP	6653	1262.5	3302.5	27.70%
96	PCP	360	36	240	13.00%
97	PCP	262	11.8	72.5	14.20%
101	PCP	1978	122.5	395	23.60%

Table 4.2. Digital PCR showing BRAF V600E mutations in human PCP samples

4.2.2 Analysis of MAPK activation in postnatal pituitary stem cells

Due to the observed neonatal lethality observed when activating MAPK signaling in pituitary progenitor cells (*Hesx1*$^{Cre/+}$*;Braf*$^{V600E/+}$ and *Hesx1*$^{Cre/+}$*;Kras*$^{G12D/+}$) a second strategy was adopted to attempt to bypass this through expressing oncogenic *Braf* or *Kras* in Sox2+ postnatal pituitary stem cells.

4.2.2.1 MAPK pathway activation in pituitary stem cells does not lead to the acquisition of a senescent phenotype

To drive the expression of oncogenic *Braf* and *Kras* in postnatal pituitary stem cells, *Sox2*$^{CreERT2/+}$*; Rosa26*$^{YFP/+}$ mice were crossed with either *Braf*$^{V600E/+}$ or *Kras*$^{G12D/+}$ mice to generate triple heterozygotes and the resulting *Sox2*$^{CreERT2/+}$*; Braf*$^{V600E/+}$*; Rosa26*$^{YFP/+}$ and *Sox2*$^{CreERT2/+}$*; Kras*$^{G12D/+}$; *Rosa26*$^{YFP/+}$ mice were induced with tamoxifen at 4 weeks of age to induce recombination and activation of the

oncogenes and YFP lineage reporter. However, it was found that induced mice rarely survived longer than 3 weeks (average survival of 20.4 days, ranging from 8 to 47 days, n=8) post-tamoxifen administration. This was due to mice developed severe acute weight loss, which necessitated humane culling, preventing the long-term analysis of the effects of MAPK activation on pituitary stem cell population. Therefore, the pituitaries from induced were analysed between 2 to 4 weeks post-tamoxifen administration.

Analysis of these pituitaries revealed no gross morphological defects, which was not anticipated due to the profound hyperplasia that was observed following MAPK activation in pituitary progenitor cells (see section 4.2.1) (Figure 4.18). Furthermore, analysis of proliferation by Ki67 by IF reveled no qualitative differences between control (*Sox2*$^{CreERT2/+}$*; Rosa26*$^{YFP/+}$) and mutant (*Sox2*$^{CreERT2/+}$*; Braf*$^{V600E/+}$*; Rosa26*$^{YFP/+}$ and *Sox2*$^{CreERT2/+}$*; Kras*$^{G12D/+}$*; Rosa26*$^{YFP/+}$) pituitaries (Figure 4.18 G). To examine whether challenging the postnatal pituitary stem cells with MAPK pathway activation resulted in the acquisition of senescent characteristics, mutant and control pituitaries were examined by IF for the senescence effectors p16 and p21. This analysis revealed that in either the Sox2+ pituitary stem cell compartment or the pituitary parenchyma, there was no increased expression of either of these markers, suggesting that cellular senescence was not induced (Fig. 4.18 A-F).

Together these results suggest that targeting postnatal pituitary stem cells with oncogenic *Braf* or *Kras* has no effect on the proliferation of either the stem cells compartment or the organ as a whole. Moreover the induction of characteristic cellular senescence markers was not observed.

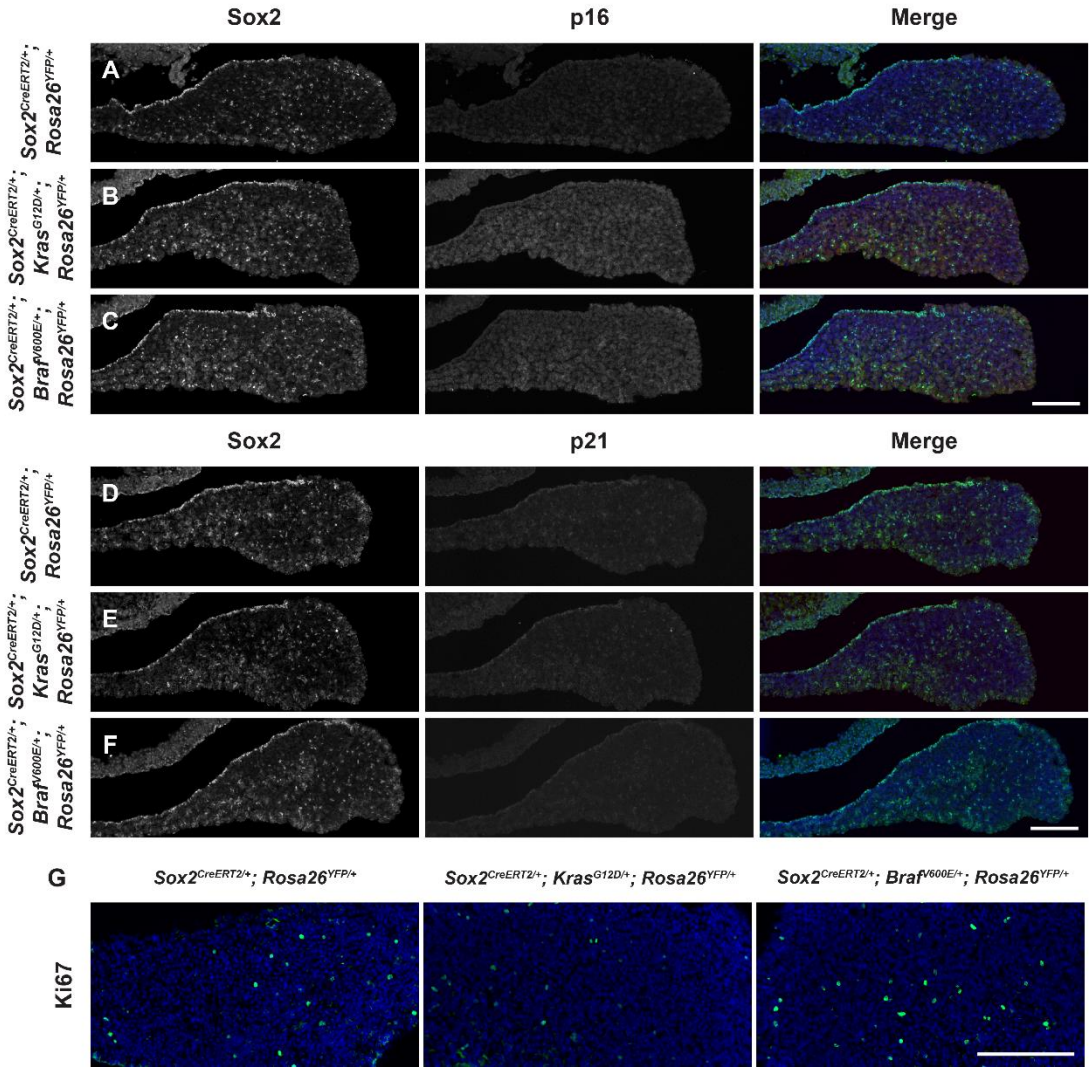

Figure 4.18 Absence of senescence-associated markers in *Sox2$^{CreERT2/+}$; Braf$^{V600E/+}$; Rosa26$^{YFP/+}$* and *Sox2$^{CreERT2/+}$; Kras$^{G12D/+}$; Rosa26$^{YFP/+}$* mutants. IHC staining against the cellular senescence effectors p21 and p16 and the proliferation marker Ki67 on histological sections of control and mutant pituitaries at induced with tamoxifen at 4 weeks of age and analysed 2-4 weeks later. **(A-F)** p21 and p16 are not expressed in control or mutant pituitaries. (**G**) Anterior lobe of the pituitary IHC stained for Ki67 showing no qualitative difference between control and mutant pituitaries. Representative immunofluorescence images from *Sox2$^{CreERT2/+}$; Braf$^{V600E/+}$; Rosa26$^{YFP/+}$* (n=4), *Sox2$^{CreERT2/+}$; Kras$^{G12D/+}$; Rosa26$^{YFP/+}$* (n=4) and control pituitaries (n=4). Scale bars; 200μm.

4.2.2.2 Overactivation of the MAPK pathway in Sox2+ stomach cell populations results in severe gastric hyperplasia and early lethality

(Analysis of stomach phenotype in *Sox2*$^{CreERT2/+}$*; Braf*$^{V600E/+}$*; Rosa26*$^{YFP/+}$ and *Sox2*$^{CreERT2/+}$*; Kras*$^{G12D/+}$*; Rosa26*$^{YFP/+}$ mice was perfomed by Dr Jean Marie Delalande at Queen Mary, University of London)

To understand why the health of induced *Sox2*$^{CreERT2/+}$*; Braf*$^{V600E/+}$*; Rosa26*$^{YFP/+}$ and *Sox2*$^{CreERT2/+}$*; Kras*$^{G12D/+}$*; Rosa26*$^{YFP/+}$ mice declined so rapidly, in the absence of any discernible pituitary phenotype, the animals were subjected to a whole body autopsy. This examination revealed that the anterior region of the stomach, corresponding to the fundus, was profoundly hyperplasic and had undergone involution towards the interior of the stomach cavity in all animals analysed (n=8) (Figure 4.19). Therefore, providing an explanation for the severe weight loss observed.

Examination of freshly dissected stomachs from control and mutant mice reveled that strong YFP fluorescence could be observed in the fundus, indicating that the activated oncogenes were expressed there (Figure 4.19). This was not unexpected as it is known that the anterior foregut is known to contain populations of Sox2-expressin cells, therefore also allowing them to be targeted with oncogenic Braf or Kras under the current experimental paradigm (Gracz & Magness 2011).

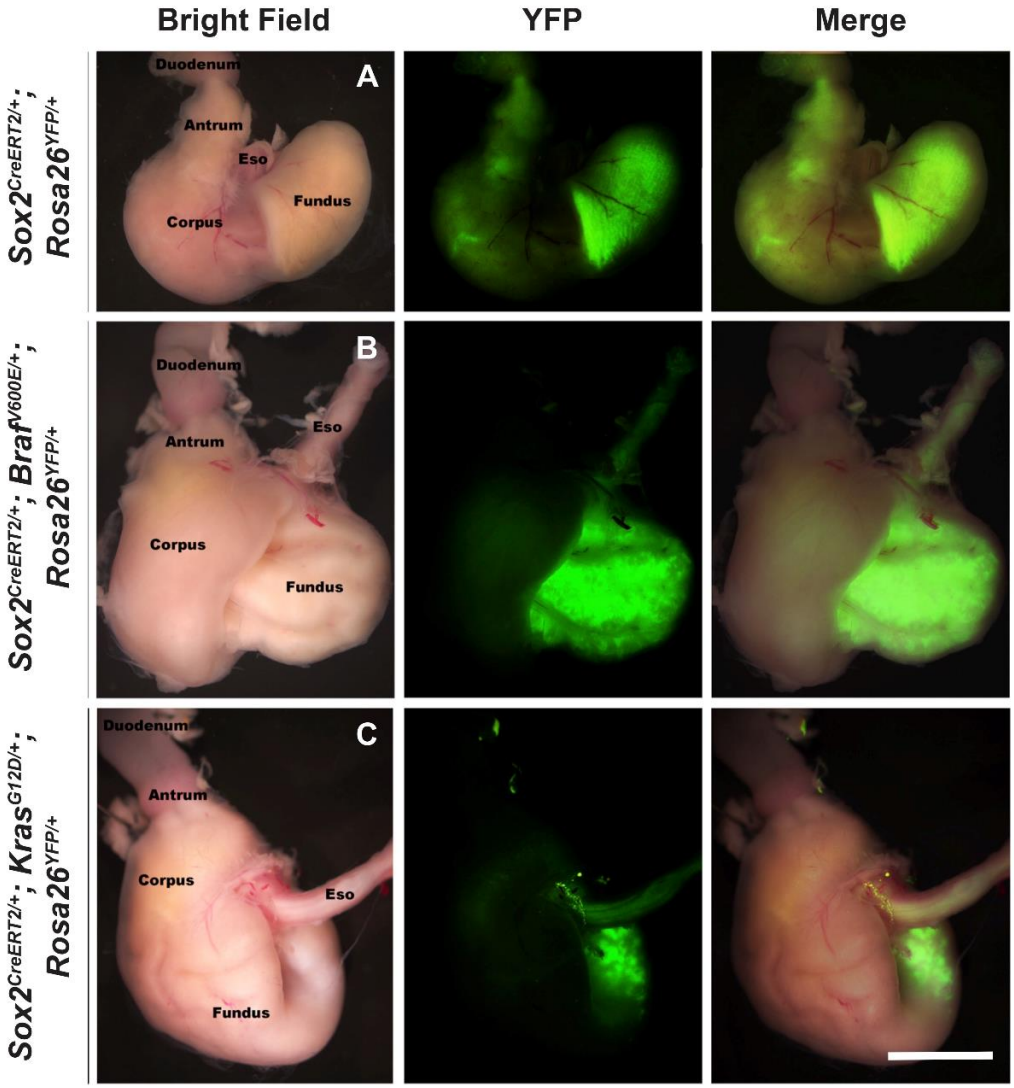

Figure 4.19. Stomachs from *Sox2*$^{CreERT2/+}$; *Braf*$^{V600E/+}$; *Rosa26*$^{YFP/+}$ and *Sox2*$^{CreERT2/+}$; *Kras*$^{G12D/+}$; *Rosa26*$^{YFP/+}$ mice display abnormal morphology. (**A-C**) Whole mount fluorescence imaging of control, *Sox2*$^{CreERT2/+}$; *Braf*$^{V600E/+}$; *Rosa26*$^{YFP/+}$ and *Sox2*$^{CreERT2/+}$; *Kras*$^{G12D/+}$; *Rosa26*$^{YFP/+}$ stomachs showing the presence of recombined cells in the fundus and its abnormal involution in mutants. Representative wholemount fluorescence images from *Sox2*$^{CreERT2/+}$; *Braf*$^{V600E/+}$; *Rosa26*$^{YFP/+}$ (n=3), *Sox2*$^{CreERT2/+}$; *Kras*$^{G12D/+}$; *Rosa26*$^{YFP/+}$ (n=3) and control stomachs (n=3). Scale bar; 1cm.

Histological examination of control and mutant stomachs stained with alcian blue or nuclear fast red, to visualise mucus and cellular nuclei respectively, revealed that cellular expansion but not increased mucus production was the cause of obstruction to the cavity (Figure 4.20).

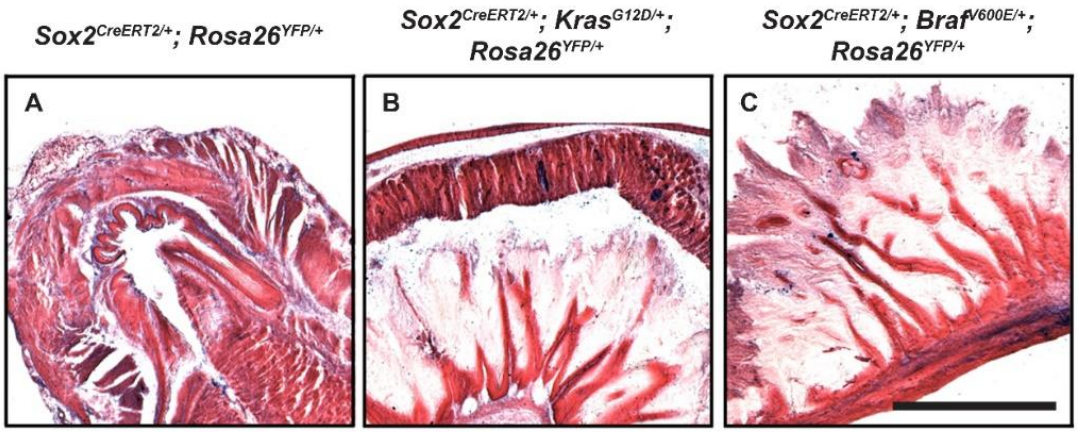

Figure 4.20. Mucus production is not the cause of stomach obstruction in mutant stomachs. (**A**-**C**) Alcian blue (mucus) and nuclear fast red (cellular nuclei) staining of control, *Sox2*$^{CreERT2/+}$*; Braf*$^{V600E/+}$*; Rosa26*$^{YFP/+}$ and *Sox2*$^{CreERT2/+}$*; Kras*$^{G12D/+}$*; Rosa26*$^{YFP/+}$ stomachs showing that the material occupying the stomach cavity in the mutants is predominantly cellular and is not the accumulation of mucus. Representative images from *Sox2*$^{CreERT2/+}$*; Braf*$^{V600E/+}$*; Rosa26*$^{YFP/+}$ (n=3), *Sox2*$^{CreERT2/+}$*; Kras*$^{G12D/+}$*; Rosa26*$^{YFP/+}$ (n=3) and control (*Sox2*$^{CreERT2/+}$*; Rosa26*$^{YFP/+}$) stomachs (n=3). Scale bar; 0.5cm.

To see what cells may be causing the obstruction, IF analysis was performed for Sox2 expression and the YFP lineage reporter. This demonstrated a dramatic cell-autonomous enlargement of Sox2 cell compartment, which had expanded into the inner cavity of the stomach (Figure 4.21). Furthermore, analysis of proliferation through Ki67 IF staining revealed that, unsurprisingly, the Sox2+ cells were significantly more proliferative in the mutant context, relative to controls (Figure 4.22). Interestingly, comparison of the proliferative index of YFP+ and YFP-/Sox2+ populations revealed no difference, suggesting either a recombination artifact or a potential paracrine pro-mitotic influence of YFP+/Sox2+ cells on YFP-/Sox2+ cells (Figure 4.22).

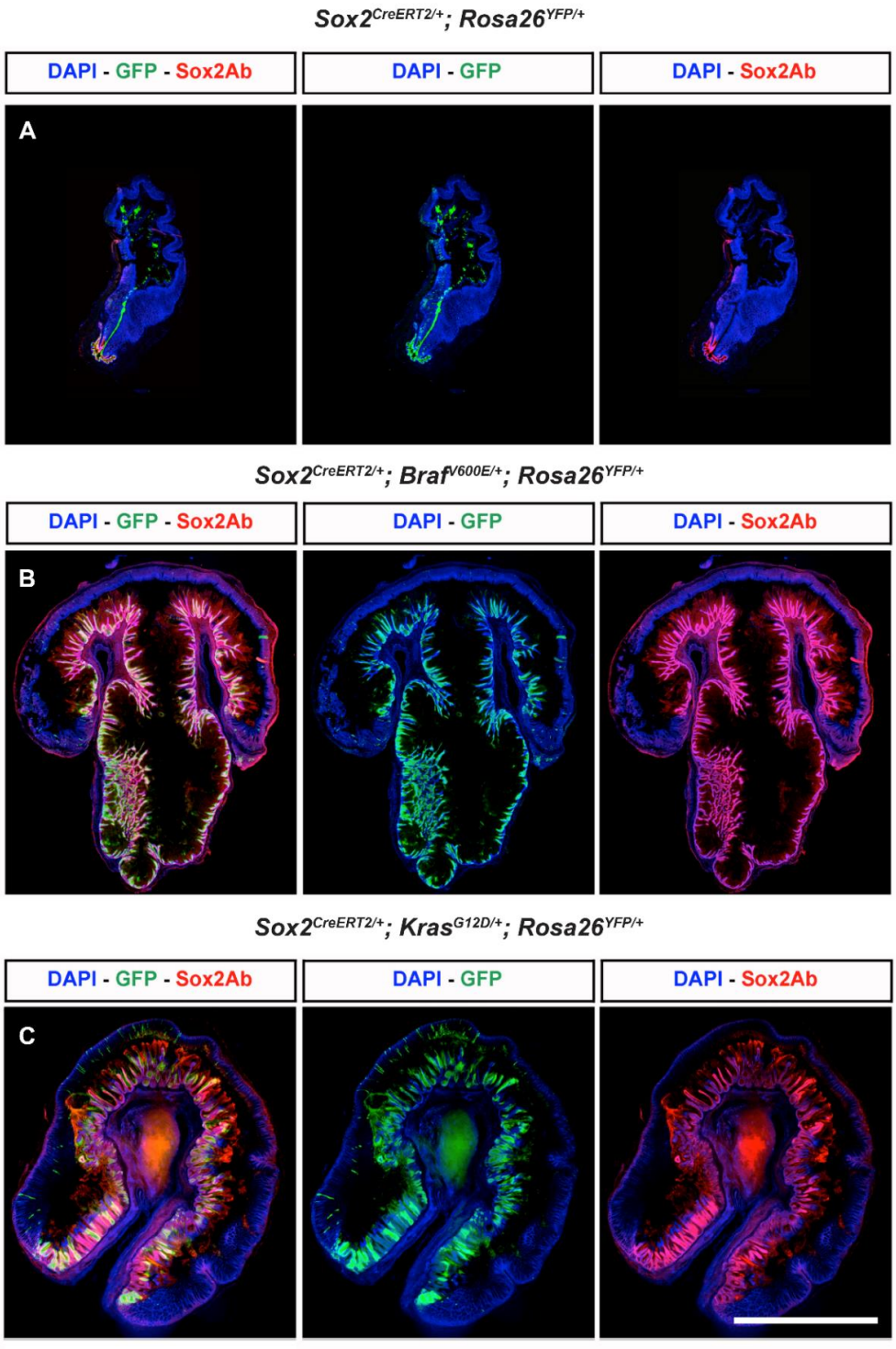

Figure 4.21. The cell-autonomous expansion of the gastric Sox2+ population is responsible for obstructing the stomach cavity. (**A**-**C**) IHC staining against GFP (green) and Sox2 (red) in control, *Sox2*$^{CreERT2/+}$*; Braf*$^{V600E/+}$*; Rosa26*$^{YFP/+}$ and *Sox2*$^{CreERT2/+}$*; Kras*$^{G12D/+}$*; Rosa26*$^{YFP/+}$ stomachs showing the cell-autonomous expansion of the Sox2+ cell population to fill the interior of the stomach. Representative immunofluorescence images from *Sox2*$^{CreERT2/+}$*; Braf*$^{V600E/+}$*; Rosa26*$^{YFP/+}$ (n=3), *Sox2*$^{CreERT2/+}$*; Kras*$^{G12D/+}$*; Rosa26*$^{YFP/+}$ (n=3) and control (*Sox2*$^{CreERT2/+}$*; Rosa26*$^{YFP/+}$) stomachs (n=3). Scale bar; 1cm.

Together, this analysis shows that targeting of Sox2-expressing cell populations in the stomach with oncogenic *Braf* or *Kras results* in a extremely rapid expansion of the gastric Sox2+ compartment, resulting in obstruction of the stomach, which is incompatible with long term survival.

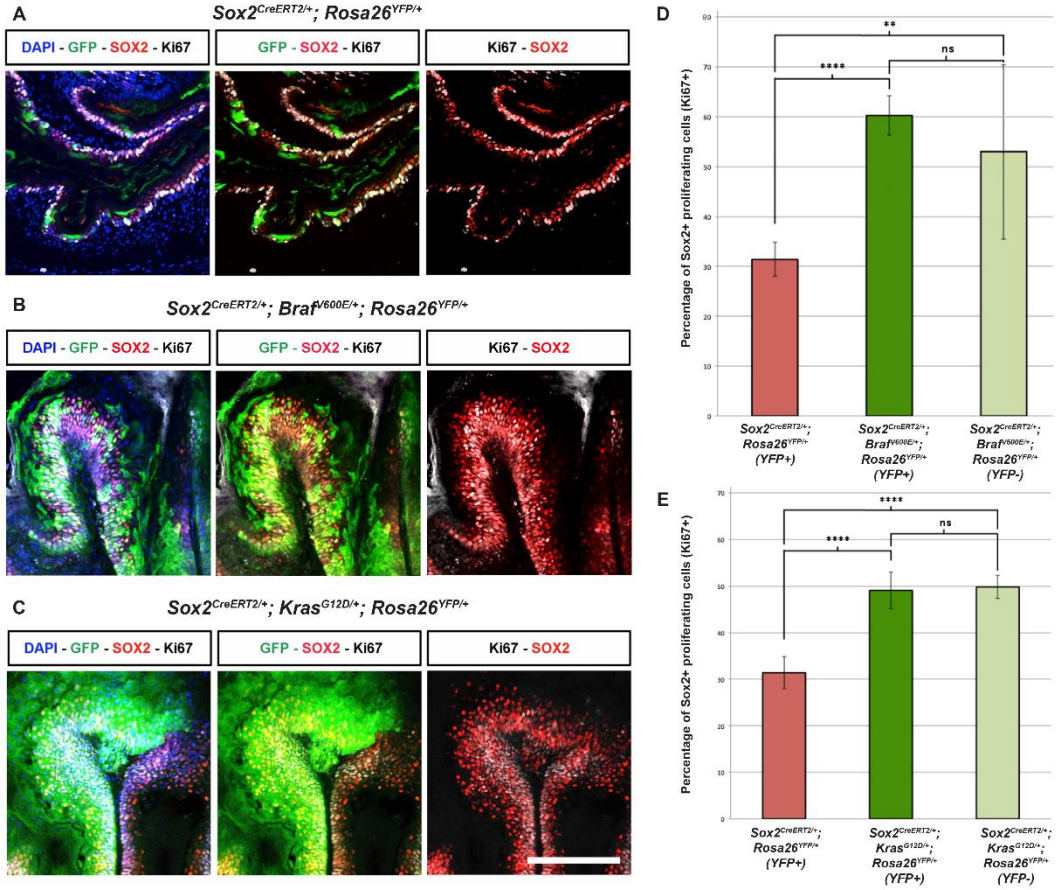

Figure 4.22. High levels of proliferation are observed in the YFP+ and YFP- Sox2+ gastric cell populations. (**A**-**C**) IHC staining against GFP (green), Sox2 (red) and Ki67 (white) in control, *Sox2*$^{CreERT2/+}$*; Braf*$^{V600E/+}$*; Rosa26*$^{YFP/+}$ and *Sox2*$^{CreERT2/+}$*; Kras*$^{G12D/+}$*; Rosa26*$^{YFP/+}$ stomachs. Note the similar proportions of Ki67 in the YFP+ and YFP- tissue in the mutant stomachs. (**D**) Quantification of the proliferative index of Sox2+ cells in control and *Sox2*$^{CreERT2/+}$*; Braf*$^{V600E/+}$*; Rosa26*$^{YFP/+}$ YFP+ and YFP- Sox2+ cells. (**E**) Quantification of the proliferative index of Sox2+ cells in control and *Sox2*$^{CreERT2/+}$*; Kras*$^{G12D/+}$*; Rosa26*$^{YFP/+}$ YFP+ and YFP- Sox2+ cells. (**P≤0.01, ***P≤0.001, ****P≤0.0001 Student's t-test). Data are mean±s.e.m. Representative immunofluorescence images from *Sox2*$^{CreERT2/+}$*; Braf*$^{V600E/+}$*; Rosa26*$^{YFP/+}$ (n=3), *Sox2*$^{CreERT2/+}$*; Kras*$^{G12D/+}$*; Rosa26*$^{YFP/+}$ (n=3) and control (*Sox2*$^{CreERT2/+}$*; Rosa26*$^{YFP/+}$) stomachs (n=3). Cell count quantification performed on 3 mice per genotype. Scale bars; 200μm.

4.3 CONCLUSIONS

In this chapter it was found that activation of the MAPK signaling pathway in the embryonic precursors of the pituitary gland did not results in the induction of cellular senescence as hypothesized, potentially due to the cellular context in which the oncogenes were expressed. Therefore, this prevented experimental testing of whether this induction of senescence in the context of wild type β-Catenin can drive non-cell autonomous tumour formation. Furthermore, the observed neo-natal lethality also prevented long-term examination of mutant mice for any potential tumourigenic effects.

However, significant pituitary developmental abnormalities were observed which warranted further investigation. MAPK pathway over-activation in the precursors of RP resulted in sustained and increased proliferation, as well as defects in terminal differentiation of the Sox2+ stem/progenitor cell compartment during development. By the end of gestation this results in a grossly enlarged pituitary gland that was predominantly composed of Sox2+ cells. Of translational significance, a population of proliferating Sox2+ cells were found for the first time in human PCP tumours, which is a situation comparable to the activated MARK-signaling mutants.

Attempts to bypass the neonatal lethality observed when activating MAPK signaling in pituitary progenitors by targeting postnatal stem cells was confounded by the development of severe gastric hyperplasia, which prevented long term examination of the pituitary. Analysis of the pituitaries before the gastric phenotype became too severe demonstrated no discernable difference in organ proliferation,

stem cell compartment size or induction of cellular senescence markers. This was potentially due to either the postnatal context, and therefore competence of the pituitary stem cells to be perturbed by activating the MAPK pathway, or the inability to follow the fate of targeted cells for longer durations.

CHAPTER 5: ELUCIDATING THE ROLE OF CELLULAR SENESCENCE DURING LUNG TUMORIGENESIS *IN VIVO*

5.1 INTRODUCTION

As discussed previously in the introduction, elucidating the role of cellular senescence *in vivo* has been hampered by a lack of tools to visualise and ablate these populations. This situation has been improved in recent years by the development of the *p16*-3MR and *INK-ATTAC* mouse models that permit the visualisation and ablation of *p16*-expressing cell populations *in vivo* (Demaria. 2014; Baker et al. 2011). However, the question of whether senescence escape occurs as a tumourigenic mechanism *in vivo* persists due to the absence of tools to lineage trace putatively senescent cell populations. This has resulted in current attempt to address this question being limited to either retrospective analysis of cells that are believed to have escaped senescence for molecular signatures of the escape, or by experimentally forcing escape and examining the cells for commonalities with advanced tumours.

The role of cellular senescence during NSCLC initiation and progression has not been extensively studied. Indeed, controversial evidence exists for whether cellular senescence acts as a tumour-suppressive mechanism to prevent the transition from adenoma to adenocarcinoma, with some studies observing cellular senescence limiting the expansion of benign lung adenoma (Collado et al. 2005a; Dankort et al. 2007; Michaloglou et al. 2005; Dhomen et al. 2009a), whereas others do not (Tuveson et al. 2004). Furthermore, it is known that senescent cells can have profoundly pleiotropic effects in the context of tumourigenesis, therefore investigations into the functional consequences of cellular senescence during lung cancer development is warranted. To date, none of the currently available genetic tools for exploring cellular senescence *in vivo* (*p16*-

3MR and *INK-ATTAC*) have been used to investigate the role of senescence in lung cancer.

5.2 RESULTS

5.2.1 Generation of the *p16FDR* mouse model

To address the role of cellular senescence during NSCLC initiation and progression in mice a novel genetically engineered mouse model, termed $p16^{FDR}$, was developed to take advantage of the commonly observed $p16^{INK4A}$ expression in senescent cells. The $p16^{FDR}$ model was used to test the hypothesis that benign lung adenomas enter into cellular senescence to limit their expansion into malignant adenocarcinomas and that their pharmacogenetic ablation would reduce tumour burden.

5.2.1.1 Generation of the *FDR* cassette

To allow for the visualisation, lineage tracing and specific ablation of cell populations a construct was designed which contained the sequences for a mammalian optimised FLP-recombinase, flanked by two *P2A* sequences, upstream of a diphtheria toxin (DT) receptor (a human membrane-anchored form of the heparin binding EGF-like growth factor with I117V and L148V mutations to repress the growth factor activities) fused to a mCherry reporter (Figure 5.1 A).

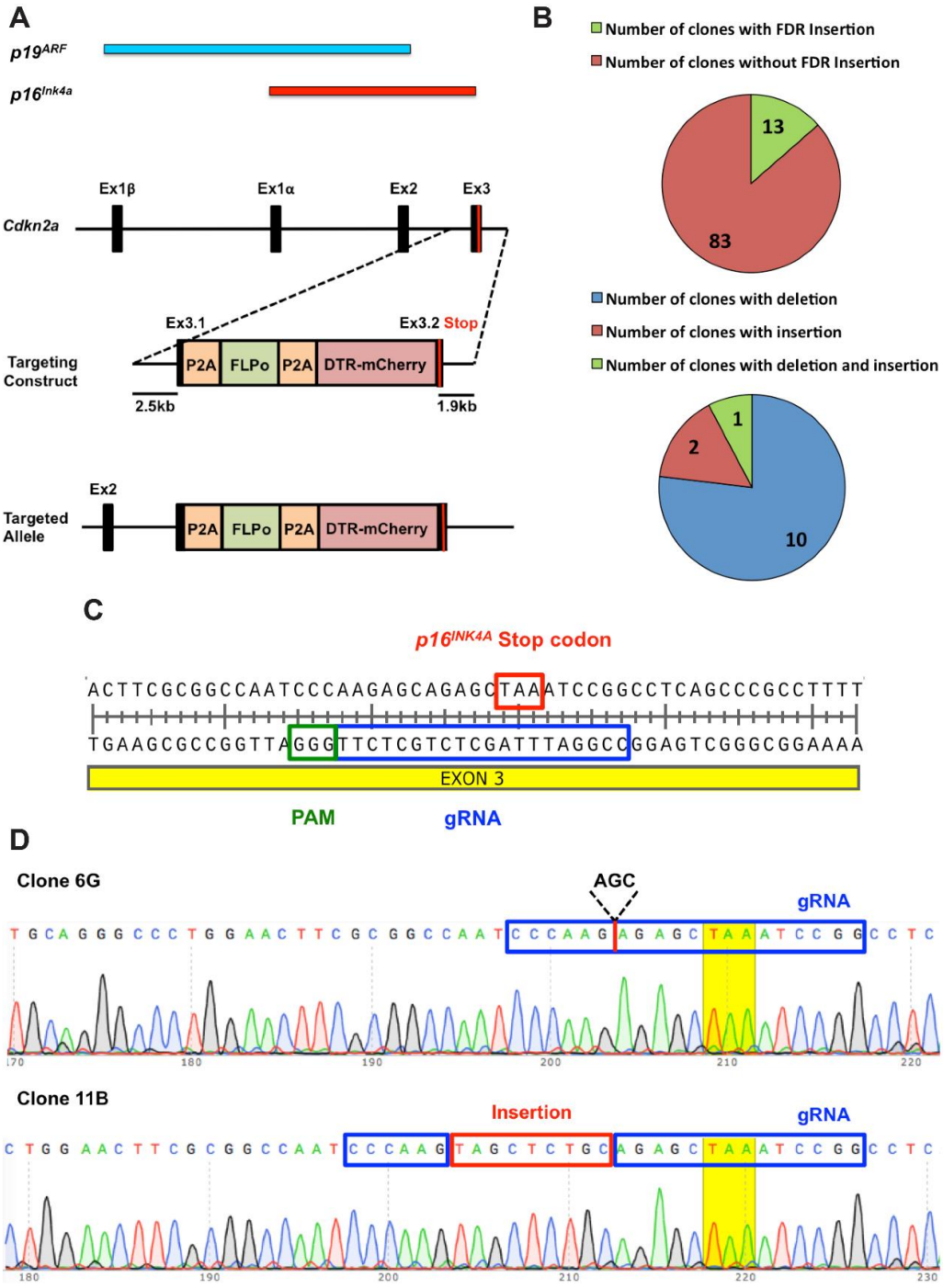

Figure 5.1. Targeting of the *Cdkn2a* locus to generate the *p16^{FDR}* mouse line. (**A**) Schematic representation of the *Cdkn2a* locus showing the exons utilitsed by the *p19^{ARF}* and *p16^{INK4A}* genes. The targeting construct is detailed showing the presence of the flanking homology arms to mediate targeting to the *Cdkn2a* locus. The *FDR* cassette is also detailed showing the locations of the mammalian optimised FLP-recombinase (FLPo), Diphtheria toxin receptor/mCherry fusion construct (DTR-mCherry) and the *P2A* sequences which mediate ribosomal skipping during translation. Beneath this is the structure of the targeted *Cdkn2a* locus showing insertion of the *FDR* cassette into the 3' end of the *p16^{INK4A}* gene,

upstream of the endogenous stop codon (highlighted in red). (**B**) Pie charts showing the number of ES cell clones which showed insertion of the FDR cassette (Top) and the proportion of insertion and deletion events near the PAM site on the second *p16*^{INK4A} allele of targeted clones (Bottom). (**C**) Sequence of part of the 3rd exon of *p16*^{INK4A} showing the location of the endogenous stop codon (Red), as well as the qRNA sequence (Blue) and PAM site (Green). (**D**) Sequencing information on the second allele of *p16*^{INK4A} which did not show insertion of the FDR cassette in previously identified targeted clones. Clone 6G shows a deletion 3rd last amino acid and clone 11B demonstrate the deletion of the final three amino acids and their replacement with the amino acid sequence VALQS.

Together this construct was termed FDR (Flippase, Diphtheria toxin receptor and Reporter) and was synthesised by GenScript. The purpose of the included elements was to allow for lineage tracing of cells through FLP-mediated recombination of a separately introduced genetic reporter construct (i.e. a modified Rosa26 locus containing an FRT-flanked transcriptional stop sequence upstream of a reporter gene such as EGFP) and their ablation/visualisation through the DTR-mCherry fusion protein. The purpose of the P2A sequences flanking the FLP-recombinase was to allow for the cassette to be introduced, in-frame, to the 3' end of a gene to allow for the generation of a poly-cistronic open-reading frame that results in the production of the, minimally perturbed, endogenous gene product, FLP-recombinase and the DTR-mCherry fusion protein. P2A sequences permit this through their ability to facilitate ribosomal "skipping" over these regions during translation of the poly-cistronic mRNA.

5.2.1.2 Validation of the FDR cassette in vitro in HEK-293T cells

Initially, the *FDR* construct was tested in HEK-293T cells to ascertain whether mCherry expression was able to be visualised and if the FLP-recombinase could be expressed in a biochemically active manner. Transfection of HEK-293T

cells with a plasmid containing the FDR construct under the control of a CMV promoter resulted in clearly visible mCherry expression (Figure 5.2 A). The mCherry was also found to be localised to the cell membrane, as expected due to its fusion to the diphtheria toxin receptor, which should localise to the cell membrane. Furthermore, co-transfection of the FDR construct with a FLP recombination reporter plasmid, which contains a CMV-driven GFP which is prevented from being expressed due to an upstream FRT-flanked transcriptional stop cassette (Addgene plasmid – 13772), resulted in robust GFP expression (Figure 5.2 B).

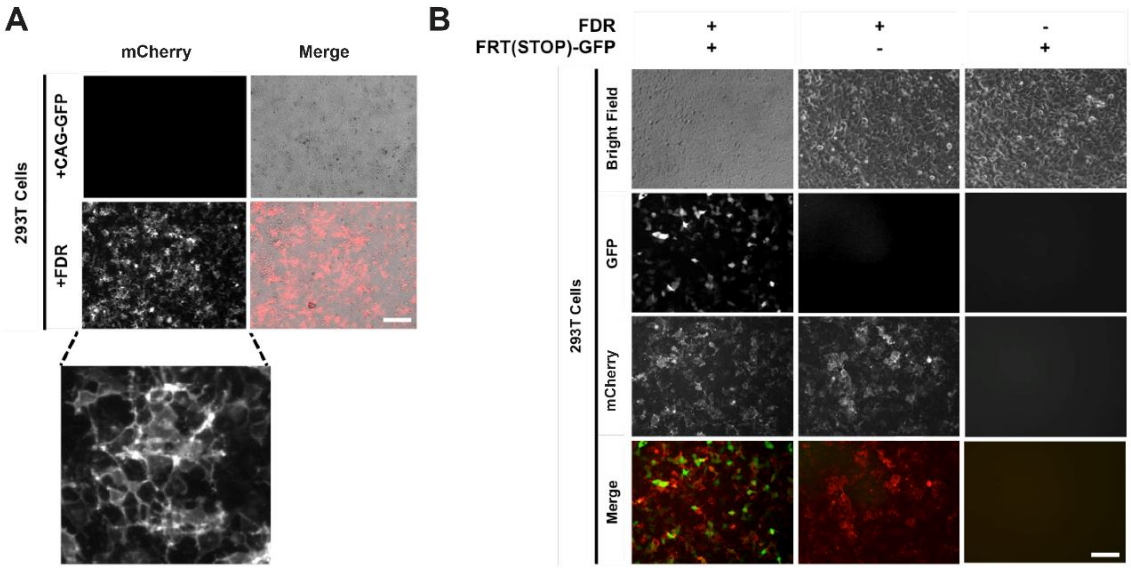

Figure 5.2. Transfection of HEK-293T cells results in the expression of mCherry and functional FLP-recombinase. (**A**) Transfection of HEK-293T cells with either the *FDR* cassette expressed under a CMV promoter construct or a GFP expressing plasmid as a control, resulted the in the membrane localised expression of mCherry after transfection with the *FDR* construct. (**B**). Transfection of HEK-293T cells with either the FDR construct in the absence or presence of a plasmid which reports FLP-recombination activity through the expression of GFP showing GFP expression only when both plasmids were co-transfected. Representative fluorescence images shown. Transfection experiment was conducted independently three times with consistant results. Scale bars; 50 µm.

Therefore, the FLP-recombinase contained within the FDR construct is expressed and is able to mediate recombination of FRT-flanked sequences. The

ability of transfected cells to be ablated with diphtheria toxin administration was not able to be ascertained with these experiments as HEK-293T, which are of human origin, are endogenously sensitive to diphtheria toxin.

5.2.1.3 Generation of the *p16^{FDR}* mouse model

(ES cells transfection and blastocyst injections were performed by Massimo Signore at the Institute of Child Health, University College London).

In order to understand the biology of senescent cells *in vivo*, the *FDR* cassette was introduced in-frame into the 3' end of the *p16^{INK4A}* gene. *p16^{INK4A}* was chosen as it is one of the most commonly expressed senescence-associated genes and its expression is seen in a variety of cellular senescent contexts including; replicative senescence, OIS and SIPS, among others (Dai & Enders 2000; Ohtani & Hara 2013; Darren J. Baker et al. 2011; Demaria, Ohtani, Youssef, Rodier, Toussaint, Mitchell, Laberge, Vijg, VanSteeg, Martijn E T Dollé, et al. 2014; Burd et al. 2013; Sato et al. 2015). The 3' end of the gene was chosen as the site of insertion to facilitate minimal disruption to the targeted endogenous *p16^{INK4A}* copy and to prevent its expression under the control of *p19^{ARF}*, another gene that is part of the *Cdkn2a* locus (Figure 5.1 A).

A guide RNA (gRNA) was designed which targeted a region 12 nt upstream the *p16^{INK4A}* stop codon (Figure 5.1 C). This gRNA was cloned into the px330 plasmid, which contains Cas9 and the regulatory element necessary for its expression. To mediate targeting of the 3' end of the *p16^{INK4A}* gene, two homology

arms were generated through PCR amplification, which corresponded to 2.5 kb upstream and 1.9 kb downstream of the gRNA protospacer adjacent motif (PAM) site (12 nt upstream of the p16INK4A stop codon). These homology arms were cloned flanking the *FDR* cassette (Figure 5.1 A) to generate the *p16-FDR* targeting vector. To avoid degradation of the targeting vector by Cas9 the PAM region in the targeting vector was mutated. Moreover, the antisense primer used to clone the 5'-*p16*-homology arm was modified to allow for the generation of an in frame insertion. The *FDR* targeting vector, px330 plasmid containing the gRNA and a vector containing a *puromycin* resistance cassette was co-transfected into wild type CCE ESCs to mediate CRISPR/Cas9 genome editing. The *puromycin* resistance cassette was used as a selection marker for potentially targeted ESC clones.

Following selection with Puromycin, 96 resistant ESC colonies were analysed for targeting efficiency. Specifically, a 2915 bp fragment was generated from the DNA of targeted clones using a forward primer which was upstream of the 5' homology arm and a reverse primer which was inside the FDR cassette (Figure 2.1 B). A second primer was also used which was near the end of the 5' homology arm, close the insertion point of the FDR cassette to allow for Sanger sequencing of the insertion site. Analysis of the 96 selected clones revealed that 13.5% (n=13) were correctly targeted in the region neighboring the PAM and showed in frame insertion of the FDR cassette (Figure 5.1 B). To determine if only one or both of the $p16^{INK4A}$ alleles were targeted, amplification of a 312bp PCR product using primers which flanked the targeted PAM site was performed (Figure 2.1 B). With this experimental approach, amplification of the allele containing the FDR cassette (targeted allele) was not achievable by PCR amplification due to its large size, generating only one product corresponding to the second allele, which was sent for Sanger sequencing to check for alteration in the proximity of the PAM region. This

analysis demonstrated that of the 13 targeted clones all showed heterozygous insertion of the FDR cassette, with no homozygous insertions being detected. Sequencing of the allele which did not show insertion of the FDR cassette in the 13 targeted clones revealed 77% possessed small deletions (n=10), 15% had small insertions (n=2) and 8% harbored both insertions and deletions (n=1) (Figure 5.1 B).

Two clones were selected for blastocyst injection to generate chimeric animals which harbored the $p16^{FDR}$ gene (Clones 6G and 11B). Clones 6G and 11B showed a respective deletion and an insertion mutational event. This resulted in the loss of the second last codon in clone 6G and the deletion of the final 3 codons in 11B, which were replaced with 5 amino acids (VALQS) (Figure 5.1 D). Following the generation of the two chimeric $p16^{FDR}$ lines, these mice were crossed with C57BL/6 mice to generate founder lines. Both founder lines were examined by the same sequencing strategy to select for mice that had inherited a true wild type copy of the $p16^{INK4A}$ gene, thereby generating $p16^{FDR/+}$ mice. Mice derived from the 11B clone were chosen to be used for further analysis and these mice were backcrossed for 5 generations before being used for experimentation.

5.2.1.4 Validation of *p16^{FDR}* function following MEF senescence induction *in vitro*

(Analysis of *p16^{FDR}* MEFs was performed in collaboration with Suchira Gallage at Imperial College London).

Following the generation of the *p16^{FDR}* mouse line, MEFs were isolated in order to test whether the FDR construct functioned as expected in an *in vitro* senescence induction system. Crossing of *p16^{FDR}* heterozygotes allowed for the generation of embryos that were either wild type, *p16^{FDR}* homozygotes or *p16^{FDR}* heterozygotes. These embryos were harvested at 13.5 dpc and MEFs were isolated. Three independent MEF cell lines were derived from each of the genotypes to be used as three biological replicates for the expreiments detailed in this section. Senescence was induced in these cells by serial passage in the presense of 20% oxygen, which has been demonstrated to induce senescence by causing extensive DNA damage through severe oxidative stress (Parrinello et al. 2003), to determine if they can express the FDR construct components and become sensitive to DT mediated ablation.

Initially, differences were noted in the growth dynamics between *p16^{FDR}* homo- and heterozygotes as well as wild type MEFs. Specifically, population doubling times were reduced by nearly 2-fold between heterozygotes and wild types, and 4-fold between homozyogotes and wild types (Figure 5.3 A). This was also reflected in crystal violet staining of fixed MEFs at the time of passage, which showed increased number of cells in plates containing homozygous or heterozygous *p16^{FDR}* MEFs, relative to wild type MEFs (Figure 5.3 B). However,

staining of the cells for SA-β-Gal, as a readout of cellular senescence induction, revealed qualitatively robust expression of the senescence marker in passage 6 wild type MEFs, with complete absence at passage 2. This observation was also true for *p16*$^{FDR/+}$ MEFs at passage 6, however p16FDR/FDR cells showed very little SA- β -Gal positivity at either passage (Figure 5.3 C).

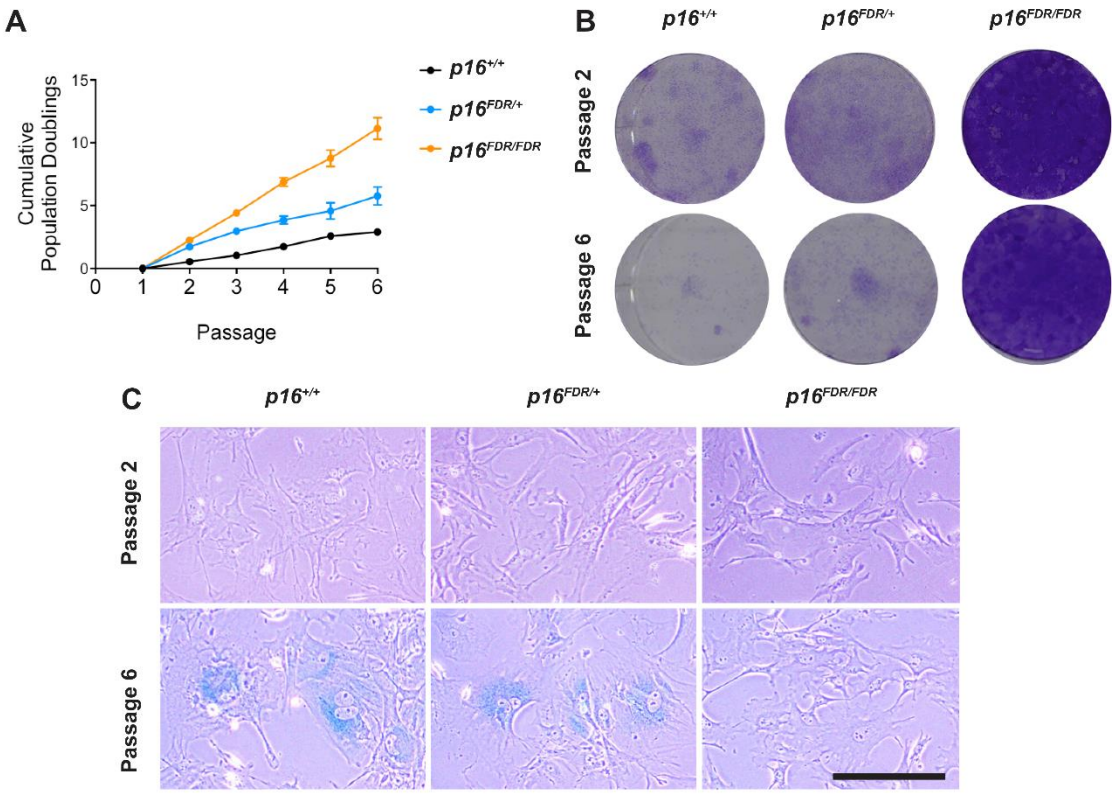

Figure 5.3. *p16*$^{FDR/+}$ MEFs are capable of entering oxidative stress-induced senescence. (**A**) Line graph demonstrating cumulative population doubling between wild type, *p16*$^{FDR/+}$ and *p16*$^{FDR/FDR}$ MEFs (n=3 per genotype) showing increase proliferation in *p16*^{FDR} homozygous and heterozygous cells. (**B**) Representative images of crystal violet stained wild type, *p16*$^{FDR/+}$ and *p16*$^{FDR/FDR}$ MEFs at passages 2 and 6 showing the increase cell density in *p16*^{FDR} homozygous and heterozygous cells. (**C**) Representative images of SA-β-Gal stained wild type, *p16*$^{FDR/+}$ and *p16*$^{FDR/FDR}$ MEFs at passages 2 and 6 showing the induction of oxidative stress-induced senescence in wild type and *p16*^{FDR} heterozygous cells. Data are mean±s.e.m. Scale bars; 50 μm.

Analysis of endogenous mCherry expression by fluorescent microscopy and cell count analysis was conducted to ascertain whether expression of the reporter increased in a passage dependent manner, which would be expected due to the induction of oxidative stress-induced senescence. As expected wild type MEFs displayed negligible levels of mCherry, which was most likely background auto-fluorescence, and these levels did not appreciably change between passage 2 and 6 (passage 2 - 3%, passage 6 - 1%; p=0.0681) (Figure 5.4). However, mCherry expression was found to be statistically significant increased from 13% of cells at passage 2 to 44% of cells at passage 6 in $p16^{FDR/+}$ MEFs (p=0.004) (Figure 5.4). Examination of $p16^{FDR/FDR}$ MEFs revealed that at passage 2 the cells already expressed mCherry is a large proportion of cells (72%), which showed a non-significant increase at passage 6 (87%, p=0.1583) (Figure 5.4).

qRT-PCR was performed on wild type, $p16^{FDR/+}$ and $p16^{FDR/FDR}$ MEFs at passages 2, 4 and 6 in order to determine if the *FDR* cassette components are expressed in a passage dependent manner as expected. Initially the expression of $p16^{INK4A}$ was profiled as a marker of cellular senescence, which has previously been shown to be upregulated in response to oxidative stress-induced senescence *in vitro* (Parrinello et al. 2003). In wild type cells $p16^{INK4A}$ expression rose by 1.5-fold and 2.6-fold between passages 4 and 6, respectively, relative to passage 2 (Figure 5.5 A). However, $p16^{FDR/+}$ MEFs showed much greater levels of $p16^{INK4A}$ mRNA than wild type MEFs at all 3 passages analysed. Although the levels of $p16^{INK4A}$ transcripts were higher in $p16^{FDR}$ heterozygotes than wild type they did show a passage-dependent increase, consistent with the induction of culture stress-induced senescence. Relative to wild type cells at passage 2, $p16^{FDR/+}$ cells showed a 1.9-fold increase at passage 2, a 4.4-fold increase at passage 4 and a 5.3-fold increase at passage 6 (Figure 5.5 A). $p16^{FDR}$ homozygotes showed an even greater elevation

in *p16*^{INK4A} mRNA than either *p16*$^{FDR/+}$ or wild type cells. Relative to passage 2 wild type cells, *p16*$^{FDR/FDR}$ MEFs expressed p16^{INK4A} 3-fold higher at passage 2 and 6-fold higher at passages 4 and 6 (Figure 5.5 A). Analysis of *FLP* and *DTR* expression found, as expected, that there was no expression in the wild type cells (Figure 5.5 B, C). However, *p16*^{FDR} homozygotes and heterozygotes were found to express both of these transcripts in both a gene-dosage and passage-dependent manner (Figure 5.5 B, C).

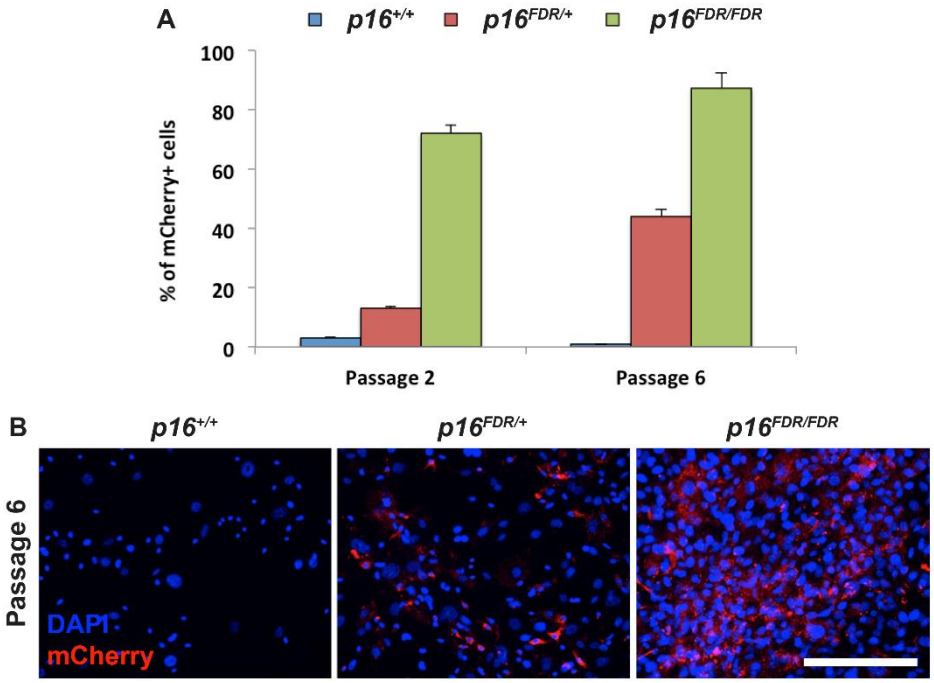

Figure 5.4. mCherry is expressed in a passage dependent manner in *p16*^{FDR} MEFs during the induction of senescence. (**A**) Quantification of the percentage of total cells which express the mCherry reporter from the *FDR* cassette between genotypes and cell culture passages (n=3 per genotype). Note the absence of mCherry+ cells in the wild type cultures but the passage dependent increase in cells which possess *p16*^{FDR}. (**B**) Representative fluorescence images of wild type, *p16*$^{FDR/+}$ and *p16*$^{FDR/FDR}$ MEFs at passage 6 showing the expression mCherry protein. Data are mean±s.e.m. Scale bars; 100 μm.

Specifically, relative to wild type cells at passage 2, *p16*$^{FDR/+}$ cells showed an increase in *FLP* expression that was 6702-fold, 14521-fold and 16961-fold higher at passages 2, 4 and 6, respectively. *p16*$^{FDR/FDR}$ MEFs expressed *FLP* 17676-fold,

31054-fold and 32036-fold higher at passage 2, 4 and 6, relative to wild type MEFs at passage 2 (Figure 5.5 B, C). Relative to wild type MEFs at passage 2, *DTR* expression in $p16^{FDR/+}$ cells was also elevated 757-fold, 1704-fold and 1883-fold higher at passages 2, 4 and 6, respectively. $p16^{FDR}$ homozygotes showed higher levels of DTR expression than heterozygotes with gene expression being measured 2284-fold, 3648-fold and 3510-fold higher at passages 2, 4 and 6, relative to wild type cells at passage 2 (Figure 5.5 B, C).

The ability of DT to clear senescent MEFs was ascertained through treatment of wild type, $p16^{FDR/+}$ and $p16^{FDR/FDR}$ cells at either passage 2 (replicating) or passage 6 (senescent) with either 0, 1, 10 or 100 ng/ml of DT. Cells were anlaysed 3 days following treatment. As expected, DT treatment had negligible effect on wild type cells, regardless of the passage (Figure 5.5 D, E). $p16^{FDR/+}$ cells at passage 2 were relatively insensitive to DT, apart from at a concentration of 100 ng/ml where a 34% reduction in cells, relative to vehicle treated $p16^{FDR/+}$ cells, was observed (Figure 5.5 D). At passage 6 however, treatment of $p16^{FDR/+}$ cells with 10 ng/ml of DT resulted in a relative loss of 55% of cells, which was more pronounced at a concentration of 100 ng/ml of DT where a relative loss of 88% of cells was observed (Figure 5.5 E). The effect of DT treatment on $p16^{FDR}$ homozygous MEFs was unsurprisingly greater when compared with heterozygotes. At passage 2, $p16^{FDR/FDR}$ cells showed a reduction in cell numbers of 51% and 88% at DT concentrations of 10 ng/ml and 100 ng/ml, respectively (Figure 5.5 D). At passage 6, $p16^{FDR/FDR}$ cells were reduced by 78% at a DT concentration of 10 ng/ml and at 100 ng/ml the cells were almost completely ablated ($p16^{FDR/FDR}$ cells were reduced by 99% compared with vehicle treated control $p16^{FDR/FDR}$ cells) (Figure 5.5 E).

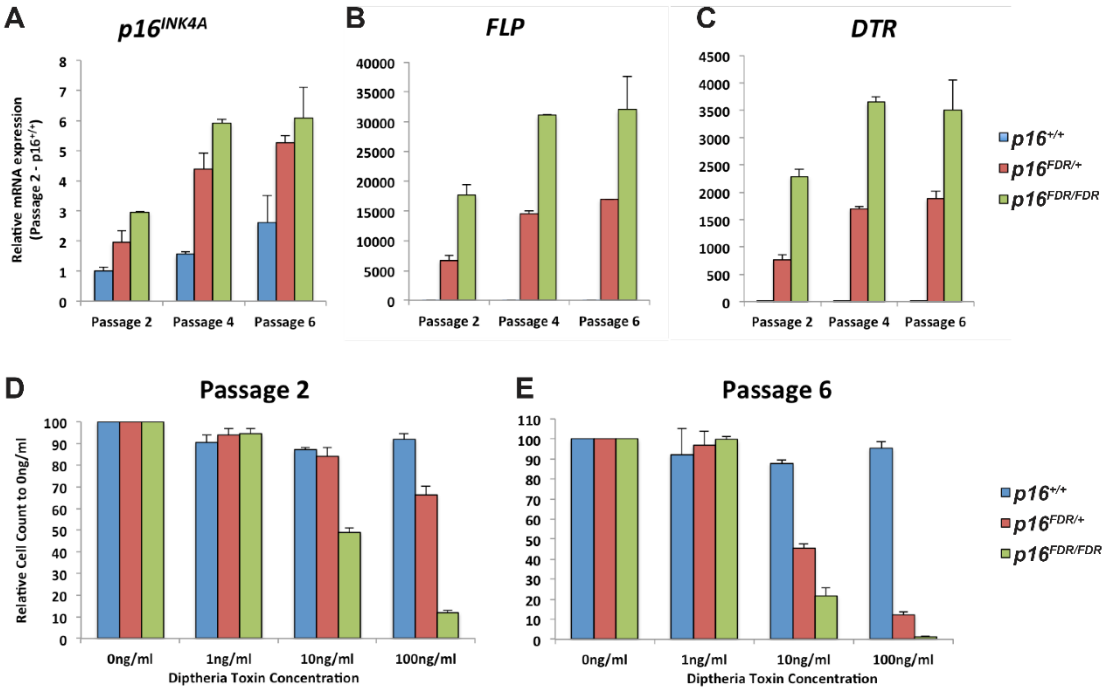

Figure 5.5. *p16*$^{FDR/+}$ MEFs express the components of the FDR cassette and are able to be ablated by DT following the induction of senescence. (**A**, **B**, **C**) Expression of *p16*^{INK4A} (**A**), *FLP* (**B**) and *DTR* (**C**) in wild type, *p16*$^{FDR/+}$ and *p16*$^{FDR/FDR}$ MEFs at passages 2, 4 and 6 (n=3 per genotype). Note the elevated expression of p16INK4A in *p16*$^{FDR/+}$ and *p16*$^{FDR/FDR}$ MEFs relative to wild type controls. *FLP* and *DTR* expression rises in a both a passage and gene dosage dependent manner. All gene expression data normalised to passage 2 wild type cells. (**D**, **E**) Relative cell counts, normalised to vehicle treated cells, showing the ability of wild type, *p16*$^{FDR/+}$ and *p16*$^{FDR/FDR}$ MEFs to be ablated thorough DT treatment (n= 3 per genotype). Note the specific sensitivity of *p16*$^{FDR/+}$ cells to be ablated only at passage 6, following senescence induction. Data are mean±s.e.m.

Together these results indicate that *p16*^{FDR} MEFs show a propensity towards a more proliferative behavior than wild type cells, with *p16*^{FDR} homozygotes showing the highest rate of proliferation. Analysis of the cellular senescence marker SA-β-Gal indicated that both the wild type cells and the *p16*^{FDR} heterozygotes are able to enter into oxidative stress-induced senescence, however the *p16*^{FDR} homozygous cells appear to be impaired in their ability to do so. This is possibly due to disruption of the poly-cistronic *p16*^{INK4A} mRNA in *p16*^{FDR} cells to be either transcribed or

translated at appropriate levels, leading to difficulties in activating the senescence program. In support of this hypothesis gene expression analysis revealed elevated levels of *p16*^{INK4A} transcripts in *p16*^{FDR} cells, relative to wild types cells, with *p16*^{FDR} homozygotes showing the greatest increase in expression. Gene expression analysis also revealed that *p16*^{FDR} cells increase the expression of *FLP*-recombinase and the *DTR* as well as showing mCherry fluorescence in a passage-dependent manner, correlating with the onset of oxidative stress-induced senescence. Moreover, *p16*^{FDR} cells, but not wild type cells at higher passages, once oxidative stress-induced senescence has initiated, demonstrated the ability to be ablated in the presence of DT.

5.2.1.5 *p16*^{FDR} homozygous mice have reduced lifespan compared with heterozygotes

p16^{FDR} homozygotes and heterozygotes were allowed to naturally age to determine if the introduction of the *p16FDR* allele produced any effects on their longevity or healthspan. This was investigated due to the proliferative abnormalities that were observed in the previous *p16*^{FDR} MEF experiments.

This analysis demonstrated that *p16*^{FDR} heterozygous mice showed a normal life and health span, with no spontaneous tumourigenesis observed in 26 mice analysed after 600 days (Figure 5.6 A). However, it was observed that *p16*^{FDR} homozygotes showed early lethality, with a mean life expectancy of 355 days (108-516 days, n=15) (Figure 5.6 A). Analysis of *p16*$^{FDR/FDR}$ mice upon death revealed that they predominantly developed spontaneous tumourigenesis in the liver (n=7 mice) and spleen (n=10 mice) (Figure 5.6 B). The high incidence of spontaneous

tumourigenesis in p16FDR homozygotes is likely due to the homozygosity of *p16*^{INK4A} hypomorphic alleles (discussed in further detail in section 6.5).

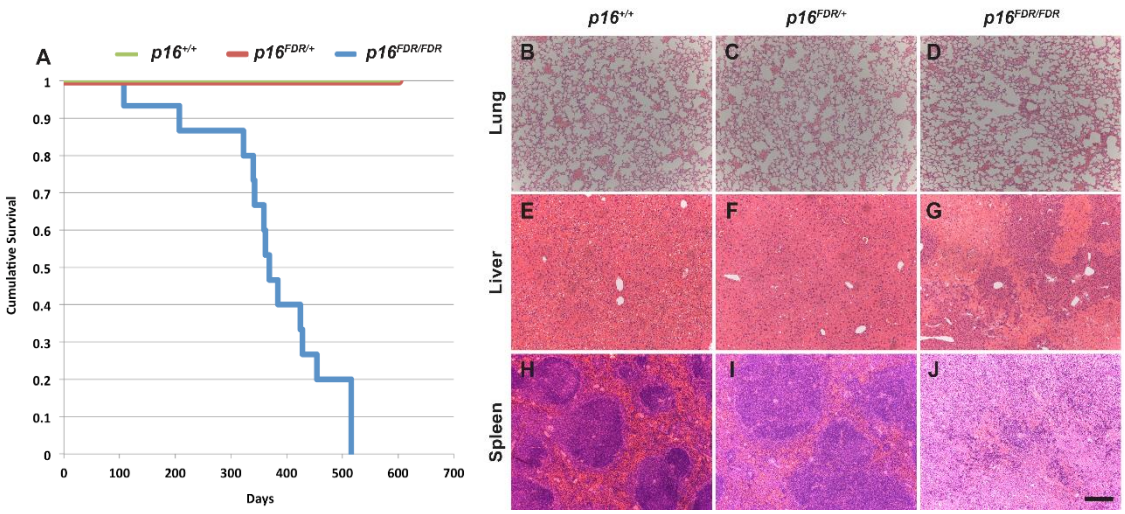

Figure 5.6. *p16*^{FDR} homozygous mice display early lethality associated with spleen and liver tumourigenesis. (**A**) Kaplan-meier plot comparing the survival of wild type, *p16*$^{FDR/+}$ and *p16*$^{FDR/FDR}$ mice. (**B**-**J**) H&E images of organs from wild type, *p16*$^{FDR/+}$ and *p16*$^{FDR/FDR}$ mice collected at 1 year of age. (**B**, **C**, **D**) Lung histology of wild type (**B**), *p16*$^{FDR/+}$ (**C**) and *p16*$^{FDR/FDR}$ (**D**) mice showing absence of spontaneous tumourigenesis. (**E**, **F**, **G**) liver histology of wild type (**E**), *p16*$^{FDR/+}$ (**F**) and *p16*$^{FDR/FDR}$ (**G**) mice demonstrating the presence of cancerous cells in *p16*^{FDR} homozygous mice. (**H**, **I**, **J**) Spleen histology of wild type (**H**), *p16*$^{FDR/+}$ (**I**) and *p16*$^{FDR/FDR}$ (**J**) mice showing the presence of cancerous cells in *p16*^{FDR} homozygous mice. Scale bars; 200 μm.

5.2.2 Investigating the effect of ablation of *p16* (mCherry)-expressing cell populations in NSCLC development

In order to model NSCLC development in mice the previously described oncogenic conditional *Kras*$^{G12D/+}$ allele was used (Jackson et al. 2001), which allows for lung tumour development following Cre-mediated recombination (see section 1.5.5 for details on the *Kras*$^{G12D/+}$ murine lung cancer model). Cre was delivered to

the lungs through the intra-nasal administration of adenoviruses that carried a Cre-recombinase expression construct (AdCre). To probe the role of cellular senescence during mouse NSCLC initiation and progression the *p16*^{FDR} mouse line was crossed with *Kras*$^{G12D/+}$ and *Rosa26*$^{YFP/+}$ mice to generate *Kras*$^{G12D/+}$*; p16*$^{FDR/+}$*; Rosa26*$^{YFP/+}$ triple heterozygotes. The *Rosa26*$^{YFP/+}$ allele allows for the lineage tracing of oncogenic *Kras* mutation sustaining cells that derive the tumour and the *p16*$^{FDR/+}$ allele permits the visualisation and selective ablation of *p16*^{INK4A}-expressing cell populations during tumourigenesis.

5.2.2.1 A similar media survival and tumour histology is observed in *Kras*$^{G12D/+}$*; p16*$^{FDR/+}$*; Rosa26*$^{YFP/+}$ and *Kras*$^{G12D/+}$*; p16*$^{+/+}$; *Rosa26*$^{YFP/+}$ mice following NSCLC induction

Initially a survival analysis was performed on *Kras*$^{G12D/+}$*; p16*$^{FDR/+}$*; Rosa26*$^{YFP/+}$ mice induced to form lung tumours to ascertain whether their survival was reduced compared with induced *Kras*$^{G12D/+}$*; Rosa26*$^{YFP/+}$ mice. The purpose of this was to determine if the introduction of the *p16*^{FDR} allele was itself having a tumour promoting or retarding effect. Specifically, *Kras*$^{G12D/+}$*; p16*$^{FDR/+}$*; Rosa26*$^{YFP/+}$ and *Kras*$^{G12D/+}$*; p16*$^{+/+}$*; Rosa26*$^{YFP/+}$ mice were induced with 2.5x10^{7} AdCre viral particles at 4 weeks of age to induce lung tumourigenesis. Following these mice long term demonstrated an equal mean survival of 180 days in both *Kras*$^{G12D/+}$*; p16*$^{FDR/+}$*; Rosa26*$^{YFP/+}$ (158-225 days, n=6) and *Kras*$^{G12D/+}$*; p16*$^{+/+}$*; Rosa26*$^{YFP/+}$ mice (134-211 days, n=8), which was not statistically significantly different (p=0.6956) (Figure 5.7 A). Therefore, this survival analysis showed that introduction of the *FDR* cassette into the *Cdkn2a* locus does not affect lung tumour survival. Furthermore, analysis of the lung tumours after 8 weeks of development, with and without the

presence of the *FDR* cassette, revealed the presence of tumours of similar size and histology (Figure 5.7 B, C). Moreover, the tumour formed in both of these models demonstrated immunoreactivity for thyroid transcription factor-1 (TTF-1), a marker for lung adenocarcinomas (Moldvay et al. 2004) (Figure 5.7 D, E). Therefore, this indicated that the presence of the *FDR* cassette is not overtly affecting the tumourigenesis process in the lungs.

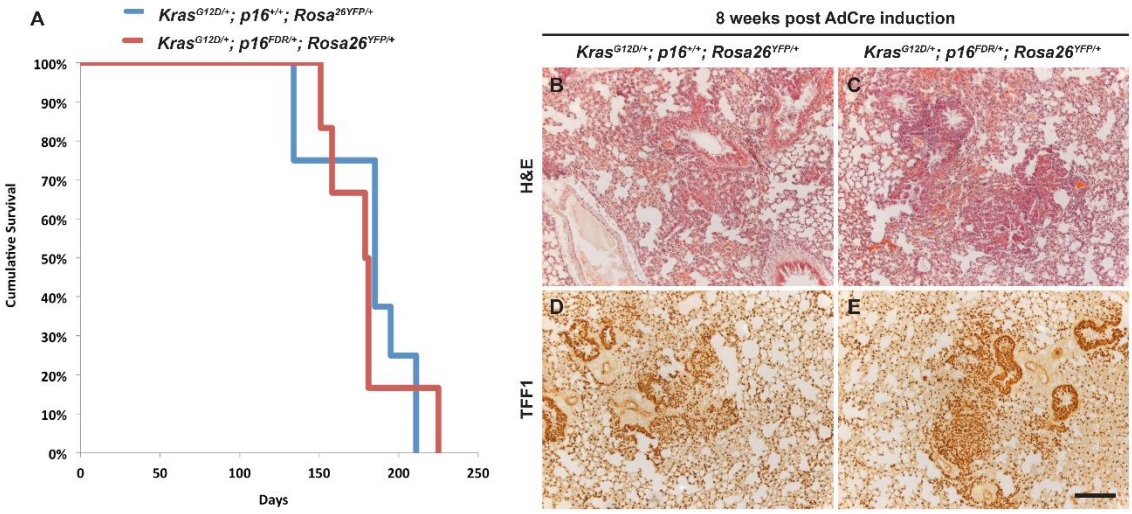

Figure 5.7. No difference in survival or tumour histology observed between *Kras$^{G12D/+}$; Rosa26$^{YFP/+}$* and *Kras$^{G12D/+}$; p16$^{FDR+/}$; Rosa26$^{YFP/+}$* mice. (**A**) Kaplan-meier plot comparing the survival of *Kras$^{G12D/+}$*; *Rosa26$^{YFP/+}$* and *Kras$^{G12D/+}$; p16$^{FDR/+}$*; *Rosa26$^{YFP/+}$* mice. (**B**, **C**) H&E images of lung tumours found in *Kras$^{G12D/+}$*; *Rosa26$^{YFP/+}$* (**B**) and *Kras$^{G12D/+}$; p16$^{FDR/+}$*; *Rosa26$^{YFP/+}$* (**C**) mice induced at 4 weeks of age to form tumour and analysed 8 week later, indicating similar size and histology of the tumours. (**D**, **E**) TFF1 IHC on the same lung tumour sections from of *Kras$^{G12D/+}$*; *Rosa26$^{YFP/+}$* and *Kras$^{G12D/+}$; p16$^{FDR/+}$*; *Rosa26$^{YFP/+}$* mice showing the similar presence of the lung adenocarcinoma marker in the tumour lesions. Scale bars; 200 µm.

5.2.2.2 mCherry+ cells are senescent and can be ablated

To examine whether the *p16^{FDR}* allele appears to be functioning appropriately *in vivo*, lung tumour bearing mice that carried *p16^{FDR}* in heterozygosity

(*Kras*$^{G12D/+}$*; p16*$^{FDR/+}$*; Rosa26*$^{YFP/+}$) were analysed by a combination of IHC, flow cytometry, qRT-PCR and DT ablation assays.

Initially, *Kras*$^{G12D/+}$*; p16*$^{FDR/+}$*; Rosa26*$^{YFP/+}$ mice were induced with AdCre at 4 weeks of age and the lungs were analysed for the presence of mCherry+ cells at 2, 4 and 8 weeks post viral induction. IHC against mCherry revealed that a large number of scattered single mCherry+ cells could be seen throughout the lung parenchyma at all timepoints analysed (Figure 5.8 A, B). On average 14**%** of cells were mCherry+ at 2 weeks post viral induction and this proportion was generally maintained during the tumourigenesis process, with a non-significant trend towards a reduction at later time points (4 weeks - 10%, 2 weeks versus 4 weeks p=0.1254; 8 weeks - 8%, 2 weeks versus 8 weeks p=0.3519) (Figure 5.8 B). This presence of mCherry+ cells was also explored by performing flow cytometry on dissociated tumour bearing lungs from *Kras*$^{G12D/+}$*; p16*$^{FDR/+}$*; Rosa26*$^{YFP/+}$ mice at the previously analysed timepoints. This showed a similar result to the histological quantification of mCherry+ cells, with 0.25%, 0.39% and 0.3% of total lung cells expressing mCherry at 2, 4 and 8 weeks post viral induction, respectively (Figure 5.8 C).

To gain an understanding if these mCherry-expressing cells are senescent they were probed by IHC analysis for common markers of cellular senescence. As one of the defining hallmarks of senescence is irreversible proliferative arrest, mCherry cells were initially stained for markers of cell division. IHC for Ki67 and mCherry revealed that these cells were negative for markers of proliferation, which would be expected if the *p16*^{FDR} allele is reporting senescent cells (Figure 5.8 G). Moreover, around 80% and 75% of the mCherry+ cells were found to be positive for the senescence effectors p16 and p21, respectively (Figure 5.8 D, E, H).

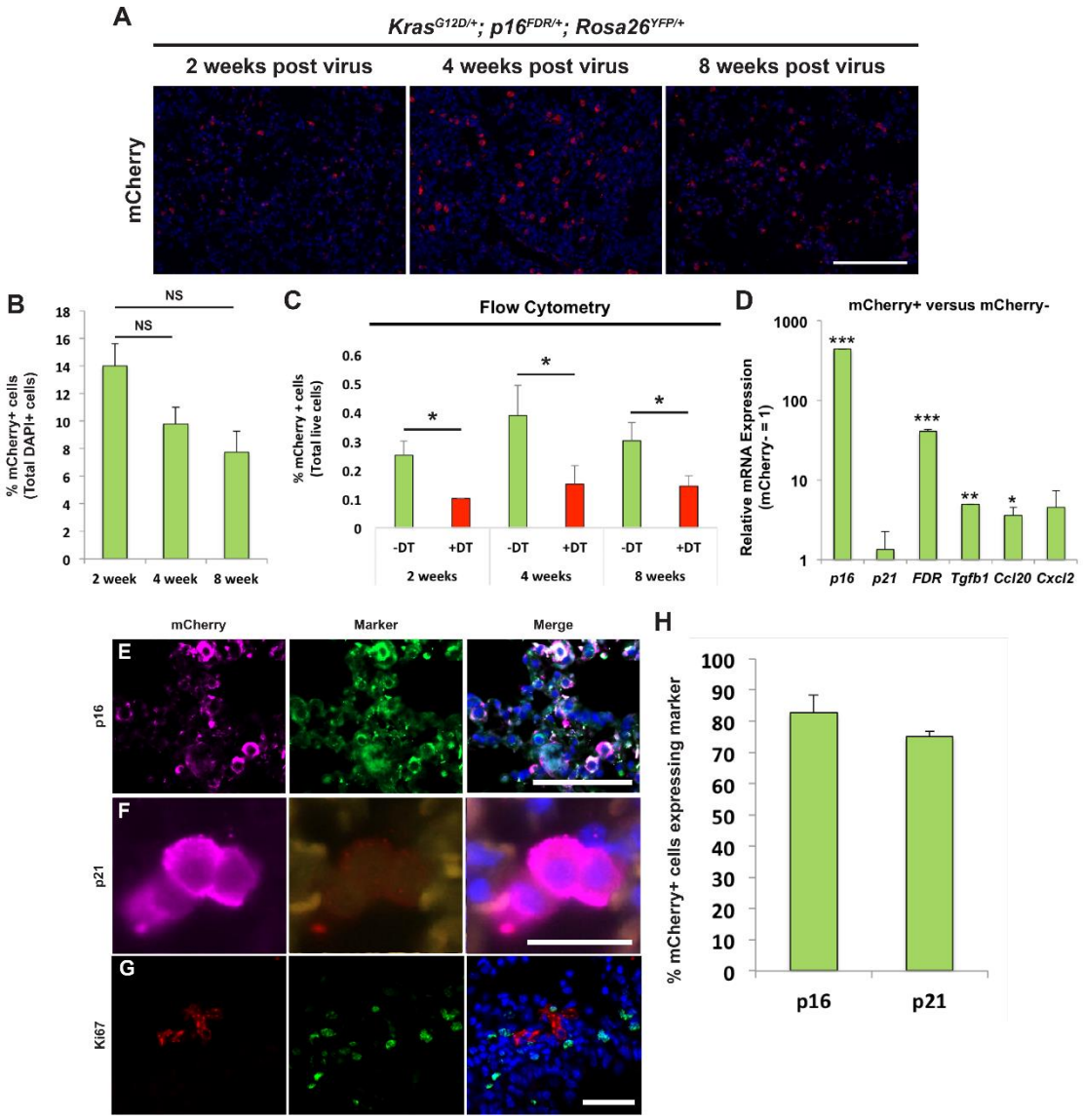

Figure 5.8. mCherry cells can be visualised, appear senescent and can be ablated by DT administration during lung tumourigenesis *in vivo*. (**A**) IF analysis for the presence of mCherry+ cells in the lungs from *Kras$^{G12D/+}$; p16$^{FDR/+}$; Rosa26$^{YFP/+}$* mice induced at 4 weeks of age and analysed 2, 4 and 8 weeks later, showing comparable levels of mCherry cells. (**B**) Quantification of the proportion of mCherry cells found in the same lung tissue section (n=3 per timepoint). (**C**) FACS quantification of the proportion of mCherry cells to total live cells before and after DT treatment, 2, 4 and 8 weeks post viral induction (2 weeks -DT n=3 +DT n=3, 4 weeks -DT n=4 +DT n=6, 8 weeks -DT n=4 +DT n=5). (**D**) qRT-PCR comparing FACS isolated mCherry+ and mCherry- cell fractions, showing an increase in senescence effectors, FDR components and SASP factors in the mCherry+ cell fraction. Gene expression data normalised to mCherry- cells (mCherry+ n=4, mCherry- n=4). (**E**-**G**) IF staining showing the colocalisation of mCherry with p16 (**E**) and p21 (**F**). mCherry cells are negative for the proliferation marker Ki67 (**G**). (**H**) Quantification of the proportion of mCherry

cells which express either p16 or p21 in *Kras*$^{G12D/+}$; *p16*$^{FDR/+}$; *Rosa26*$^{YFP/+}$ mice induced at 4 weeks of age and analysed 8 weeks later (n=3 per marker). *P≤0.05, **P≤0.01, ***P≤0.001, Student's t-test. Data are mean±s.e.m. NS = not significant. Scale bars; 50 μm (A, E, G), 15 μm (F).

To further explore whether the mCherry+ cells have activated the senescent phenotype, mCherry+ and mCherry- cells were isolated from the lungs of *Kras*$^{G12D/+}$; *p16*$^{FDR/+}$; *Rosa26*$^{YFP/+}$ mice, 8 weeks post AdCre induction, by flow cytometry to probe their gene expression profile by qRT-PCR. Comparison of mCherry+ and mCherry- cells revealed high levels of *FDR* mRNA, as expected, providing confidence in the successful isolation of mCherry+ cells by FACS. Furthermore, a significant enrichment for the senescence effector *p16* and a trend towards increased *p21* expression in mCherry+ cells. Furthermore, a significant enrichment for the SASP factors *Tgfb1* and *Ccl20* and a trend towards increased *Cxcl2* expression was also observed in mCherry+ cells (Figure 5.8 D).

To test whether the identified mCherry+ cells are able to be pharmacogenetically ablated through DT administration, *Kras*$^{G12D/+}$; *p16*$^{FDR/+}$; *Rosa26*$^{YFP/+}$ mice were induced with AdCre at 4 weeks of age and treated twice weekly with either 10 ng/g of DT or PBS, as a vehicle control. The lungs of these mice were then analysed by flow cytometry 2, 4 and 8 weeks later for any change to the mCherry+ cell population. This analysis revealed that on average, DT treatment resulted in the ablation of 50-60% of mCherry+ cells. Specific proportions of mCherry+ cells were: (i) At 2 weeks post virus induction, control samples, 0.25% and DT treated, 0.10%, p=0.042; (ii) At 4 weeks post induction, control 0.39% and DT treated, 0.15%, p=0.049; (iii) and at 8 weeks post induction, control 0.30% and DT treated, 0.14%, p=0.0351 (Figure 5.8 C). Greater levels of mCherry+ cell ablation could be achieved at higher DT concentrations, however, animals showed

deleterious health effects such as significant weight loss, therefore all experiments involving DT ablation were performed at 10 ng/gr of body weight (Data not shown).

Together, these results show that mCherry+ cells are found within the lungs of mice induced to form NSCLC and that their proportion does not appear to change with time. These cells appear to express the senescence markers p16 and p21 as well as a subset of canonical SASP molecules. Further to this, a significant proportion of putatively senescent mCherry+ cells are able to be pharmacogenetically ablated through DT administration *in vivo*.

5.2.2.3 A low proportion of developing tumour cells are mCherry+

Following the identification that mCherry+ cells bear hallmarks of cellular senescence, their presence within developing tumour lesions was assessed. The purpose of this was to determine the degree of senescence within the tumour, to understand if senescence was acting as a tumour-suppressive mechanism as is generally believed, as well as to assess the potential therapeutic potential of their ablation.

To achieve this, tumour bearing lungs from KrasG12D/+; p16FDR/+; Rosa26YFP/+ mice, induced with AdCre at 4 weeks of age, were collected 2, 4 and 8 weeks post-induction and studied by IF for both mCherry (putatively senescent cells) and YFP (KrasG12D mutation sustaining tumour cells). Immunofluorescence analysis of lung tissue sections 2 weeks post viral induction from KrasG12D/+; p16FDR/+; Rosa26YFP/+ mice showed a small number of scattered nascent

tumour foci that are comprised of around 9 YFP+ cells (+/- 3.2 cells). This increased to an average of 43 cells (+/- 19 cells) at 4 weeks and to 146 cells at 8 weeks (+/- 38 cells) (Figure 5.9 A-C).

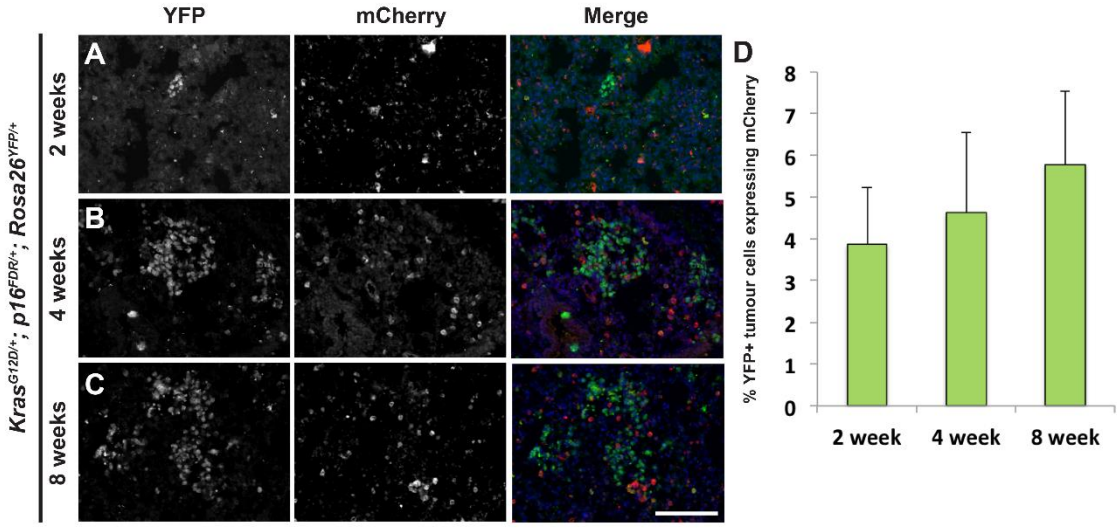

Figure 5.9. Very few mCherry cells are found within developing lung tumour lesions. (**A**-**C**) Double IF staining of *Kras*$^{G12D/+}$*; p16*$^{FDR/+}$*; Rosa26*$^{YFP/+}$ lungs 2 (**A**), 4 (**B**) and 8 (**C**) weeks post viral induction for YFP and mCherry colocalisation. (**D**) Quantification of the number of YFP+ tumour cells which express mCherry at the indicated age post viral induction (n=3 per timepoint). Data are mean±s.e.m. Scale bars; 100 μm.

Interestingly, analysis of mCherry/YFP colocalisation revealed only a small percentage of tumour cells expressed the *FDR* mCherry reporter. At 2 weeks post virus mCherry expression was almost undetectable in YFP+ tumour cells (Figure 5.9 A, D). At 4 and 8 weeks post-viral induction it was found that only 4.6% and 5.7% of YFP+ tumour cells were positive for mCherry, respectively (Figure 5.9 B, C, D). Therefore, this provides evidence that the majority of tumour cells are negative for p16 expression.

Furthermore, evidence for the low burden of *p16*-expressing mCherry+ cells in the growing tumours was also provided by flow cytometry. Analysis of dissociated lungs from *Kras*$^{G12D/+}$*; p16*$^{FDR/+}$*; Rosa26*$^{YFP/+}$ mice for mCherry+ and YFP+ cells revealed that the vast majority of mCherry+ cells appeared to be YFP- at all timepoints analysed. This could be in part due to difficulty of the flow cytometric approach to differentiate between YFP+/mCherry- and YFP+/mCherry+. However, comparison of *Kras*$^{G12D/+}$*; p16*$^{FDR/+}$*; Rosa26*$^{YFP/+}$ and *Kras*$^{G12D/+}$*; Rosa26*$^{YFP/+}$ mice induced with AdCre at 4 weeks of age and analysed by FACS found comparable numbers of YFP+ cells (*Kras*$^{G12D/+}$*; p16*$^{FDR/+}$*; Rosa26*$^{YFP/+}$ YFP+ cells = 2.75%, *Kras*$^{G12D/+}$*; Rosa26*$^{YFP/+}$ YFP+ cells = 2.65%, p=0.9245) at 8 weeks post viral induction. This indicates that if there is a population of YFP+/mCherry+ cells in *Kras*$^{G12D/+}$*; p16*$^{FDR/+}$*; Rosa26*$^{YFP/+}$ mice they are very low in proportion to the predominantly YFP+/mCherry- tumour cells.

Therefore, these results indicate that there is a slight increase in the number of *p16*-expressing cells in lung tumours between 2 and 4 weeks post-induction, however the overall burden of mCherry+ cells is very low between 4 and 8 weeks post viral induction. This suggests that senescence is not acting to cell-autonomously limit tumour expansion, to any considerable degree, at the timepoints analysed, contrary to the initial hypothesis. In agreement with this, the co-localisation of mCherry and YFP is very low.

5.2.2.4 Ablation of *p16* (mCherry)-expressing cells results in a reduced tumour burden in *Kras$^{G12D/+}$; p16$^{FDR/+}$; Rosa26$^{YFP/+}$* mice

Due to the very low degree of co-localisation between senescent mCherry+ and tumour YFP+ cells, it was anticipated that there would be little efficacy in DT treatment reducing the tumour burden. However, the fact that mCherry cells are predominantly found outside the tumour led to the refined hypothesis that they may have non-cell autonomous functions that may influence tumour development, similar to what was observed in the mouse model of ACP (see chapter 3). Therefore, the effect of mCherry+ cell ablation on NSCLC tumour initiation and progression was ascertained.

This was achieved by treating *Kras$^{G12D/+}$; p16$^{FDR/+}$; Rosa26$^{YFP/+}$* mice with DT (under the same dosing regime performed previously in section 5.2.2.3) and assessing tumour burden. Remarkably, the lungs from *Kras$^{G12D/+}$; p16$^{FDR/+}$; Rosa26$^{YFP/+}$* mice, 8 weeks post viral induction, treated with DT showed a dramatic reduction in the number of visible tumours on the surface of the lung, when compared with the lungs from vehicle treated control mice (Figure 5.10 A). Moreover, analysis of whole mount YFP fluorescence in these animals revealed greatly reduced levels of YFP, potentially indicating that DT was having an anti-tumourigenic effect (Figure 5.10 B).

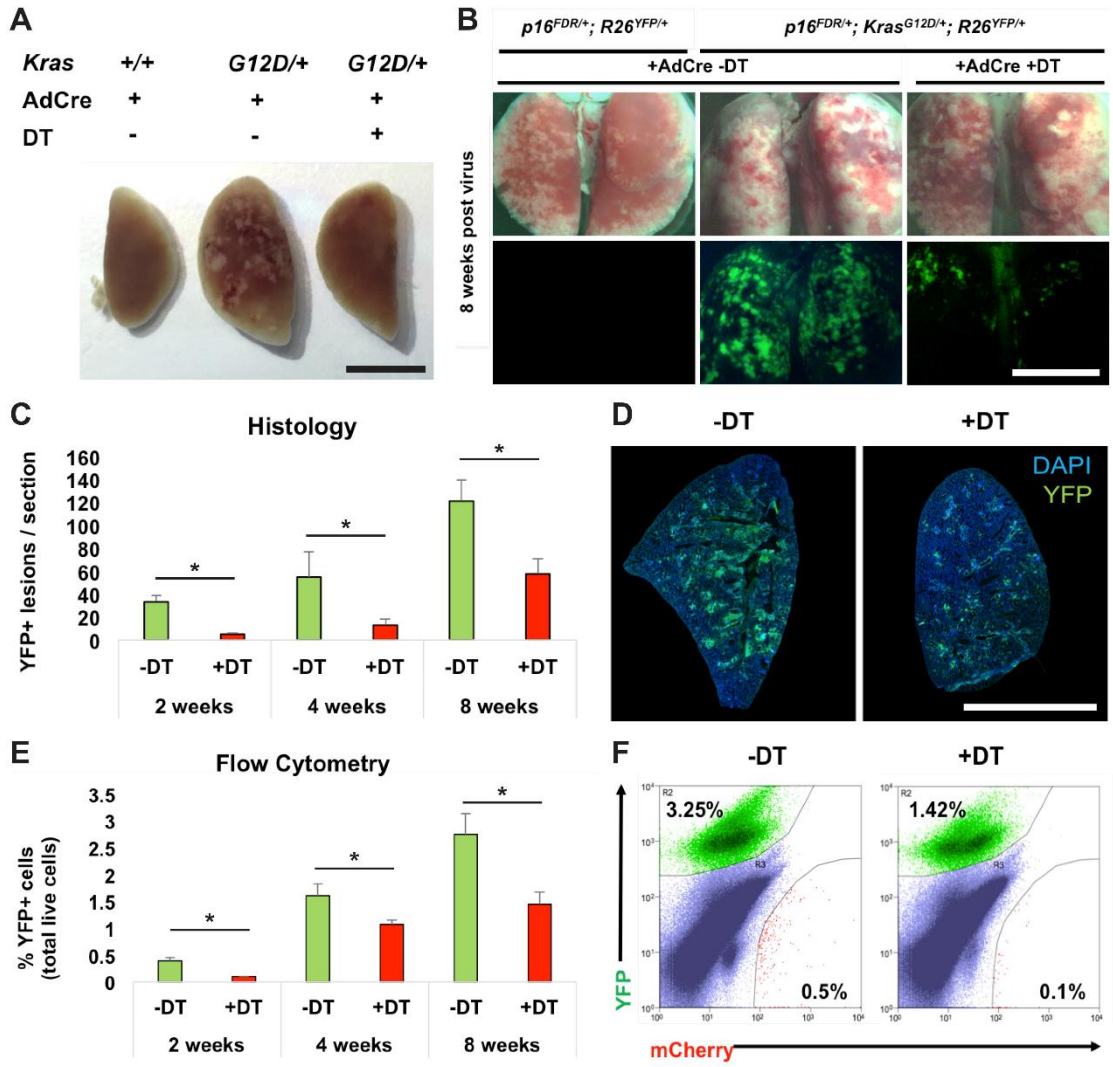

Figure 5.10. Ablation of mCherry cells resulting in a dramatic reduction in tumour burden in *Kras$^{G12D/+}$; p16$^{FDR/+}$; Rosa26$^{YFP/+}$* mice. (**A**) Representative gross morphology of lungs from *p16$^{FDR/+}$; Rosa26$^{YFP/+}$* and *Kras$^{G12D/+}$; p16$^{FDR/+}$; Rosa26$^{YFP/+}$* mice induced at 4 weeks of age and analysed 8 weeks later. Not the reduced incidence of surface tumour lesions in the DT treated *Kras$^{G12D/+}$; p16$^{FDR/+}$; Rosa26$^{YFP/+}$* mice (n=5 per group). (**B**) Representative whole mount fluorescence images of *p16$^{FDR/+}$; Rosa26$^{YFP/+}$* and *Kras$^{G12D/+}$; p16$^{FDR/+}$; Rosa26$^{YFP/+}$* mice for the presence of YFP+ tumours, indicating a reduction in *Kras$^{G12D/+}$; p16$^{FDR/+}$; Rosa26$^{YFP/+}$* mice treated with DT (n=5 per group). (**C**) Histological analysis of the number of tumour lesions in *Kras$^{G12D/+}$; p16$^{FDR/+}$; Rosa26$^{YFP/+}$* mice treated with either vehicle control or DT, showing a reduction in the number of lesions (n=3 mice per group per timepoint). (**D**) Representative histological lung sections from *Kras$^{G12D/+}$; p16$^{FDR/+}$; Rosa26$^{YFP/+}$* mice treated with either vehicle control or DT and IF stained for YFP+ tumour cells. (**E**) FACS analysis of the proportion of YFP tumour cells (relative to total live cells) between *Kras$^{G12D/+}$; p16$^{FDR/+}$; Rosa26$^{YFP/+}$* mice treated with either vehicle control or DT, showing a reduction in the number of YFP+ cells (2 weeks -DT n=3 +DT n=3, 4 weeks -DT

n=4 +DT n=6, 8 weeks -DT n=4 +DT n=5). (**F**) Representative FACS plot from *Kras*$^{G12D/+}$; *p16*$^{FDR/+}$; *Rosa26*$^{YFP/+}$ mice treated with either vehicle control or DT, showing a reduction in both the number of YFP (Green, top left) and mCherry+ (Red, bottom right) cells. *P≤0.05, Student's t-test. Data are mean±s.e.m. Scale bars; 5 mm.

To better characterise the effect of DT treatment on tumour burden, the lung tumours from *Kras*$^{G12D/+}$; *p16*$^{FDR/+}$; *Rosa26*$^{YFP/+}$ mice were assessed at 2, 4 and 8 week post-viral induction by a combination of histology and flow cytometry. FACS analysis of vehicle treated *Kras*$^{G12D/+}$; *p16*$^{FDR/+}$; *Rosa26*$^{YFP/+}$ mice revealed that, relative to the total cells in the lung, the number of YFP+ tumour cells increased from 0.39% at 2 weeks post induction to 1.6% at 4 weeks and finally to 2.75% at 8 weeks (Figure 5.10 E). Remarkably, DT treatment resulted in a significant reduction in the number of YFP+ cells at all three timepoints. At 2 weeks post induction the number of YFP+ cells fell to 0.10% (74.4% reduction, p=0.0424), at 4 weeks the number of tumour cells were reduced to 1.07% (33.2% reduction, p=0.0274) and at 8 weeks the number of YFP+ cells fell to 1.44% (47.6% reduction, p=0.0155) following DT treatment (Figure 5.10 E,F). Histological analysis of *Kras*$^{G12D/+}$; *p16*$^{FDR/+}$; *Rosa26*$^{YFP/+}$ lungs treated with either vehicle or DT revealed similar results. The number of YFP+ tumour lesions were manually counted from histological sections IF stained with YFP from tumour bearing lungs collected from *Kras*$^{G12D/+}$; *p16*$^{FDR/+}$; *Rosa26*$^{YFP/+}$ mice 2, 4 and 8 weeks post viral induction. This analysis showed that at 2 weeks, the number of tumour lesions decreased by 85.42% (control, 33.33 lesions; DT treated 4.86 lesions; p=0.0391), at 4 weeks there was a decrease of 76.32% (control, 54.89 lesions; DT treated - 13.23 lesions; p=0.0426) and at 8 weeks a reduction of 52.55% (control, 121.17 lesions; DT treated, 57.5 lesions; p=0.0351) was observed (Figure 5.10 C, D).

It is important to know whether the effect of DT treatment on tumour burden was specifically through the action of the *p16*^{FDR} gene or through a non-specific chemotherapeutic mechanism. To test this *Kras*$^{G12D/+}$*; Rosa26*$^{YFP/+}$ mice were induced with AdCre at 4 weeks of age to induce lung tumourigenesis and for 8 weeks the mice were treated with either a vehicle control or DT, twice a week as in the previous experiment. Following this the lungs were collected for analysis. Whole-mount fluorescence imaging of these lungs revealed comparable levels of YFP fluorescence, indicating an analogous tumour burden (Figure 5.11 A). Analysis of the proportion of YFP+ cells between DT treated and control lungs by FACS revealed no significant difference between the groups (Control, 2.65%; DT treated, 2.15%; n=3 per group; *p*=0.6315 students t-test) (Figure 5.11 B).

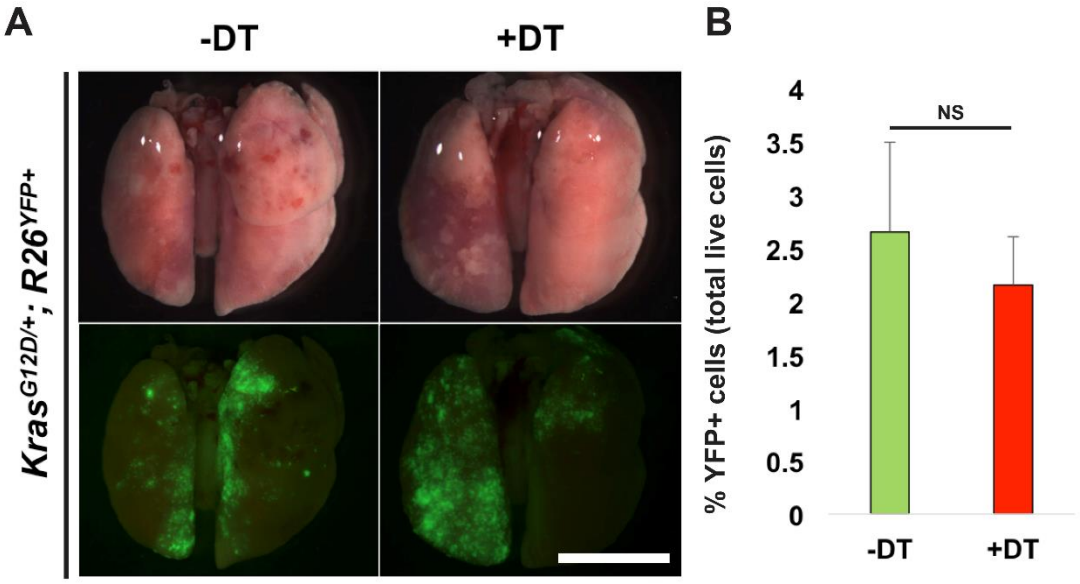

Figure 5.11. The presence of the *FDR* cassette is required to mediate a reduction in lung tumour burden following DT treatment. (**A**) Whole mount fluorescence analysis of *Kras*$^{G12D/+}$*; Rosa26*$^{YFP/+}$ mice induced at 4 weeks of age and treated with either vehicle control or DT for 8 weeks (n=3 mice per treatment group). Note the similar area of the lung containing tumour cells, regardless of treatment regime. (**B**) FACS analysis of the proportion of YFP tumour cells (relative to total live cells) in *Kras*$^{G12D/+}$*; Rosa26*$^{YFP/+}$ mice treated with either vehicle control or DT, showing similar levels of YFP+ cells between treatment groups (n=3 mice per treatment group). NS = not significant. Data are mean±s.e.m. Scale bars; 5 mm.

Together, these results indicate that the ablation of *p16*-expressing cells significantly reduces the tumour burden in a mouse model of NSCLC. DT treatment improved the gross appearance of tumour bearing lungs by visibly reducing the size and number of tumours. Furthermore, analysis of treated lungs histologically and by flow cytometry confirmed that the overall number of tumour cells was significantly lower. Analysis of DT treated lung tumour bearing animals, which did not possess the $p16^{FDR}$ gene, confirmed that tumour-reducing effect of DT treatment was due to the ablation of mCherry+ cells.

5.2.2.5 Reduction of *p16* (mCherry)-expressing cells retards tumour cell proliferation

As it was observed that the majority of *p16*-expressing cells are found outside of the tumour lesions and that their ablation led to a reduction in tumour burden, this implies that the *p16*-expressing cells are able to non-cell autonomously influence the development of the tumour. This situation is potentially analogous to the work described in chapter 3, where senescent cluster cells in the pituitary of $Sox2^{CreERT2/+}$; $Ctnnb1^{lox(ex3)/+}$; $Rosa26^{YFP/+}$ mice have a mitogenic effect on surrounding cells and are able to non-cell autonomously induce tumourigenesis. Furthermore, studies by other groups have shown that senescent cells are able to promote proliferation in both normal and tumour tissue by the paracrine action of the SASP (Coppé, Christopher K. Patil, et al. 2010; Laberge et al. 2015; Kuilman et al. 2008; Bavik et al. 2006).

Therefore, the effect on lung tumour proliferation following the ablation of *p16*-expressing cells was ascertained to determine whether these cells might be having pro-mitogenic effects. To achieve this *Kras*$^{G12D/+}$*; p16*$^{FDR/+}$*; Rosa26*$^{YFP/+}$ mice were induced with AdCre at 4 weeks of age to induce lung tumourigenesis. Following this, they were treated with either a vehicle control or DT twice weekly and the lungs analysed after 2, 4 or 8 weeks for makers of proliferation in the developing tumours. This analysis revealed that in vehicle treated mice at 2 weeks post-viral induction around 70% of YFP+ tumour cells were Ki67+, indicating a high degree of cell division which correlated with the low level of mCherry expression previously observed within the tumour at this timepoint (Figure 5.12). As tumourigenesis progressed, tumour cells were observed to be significantly less proliferative than at the initial timepoint investigated. Specifically, the proportion of tumour cells expressing Ki67 fell to 17% at 4 weeks and 25% at 8 weeks post viral-induction (Figure 5.12). Interestingly, analysis of the lungs of DT treated *Kras*$^{G12D/+}$*; p16*$^{FDR/+}$*; Rosa26*$^{YFP/+}$ mice revealed that tumours had significantly lower proliferative indexes at all three timepoints. Strikingly, at 2 weeks post viral induction only 3.4% of tumour cells were found to be Ki67+ (Figure 5.12). This tumour quiescence was also observed at 4 and 8 weeks post viral induction in DT treated mice, with only 4.6% and 7% of tumour cells showing Ki67 expression, respectively (Figure 5.12).

Together these results show that a reduction in *p16*-expressing cells retards the growth of lung tumours, which is consistent with previous reports that senescent cells, through the action of the SASP, can have pro-mitotic effects on neighboring cells, accelerating tumourigenesis. The mechanisms by which these *p16*-expressing lung cells can non-cell autonomously promote cell division are currently unknown. However, unbiased transcriptomic analysis may aid in dissecting this. Comparison of the gene expression profiles of both senescent (mCherry+/p16+) and lung tumour

(YFP+) cell populations will allow for the characterisation of the SASP produced by the senescent cells and the activated signaling pathway in tumour cells, which could be used to infer paracrine signaling between senescent and tumour cells.

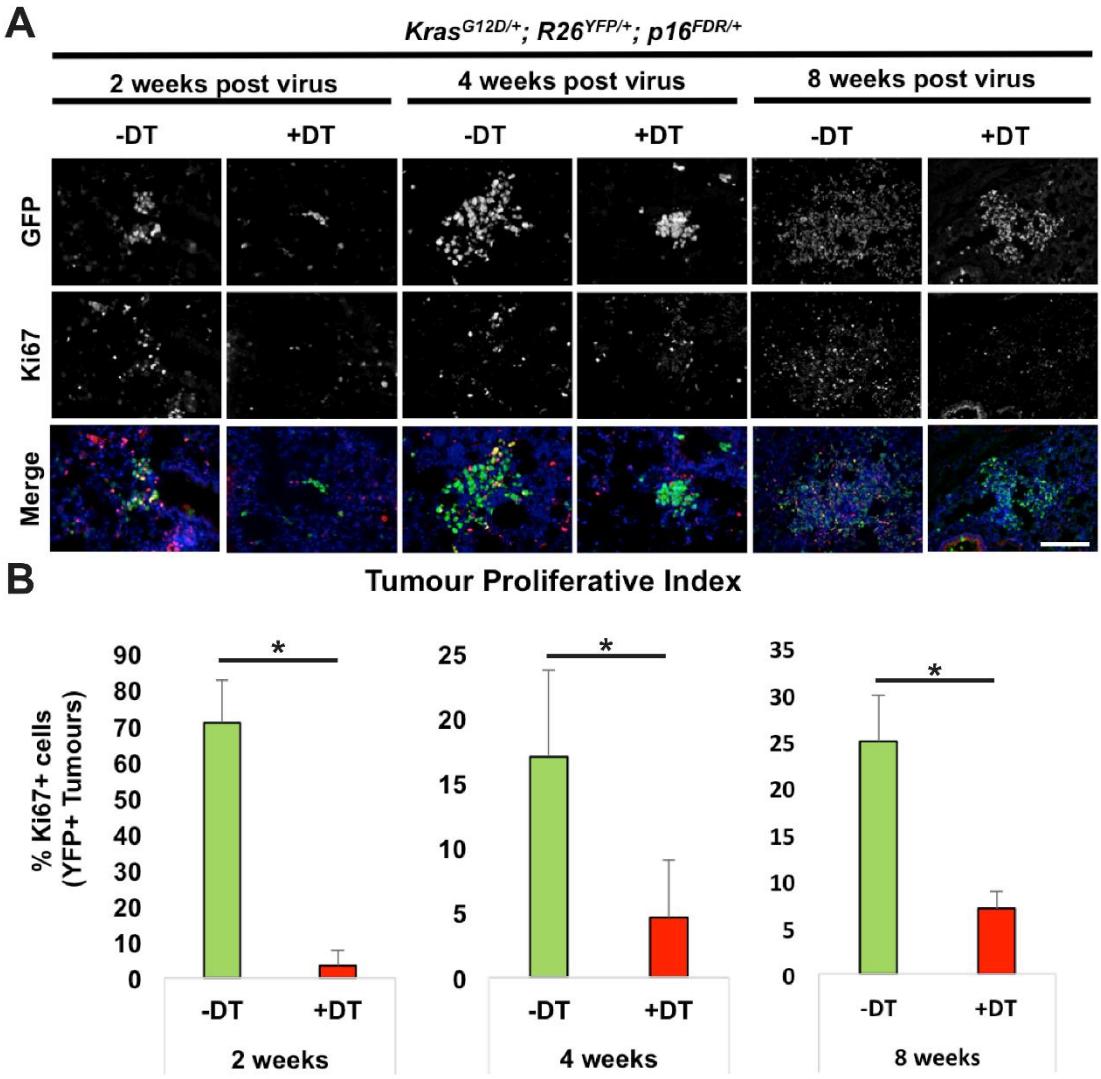

Figure 5.12. Ablation of mCherry cells results in reduction in the proliferation of lung tumour cells. (**A**) Representative IF staining of lungs from *Kras$^{G12D/+}$; p16$^{FDR/+}$; Rosa26$^{YFP/+}$* mice with the proliferation marker Ki67 and YFP to visualise tumours. Mice were subjected to viral induction at 4 weeks of age and the lungs were analysed 2, 4 and 8 weeks later. (**B**) Quantification of tumour cell proliferation 2, 4 and 8 weeks post viral induction showing a significant decrease at all timepoints analysed (n=3 mice per treatment group per timepoint). *P≤0.05, Student's t-test. Data are mean±s.e.m. Scale bars; 200 μm.

5.3 CONCLUSIONS

In this chapter a novel mouse line, termed *p16*^{FDR}, was generated to allow for the visualisation, lineage tracing and selective ablation of *p16*-expressing cell populations. The purpose of this mouse was to aid the study of cellular senescence in an *in vivo* setting. Validation of the *FDR* construct demonstrated that it was able to express membrane-tethered mCherry expression and facilitate FLP-mediated recombination. Furthermore, analysis of MEFs derived from *p16*^{FDR} mice found that heterozygous cells behaved relatively normally in culture as they are able to undergo oxidative stress-induced senescence, with concomitant expression of mCherry and sensitivity of DT-mediated ablation. However, homozygous MEFs from *p16*^{FDR} mice demonstrated impairment in entering oxidative stress-induced senescence, potentially indicating that the insertion of the *FDR* cassette into the *Cdkn2a* locus resulted in a hypomorphic *p16*^{INK4A} allele. *p16*^{FDR} heterozygotes had normal health and lifespans, with no incidences of tumourigensis observed. Homozygous mice on the other had demonstrated early lethality due to the development of spontaneous tumourigenesis in several organ systems, which would be consistent with the effects expected from homozygosity of hypomorphic *p16*^{INK4A} alleles.

Following the generation of the *p16*^{FDR} mouse line, the role of *p16*-expressing senescent cell populations was explored during lung tumourigenesis. Analysis of the survival of mice induced to form lung tumours that were either wild type for *p16*^{INK4A} or carried a single copy of *p16*^{FDR} demonstrated that the presence of the *p16*^{FDR} gene did not exacerbate tumourigenesis. Strikingly, ablation of the *p16*-expressing cells resulted in a dramatic reduction in tumour burden as well as

the tumour cell proliferation. Interestingly, it was observed that there is very low levels of p16 and mCherry expression in the tumours as most of these cells are instead found in the lung parenchyma. This indicates that the tumour cells do not appear to activate the senescence program to any considerable degree at the timepoints analysed, which is contrary to the initial hypothesis that senescence is acting to cell-autonomously limit tumour expansion. Low expression of mCherry/p16 in lung tumour cells demonstrated that the significant reduction in tumour burden cannot solely be explained by the cell autonomous ablation of tumour cells. This is because the numbers of mCherry+ tumour cells are too low to explain the overall reduction in tumour cell numbers observed. This indicates that these senescent cells are likely promoting the growth of the tumour in a paracrine manner, presumably through the action of the SASP.

CHAPTER 6: GENERAL DISCUSSION

In this thesis, the role of cellular senescence and the SASP was explored in both the induction of non-cell autonomous tumours of the pituitary gland and during lung cancer progression. This was achieved using genetically engineered mouse models of ACP (*Sox2*$^{CreERT2/+}$*; Ctnnb1*$^{lox(ex3)/+}$) and NSCLC (*Kras*$^{G12D/+}$). In chapter 3, an inducible model of ACP was validated for investigating paracrine tumour formation. The senescent phenotype and the SASP of pituitary stem cells targeted with oncogenic β-Catenin was characterised and the effect of physiological ageing on this phenotype was ascertained. In chapter 4, attempts were made to activate the cellular senescence program in the context of wild type β-Catenin, through the overactivation of the MAPK signalling pathway, to further explore the role of senescence in the pituitary. Due to unforeseen experimental outcomes this was not achievable, however, the experimental approach allowed for an exploration into the role that MAPK signalling has in regulating pituitary organogenesis and provided insight into the potential pathogenesis of PCP. In chapter 5, a novel mouse line (*p16-FDR*) was developed and validated for exploring the functions of cellular senescence *in vivo*. This model was then used to preliminarily explore the effect of senescent cell ablation on NSCLC initiation and progression, which revealed a potential paracrine pro-tumourigenic role for senescent cell populations.

6.1 Pituitary stem cells senescence drives age-attenuated induction of non-cell autonomous tumourigenesis

Previously, lineage tracing studies have been performed using *Sox2*$^{CreERT2/+}$*; Ctnnb1*$^{lox(ex3)/+}$*; Rosa26*$^{YFP/+}$ mice, in which the pituitary stem cell compartment is targeted with oncogenic β-Catenin. Intriguingly this revealed that pituitary tumours are able to form non-cell autonomously from the mutation-targeted cells

(Cynthia Lilian Andoniadou et al. 2013), a result that was also reproduced in this thesis (Figure 3.1). This discovery of paracrine tumourigenesis in the pituitary gland has also been validated in a recent study using a different ACP mouse model (*Hesx1$^{Cre/+}$; Ctnnb1$^{lox(ex3)/+}$; Rosa26$^{YFP/+}$*), which facilitates oncogene activation in the vast majority of the embryonic precursors of the pituitary gland. Therefore, paracrine tumourigenesis is not a phenomenon unique to a single experimental context (Gonzalez-Meljem et al. 2017b).

These findings were surprising as they deviate significantly from the canonical cancer stem cell paradigm. Similar lineage tracing studies have demonstrated canonical cell-autonomous tumourigenesis in many other organ systems such as the mammary gland, intestine, prostate and skin, among others (Schepers et al. 2012; Nakanishi et al. 2013; Zomer et al. 2013). Therefore, this reinforces that tumours stereotypically originate cell-autonomously from mutation sustaining cells. However, there does exist evidence for non-cell autonomous tumourigenesis in a variety of organ systems outside of the pituitary gland. Paracrine skin tumourigenesis is induced by targeting Notch1 or β-Catenin mutations to either mouse epidermis or hair follicles, respectively. This leads to the overactivation of the WNT pathway and tumourigenesis in wild type cells neighboring mutation-sustaining cells (Deschene et al. 2014; Nicolas et al. 2003). Furthermore, another study demonstrated non-cell autonomous induction of acute myeloid leukaemia (AML) by targeting oncogenic β-Catenin expression specifically in osteoblasts. This resulted in the transformation of neighboring hematopoietic stem cells (HSC) that possessed a divergent set of genetic alteration, relative to the oncogene targeted osteoblasts. Moreover, transplantation of wild type HSCs into lethally irradiated mice that had oncogenic β-Catenin targeted to their osteoblast compartment, also resulted in the development of AML, signifying that the wild type

HSC were able to be transformed in a paracrine manner to become CSCs (Kode et al. 2014).

6.1.1 β-Catenin accumulating cell clusters in a mouse model of ACP enter into cellular senescence and activate the SASP

The presence of cluster cells which accumulated β-Catenin in their nucleus and cytoplasm is a characteristic hallmark of human ACP. However, the function of the cluster cells in the pathogenesis of the disease is poorly understood. Following the activation of oncogenic β-Catenin in the pituitary stem cells compartment, using the inducible *Sox2*$^{CreERT2/+}$*; Ctnnb1*$^{lox(ex3)/+}$*; Rosa26*$^{YFP/+}$ mouse model of ACP, clusters of cells which accumulate nucleocytoplasmic β-Catenin are formed cell-autonomously after a latency period of around 4 weeks. These cells persist for long periods of time and do not show evidence of proliferation or apoptosis. Around 3 to 4 months following oncogene activation non-cell autonomous pituitary tumours begin to form that are negative for lineage trace markers of mutation-sustaining cells, markers of hormonal differentiation or the endocrine cell type marker, synaptophysin (Cynthia Lilian Andoniadou et al. 2013) (Figure 3.1). The fact that the cluster cells precede tumour formation and persist in long-term association with the lesions indicated that they may be involved in tumour formation.

Previously it was suggested that the lack of proliferation in the cluster cells found in human ACP indicated that the cells were in a quiescent state (Buslei et al. 2007a; Gaston-massuet et al. 2011). Furthermore, the discovery that cluster cells express stem cell markers lead to them being considered as being stem-like in nature (Gaston-massuet et al. 2011; Garcia-Lavandeira et al. 2011; Hölsken et al.

2013). However, this view has been challenged by the previously discussed study that lineage traced the pituitary stem cell compartment following oncogenic β-Catenin expression (Cynthia Lilian Andoniadou et al. 2013). This demonstrated that in the mouse, cluster cells, while being derived from the pituitary stem cells, do not cell-autonomously give rise to the tumour, as would be expected by a CSC model (Figure 1.4).

Therefore, this lead to the hypothesis that the cluster cells may have entered into cellular senescence and that through the paracrine activities of the SASP, result in transformation of neighboring cells, leading to non-cell autonomous tumourigenesis. This hypothesis would explain the non-proliferative nature of the cluster cells and the reason behind which they persist in long-term association with the developing tumour, which they do not cell-autonomously contribute to. Furthermore, it would also provide a potential biological function for the wide variety of signalling molecules that the cluster cells have been previously reported to produce in both human and mouse clusters (Gaston-Massuet et al. 2011; Cynthia L Andoniadou et al. 2012).

In chapter 3, this hypothesis was explored using an inducible model of ACP (*Sox2*$^{CreERT2/+}$*; Ctnnb1*$^{lox(ex3)/+}$*; Rosa26*$^{YFP/+}$), which allowed for the generation of cluster cells and pituitary tumours following tamoxifen administration. Initially it was confirmed that the mouse cluster cells showed absence of markers of proliferation, indicating a permanent cell cycle arrest (Figure 3.2), which is in agreement with what is known about cellular senescence *in vivo* (Michaloglou et al. 2005; Xue et al. 2007b). This situation is also observed in human ACP cluster cells which are known

to be neither proliferative nor apoptotic (Buslei et al. 2007a; Gaston-massuet et al. 2011; Zhu & You 2015).

As it is known that cellular senescence is a tremendously heterogeneous cellular phenotype, several markers and transcriptomic analyses were performed on the cluster cells to confirm their entry into senescence. IF analysis demonstrated that mouse cluster cells were found to harbor DNA damage as evidenced by phosphorylated-DNA-PKcs expression and express the cyclin-dependent kinase inhibitor, and senescence cell-cycle arrest mediator, p21 (Figure 3.2).

These results were corroborated by recent work which performed detailed characterisation of the cluster cells found in both human ACP and an embryonic mouse model of ACP (*Hesx1*$^{Cre/+}$*; Ctnnb1*$^{lox(ex3)/+}$), which found that they express a plethora of markers that are constant with a senescent state (Gonzalez-Meljem et al. 2017b). Specifically this study found that cluster cells accumulate SA-β-Gal, the most commonly employed methods for histologically detecting senescent cells, lysosomal proteins such as LAMP1, LAMP2 and Lysozyme C and the senescence markers p53 and p21 (Gonzalez-Meljem et al. 2017b). Expansion of the lysosomal compartment is commonly observed in senescent cells due to their increased metabolic demands that are required to maintain their high levels of secretion (Kurz et al. 2000; Jan R. Dörr et al. 2013). The p53/p21 pathway is also known to be critical for mediating OIS in many *in vivo* cellular contexts (Serrano et al. 1997; Ventura et al. 2007; Sarkisian et al. 2007), including overactivation of the WNT pathway (Sato et al. 2015; Debies et al. 2008). The presence of DNA damage in the cluster cells is also a commonality the cells share with senescent cells. Oncogene signalling is known to produce DNA damage and the resulting DDR is

considered to be essential for activation of the senescence and SASP programs (Bartkova et al. 2006; Mallette, Ferbeyre, et al. 2007; Fumagalli et al. 2014; Rodier et al. 2009; Kang et al. 2015).

Work from other groups has demonstrated that overactivation of the WNT pathway is capable of inducing the onset of cellular senescence with concomitant DNA-damage in both *in vitro* and *in vivo* settings (Gu et al. 2014; Zhang et al. 2011; Xu et al. 2008a). Of relevance to this thesis, it has recently been demonstrated that the clusters from human ACP and the embryonic ACP model (*Hesx1*$^{Cre/+}$*; Ctnnb1*$^{lox(ex3)/+}$) show activation of the $NF_{\kappa}B$ pathway due to the expression of RelA/p65, NEMO and phosphorylated $I_{\kappa}B\alpha$ (Gonzalez-Meljem et al. 2017b). Further work is required to confirm that this is also true in the *Sox2*$^{CreERT2/+}$*; Ctnnb1*$^{lox(ex3)/+}$*; Rosa26*$^{YFP/+}$ model of ACP.

In order to perform and more detailed and unbiased exploration of the senescent and SASP phenotype of the cluster cells in the inducible ACP model a flow cytometry-based approach was adopted to isolate the clusters to interrogate their gene expression profile (Figures 3.3 and 3.4). This approach demonstrated validity as cells could be isolated from oncogenic pituitaries that possessed transcriptomic signatures of WNT pathway activation and stem cell related transcripts, while showing low expression of makers of differentiated pituitary cells, which is indicative of cluster cell isolation (Figure 3.3). Moreover, this analysis demonstrated expression of previously described signalling molecules, belonging to the FGF, BMP and HH families, that have been previously observed to be produced by the cluster cells in both mouse (*Hesx1*$^{Cre/+}$*; Ctnnb1*$^{lox(ex3)/+}$) and human ACP (Gaston-massuet et al. 2011; Cynthia L. Andoniadou et al. 2012) (Figure 3.5 A).

Furthermore, the expression of these signalling molecules have been previously demonstrated to be downstream of $NF_{\kappa}B$ pathway activation (Kasperczyk et al. 2009; Salminen et al. 2012; Park et al. 2016; Du & Geller 2010). Interrogation of senescence and SASP related mRNA expression from FACS isolated cluster cells found that they upregulated expression of the senescence effectors *Cdkn1a* and *Cdkn2a* and well as common SASP factors (*Il1α, Il1β, Cxcl1, Ccl20* and *Tgfβ1*). Furthermore, OIS and SASP gene expression profiles, previously described by other laboratories (Acosta et al. 2013) were found to be enriched in the cluster cells derived from the inducible model of ACP (Figure 3.5). Interestingly, comparison of the cluster gene expression profile derived in chapter 3, with recently reporter cluster gene expression data from human ACP clusters (Gonzalez-Meljem et al. 2017b) revealed the clusters from mouse and human share molecular homogeneity. Therefore, this indicates that a senescence response to overactivation of the WNT pathway appears to be conserved (Figure 3.6).

6.1.2 SASP is the mediator of paracrine tumourigenesis in the pituitary

It is known that cancer incidence is unevenly distributed across various organ and tissue systems in an organism. Furthermore, adults and children are known to develop different types of malignancies (Howlader et al. 2012). This observation is partly explained by the intrinsic susceptibility of certain organs to inherited oncogenic mutations or carcinogen exposure (Danaei et al. 2005; Futreal et al. 2004). Furthermore, it has been recently proposed that the rate of proliferation of a tissues stem cell compartment may dictate its cancer risk (Tomasetti & Vogelstein 2015). This hypothesis postulates that cancer may be

induced by the propagation of chance mutations found in highly mitotic stem cell compartments. However, this concept of great importance being placed on cell-intrinsic factors in the development of cancer has been met with significant controversy from others who estimate that extrinsic factors are of higher significance (Ashford et al. 2015; Gotay et al. 2015; O'Callaghan 2015; Potter & Prentice 2015; Song & Giovannucci 2015; Wild et al. 2015; Wu et al. 2016). However, recently an elegant study by the Gilbertson group demonstrated the varying susceptibility of organs to develop cancer when challenged with different oncogenic mutations and ablation of tumour-suppressor genes in both neonatal and adult mice (L. Zhu et al. 2016). This work provided evidence that tumour incidence is strongly influenced by the replicative capacity of a tissues resident stem cell population. However extrinsic variables such as organ damage did exacerbate cancer risk through activation of the resident stem cells.

Work from this thesis and other studies performed on pituitary stem cell populations have demonstrated that the proliferation rates of pituitary stem cells markedly fall after early postnatal development (Nolan et al. 1998; Levy 2002). Therefore, their ability to drive paracrine tumourigenesis at varying ages was assessed in chapter 3. Specifically, the pituitary stem cell population was challenged with oncogenic β-Catenin expression at either 1 or 6 months of age using the inducible ACP mouse model (*Sox2*$^{CreERT2/+}$*; Ctnnb1*$^{lox(ex3)/+}$*; Rosa26*$^{YFP/+}$). Strikingly, results from this experiment revealed that targeting stem cells at 6 months of age dramatically reduced the incidence of tumours forming in the pituitary gland (Table 3.1). Intriguingly, analysis of the pituitaries targeted at 6 months of age, prior to tumour formation, revealed that they possessed cell clusters that accumulated nucleocytoplasmic β-Catenin, similar to what was observed in targeted younger mice (Figure 3.7 B). However, the cluster cells in older mice are reduced in

size (Figure 3.7 C). Further analysis revealed more similarities with the cluster cells formed in younger animals, including the absence of proliferation markers, presence of nuclear p21 and a similar gene expression profile (i.e. upregulation of the WNT target genes *Lef1* and *Axin2*, the cluster-related developmental signalling ligands *Shh*, *Bmp4* and *Fgf20* as well as senescence and SASP-related transcripts *Cdkn1a*, *Cdkn2a* and *Il1b*) (Figure 3.7 B,D). However, comparison of the clusters formed in older or younger mice revealed that the levels of SASP-related mRNAs (*Shh*, *Bmp4*, *Fgf20*, *Cdkn1a*, *Cdkn2a*, *Trp53*, *Il1b*, *Cxcl2* and *Tgb1*) were significantly reduced (Figure 3.8 A). This quantitative reduction in the SASP from cluster cells in older mice not only correlated with a greatly reduced tumourigenic burden, but also the non-cluster cells in older animals showed an ameliorated mitogenic response to the presence of the clusters, which was observed in the pituitary of younger mice harboring cell cluster (Figure 3.8 B).

Therefore, similar to what has been reported by the Gilbertson group in other organ system, it is observed that the replicative capacity of the pituitary stem cell compartment correlates with their ability to form large cluster cells with a robust SASP, which is capable of mediating paracrine tumourigenesis. In support of this, analysis of the pituitary stem cells compartment between young and older wild type mice revealed an increased expression of senescence/quiescence related transcripts (*Cdkn2a* and *Trp53*) in the stem cells of older animals (Figure 3.8 C). It is known that quiescent cell populations are significantly more resistant than proliferating cells to the induction of cellular senescence following DNA-damaging insults (Leontieva & Blagosklonny 2010). Therefore, potentially the pituitary stem cells in the older mice, having gone through many more rounds of cell division, are more quiescent than their younger counterparts, resulting in a reduced capacity to respond to the senescence-inducing oncogenic β-Catenin stimulus.

In support of the data obtained in this thesis, a model for SASP to be required non-cell autonomously for tumour induction, has been recently been proposed. WNT-pathway activation in Hesx1-derived pituitary precursors was induced in the context of wild-type β-catenin through deletion of the β-catenin-repressor protein *Apc* (*Hesx1*$^{Cre/+}$*; Apc*$^{fl/fl}$), resulting in elevated WNT pathway activation (Gonzalez-Meljem et al. 2017b). Strikingly in this experimental paradigm there was no incidence of tumourigenesis observed in the pituitary at all. While these pituitaries also contained senescent β-Catenin accumulating cell clusters, they were very small in size when compared with cluster from mice that were competent to form tumours by expressing oncogenic beta-catenin (young *Sox2*$^{CreERT2/+}$*; Ctnnb1*$^{lox(ex3)/+}$ and *Hesx1*$^{Cre/+}$*; Ctnnb1*$^{lox(ex3)/+}$ mice). Moreover, expression analysis of the SASP in *Hesx1*$^{Cre/+}$*; Apc*$^{fl/fl}$ mice revealed that SASP production was also greatly reduced. Therefore, this situation appears to phenocopy what was observed in the experiments involving *Sox2*$^{CreERT2/+}$*; Ctnnb1*$^{lox(ex3)/+}$ mice induced at older ages.

Further work is required to explore in more depth the differences in the composition and intensity of the SASP. This could be achieved through un-biased transcriptomic analysis by RNA-sequencing of cluster cells derived from older and younger mice. Such an analysis may provide insight into SASP factors that are missing or show the greatest degree of downregulation in the older cluster cells, which could facilitate more refined experiments to probe the function of these molecules in mediating paracrine tumourigenesis. If the future identification of the tumour cell of origin is successful (see sections 3.2.4 and 6.2) then this would provide an excellent platform for the testing of identified SASP components for their ability to induce non-cell autonomous transformation. Furthermore, it would be of interest to test the ability of senolytic and SASP neutralizing molecules to ablate the

senescent cluster cells in mouse models of ACP. By clearing the senescent cluster cells or blocking their SASP production it would be expected that non-cell autonomous tumourigenesis would not proceeed. This would provide further evidence for the role of SASP factors in mediating paracrine tumourigenesis in the pituitary gland. Such experiments may also produce clinically beneficial results which may aid in the treatment of human ACP patients.

6.1.3 Proposed model for non-cell autonomous tumourigenesis in the pituitary gland

Together the results from chapter 3 provide a framework for forming an explanation of non-cell autonomous tumourigenesis in the pituitary gland that is in contrast with the currently prevailing CSC model. In two mouse models of ACP, tumours form non-cell autonomously from non-targeted cells, indicating a model of paracrine tumourigenesis (Gonzalez-Meljem et al. 2017b; Cynthia Lilian Andoniadou et al. 2013) (Figure 3.1). The results described in chapter 3 provide evidence that pituitary stem cells, following oncogenic β-Catenin expression enter into cellular senescence and secrete SASP molecules, which are known to be a pro-tumourigenic signalling mechanism in some contexts. Furthermore, molecular similarities were found between mouse and human clusters suggesting that they may act biologically analogously in the pathogenesis of ACP. A significant proportion of canonical SASP factors are known to act as growth factors, which may activate oncogenic pathway resulting in excessive proliferation and potentially replicative stress. Replicative stress can lead to genomic instability, promoting DNA damage and mutation acquisition. Moreover, the SASP has recently been shown to be capable of mediating cell reprogramming, predominantly

through IL6 (Mosteiro et al. 2016) and potentiating regeneration and cellular plasticity (Ritschka et al. 2017). Potentially, the SASP could expand the population of stem/progenitor cells and bolster their chance of acquiring mutations. Another means of inducing DNA damage and mutations in a paracrine manner is through the generation of a pro-inflammatory microenvironment around senescent cells, which increases the abundance of damaging reactive oxygen and nitrogen species (Figure 6.1).

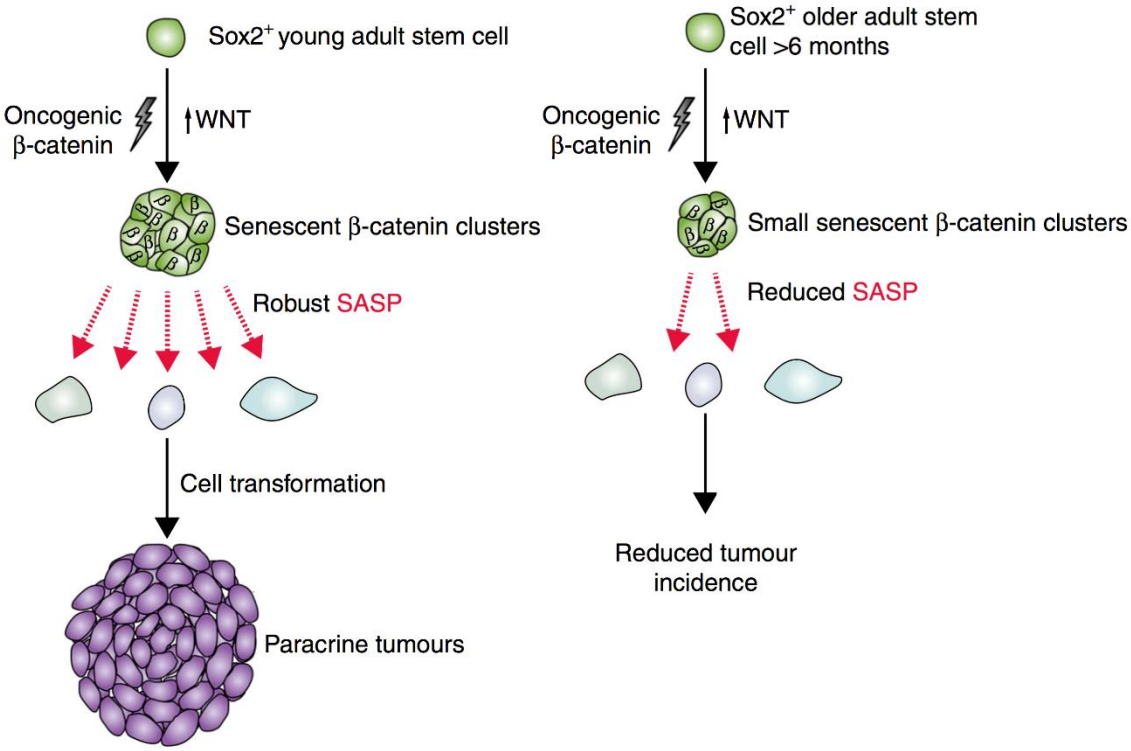

Figure 6.1. Model for non-cell autonomous tumourigenesis in the pituitary gland. WNT pathway activation, through oncogenic β-Catenin expression in pituitary adult stem cells found in young mice, results in the formation of senescent cell clusters that accumulate nucleocytoplasmic β-Catenin. Through the action of a robust SASP neighboring cells are transformed resulting in the development of non-cell autonomous tumourigenesis. If oncogenic β-Catenin is instead targeted to pituitary stem cells in older mice, smaller senescent cell clusters are formed with a reduced intensity in the SASP, which correlates with a profound reduction in tumourigenic incidence.

6.2 The Vav1 haematopoietic lineage is not the cell of origin for paracrine tumours in the pituitary gland

Gaining an understanding of the cell of origin for the paracrine tumours formed in both *Sox2*$^{CreERT2/+}$*; Ctnnb1*$^{lox(ex3)/+}$ and *Hesx1*$^{Cre/+}$*; Ctnnb1*$^{lox(ex3)/+}$ models is an important objective for dissecting the mechanisms behind paracrine tumourigenesis. Results from lineage tracing studied targeting oncogenic β-Catenin to either the pituitary stem cell compartment (Sox2+) or pituitary precursor cells (Hesx1+) developmentally revealed that not only do the tumours form in a paracrine manner, but that the tumour cell of origin is not derived from the Hesx1 lineage which gives rise to all endocrine cell types in the anterior lobe (Gonzalez-Meljem et al. 2017b; Cynthia Lilian Andoniadou et al. 2013).

In chapter 3, a preliminary investigation into the tumour cell of origin was performed. This involved the generation of chimeric mice that allowed for the targeting of oncogenic β-Catenin to the postnatal pituitary stem cell compartment while simultaneously lineage tracing candidate tumour cell or origin lineage (Figure 3.9 A). As the tumour is not derived from the Hesx1 lineage candidates for the tumour cell or origin include cells resident in the pituitary but not derived from this lineage. Therefore the most likely candidates include the Vav1-derived hematopoietic/bone marrow lineage, the Wnt1-derived neural crest lineage, which gives ride to pericytes found in the pituitary and the Tie2-derived endothelial cell lineage. In this thesis the Vav1 cell haematopoietic cell lineage was investigated for its ability to be transformed and give rise to the paracrine tumours. This analysis did not reveal contribution from this lineage however, excluding it as a candidate for the tumour cell of origin (Figure 3.9 C).

Knowledge of the tumour cell of origin would facilitate the designing of refined experiments that would allow the contribution of SASP factors to be investigated. For example, isolated cluster cells from *Sox2*$^{CreERT2/+}$*; Ctnnb1*$^{lox(ex3)/+}$ mice could be used to generate conditioned medium or directly co-cultured with un-transformed tumour cell of origin cells to facilitate their transformation. This process could theoretically be biochemically monitored to describe the process of transformation and specific SASP factors in isolation or combination could be added to the medium of cultured tumour cell of origin cells to recapitulate results from co-culture or conditioned medium experiments. However, previous attempts by myself to culture isolated oncogenic β-Catenin-targeted pituitary stem cells has been met with little success due to the senescent and therefore non-replicating nature of these cells (data not shown). Attempts to generate cluster cells *in vitro,* through inducing recombination of oncogenic β-Catenin by exposing cultured *Sox2*$^{CreERT2/+}$*; Ctnnb1*$^{lox(ex3)/+}$*; Rosa26*$^{YFP/+}$ pituitaries to tamoxifen, was also unsuccessful. This potentially indicates that cell cluster formation in the pituitary is not a simple cell-autonomous process induced by WNT-pathway activation. Instead, non-cell autonomous interactions between oncogene-targeted pituitary stem cells and their local environment may be necessary for cluster formation. Further investigation is required to test this hypothesis and ascertain the feasibility of generating pituitary cluster cells *in vitro*.

6.3 Overexpression of either oncogenic *Braf*^{V600E} or *Kras*^{G12D} is not sufficient to induce cellular senescence in pituitary stem/progenitor cells developmentally or postnatally

In chapter 3, it was shown that there exists a correlation between the intensity of SASP production and non-cell autonomous tumour development. Chapter 4 attempted to expand on this through experiments to induce cellular senescence in the context of wild type β-Catenin to test whether the senescence and SASP programs alone were sufficient to induce paracrine tumour production. This was attempted through conditional expression of oncogenic components of the MAPK signalling pathway (*Braf*^{V600E} and *Kras*^{G12D}) in either postnatal pituitary stem cells or in the precursors of the pituitary gland during development. These oncogenes were chosen due to their previously reported abilities to be strong inducers of cellular senescence in both *in vitro* and *in vivo* contexts (Dhomen et al. 2009; Mercer et al. 2005; Tuveson et al. 2004).

Oncogenic activation of the MAPK pathway in Hesx1+ pituitary progenitor cells unexpectedly resulted in neo-natal lethality due to the aberrant development of the lungs, presumably through off-target expression of the oncogenes, which was incompatible with life. Analysis at late gestational stages found that there was no induction of the senescence-related markers p16 or p21, relative to stage-matched wild type control pituitaries. This indicates that the oncogenic overactivation of the MAPK pathway is insufficient to drive the expression of the senescence cell cycle arrest mediators p16 and p21 developmentally in pituitary Hesx1 derivatives. It was observed in chapter 4 that cells in the developing pituitary physiologically expressed both *Braf* and *Kras* mRNA and that a subset of targeted cells (Sox2+

stem/progenitor cells) upregulated pERK1/2 expression. Therefore the expression of the oncogenes was effective in facilitating a cellular phenotype and activation of the MAPK pathway, however, there was no induction of cellular senescence. There is the possibility that the hyper-replicative nature of the Sox2+ compartment would eventually lead to the induction of cellular senescence. An example of this may be replicative senescence induced through proliferation-mediated telomere attrition. However, the complete penetrance of neonatal lethality in experimental mice precluded the testing of this hypothesis.

This failure to induce senescence could be due to the developmental context in which the oncogenes were expressed. These embryonic progenitor cells are already primed to be highly mitotic which may mean ectopic mitogenic signals (oncogenic *Braf*^{V600E} and *Kras*^{G12D} expression) results in an increase in their proliferation, rather than retarding it. Therefore, this provided a rational for targeting Sox2+ pituitary stem cells postnatally, using *Sox2*^{CreERT2}, mice at a time when they are more quiescent in nature and may be more susceptible to senescence induction. The conditional activation of these oncogenes was performed in *Sox2*$^{CreERT2/+}$*; Braf*$^{V600E/+}$ and *Sox2*$^{CreERT2/+}$*; Kras*$^{G12D/+}$ mice at 4 weeks of age, at an identical stage to when the β-Catenin mutations were activated in the *Sox2*$^{CreERT2/+}$*; Ctnnb1*$^{lox(ex3)/+}$ model of ACP to induce cellular senescence.

Unexpectedly, this second strategy presented experimental challenges that also prevented the long-term study of mutant mice. Both of the mutant genotypes in which oncogenic *Braf* or *Kras* were targeted was targeted to *Sox2*-expressing cell compartments developed rapidly growing stomach neoplasms that necessitated

the humane culling of the experimental animals within 3 weeks following oncogene induction (see section 4.2.2).

This provided a short opportunity to examine the effects of oncogenic stimulation of the MAPK pathway on postnatal pituitary stem cells. Surprisingly, however, unlike the profound effect on pituitary development that were characterised, the mutant pituitaries appeared normal in both gross morphology and cellular characteristics (Figure 4.18). Specifically, examination of markers of cellular senescence, p16 and p21, revealed that both the mutant and control pituitaries were almost completely negative. A qualitative assessment of proliferation also revealed that their appeared to be no difference in cellular turnover. Furthermore, Sox2 expression appeared normally distributed between the marginal zone and the anterior lobe parenchyma.

Therefore, unlike the stem/progenitor cells found developmentally, the postnatal pituitary stem cells appear to be refractory to perturbation by oncogenic MAPK signalling. Potentially this difference is due to the divergent adult versus embryonic context in which the cells are situated. Another explanation is certain intrinsic variables in adult pituitary stem cells could make them insensitive to MAPK perturbation, such as the absence of either *Braf* or *Kras* expression. Further research is required to clarify this.

6.4 The MAPK signaling pathway is important for regulating self-renewal and differentiation of pituitary progenitor cells developmentally

While activation of oncogenic *Braf*^{V600E} and *Kras*^{G12D} in Hesx1+ pituitary progenitor cells did not appear to induce cellular senescence, analysis of the pituitaries developmentally revealed a profound hyperplasic phenotype. This was due to oncogene-targeted pituitaries showing increased and sustained proliferation of the Sox2+ stem/progenitor compartment along with an impaired differentiation potential. This resulted in the pituitary being almost completely comprised of Sox2+ cells and devoid of terminally differentiated hormonal cells by the end of gestation (see section 4.2.1). As the *Hesx1-Cre* mouse is known to drive Cre-mediated recombination in the anterior hypothalamus, non-cell autonomous contributions from this structure to the observed developmental defects cannot be completely ruled out. However, the observation that the patterning of the hypothalamus was normal at 10.5 dpc seems to argue that the phenotype is due to the effects of MAPK dysregulation in the developing RP. Intriguingly, and of translational relevance, it was observed for the first time that human PCP tumours contain a population of Sox2+ cells. These cells also appear to account for the vast majority of proliferation events in the tumour but do not show evidence of any form of differentiation into the pituitary cell lineages.

6.4.1 Physiological implication of studying overactivation of MAPK signalling on pituitary development

Ligands belonging to the FGF family bind to tyrosine kinase FGF receptors (FGFRs) and activate the downstream MAPK signalling pathway. During development, several FGFs, including Fgf8, Fgf10 and Fgf18 are expressed in the ventral dienchephalon between 9.5 and 10.5 dpc (Treier et al. 1998; Treier, O'Connell, A. Gleiberman, et al. 2001). In support of the observations made in this thesis, that MAPK activation results in stem cell compartment expansion, loss-of-function mutants of FGF and FGFR2 have lower proliferation in RP progenitors and abnormal pituitary morphogenesis (De Moerlooze et al. 2000; Ohuchi et al. 2000). Furthermore, *ex vivo* culture of RP tissue with either FGF ligands or FGF pathway inhibitors demonstrated a crucial role for the FGF pathway in controlling RP proliferation and that downregulation of the pathway is required for the normal specification of the Pit1 lineage (Ericson et al. 1998; Norlin et al. 2000). Other experiments which activated the FGF signalling pathway through ectopic and transgenic expression of Fgf8 during pituitary development (by using a Cga (α-GSU) promoter) found it resulted in pituitary hyperplasia and enlargement of the corticotroph population. Moreover, in this experimental approach, a severe reduction in the numbers of gonadotrophs, thyrotrophs, somatotrophs and gonadotrophs was observed, which closely resembles the phenotype observed following MAPK pathway activation in Hesx1 pituitary descendants.

As the MAPK pathway in this study was activated through the expression of oncogenic variants of downstream MAPK signal transducing components, it raises the possibility that other ligands that activate this pathway may have poorly

described roles in pituitary development. Examples of such ligands include PDGF, EGF and TGFα. However, it is conceivable that none of these factors are expressed and that FGFs are the only ligand involved at these developmental timepoints. Further research will be required to clarify the contribution of upstream MAPK pathway ligands to pituitary development.

6.4.2 Insights into the molecular pathogenesis of PCP

Sequencing studies have shown that mutations in BRAF and KRAS are uncommon in pituitary adenomas, but activation of the MAPK pathway has been reported in these tumours (Newey et al. 2013.; Reincke et al. 2015; Ronchi et al. 2016; Välimäki et al. 2015). However, several studies have provided evidence of the involvement of MAPK signalling in pituitary tumourigenesis. In a highly invasive recurrent prolactinoma, which proved to be fatal, a mutation was found in codon 12 of *HRAS* (Gly to Val) (Karga et al. 1992). Moreover, a study on pituitary adenomas uncovered overexpression of both *BRAF* mRNA and protein (Ewing et al. 2007). *In vitro* experiments in which the MAPK pathway was constitutively activated through the expression of oncogenic $KRAS^{G12V}$ in the bi-hormonal somatolactotroph GH4 precursor cell line, promoted differentiation to a prolactin-secreting cell type. However, this was not found to be sufficient to drive tumourigenesis (Booth et al. 2014). This differs from the work presented in this thesis, where the differentiation of lactotrophs is reduced rather than induced. This is potentially due the cell context in which the MAPK pathway is activated (i.e. Hesx1 embryonic precursors versus GH4 cells) or the *in vitro* experimental context.

As discussed in chapter 1, PCPs are tumours of the sellar region which are mostly benign in nature. They are generally found in the elderly population and can result in severe morbidity when aggressive. Sequencing studies have shown that the vast majority of PCP tumours harbour BRAF p.V600E mutations, however little is known regarding the pathogenesis of the disease (Brastianos et al. 2014). Furthermore, recent clinical data has shown that the MAPK pathway is important for tumour maintenance as the use of BRAF-V600E and MEK inhibitors showed preliminary therapeutic benefit (Aylwin et al. 2016; Brastianos et al. 2016).

Analysis of mutant mice with MAPK overactivation in the embryonic precursors of the pituitary provided insight into the molecular etiology of PCP tumourigenesis. A population of proliferative SOX2-expressing cells was identified in PCP tumours, specifically in the basal cells lining fibrovascular cores (see section 4.2.1.6). Interestingly it was found that the vast majority of dividing cells were found in the SOX2+ compartment, implicating these cells as drivers of tumour growth. While BRAF-V600E mutant protein was detected throughout PCP tumour samples, pERK1/2 expression was restricted to the cells lining fibrovascular cores, where the majority of the SOX2-expressing cells are found. This is analogous to the situation in the mutant mouse models where pERK1/2 staining is predominantly restricted to the pituitary stem cell niche, while Braf-V600E mutant protein is found throughout the gland. Furthermore, PCP tumours are known to be negative for markers of hormonal expression, however it is speculated that the squamous cells in PCP tumours are cell-autonomously derived from the basal cells (SOX2+). This bears similarity to the situation in the mutant mouse models, as differentiation of the Sox2+ stem/progenitor cells was observed to be broadly impaired (apart from the Tpit cell lineage).

While these are differences between the mutant mouse models and PCP tumours, both systems share a SOX2+ compartment that is the predominant source of cell turnover and shows impaired potential to differentiate. The observed neonatal lethality prevented long term evaluation of these mutant mice to determine if they would go on to form pituitary tumours that resembled human PCP. Future investigations could transplant the mutant mouse pituitaries at late gestational stages into immunocompromised hosts to allow for greater amounts of time to assess tumourigenic potential. If successful this could provide a platform for preclinical research into further, or more refined, therapeutic strategies for combating human PCP.

6.4.3 Proposed model for the role of MAPK signaling during pituitary development

Together, the results from the developmental study on MAPK dysregulation in pituitary precursors, detailed in chapter 4, provide a model for the role of the MAPK signalling pathway in orchestrating correct pituitary development (Figure 6.2). Specifically, over activation of the MAPK pathway promotes the self-renewal of the Sox2 stem/progenitor cell compartment resulting in gross enlargement of the organ. This imposed bias towards self-renewal is at the expense of producing Sf1+ and Pit1+ progenitors, which results in almost complete absence of their downstream terminally differentiated progeny (Gonadotrophs from the Sf1 lineage and somatotrophs, thyrotrophs and lactotrophs from the Pit1 lineage). Furthermore, there is no bias against differentiation into Tpit+ progenitors, however greater numbers are generated, potentially due to the enlarged pool of Sox2+ stem/progenitor cells. The Tpit lineage cell-autonomously responds to MAPK activation by increasing their self- renewal, which results in a greater production of

the Acth+ corticotroph population. Analysis of human PCP tumours, in which MAPK pathway activating BrafV600E mutations are the sole genetic event, show proliferation restricted to a population of Sox2+ cells. These cells may be acting as tumour initiating cells or CSC that are responsible for proliferating to give rise to cells that comprise the bulk of the tumour.

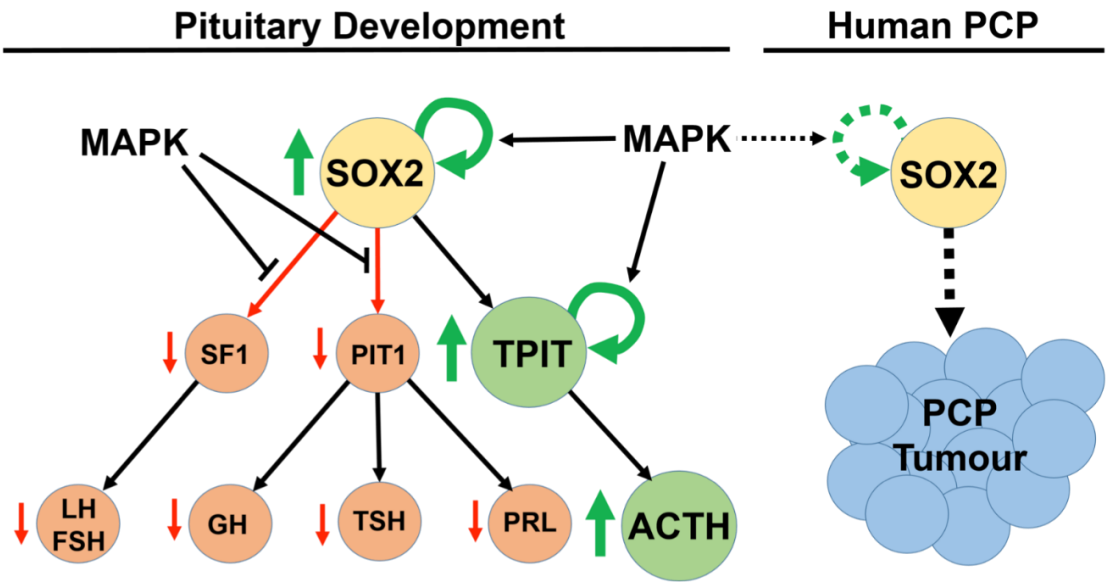

Figure 6.2. Model for the potential role of MAPK signalling in pituitary development. Activation of MAPK signalling using inducible KrasG12D or BrafV600E oncogenes resulted in gross expansion of the anterior lobe of the pituitary by the end of gestation. This was predominantly fuelled by increased self-renewal of SOX2+ stem/progenitor cells. Their differentiation was also impaired leading to a reduction in SF1 and PIT1 hormonal lineages, while TPIT+ progenitors were increased leading to an over specification of ACTH+ corticotrophs. In human PCP harbouring BRAF p.V600E mutations, activation of the MAPK pathway is also found, predominantly in groups of SOX2+ cells. These cells are also the main source of proliferation in the tumour.

6.5 Generation of a novel mouse model to explore the role of cellular senescence in vivo

Cellular senescence is a difficult phenotype to study due to the heterogeneous nature of this cellular state. While a wide variety of markers have been employed to identify these cells (see section 1.1.4), many are also commonly found on non-senescent cells such as quiescent cell populations, aged lympocytes and tissue macrophages. Therefore, the gold standard approach for the identification of cellular senescence in vivo is the use of a combinatorial array of markers to positively select for senescent cells and discriminate against confounding cell types.

To date, the most commonly employed markers of senescent cells are the expression of the cyclin-dependent kinase inhibitor *p16^{INK4A}* and positivity for SA-β-Gal (Sharpless & Sherr 2015). While expression of *p16^{INK4A}* has limitations, such as its expression in some immune cell populations such as macrophage populations and aged lymphocytes (Collado & Serrano 2006; Hall et al. 2017), it is found to be strongly expressed in senescent cells, both *in vitro* and *in vivo*, in a variety of cellular contexts (Dai & Enders 2000; Ohtani & Hara 2013; Darren J. Baker et al. 2011; Demaria, Ohtani, Youssef, Rodier, Toussaint, Mitchell, Laberge, Vijg, VanSteeg, Martijn E T Dollé, et al. 2014; Burd et al. 2013; Sato et al. 2015). As mentioned previously *p16^{INK4A}* expression has been used as the basis for several senescence reporting and ablating mouse models (see section 1.1.6), which has resulted in the successful identification of senescence acting pro-regeneratively during wound closure and detrimentally during the ageing process (Demaria, Ohtani, Youssef, Rodier, Toussaint, Mitchell, Laberge, Vijg, VanSteeg, Martijn E T

Dollé, et al. 2014; Darren J. Baker et al. 2011; Baker et al. 2016). Each of these models has intrinsic advantages and disadvantages (discussed in section 1.1.6) that must be taken into account during experimental design.

To add to the genetic toolbox for studying cellular senescence a novel mouse line was developed in chapter 5 termed *p16-FDR*. The purpose of this line is to facilitate the *in vivo* visualisation, ablation and lineage tracing of *p16*-expressing cell populations using a cassette I designed termed *FDR* (Flippase, Diphtheria toxin receptor and Reporter) (see section 5.2.1). The $p16^{INK4A}$ gene was chosen due to its previously discussed heavy involvement with the senescent phenotype. A CRISPR/Cas9 gene targeting approach was utilised targeting the 3' end of the $p16^{INK4A}$ gene to introduce minimal disruption, while allowing expression of the *FDR* cassette under endogenous regulatory control.

Initial tests of the *FDR* cassette *in vitro* demonstrated its ability to express an mCherry reporter and drive Flippase-recombinase mediated recombination of a reporter construct. Furthermore, following the generation of *p16-FDR* mice the genetic strategy was validated in isolated MEFs. Specifically, the induction of oxidative stress-induced senescence in these cells drives the expression of mCherry and confers sensitivity to diphtheria toxin mediated pharmacogenetic ablation. However, abnormally high levels of proliferation and a failure to express a marker of cellular senescence were observed in cells that were homozygous for insertion of the *FDR* cassette. This indicates that the introduction of the *FDR* cassette into the 3' end of the $p16^{INK4A}$ gene was not as neutral as anticipated, but may instead be resulting in a hypomorphic allele.

A survival analysis of homozygous and heterozygous *p16-FDR* mice demonstrated that a homozygous insertion of *FDR* resulted in significantly reduced longevity due to the development of spontaneous tumours in the spleen and liver (see section 5.2.1.5). This finding is consistent with previous reports on the survival and spontaneous tumourigenic incidence in $p16^{-/-}$ mice (Sharpless et al. 2004). As both $p16^{INK4A}$ and $p19^{ARF}$ share the *Cdkn2a* locus, introduction of the *FDR* casette into the 3' end of $p16^{INK4A}$ may have had unintended consequences on the function of $p19^{ARF}$. However, previous reports state that mice which have double knockouts of $p16^{INK4A}$ and $p19^{ARF}$ show greater spontaneous tumourigenesis than either $p19^{ARF-/-}$, $p16^{INK4A-/-}$ or the $p16^{FDR/FDR}$ mice generated in this thesis (Sharpless et al. 2004). Therefore, this suggests that *p16FDR* mice possess a hypomorphic allele of $p16^{INK4A}$ that promotes spontaneous tumourigenesis when in homozygosity. However, comparison of their survival with other published studies suggest that the effect on the nearby $p19^{ARF}$ gene is most likely minimal. As *p16-FDR* heterozygous mice did not show any overt spontaneous tumourigenesis or reduced longevity, they used for the remainder of this thesis for further experimentation.

6.6 Ablation of *p16*-expressing cell populations results in a gross reduction in the tumour burden in a mouse model of NSCLC

Lung cancer is a heterogeneous class of tumour entities that is associated with a high incidence and a low survival rate (Ferlay et al. 2015). A range of therapies are available for managing the disease, but greater research efforts are required to expand our knowledge of the molecular etiology of the disease to generate further therapeutic strategies to combat it. NSCLC comprises the majority

of newly diagnosed lung cancer cases (85%) and sequencing studies have demonstrated that the cancers possess an impressive array of different genetic alterations. Mutations that result in overactivation of the MAPK pathway, such as activating mutations in *KRAS* (25-32% of patients) or receptor tyrosine kinases (24% of patients), are particularly represented in NSCLC (see section 1.5.3) (Collisson et al. 2014; Jianjiong Gao et al. 2013).

It is believed that cellular senescence acts to cell-autonomously limit the capacity of lung tumour cells to undergo malignant transformation (Collado et al. 2005a; Dankort et al. 2007; Michaloglou et al. 2005; Dhomen et al. 2009b). A situation that is believed to occur in a number of oncogenic contexts, such as in skin papilloma formation (Dhomen et al. 2009b), pituitary hyperplasia (Lazzerini Denchi et al. 2005), prostatic intraepithelial neoplasia (Majumder et al. 2008; Caterina Nardella et al. 2008) and thymus tumourigenesis (Xu et al. 2008b). However, in contrast to this, some groups have failed to find evidence of senescence induction during lung tumourigenesis (Tuveson et al. 2004). Furthermore, it is now appreciated that senescent cells can have profoundly pleiotropic local and systemic effects that can be both beneficial and detrimental (see section 1.1.2 and 1.1.3). Little is known about the potential indirect effects that senescent cells can have during the lung tumourigenesis process and given their emerging role of importance in oncology and ageing, further investigations are warranted.

The work described in chapter 5 aimed to study the action of senescent cells during the process of lung tumourigenesis. Specifically, the *p16-FDR* mouse line generated in the first half of chapter 5 was induced to form lung tumours through viral activation of a conditional oncogenic $Kras^{G12D}$ allele. This allowed for the

visualisation of the *p16*-expressing cell populations during tumour formation and growth as well as their ablation to ascertain the functional consequences of their presence on the nascent tumours. Comparison of the survival between *Kras*^{G12D} mice with and without a *p16-FDR* allele demonstrated no difference, suggesting that the introduction of the *FDR* cassette is not accelerating tumourigenesis.

Analysis of tumour-bearing *p16-FDR* mice found that the cells carrying the reporter demonstrated characteristics indicative of a senescent state. Specifically, the vast majority of these cells expressed both p16 and p21 and are also found to be absent for markers of proliferation. In contrast to several studies that found significant levels of senescence in lung adenomas (Collado et al. 2005a; Dankort et al. 2007; Michaloglou et al. 2005; Dhomen et al. 2009a), very few of the putatively senescent cells reported by the *FDR* cassette were detected in tumour lesions between 2 and 8 weeks of growth (see section 5.2.2.3). This may be due to experimental timing, as relatively early stages of the tumour-formation process that were analysed. Therefore, a senescence growth arrest may activate in more advanced tumours and warrants further investigation. Future analysis will be required to investigate this possibility. However, senescence may also act very early in the tumourigenesis process, perhaps even at the level of a single oncogene targeted cell. If this were the case then presumably the majority of tumours analysed in this study would have already undergone a senescence escape event and therefore not be reported by the *FDR* cassette. The question of whether senescence escape is a mechanism of lung tumourigenesis is out with the scope of this thesis but is potentially addressable with the unique abilities of the *p16-FDR* mouse model in future investigations (for more details see section 6.7).

The observation that the majority of putatively senescent cells reported by the *p16-FDR* model are found outside of the tumour lesions raised the possibility that they may be acting to non-cell autonomously influence tumour development, similarly to the observations of ACP made in chapter 3. To test this, lung tumour bearing *p16-FDR* mice were treated with diphtheria toxin to pharmacogenetically ablate the senescent cells. While only a partial ablation of the reported cells was achievable, without inducing off-target effects, nevertheless a substantial reduction in tumour burden was observed in the treated mice (see section 5.2.2.4). This effect was confirmed to be mediated by the introduction of the *FDR* cassette and not due to a non-specific chemotherapeutic action of the toxin. Intriguingly, the proliferation rate of residual tumour cells in treated mice was significantly lower than in controls, suggesting a potential mitogenic paracrine influence from the *p16*-expressing cell populations (see section 5.2.2.5). In future investigations it will be of interest to perform significantly longer term DT ablation studies to ascertain if their is a survival benefit from the removal of putatively senescent cells in the context of lung tumourigenesis. Together, these preliminary results suggest that senescent cells may have a role in accelerating the development of lung cancer and that their ablation may be therapeutically beneficial.

Further work is required to better characterise the cells reported by the *FDR* cassette to give additional confidence in their senescent state. This will also help rule out the contribution of other cell types that may mimic cellular senescence, such as aged lymphocytes and macrophages (Collado & Serrano 2006; Hall et al. 2017). Furthermore, it is important to generally characterise the proportion of mCherry+ cells contributing to the different cell types found in the lung (e.g. Type I and II alveolar cells, Clara cells, BASCs, resident tissue macrophages and circulating monocyte and leukocyte populations) to assess their potential effects on

tumourigenesis. A further approach is to isolate the reported cells by their expression of fluorescent mCherry protein and then subject them to unbiased transcriptomic analysis. Signatures of cellular senescence could be interrogated in a similar manner to the gene expression data from the cell clusters derived from the mouse model of ACP investigated in chapter 3. The characteristics of other confounding cell types could also be investigated in a similar manner. Furthermore, signalling interactions between the tumour cells and the putatively senescent cells could be inferred bioinformatically. This could be achieved by analysis of signalling pathways activated in tumour cells that are downstream of identified ligands produced from the senescent cells. This information could be used to form the basis of a molecular mechanism describing the interaction between senescent cells and nascent lung tumours, which may yield novel strategies for managing the disease. Furthermore, treatment of lung tumour bearing mice with either senolytics or SASP neutralizing agents, to attempt to recapitulate the observed effects of pharmacogenetic p16-expressing cell ablation, is warrented and may provide insights into the translational potential of this research in comabting human NSCLC.

6.7 Strategy for investigating the involvement of senescence escape in the tumourigenesis process

Is the proliferative arrest of senescent cells truly irreversible in vivo? The answer to this question is important not just for furthering basic biological research but also has significant implications for cancer therapy. Efforts are being made to clinically employ therapeutics to induce cellular senescence in tumour cells to cell-autonomously prevent further growth (Kirkland et al. 2017). If senescent cells can revert to a proliferative state *in vivo* then these cells may be a significant source of

recurrent cancers. Even if they do not, their paracrine influence on the tissue and tumour microenvironments, through the SASP, may also act in a pro-tumourigenic manner, as proposed in chapters 3 and 5. To explore the question of senescence bypass and escape the *p16-FDR* mouse line could be employed. As *p16*-expressing senescent cell populations will express Flippase-recombinase, this can be employed to activate an irreversible reporter system (such as an FRT-flanked transcriptional stop cassette upstream of fluorescent reporter coding sequence, under the regulatory control of a ubiquitous promoter) to facilitate lineage tracing of senescent cell populations *in vivo* (Figure 6.3). This strategy could be used in the mouse lung cancer model employed in chapter 5 to ascertain whether the tumour cells arise from a senescent precursor cells that escaped. Furthermore, "pre-treatment" of the mice used in chapter 5 mice with DT, prior to the initiation of lung tumourigenesis could result in the ablation of tumour cell(s) of origin, potentially, reducing or preventing tumour formation.

It would be interesting to study the question of senescence escape in a variety of oncological context to look for convergent and divergent role of cellular senescence during the tumourigenesis process. If senescence escape is found to be a tumourigenic mechanism *in vivo* then this leads to potential hypothesis that ablation of senescent cells could be a novel prophylactic approach to cancer therapy.

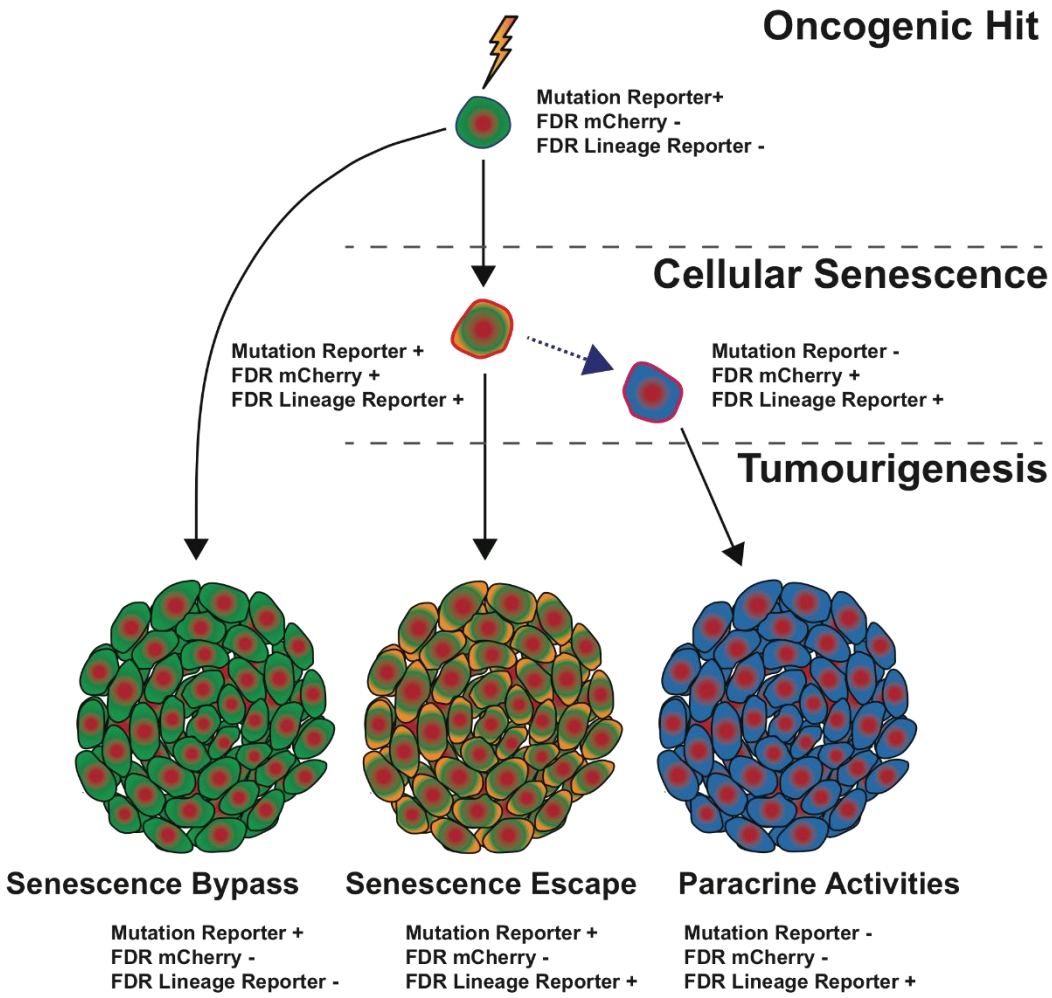

Figure 6.3. Strategy for investigating senescence escape and bypass *in vivo*. By independently lineage tracing Cre and FLP expressing cell population there is the possibility to address the question of senescence escape and bypass *in vivo*. This would be achieved by Cre-activation of an oncogene, to initiate tumourigenesis, and a reporter construct to enable the lineage tracing of mutation sustaining cells for their cellular contribution to tumour formation. The introduction of the *p16-FDR* allele then allows for the independent lineage tracing of *p16*-expressing cell populations, through the action of the FLP-recombinase to irreversibly activate the expression of a second reporter construct. Therefore, this strategy allows for the simultaneous investigation of the contribution of mutations sustaining cells (Cre-reporter+) and cells that currently (mCherry+/FLP-reporter+) or previously expressed $p16^{INK4A}$ (mCherry-/FLP-reporter+).

6.8 General conclusions

The purpose of this thesis was to explore the involvement of cellular senescence during lung and pituitary tumourigenesis. Two main hypotheses were explored: (1) that cluster cells generated in a mouse model of ACP enter into cellular senescence and drive non-cell autonomous tumourigenesis through the SASP and (2) Lung adenomas enter into cellular senescence to prevent their malignant transformation and that their ablation, while senescent, will decrease tumour burden.

In chapter 3, a mouse model of ACP that demonstrated non-cell autonomous tumourigenesis was analysed. In agreement with the first hypothesis, cell clusters, derived from WNT pathway activated stem cells, were found to enter into cellular senescence with concomitant activation of the SASP. Furthermore, the SASP from these cell clusters was ameliorated with age and correlated with a profound reduction in tumourigenic incidence. Together, evidence was provided for a model where a robust SASP mediates the paracrine induction of tumour formation. This unusual mode of tumourigenesis is found in disparate oncogenic contexts, however the mechanisms behind it are poorly understood. Investigations into the role of cellular senescence in these contexts may provide insight and is warranted in future investigations. Furthermore, these results, along with other investigations into ACP biology, may aid in the identification of targetable pathway that are of therapeutic benefit to patients.

In chapter 4, attempts were made to further investigate the first hypothesis by asking whether the activation of senescence and SASP alone (i.e independent of

the activating β-Catenin mutations that drive cellular senescence in the inducible ACP model) is sufficient to drive paracrine tumourigenesis. This was performed in the context of pituitary precursors cells developmentally and pituitary stem cells postnatally by constitutively activating an oncogenic signalling pathway (MAPK). Experimental complications prevented the long-term evaluation of the mice and the pituitaries did not show evidence of senescence induction at analysed time points. However, oncogene targeted embryos displayed profoundly hyperplastic pituitary phenotype. This was characterised and found to consist of an expansion of the stem/progenitor cell compartment, which was severely impaired in its ability to differentiate. Similarities were found in the phenotypes of these mice and human PCP tumours due to the identification of a population of proliferating cells, which expressed a pituitary stem cell marker, which appears to drive PCP tumour growth. While this work did not further the first main hypothesis, it furthered our knowledge into the role of the MAPK pathway in regulating pituitary development. Furthermore, insight was gained into the potential molecular pathogenesis of human PCP.

The final results chapter detailed the development and validation of a novel mouse model to facilitate the lineage tracing, direct visualisation and ablation of *p16*-expressing cell populations. The purpose of which is to aid in the study of cellular senescence *in vivo*. This model was then used in a mouse model of lung tumourigensis. Contrary to the second main hypothesis of this thesis, significant induction of cellular senescence was not observed in developing lung adenomas. However, large numbers of senescent cells were found outside and in association with the tumours and their ablation revealed a non-cell autonomous role for *p16*-expressing cells in driving proliferation of the tumour cells. This work furthers our knowledge of the molecular milieu that is occurring during lung cancer development and provides evidence to support the therapeutic clearance of senescent cells.

Furthermore, a new mouse model was developed to aid in the study of cellular senescence *in vivo* and also provide a novel strategy for understanding the role of senescence escape in tumourigensis.

In conclusion, cellular senescence is a fascinating and rich topic. What was originally considered a cell autonomous tumour-suppresive mechanism is now appreciated to have widespread role in regulating a myriad of physiological functions, including development, ageing and regeneration. Cellular senescence also paradoxically plays a detrimental role, impacting negatively on numerous age-associated pathologies, including cancer. Excellent work has been done over the last several decades in characterising the biochemical pathways that enforce and the stimuli that induce the senescent state. With the recent development of new tools to explore this phenotype in vivo future investigations are primed to significantly change our understanding of both normal and pathological physiology. Optimistically, future investigations into the senescent phenotype may induce a re-evaluation of the origins of cancer and possibly, the irreversibility of the ageing process.

BIBLIOGRAPHY

Acosta, J.C. et al., 2013. A complex secretory program orchestrated by the inflammasome controls paracrine senescence. *Nature cell biology*, 15(8), pp.978–90.

Acosta, J.C. et al., 2008. Chemokine signaling via the CXCR2 receptor reinforces senescence. *Cell*, 133(6), pp.1006–18.

Adam, R.C. et al., 2015. Pioneer factors govern super-enhancer dynamics in stem cell plasticity and lineage choice. *Nature*, 521(7552), pp.366–70.

Agostini, A. et al., 2012. Targeted cargo delivery in senescent cells using capped mesoporous silica nanoparticles. *Angewandte Chemie - International Edition*, 51(42), pp.10556–10560.

Aird, K.M. et al., 2016. HMGB2 orchestrates the chromatin landscape of senescence-associated secretory phenotype gene loci. *The Journal of Cell Biology*, 215(3), pp.325–334.

Akiyama, H. et al., 2004. Essential role of Sox9 in the pathway that controls formation of cardiac valves and septa. *Proceedings of the National Academy of Sciences of the United States of America*, 101(17), pp.6502–7.

Alimonti, A. et al., 2010. A novel type of cellular senescence that can be enhanced in mouse models and human tumor xenografts to suppress prostate tumorigenesis. *The Journal of Clinical Investigation*, 120(3), pp.681–693.

Anastas, J.N. & Moon, R.T., 2013. WNT signalling pathways as therapeutic targets in cancer. *Nature Reviews Cancer*, 13(1), pp.11–26.

Ancrile, B., Lim, K.-H. & Counter, C.M., 2007. Oncogenic Ras-induced secretion of IL6 is required for tumorigenesis. *Genes & development*, 21(14), pp.1714–1719.

Andoniadou, C.L. et al., 2011. HESX1- and TCF3-mediated repression of Wnt/ B-catenin targets is required for normal development of the anterior forebrain. *Development*, 4942, pp.4931–4942.

Andoniadou, C.L. et al., 2012. Identification of novel pathways involved in the pathogenesis of human adamantinomatous craniopharyngioma. *Acta neuropathologica*.

Andoniadou, C.L. et al., 2012. Identification of novel pathways involved in the pathogenesis of human adamantinomatous craniopharyngioma. *Acta Neuropathologica*, 124(2), pp.259–271.

Andoniadou, C.L. et al., 2007. Lack of the murine homeobox gene Hesx1 leads to a posterior transformation of the anterior forebrain. *Development (Cambridge, England)*, 134(8), pp.1499–508.

Andoniadou, C.L. et al., 2013. Sox2+ Stem/Progenitor Cells in the Adult Mouse Pituitary Support Organ Homeostasis and Have Tumor-Inducing Potential. *Cell Stem Cell*, 13(4), pp.433–445.

Andoniadou, C.L. et al., 2013. The Sox2 + population of the adult murine pituitary includes progenitor / stem cells with tumour-inducing potential. *Cell stem cell*.

Apps, J.R. et al., 2018. Tumour compartment transcriptomics demonstrates the activation of inflammatory and odontogenic programmes in human adamantinomatous craniopharyngioma and identifies the MAPK/ERK pathway as a novel therapeutic target. *Acta Neuropathologica*, 135(5), pp.757–777..

Arthur, J.S.C., 2008. MSK activation and physiological roles. *Frontiers in bioscience : a journal and virtual library*, 13, pp.5866–79.

Ashford, N.A. et al., 2015. Cancer risk: Role of environment. *Science*, 347(6223), pp.727–727.

Aylwin, S.J.B., Bodi, I. & Beaney, R., 2016. Pronounced response of papillary craniopharyngioma to treatment with vemurafenib, a BRAF inhibitor. *Pituitary*, 19(5), pp.544–546.

Baar, M.P. et al., 2017. Targeted Apoptosis of Senescent Cells Restores Tissue Homeostasis in Response to Chemotoxicity and Aging. *Cell*, 169(1), pp.132–147.

Bai, L. & Wang, S., 2014. Targeting Apoptosis Pathways for New Cancer Therapeutics. *Annual Review of Medicine*, 65(1), pp.139–155.

Baker, D.J. et al., 2011. Clearance of p16Ink4a-positive senescent cells delays ageing-associated disorders. *Nature*, 479(7372), pp.232–236.

Baker, D.J. et al., 2011. Clearance of p16Ink4a-positive senescent cells delays ageing-associated disorders. *Nature*, 479(7372), pp.232–236.

Baker, D.J. et al., 2016. Naturally occurring p16 Ink4a-positive cells shorten healthy lifespan. *Nature*, 530(7589), pp.184–189.

Baker, D.J. et al., 2008. Opposing roles for p16Ink4a and p19Arf in senescence and ageing caused by BubR1 insufficiency. *Nature Cell Biology*, 10(7), pp.825–836.

Barkhoudarian, G. & Laws, E.R., 2013. Craniopharyngioma: history. *Pituitary*, 16(1), pp.1–8.

Baroja-Mazo, A. et al., 2016. Immunosuppressive potency of mechanistic target of rapamycin inhibitors in solid-organ transplantation. *World Journal of Transplantation*, 6(1), p.183.

Bartkova, J. et al., 2006. Oncogene-induced senescence is part of the tumorigenesis barrier imposed by DNA damage checkpoints. *Nature*, 444(November), pp.633–637.

Bavik, C. et al., 2006. The gene expression program of prostate fibroblast senescence modulates neoplastic epithelial cell proliferation through paracrine mechanisms. *Cancer research*, 66(2), pp.794–802.

Beauséjour, C.M. et al., 2003. Reversal of human cellular senescence: roles of the p53 and p16 pathways. *The EMBO journal*, 22(16), pp.4212–4222.

Bieging, K.T., Mello, S.S. & Attardi, L.D., 2014. Unravelling mechanisms of p53-mediated tumour suppression. *Nature Reviews Cancer*, 14(5), pp.359–370.

Bilodeau, S., Roussel-Gervais, A. & Drouin, J., 2009. Distinct developmental roles of cell cycle inhibitors p57Kip2 and p27Kip1 distinguish pituitary progenitor cell cycle exit from cell cycle reentry of differentiated cells. *Molecular and cellular biology*, 29(7), pp.1895–908.

Blasco, R.B. et al., 2011. c-Raf, but Not B-Raf, Is Essential for Development of K-

Ras Oncogene-Driven Non-Small Cell Lung Carcinoma. *Cancer Cell*, 19(5), pp.652–663.

Bodmer, W.F. et al., 1987. Localization of the gene for familial adenomatous polyposis on chromosome 5. *Nature*, 328(6131), pp.614–6.

Bodnar, A.G. et al., 1998. Extension of life-span by introduction of telomerase into normal human cells. *Science (New York, N.Y.)*, 279(5349), pp.349–52.

Bonner, W.M. et al., 2008. $γ$H2AX and cancer. *Nature Reviews Cancer*, 8(12), pp.957–967.

Booth, A. et al., 2014. Persistent ERK/MAPK activation promotes lactotrope differentiation and diminishes tumorigenic phenotype. *Molecular endocrinology (Baltimore, Md.)*, 28(12), pp.1999–2011

Boots, A.W., Haenen, G.R.M.M. & Bast, A., 2008. Health effects of quercetin: From antioxidant to nutraceutical. *European Journal of Pharmacology*, 585(2–3), pp.325–337.

Braig, M. et al., 2005. Oncogene-induced senescence as an initial barrier in lymphoma development. *Nature*, 436(7051), pp.660–5.

Brastianos, P.K. et al., 2016. Dramatic Response of BRAF V600E Mutant Papillary Craniopharyngioma to Targeted Therapy. *Journal of the National Cancer Institute*, 108(2), p.djv310.

Brastianos, P.K. et al., 2014. Exome sequencing identifies BRAF mutations in papillary craniopharyngiomas. *Nature Publishing Group*, 46(2).

Breyer, B. et al., 2001. Adenoviral vector-mediated gene transfer for human gene therapy. *Current gene therapy*, 1(2), pp.149–62.

Bric, A. et al., 2009. Functional identification of tumor-suppressor genes through an in vivo RNA interference screen in a mouse lymphoma model. *Cancer cell*, 16(4), pp.324–35.

Bunin, G.R. et al., 1998. The descriptive epidemiology of craniopharyngioma. *Journal of Neurosurgery*, 89(4), pp.547–551.

Burd, C.E. et al., 2013. Monitoring Tumorigenesis and Senescence In Vivo with a p16INK4a-Luciferase Model. *Cell*, 152(1–2), pp.340–351.

Burotto, M. et al., 2014. The MAPK pathway across different malignancies: a new perspective. *Cancer*, 120(22), pp.3446–56.

Buslei, R. et al., 2005. Common mutations of β-catenin in adamantinomatous craniopharyngiomas but not in other tumours originating from the sellar region. *Acta Neuropathologica*, 109(6), pp.589–597.

Buslei, R. et al., 2007a. Nuclear beta-catenin accumulation associates with epithelial morphogenesis in craniopharyngiomas. *Acta neuropathologica*, 113(5), pp.585–90.

Buslei, R. et al., 2007b. Nuclear β-catenin accumulation associates with epithelial morphogenesis in craniopharyngiomas. *Acta Neuropathologica*, 113(5), pp.585–590.

Buxade, M., Parra-Palau, J.L. & Proud, C.G., 2008. The Mnks: MAP kinase-interacting kinases (MAP kinase signal-integrating kinases). *Frontiers in bioscience : a journal and virtual library*, 13, pp.5359–73.

Cahu, J., Bustany, S. & Sola, B., 2012. Senescence-associated secretory phenotype favors the emergence of cancer stem-like cells. *Cell death & disease*, 3(12), p.e446.

Campisi, J., 2013. Aging, Cellular Senescence, and Cancer. *Annual Review of Physiology*, 75(1), pp.685–705.

Canino, C. et al., 2012. SASP mediates chemoresistance and tumor-initiating-activity of mesothelioma cells. *Oncogene*, 31(26), pp.3148–3163.

Cano, D.A., Soto-Moreno, A. & Leal-Cerro, A., 2014. Genetically Engineered Mouse Models of Pituitary Tumors. *Frontiers in Oncology*, 4, p.203.

Capell, B.C. et al., 2016. MLL1 is essential for the senescence- associated secretory phenotype. *Genes & Development*, 2, pp.321–336.

Cargnello, M. & Roux, P.P., 2011. Activation and function of the MAPKs and their substrates, the MAPK-activated protein kinases. *Microbiology and molecular biology reviews : MMBR*, 75(1), pp.50–83.

Carreno, G. et al., 2016. Stem cells and their role in pituitary tumorigenesis. *Molecular and Cellular Endocrinology*, 445, pp.27–34.

Carriere, A. et al., 2008. The RSK factors of activating the Ras/MAPK signaling cascade. *Frontiers in bioscience : a journal and virtual library*, 13, pp.4258–75.

Castilho, R.M. et al., 2009. mTOR mediates Wnt-induced epidermal stem cell exhaustion and aging. *Cell stem cell*, 5(3), pp.279–89.

Castinetti, F. et al., 2011. PITX2 AND PITX1 regulate thyrotroph function and response to hypothyroidism. *Molecular endocrinology (Baltimore, Md.)*, 25(11), pp.1950–1960.

Ceteci, F. et al., 2011. Conditional expression of oncogenic C-RAF in mouse pulmonary epithelial cells reveals differential tumorigenesis and induction of autophagy leading to tumor regression. *Neoplasia (New York, N.Y.)*, 13(11), pp.1005–18.

Chang, J. et al., 2016. Clearance of senescent cells by {ABT263} rejuvenates aged hematopoietic stem cells in mice. *Nat Med*, 22(1), pp.78–83.

Chen, J. et al., 2005. The adult pituitary contains a cell population displaying stem/progenitor cell and early embryonic characteristics. *Endocrinology*, 146(9), pp.3985–98.

Chen, L. et al., 2014. Evidence of brain tumor stem progenitor-like cells with low proliferative capacity in human benign pituitary adenoma. *Cancer Letters*, 349(1), pp.61–66.

Chen, Y. et al., 2015. Lysyl hydroxylase 2 induces a collagen cross-link switch in tumor stroma. *The Journal of clinical investigation*, 125(3), pp.1147–62.

Chen, Z. et al., 2005. Crucial role of p53-dependent cellular senescence in suppression of Pten-deficient tumorigenesis. *Nature*, 436(7051), pp.725–30.

Chen, Z. et al., 2014. Non-small-cell lung cancers: a heterogeneous set of diseases. *Nature reviews. Cancer*, 14(8), pp.535–46.

Cheng, M., Boulton, T.G. & Cobb, M.H., 1996. ERK3 is a constitutively nuclear protein kinase. *The Journal of biological chemistry*, 271(15), pp.8951–8.

Cheung, M. & Briscoe, J., 2003. Neural crest development is regulated by the transcription factor Sox9. *Development*, 130(23), pp.5681–5693.

Chiche, A. et al., 2017. Injury-Induced Senescence Enables In Vivo Reprogramming in Skeletal Muscle. *Cell Stem Cell*, 20(3), p.407–414.e4.

Chien, Y. et al., 2011. Control of the senescence-associated secretory phenotype by NF-$κ$B promotes senescence and enhances chemosensitivity. *Genes & development*, 25(20), pp.2125–2136.

Childs, B.G. et al., 2016. Senescent intimal foam cells are deleterious at all stages of atherosclerosis. *Science*, 354(6311), pp.472–477.

Chondrogianni, N. et al., 2010. Anti-ageing and rejuvenating effects of quercetin. *Experimental Gerontology*, 45(10), pp.763–771.

Cisowski, J. et al., 2016. Oncogene-induced senescence underlies the mutual exclusive nature of oncogenic KRAS and BRAF. *Oncogene*, 35(10), pp.1328–1333.

Clevers, H., Loh, K.M. & Nusse, R., 2014. An integral program for tissue renewal and regeneration: Wnt signaling and stem cell control. *Science*, 346(6205), pp.1248012–1248012.

Colavitti, R. & Finkel, T., 2005. Reactive oxygen species as mediators of cellular senescence. *IUBMB life*, 57(4–5), pp.277–81.

Collado, M. et al., 2005a. Tumour biology: Senescence in premalignant tumours. *Nature*, 436(7051), pp.642–642.

Collado, M. et al., 2005b. Tumour biology: Senescence in premalignant tumours. *Nature*, 436(7051), pp.642–642.

Collado, M., Blasco, M.A. & Serrano, M., 2007. Cellular Senescence in Cancer and Aging. *Cell*, 130(2), pp.223–233.

Collado, M. & Serrano, M., 2010. Senescence in tumours: evidence from mice and humans. *Nature reviews. Cancer*, 10(1), pp.51–7.

Collado, M. & Serrano, M., 2010. Senescence in tumours: evidence from mice and humans. *Nature Reviews Cancer*, 10(1), pp.51–57.

Collado, M. & Serrano, M., 2006. The power and the promise of oncogene-induced senescence markers. *Nature reviews. Cancer*, 6(6), pp.472–6.

Collisson, E.A. et al., 2014. Comprehensive molecular profiling of lung adenocarcinoma. *Nature*, 511(7511), pp.543–550.

Coppé, J.-P., Patil, C.K., et al., 2010. A human-like senescence-associated secretory phenotype is conserved in mouse cells dependent on physiological oxygen. M. V. Blagosklonny, ed. *PloS one*, 5(2), p.e9188.

Coppé, J.-P., Patil, C.K., et al., 2010. A Human-Like Senescence-Associated Secretory Phenotype Is Conserved in Mouse Cells Dependent on Physiological Oxygen M. V. Blagosklonny, ed. *PLoS ONE*, 5(2), p.e9188.

Coppé, J.-P. et al., 2008a. Senescence-associated secretory phenotypes reveal cell-nonautonomous functions of oncogenic RAS and the p53 tumor suppressor. *PLoS biology*, 6(12), pp.2853–68.

Coppé, J.-P. et al., 2008b. Senescence-associated secretory phenotypes reveal

cell-nonautonomous functions of oncogenic RAS and the p53 tumor suppressor. J. Downward, ed. *PLoS biology*, 6(12), pp.2853–68.

Coulombe, P. & Meloche, S., 2007. Atypical mitogen-activated protein kinases: structure, regulation and functions. *Biochimica et biophysica acta*, 1773(8), pp.1376–87.

Courtois-Cox, S. et al., 2006. A negative feedback signaling network underlies oncogene-induced senescence. *Cancer cell*, 10(6), pp.459–72.

Crescenzi, E. et al., 2011. NF-$κ$B-dependent cytokine secretion controls Fas expression on chemotherapy-induced premature senescent tumor cells. *Oncogene*, 30(24), pp.2707–2717.

Dai, C.Y. & Enders, G.H., 2000. p16 INK4a can initiate an autonomous senescence program. *Oncogene*, 19(13), pp.1613–1622.

Danaei, G. et al., 2005. Causes of cancer in the world: comparative risk assessment of nine behavioural and environmental risk factors. *Lancet (London, England)*, 366(9499), pp.1784–93.

Dankort, D. et al., 2007. A new mouse model to explore the initiation, progression, and therapy of BRAFV600E-induced lung tumors. *Genes & Development*, 21(4), pp.379–384.

Dattani, M.T. et al., 1998. Mutations in the homeobox gene HESX1/Hesx1 associated with septo-optic dysplasia in human and mouse. *Nature genetics*, 19(2), pp.125–133.

Davalos, A.R. et al., 2010. Senescent cells as a source of inflammatory factors for tumor progression. *Cancer and Metastasis Reviews*, 29(2), pp.273–283.

Davidson, M.R., Gazdar, A.F. & Clarke, B.E., 2013. The pivotal role of pathology in the management of lung cancer. *Journal of thoracic disease*, 5 Suppl 5, pp.S463-78.

Davis, S.W. et al., 2009. Genetics, Gene Expression and Bioinformatics of the Pituitary Gland. *Hormone Research in Paediatrics*, 71(2), pp.101–115.

Davis, S.W., Mortensen, A.H. & Camper, S. a, 2011. Birthdating studies reshape models for pituitary gland cell specification. *Developmental biology*, 352(2), pp.215–227.

Debacq-Chainiaux, F. et al., 2009. Protocols to detect senescence-associated beta-galactosidase (SA-betagal) activity, a biomarker of senescent cells in culture and in vivo. *Nature protocols*, 4(12), pp.1798–1806.

Debies, M.T. et al., 2008. Tumor escape in a Wnt1-dependent mouse breast cancer model is enabled by p19Arf/p53 pathway lesions but not p16 Ink4a loss. *The Journal of clinical investigation*, 118(1), pp.51–63.

Dekkers, O.M. et al., 2006. Quality of life in treated adult craniopharyngioma patients. *European Journal of Endocrinology*, 154(3), pp.483–489.

Demaria, M., Ohtani, N., Youssef, S.A., Rodier, F., Toussaint, W., Mitchell, J.R., Laberge, R.M., Vijg, J., VanSteeg, H., Dollé, M.E.T., et al., 2014. An essential role for senescent cells in optimal wound healing through secretion of PDGF-AA. *Developmental Cell*, 31(6), pp.722–733.

Demaria, M., Ohtani, N., Youssef, S.A., Rodier, F., Toussaint, W., Mitchell, J.R., Laberge, R.M., Vijg, J., VanSteeg, H., Dollé, M.E.T., et al., 2014. An essential

role for senescent cells in optimal wound healing through secretion of PDGF-AA. *Developmental Cell*, 31(6), pp.722–733.

Demaria, M. et al., 2017. Cellular Senescence Promotes Adverse Effects of Chemotherapy and Cancer Relapse. *Cancer discovery*, 7(2), pp.165–176.

Denchi, E.L. et al., 2005. Deregulated E2F Activity Induces Hyperplasia and Senescence-Like Features in the Mouse Pituitary Gland. *Molecular and cellular biology*, 25(7), pp.2660–2672.

Denef, C., 2008. Paracrinicity: the story of 30 years of cellular pituitary crosstalk. *Journal of neuroendocrinology*, 20(1), pp.1–70.

Desai, T.J., Brownfield, D.G. & Krasnow, M.A., 2014. Alveolar progenitor and stem cells in lung development, renewal and cancer. *Nature*, 507(7491), pp.190–194.

Deschene, E.R. et al., 2014. Beta-Catenin Activation Regulates Tissue Growth Non-Cell Autonomously in the Hair Stem Cell Niche. *Science*, 343(6177), pp.1353–1356.

Deschenes-Simard, X. et al., 2013. Tumor suppressor activity of the ERK/MAPK pathway by promoting selective protein degradation. *Genes & Development*, 27(8), pp.900–915.

Devarakonda, S., Morgensztern, D. & Govindan, R., 2015. Genomic alterations in lung adenocarcinoma. *The Lancet. Oncology*, 16(7), pp.e342-51.

Dhomen, N. et al., 2009a. Oncogenic Braf Induces Melanocyte Senescence and Melanoma in Mice. *Cancer Cell*, 15(4), pp.294–303.

Dhomen, N. et al., 2009b. Oncogenic Braf Induces Melanocyte Senescence and Melanoma in Mice. *Cancer Cell*, 15(4), pp.294–303.

Dimri, G.P. et al., 1995. A biomarker that identifies senescent human cells in culture and in aging skin in vivo. *Proceedings of the National Academy of Sciences of the United States of America*, 92(20), pp.9363–7.

Ding, L. et al., 2008. Somatic mutations affect key pathways in lung adenocarcinoma. *Nature*, 455(7216), pp.1069–1075.

Dirac, A.M.G. & Bernards, R., 2003. Reversal of senescence in mouse fibroblasts through lentiviral suppression of p53. *The Journal of biological chemistry*, 278(14), pp.11731–4.

Dollé, P. et al., 1990. Expression of GHF-1 protein in mouse pituitaries correlates both temporally and spatially with the onset of growth hormone gene activity. *Cell*, 60(5), pp.809–20.

Donangelo, I. et al., 2014. Sca1+ murine pituitary adenoma cells show tumor-growth advantage. *Endocrine-Related Cancer*, 21(2), pp.203–216.

Dörr, J.R. et al., 2013. Synthetic lethal metabolic targeting of cellular senescence in cancer therapy. *Nature*, 501(7467), pp.421–5.

Du, Q. & Geller, D.A., 2010. Cross-Regulation Between Wnt and NF-$κ$B Signaling Pathways. *Forum on immunopathological diseases and therapeutics*, 1(3), pp.155–181.

DuPage, M., Dooley, A.L. & Jacks, T., 2009. Conditional mouse lung cancer models using adenoviral or lentiviral delivery of Cre recombinase. *Nature Protocols*,

4(7), pp.1064–1072.

Effros, R.M., 2006. Anatomy, development, and physiology of the lungs. *GI Motility online, Published online: 16 May 2006;* | *doi:10.1038/gimo73*.

Ehrhardt, A. et al., 2001. Development of pulmonary bronchiolo-alveolar adenocarcinomas in transgenic mice overexpressing murine c-myc and epidermal growth factor in alveolar type II pneumocytes. *British journal of cancer*, 84(6), pp.813–8.

Elzi, D.J. et al., 2012. Plasminogen activator inhibitor 1 - insulin-like growth factor binding protein 3 cascade regulates stress-induced senescence. *Proceedings of the National Academy of Sciences*, 109(30), pp.12052–12057.

Emery, P. et al., 2008. IL-6 receptor inhibition with tocilizumab improves treatment outcomes in patients with rheumatoid arthritis refractory to anti-tumour necrosis factor biologicals: results from a 24-week multicentre randomised placebo-controlled trial. *Annals of the Rheumatic Diseases*, 67(11), pp.1516–1523.

Engelman, J.A. et al., 2008. Effective use of PI3K and MEK inhibitors to treat mutant Kras G12D and PIK3CA H1047R murine lung cancers. *Nature Medicine*, 14(12), pp.1351–1356.

Ericson, J. et al., 1998. Integrated FGF and BMP signaling controls the progression of progenitor cell differentiation and the emergence of pattern in the embryonic anterior pituitary. *Development (Cambridge, England)*, 125(6), pp.1005–15.

van Es, J.H. et al., 2012. Dll1+ secretory progenitor cells revert to stem cells upon crypt damage. *Nature cell biology*, 14(10), pp.1099–104.

Ewald, J.A. et al., 2010. Therapy-induced senescence in cancer. *Journal of the National Cancer Institute*, 102(20), pp.1536–46.

Ewing, I. et al., A mutation and expression analysis of the oncogene BRAF in pituitary adenomas. *Clinical endocrinology*, 66(3), pp.348–352.

Eyman, D. et al., 2009. CCL5 secreted by senescent aged fibroblasts induces proliferation of prostate epithelial cells and expression of genes that modulate angiogenesis. *Journal of Cellular Physiology*, 220(2), pp.376–381.

Fang, Q. et al., 2016. Genetics of Combined Pituitary Hormone Deficiency: Roadmap into the Genome Era. *Endocrine reviews*, 37(6), pp.636–675.

Farr, J.N. et al., 2017. Targeting cellular senescence prevents age-related bone loss in mice. *Nat Med*, 23(9), pp.1072–1079.

Fauquier, T. et al., 2008. SOX2-expressing progenitor cells generate all of the major cell types in the adult mouse pituitary gland. *Proceedings of the National Academy of Sciences of the United States of America*, 105(8), pp.2907–12.

Fearon, E.R., 2011. Molecular Genetics of Colorectal Cancer. *Annual Review of Pathology: Mechanisms of Disease*, 6(1), pp.479–507.

Ferbeyre, G. et al., 2000. PML is induced by oncogenic ras and promotes premature senescence. *Genes & development*, 14(16), pp.2015–27.

Ferlay, J. et al., 2015. Cancer incidence and mortality worldwide: Sources, methods and major patterns in GLOBOCAN 2012. *International Journal of Cancer*, 136(5), pp.E359–E386.

Filomeni, G., De Zio, D. & Cecconi, F., 2015. Oxidative stress and autophagy: the

clash between damage and metabolic needs. *Cell Death and Differentiation*, 22(3), pp.377–388.

Fisher, G.H. et al., 2001. Induction and apoptotic regression of lung adenocarcinomas by regulation of a K-Ras transgene in the presence and absence of tumor suppressor genes. *Genes & Development*, 15(24), pp.3249–3262.

Fitzgerald, A.L. et al., 2015. Reactive oxygen species and p21Waf1/Cip1 are both essential for p53-mediated senescence of head and neck cancer cells. *Cell Death and Disease*, 6(3), p.e1678.

Flores, I., Benetti, R. & Blasco, M.A., 2006. Telomerase regulation and stem cell behaviour. *Current Opinion in Cell Biology*, 18(3), pp.254–260.

Florio, T., 2011. Adult pituitary stem cells: from pituitary plasticity to adenoma development. *Neuroendocrinology*, 94(4), pp.265–77.

Franceschi, C. & Campisi, J., 2014. Chronic inflammation (Inflammaging) and its potential contribution to age-associated diseases. *J Gerontol A Biol Sci Med Sci*, 69, pp.S4–S9.

Freund, A., Patil, C.K. & Campisi, J., 2011. p38MAPK is a novel DNA damage response-independent regulator of the senescence-associated secretory phenotype. *The EMBO journal*, 30(8), pp.1536–1548.

Fuhrmann-Stroissnigg, H. et al., 2017. Identification of HSP90 inhibitors as a novel class of senolytics. *Nature Communications*, 8(1), p.422.

Fumagalli, M. et al., 2014. Stable Cellular Senescence Is Associated with Persistent DDR Activation. *PloS one*, 9(10), p.e110969.

Futreal, P.A. et al., 2004. A census of human cancer genes. *Nature Reviews Cancer*, 4(3), pp.177–183.

Gaillard, H., García-Muse, T. & Aguilera, A., 2015. Replication stress and cancer. *Nature Reviews Cancer*, 15(5), pp.276–289.

Gao, J. et al., 2013. Integrative analysis of complex cancer genomics and clinical profiles using the cBioPortal. *Science signaling*, 6(269), p.pl1.

Gao, J. et al., 2013. Integrative Analysis of Complex Cancer Genomics and Clinical Profiles Using the cBioPortal. *Science Signaling*, 6(269), pp.pl1-pl1.

Garcia-Lavandeira, M. et al., 2009. A GRFa2/Prop1/stem (GPS) cell niche in the pituitary. J. A. L. Calbet, ed. *PloS one*, 4(3), p.e4815.

Garcia-Lavandeira, M. et al., 2011. Craniopharyngiomas Express Embryonic Stem Cell Markers (SOX2, OCT4, KLF4, and SOX9) as Pituitary Stem Cells but Do Not Coexpress RET/GFRA3 Receptors. *The Journal of clinical endocrinology and metabolism*, 97(January), pp.1–8.

Garnett, S. et al., 2017a. p53 loss does not permit escape from BrafV600E-induced senescence in a mouse model of lung cancer. *Oncogene*, 36(45), pp.6325–6335.

Garnett, S. et al., 2017b. p53 loss does not permit escape from BrafV600E-induced senescence in a mouse model of lung cancer. *Oncogene*, 36(45), pp.6325–6335.

Gaston-Massuet, C. et al., 2008. Genetic interaction between the homeobox

transcription factors HESX1 and SIX3 is required for normal pituitary development. *Developmental biology*, 324(2), pp.322–33.

Gaston-Massuet, C. et al., 2011. Increased Wingless (Wnt) signaling in pituitary progenitor/stem cells gives rise to pituitary tumors in mice and humans. *Proceedings of the National Academy of Sciences of the United States of America*, 108(28), pp.11482–7.

Gire, V. & Wynford-Thomas, D., 1998. Reinitiation of DNA synthesis and cell division in senescent human fibroblasts by microinjection of anti-p53 antibodies. *Molecular and cellular biology*, 18(3), pp.1611–21.

Gleiberman, A.S. et al., 2008. Genetic approaches identify adult pituitary stem cells. *Proceedings of the National Academy of Sciences of the United States of America*, 105(17), pp.6332–7.

Goldsmith, S., Lovell-Badge, R. & Rizzoti, K., 2016. SOX2 is sequentially required for progenitor proliferation and lineage specification in the developing pituitary. *Development (Cambridge, England)*, 143(13), pp.2376–88.

Goldstraw, P. et al., 2007. The IASLC Lung Cancer Staging Project: Proposals for the Revision of the TNM Stage Groupings in the Forthcoming (Seventh) Edition of the TNM Classification of Malignant Tumours. *Journal of Thoracic Oncology*, 2(8), pp.706–714.

Gómez-Gaviro, M.V. et al., 2012. The vascular stem cell niche. *Journal of Cardiovascular Translational Research*, 5(5), pp.618–630.

Gonzalez-Meljem, J.M. et al., 2017a. Stem cell senescence drives age-attenuated induction of pituitary tumours in mouse models of paediatric craniopharyngioma. *Nature Communications*, 8(1), p.1819.

Gonzalez-Meljem, J.M. et al., 2017b. Stem cell senescence drives age-attenuated induction of pituitary tumours in mouse models of paediatric craniopharyngioma. *Nature Communications*, 8(1), p.1819.

Gosselin, K. et al., 2009. Senescence-associated oxidative DNA damage promotes the generation of neoplastic cells. *Cancer research*, 69(20), pp.7917–25.

Gotay, C., Dummer, T. & Spinelli, J., 2015. Cancer risk: prevention is crucial. *Science (New York, N.Y.)*, 347(6223), p.728.

Govindan, R. et al., 2006. Changing epidemiology of small-cell lung cancer in the United States over the last 30 years: analysis of the surveillance, epidemiologic, and end results database. *Journal of clinical oncology : official journal of the American Society of Clinical Oncology*, 24(28), pp.4539–44.

Gracz, A.D. & Magness, S.T., 2011. Sry-box (Sox) transcription factors in gastrointestinal physiology and disease. *American journal of physiology. Gastrointestinal and liver physiology*, 300(4), pp.G503-15.

Gray-Schopfer, V.C. et al., 2006. Cellular senescence in naevi and immortalisation in melanoma: a role for p16? *British journal of cancer*, 95(4), pp.496–505.

Greulich, H., 2010. The genomics of lung adenocarcinoma: opportunities for targeted therapies. *Genes & cancer*, 1(12), pp.1200–10.

Gridelli, C. et al., 2015. Non-small-cell lung cancer. *Nature Reviews Disease Primers*, 1, p.15009.

Gu, Z. et al., 2014. Wnt/β-catenin signaling mediates the senescence of bone

marrow-mesenchymal stem cells from systemic lupus erythematosus patients through the p53/p21 pathway. *Molecular and Cellular Biochemistry*, 387(1–2), pp.27–37.

Guerra, C. et al., 2003. Tumor induction by an endogenous K-ras oncogene is highly dependent on cellular context. *Cancer cell*, 4(2), pp.111–20.

Halazonetis, T.D., Gorgoulis, V.G. & Bartek, J., 2008. An oncogene-induced DNA damage model for cancer development. *Science (New York, N.Y.)*, 319(5868), pp.1352–1355.

Hall, B.M. et al., 2016. Aging of mice is associated with p16(Ink4a)- and β-galactosidase-positive macrophage accumulation that can be induced in young mice by senescent cells. *Aging*, 8(7), pp.1294–315.

Hall, B.M. et al., 2017. p16(Ink4a) and senescence-associated β-galactosidase can be induced in macrophages as part of a reversible response to physiological stimuli. *Aging*, 9(8), pp.1867–1884.

Hameyer, D. et al., 2007. Toxicity of ligand-dependent Cre recombinases and generation of a conditional Cre deleter mouse allowing mosaic recombination in peripheral tissues. *Physiological genomics*, 31(1), pp.32–41.

Hanahan, D. & Weinberg, R. a., 2011. Hallmarks of cancer: The next generation. *Cell*, 144(5), pp.646–674.

Hanahan, D. & Weinberg, R.A., 2000. The hallmarks of cancer. *Cell*, 100(1), pp.57–70.

Harada, N. et al., 1999. Intestinal polyposis in mice with a dominant stable mutation of the beta -catenin gene. *The EMBO Journal*, 18(21), pp.5931–5942.

Hashimoto, H., Ishikawa, H. & Kusakabe, M., 1998. Three-dimensional analysis of the developing pituitary gland in the mouse. *Developmental Dynamics*, 212(1), pp.157–166.

Haston, S., Manshaei, S. & Martinez-Barbera, J.P., 2018. Stem/progenitor cells in pituitary organ homeostasis and tumourigenesis. *Journal of Endocrinology*, 236(1), pp.R1–R13.

Hasty, P. et al., 2013. mTORC1 and p53: Clash of the gods? *Cell Cycle*, 12(1), pp.20–25.

Hattori, T. et al., 2010. SOX9 is a major negative regulator of cartilage vascularization, bone marrow formation and endochondral ossification. *Development*, 137(6), pp.901–911

Haugstetter, A.M. et al., 2010. Cellular senescence predicts treatment outcome in metastasised colorectal cancer. *British Journal of Cancer*, 103(4), pp.505–509.

Hayden, M.S. & Ghosh, S., 2012. NF- B, the first quarter-century: remarkable progress and outstanding questions. *Genes & Development*, 26(3), pp.203–234.

Hayden, M.S., West, A.P. & Ghosh, S., 2006. NF-$κ$B and the immune response. *Oncogene*, 25(51), pp.6758–6780.

HAYFLICK, L. & MOORHEAD, P.S., 1961. The serial cultivation of human diploid cell strains. *Experimental cell research*, 25, pp.585–621.

Herbig, U. et al., 2006. Cellular Senescence in Aging Primates. *Science*, 311(5765),

pp.1257–1257.

Herbst, R.S., Heymach, J. V. & Lippman, S.M., 2008. Lung Cancer. *New England Journal of Medicine*, 359(13), pp.1367–1380.

Herbst, R.S., Morgensztern, D. & Boshoff, C., 2018. The biology and management of non-small cell lung cancer. *Nature 2018 553:7689*, 553(7689), p.446.

Hermesz, E., Mackem, S. & Mahon, K.A., 1996. Rpx : a novel anterior-restricted homeobox gene progressively activated in the prechordal plate , anterior neural plate and Rathke ' s pouch of the mouse embryo. *Development*, 52, pp.41–52.

Hernandez-Segura, A., Nehme, J. & Demaria, M., 2018. Hallmarks of Cellular Senescence. *Trends in Cell Biology*, 28(6), pp.436–453.

Herranz, N. et al., 2015. mTOR regulates MAPKAPK2 translation to control the senescence-associated secretory phenotype. *Nature Cell Biology*, 17(9).

Higuchi, M. et al., 2014. PRRX1 and PRRX2 distinctively participate in pituitary organogenesis and a cell-supply system. *Cell and tissue research*, 357(1), pp.323–35.

Hindson, B.J. et al., High-throughput droplet digital PCR system for absolute quantitation of DNA copy number. *Analytical chemistry*, 83(22), pp.8604–8610.

Hoare, M. et al., 2016. NOTCH1 mediates a switch between two distinct secretomes during senescence. *Nature Cell Biology*.

Hölsken, A. et al., 2013. Adamantinomatous craniopharyngiomas express tumor stem cell markers in cells with activated Wnt signaling: further evidence for the existence of a tumor stem cell niche? *Pituitary*, 17(6), pp.546–556.

Horiguchi, K. et al., 2012. Expression of chemokine CXCL12 and its receptor CXCR4 in folliculostellate (FS) cells of the rat anterior pituitary gland: the CXCL12/CXCR4 axis induces interconnection of FS cells. *Endocrinology*, 153(4), pp.1717–24.

Hosoyama, T. et al., 2010. A Postnatal Pax7 Progenitor Gives Rise to Pituitary Adenomas. *Genes & cancer*, 1(4), pp.388–402.

Howlader, N. et al., 2012. SEER Cancer Statistics Review 1975-2008.

Hsu, Y.-C., Li, L. & Fuchs, E., 2014. Emerging interactions between skin stem cells and their niches. *Nature medicine*, 20(8), pp.847–56.

Huang, B. et al., 1999. Autosomal XX sex reversal caused by duplication of SOX9. *American journal of medical genetics*, 87(4), pp.349–53.

Hubackova, S. et al., 2012. IL1- and TGFβ-Nox4 signaling, oxidative stress and DNA damage response are shared features of replicative, oncogene-induced, and drug-induced paracrine "bystander senescence". *Aging*, 4(12), pp.932–51.

Huff, V., 2011. Wilms' tumours: about tumour suppressor genes, an oncogene and a chameleon gene. *Nature reviews. Cancer*, 11(2), pp.111–21.

Hüsken, U. & Carl, M., 2013. The Wnt/beta-catenin signaling pathway establishes neuroanatomical asymmetries and their laterality. *Mechanisms of development*, 130(6–8), pp.330–5.

Iannello, A. & Raulet, D.H., 2013. Immune Surveillance of Unhealthy Cells by Natural Killer Cells. *Cold Spring Harbor Symposia on Quantitative Biology*,

78(0), pp.249–257.

Di Ieva, A. et al., 2014. Aggressive pituitary adenomas—diagnosis and emerging treatments. *Nature Reviews Endocrinology*, 10(7), pp.423–435.

Ikeda, T. et al., 2004. The combination of SOX5, SOX6, and SOX9 (the SOX trio) provides signals sufficient for induction of permanent cartilage. *Arthritis and rheumatism*, 50(11), pp.3561–73.

Imielinski, M. et al., 2012. Mapping the hallmarks of lung adenocarcinoma with massively parallel sequencing. *Cell*, 150(6), pp.1107–20.

Inomata, M. et al., 1996. Alteration of beta-catenin expression in colonic epithelial cells of familial adenomatous polyposis patients. *Cancer research*, 56(9), pp.2213–7.

Isaacs, H., 2009. Fetal brain tumors: a review of 154 cases. *American journal of perinatology*, 26(6), pp.453–66.

Ivanov, a. et al., 2013. Lysosome-mediated processing of chromatin in senescence. *The Journal of Cell Biology*, 202(1), pp.129–143.

Iwanaga, K. et al., 2008. Pten Inactivation Accelerates Oncogenic K-ras-Initiated Tumorigenesis in a Mouse Model of Lung Cancer. *Cancer Research*, 68(4), pp.1119–1127.

Jackson, E.L. et al., 2001. Analysis of lung tumor initiation and progression using conditional expression of oncogenic K-ras. *Genes & development*, 15(24), pp.3243–8.

Jackson, E.L. et al., 2005. The differential effects of mutant p53 alleles on advanced murine lung cancer. *Cancer research*, 65(22), pp.10280–8.

Jacobs, J.J.L. et al., 2004. Significant role for p16INK4a in p53-independent telomere-directed senescence. *Current biology : CB*, 14(24), pp.2302–2308.

Jayakody, S.A. et al., 2012. SOX2 regulates the hypothalamic-pituitary axis at multiple levels. *The Journal of Clinical Investigation*, 122(10), pp.3635–3646.

Jeon, O.H. et al., 2017. Local clearance of senescent cells attenuates the development of post-traumatic osteoarthritis and creates a pro-regenerative environment. *Nature Medicine*, 23(6), pp.775–781.

Ji, H. et al., 2007. LKB1 modulates lung cancer differentiation and metastasis. *Nature*, 448(7155), pp.807–10.

Ji, H. et al., 2006. The impact of human EGFR kinase domain mutations on lung tumorigenesis and in vivo sensitivity to EGFR-targeted therapies. *Cancer cell*, 9(6), pp.485–95.

Johnson, L. et al., 2001. Somatic activation of the K-ras oncogene causes early onset lung cancer in mice. *Nature*, 410(6832), pp.1111–6.

Joó, J.G. et al., 2009. Foetal craniopharyngioma diagnosed by prenatal ultrasonography and confirmed by histopathological examination. *Prenatal diagnosis*, 29(2), pp.160–3.

Jurk, D. et al., 2014. Chronic inflammation induces telomere dysfunction and accelerates ageing in mice. *Nature Communications*, 5(1), p.4172.

Jurkiewicz, E. et al., 2010. Antenatal diagnosis of the congenital

craniopharyngioma. *Polish journal of radiology*, 75(1), pp.98–102.

Kaefer, A. et al., 2014. Mechanism-based pharmacokinetic/pharmacodynamic meta-analysis of navitoclax (ABT-263) induced thrombocytopenia. *Cancer Chemotherapy and Pharmacology*, 74(3), pp.593–602.

Kamijo, T. et al., 1997. Tumor Suppression at the Mouse INK4a Locus Mediated by the Alternative Reading Frame Product p19 ARF. *Cell*, 91(5), pp.649–659.

Kang, C. et al., 2015. The DNA damage response induces inflammation and senescence by inhibiting autophagy of GATA4. *Science (New York, N.Y.)*, 349(6255), p.aaa5612.

Kang, C. & Elledge, S.J., 2016. How autophagy both activates and inhibits cellular senescence. *Autophagy*, 12(5), pp.898–899.

Kang, P. et al., 2012. Sox9 and NFIA coordinate a transcriptional regulatory cascade during the initiation of gliogenesis. *Neuron*, 74(1), pp.79–94.

Kang, T.-W. et al., 2011. Senescence surveillance of pre-malignant hepatocytes limits liver cancer development. *Nature*, 479(7374), pp.547–551.

Kang, Y. et al., 2010. Proliferation of human lung cancer in an orthotopic transplantation mouse model. *Experimental and therapeutic medicine*, 1(3), pp.471–475.

Karavitaki, N., 2012. Prevalence and incidence of pituitary adenomas. *Annales d'Endocrinologie*, 73(2), pp.79–80.

Karga, H.J. et al., Ras mutations in human pituitary tumors. *The Journal of clinical endocrinology and metabolism*, 74(4), pp.914–919.

Kasperczyk, H. et al., 2009. Characterization of sonic hedgehog as a novel NF-kappaB target gene that promotes NF-kappaB-mediated apoptosis resistance and tumor growth in vivo. *FASEB journal : official publication of the Federation of American Societies for Experimental Biology*, 23(1), pp.21–33.

Kato, K. et al., 2004. Possible linkage between specific histological structures and aberrant reactivation of the Wnt pathway in adamantinomatous craniopharyngioma. *Journal of Pathology*, 203(3), pp.814–821.

Kelberman, D. et al., 2009. Genetic Regulation of Pituitary Gland Development in Human and Mouse. *Endocrine Reviews*, 30(7), pp.790–829.

Kelberman, D. et al., 2006. Mutations within Sox2/SOX2 are associated with abnormalities in the hypothalamo-pituitary-gonadal axis in mice and humans. *The Journal of clinical investigation*, 116(9), pp.2442–55.

Kim, C.F.B. et al., 2005. Identification of Bronchioalveolar Stem Cells in Normal Lung and Lung Cancer. *Cell*, 121(6), pp.823–835.

Kim, Y.H. et al., 2017. Senescent tumor cells lead the collective invasion in thyroid cancer. *Nature Communications*, 8, p.15208.

Kim, Y.H. et al., 2014. TSH Signaling Overcomes B-RafV600E–Induced Senescence in Papillary Thyroid Carcinogenesis through Regulation of DUSP6. *Neoplasia*, 16(12), pp.1107–1120.

Kinzler, K.W. & Vogelstein, B., 1996. Lessons from hereditary colorectal cancer. *Cell*, 87(2), pp.159–70.

Kirkland, J.L. et al., 2017. The Clinical Potential of Senolytic Drugs. *Journal of the American Geriatrics Society*, 65(10), pp.2297–2301.

Kissil, J.L. et al., 2007. Requirement for Rac1 in a K-ras induced lung cancer in the mouse. *Cancer research*, 67(17), pp.8089–94.

Klaus, A. & Birchmeier, W., 2008. Wnt signalling and its impact on development and cancer. *Nature Reviews Cancer*, 8(5), pp.387–398.

Kode, A. et al., 2014. Leukaemogenesis induced by an activating β-catenin mutation in osteoblasts. *Nature*, 506(7487), pp.240–4.

Koesters, R. et al., 1999. Mutational activation of the beta-catenin proto-oncogene is a common event in the development of Wilms' tumors. *Cancer research*, 59(16), pp.3880–2.

Konstantinidou, G. et al., 2013. RHOA-FAK Is a Required Signaling Axis for the Maintenance of KRAS-Driven Lung Adenocarcinomas. *Cancer Discovery*, 3(4), pp.444–457.

Kostadinov, S. et al., 2014. Fetal Craniopharyngioma: Management, Postmortem Diagnosis, and Literature Review of an Intracranial Tumor Detected in Utero. *Pediatric and Developmental Pathology*, 17(5), pp.409–412.

Kramer, B.W., Götz, R. & Rapp, U.R., 2004. Use of mitogenic cascade blockers for treatment of C-Raf induced lung adenoma in vivo: CI-1040 strongly reduces growth and improves lung structure. *BMC cancer*, 4(1), p.24.

Krizhanovsky, V. et al., 2008. Senescence of Activated Stellate Cells Limits Liver Fibrosis. *Cell*, 134(4), pp.657–667.

Krtolica, A. et al., 2001. Senescent fibroblasts promote epithelial cell growth and tumorigenesis: a link between cancer and aging. *Proceedings of the National Academy of Sciences of the United States of America*, 98(21), pp.12072–7.

Kuilman, T. et al., 2008. Oncogene-induced senescence relayed by an interleukin-dependent inflammatory network. *Cell*, 133(6), pp.1019–1031.

Kuilman, T. et al., 2010. The essence of senescence. *Genes & development*, 24(22), pp.2463–79.

Kurz, D.J. et al., 2000. Senescence-associated (beta)-galactosidase reflects an increase in lysosomal mass during replicative ageing of human endothelial cells. *Journal of cell science*, 113 (Pt 2, pp.3613–3622.

Kwon, M. & Berns, A., 2013. Mouse models for lung cancer. *Molecular oncology*, 7(2), pp.165–77.

, J., 2012. Mammalian MAPK Signal Transduction Pathways Activated by Stress and Inflammation: A 10-Year Update. *Physiological Reviews*, 92(2), pp.689–737.

Laberge, R.-M. et al., 2015. MTOR regulates the pro-tumorigenic senescence-associated secretory phenotype by promoting IL1A translation. *Nature cell biology*, Advance On(November 2014), pp.1–15.

Labeur, M. et al., 2010. Pituitary tumors: cell type-specific roles for BMP-4. *Molecular and cellular endocrinology*, 326(1–2), pp.85–8.

Lamolet, B. et al., 2001. A pituitary cell-restricted T box factor, Tpit, activates POMC transcription in cooperation with Pitx homeoproteins. *Cell*, 104(6), pp.849–59.

Langer, C.J. et al., 2010. The Evolving Role of Histology in the Management of Advanced Non–Small-Cell Lung Cancer. *Journal of Clinical Oncology*, 28(36), pp.5311–5320.

Larkin, S. & Ansorge, O., 2000. *Pathology and Pathogenesis of Pituitary Adenomas and Other Sellar Lesions*, MDText.com, Inc.

Lawrence, T., 2009. The nuclear factor NF-kappaB pathway in inflammation. *Cold Spring Harbor perspectives in biology*, 1(6), p.a001651.

Lazzerini Denchi, E. et al., 2005. Deregulated E2F activity induces hyperplasia and senescence-like features in the mouse pituitary gland. *Molecular and cellular biology*, 25(7), pp.2660–72.

Le, O.N.L. et al., 2010. Ionizing radiation-induced long-term expression of senescence markers in mice is independent of p53 and immune status. *Aging Cell*, 9(3), pp.398–409.

Lee, B.Y. et al., 2006. Senescence-associated beta-galactosidase is lysosomal beta-galactosidase. *Aging cell*, 5(2), pp.187–195.

Lemjabbar-Alaoui, H. et al., 2015. Lung cancer: Biology and treatment options. *Biochimica et Biophysica Acta (BBA) - Reviews on Cancer*, 1856(2), pp.189–210.

Leontieva, O. V. & Blagosklonny, M. V., 2010. DNA damaging agents and p53 do not cause senescence in quiescent cells, while consecutive re-activation of mTOR is associated with conversion to senescence. *Aging*, 2(12), pp.924–935.

Lepore, D.A. et al., 2005. Identification and enrichment of colony-forming cells from the adult murine pituitary. *Experimental cell research*, 308(1), pp.166–76.

Leppert, M. et al., 1987. The gene for familial polyposis coli maps to the long arm of chromosome 5. *Science (New York, N.Y.)*, 238(4832), pp.1411–3.

Levy, A., 2002. Physiological implications of pituitary trophic activity. *Journal of Endocrinology*, 174(2), pp.147–155.

Liao, E.-C. et al., 2014. Radiation induces senescence and a bystander effect through metabolic alterations. *Cell death & disease*, 5(5), p.e1255.

Lines, K.E., Stevenson, M. & Thakker, R.V., 2016. Animal models of pituitary neoplasia. *Molecular and Cellular Endocrinology*, 421, pp.68–81.

Liu, K. et al., 2013. The multiple roles for Sox2 in stem cell maintenance and tumorigenesis. *Cellular Signalling*, 25(5), pp.1264–1271.

Liu, Y. et al., 2006. Aberrant promoter methylation of p16 and MGMT genes in lung tumors from smoking and never-smoking lung cancer patients. *Neoplasia (New York, N.Y.)*, 8(1), pp.46–51.

Louis, D.N. et al., 2016. WK, C. of Tumours of the Central Nervous of Tumours, vol. Volume 1.

Lujambio, A. et al., 2013. Non-cell-autonomous tumor suppression by p53. *Cell*, 153(2), pp.449–60.

Luo, X. et al., 2016. Stromal-Initiated Changes in the Bone Promote Metastatic Niche Development Article Stromal-Initiated Changes in the Bone Promote Metastatic Niche Development. *CellReports*, 14(1), pp.82–92.

Mainardi, S. et al., 2014. Identification of cancer initiating cells in K-Ras driven lung adenocarcinoma. *Proceedings of the National Academy of Sciences of the United States of America*, 111(1), pp.255–60.

Majumder, P.K. et al., 2008. A Prostatic Intraepithelial Neoplasia-Dependent p27Kip1 Checkpoint Induces Senescence and Inhibits Cell Proliferation and Cancer Progression. *Cancer Cell*, 14(2), pp.146–155.

Mallette, F.A., Gaumont-Leclerc, M.-F., et al., 2007. Myc down-regulation as a mechanism to activate the Rb pathway in STAT5A-induced senescence. *The Journal of biological chemistry*, 282(48), pp.34938–44.

Mallette, F.A., Ferbeyre, G. & Mallette, F.A., 2007. The DNA damage signaling pathway is a critical mediator of oncogene-induced senescence service The DNA damage signaling pathway is a critical mediator of oncogene-induced senescence. , (514), pp.43–48.

Maretto, S. et al., 2003. Mapping Wnt/beta-catenin signaling during mouse development and in colorectal tumors. *Proceedings of the National Academy of Sciences of the United States of America*, 100(6), pp.3299–304.

Markakis, E.A., 2002. Development of the neuroendocrine hypothalamus. *Frontiers in neuroendocrinology*, 23(3), pp.257–91.

Martinez-Barbera, J.P. & Andoniadou, C.L., Concise Review: Paracrine Role of Stem Cells in Pituitary Tumors: A Focus on Adamantinomatous Craniopharyngioma.

Matos, L., Gouveia, A.M. & Almeida, H., 2015. ER Stress Response in Human Cellular Models of Senescence. *The Journals of Gerontology Series A: Biological Sciences and Medical Sciences*, 70(8), pp.924–935.

Meek, D.W., 2009. Tumour suppression by p53: a role for the DNA damage response? *Nature reviews. Cancer*, 9(10), pp.714–723. Available at: http://dx.doi.org/10.1038/nrc2716.

Melmed, S., 2003. Mechanisms for pituitary tumorigenesis: the plastic pituitary. *The Journal of clinical investigation*, 112(11), pp.1603–18.

Melmed, S., 2011. Pathogenesis of pituitary tumors. *Nature Reviews Endocrinology*, 7(5), pp.257–266.

Menendez, D., Inga, A. & Resnick, M. a, 2009. The expanding universe of p53 targets. *Nature reviews. Cancer*, 9(10), pp.724–737.

Mercer, K. et al., Expression of endogenous oncogenic V600EB-raf induces proliferation and developmental defects in mice and transformation of primary fibroblasts. *Cancer research*, 65(24), pp.11493–11500.

Mertens, F. et al., 2015. Pituitary tumors contain a side population with tumor stem cell-associated characteristics. *Endocrine-Related Cancer*, 22(4), pp.481–504.

Meuwissen, R. et al., 2003. Induction of small cell lung cancer by somatic inactivation of both Trp53 and Rb1 in a conditional mouse model. *Cancer Cell*, 4(3), pp.181–189.

Meuwissen, R. et al., 2001. Mouse model for lung tumorigenesis through Cre/lox controlled sporadic activation of the K-Ras oncogene. *Oncogene*, 20(45), pp.6551–8.

Di Micco, R. et al., 2006. Oncogene-induced senescence is a DNA damage

response triggered by DNA hyper-replication. *Nature*, 444(7119), pp.638–642.

Michaloglou, C. et al., 2005. BRAFE600-associated senescence-like cell cycle arrest of human naevi. *Nature*, 436(7051), pp.720–4.

Mikels, A.J. & Nusse, R., 2006. Wnts as ligands: processing, secretion and reception. *Oncogene*, 25(57), pp.7461–8.

Milanovic, M. et al., 2017. Senescence-associated reprogramming promotes cancer stemness. *Nature*, 553(7686), pp.96–100.

De Moerlooze, L. et al., 2000. An important role for the IIIb isoform of fibroblast growth factor receptor 2 (FGFR2) in mesenchymal-epithelial signalling during mouse organogenesis. *Development (Cambridge, England)*, 127(3), pp.483–92.

Moldvay, J. et al., 2004. The role of TTF-1 in differentiating primary and metastatic lung adenocarcinomas. *Pathology oncology research : POR*, 10(2), pp.85–8.

Mollard, P. et al., 2012. A tridimensional view of pituitary development and function. *Trends in Endocrinology & Metabolism*, 23(6), pp.261–269.

Moniot, B. et al., 2004. SOX9 specifies the pyloric sphincter epithelium through mesenchymal-epithelial signals. *Development (Cambridge, England)*, 131(15), pp.3795–804.

Mosteiro, L. et al., 2016. Tissue damage and senescence provide critical signals for cellular reprogramming in vivo. *Science*, 354(6315).

Müller, H.L., 2014a. Childhood craniopharyngioma: treatment strategies and outcomes. *Expert Review of Neurotherapeutics*, 14(2), pp.187–197.

Müller, H.L., 2013. Childhood craniopharyngioma. *Pituitary*, 16(1), pp.56–67.

Müller, H.L., 2014b. Craniopharyngioma. *Endocrine reviews*, 35(3), pp.513–543.

Müller, H.L. et al., 2004. Longitudinal Study on Growth and Body Mass Index before and after Diagnosis of Childhood Craniopharyngioma. *The Journal of Clinical Endocrinology & Metabolism*, 89(7), pp.3298–3305.

Muñoz-Espín, D. et al., 2013. Programmed cell senescence during mammalian embryonic development. *Cell*, 155(5), pp.1104–18.

Muñoz-Espín, D. & Serrano, M., 2014. Cellular senescence : from physiology to pathology. *Nature reviews. Molecular cell biology*, 15(7), pp.482–496.

Muñoz-Espín, D. et al., 2018. A versatile drug delivery system targeting senescent cells. *EMBO Molecular Medicine*, 10(9), p.e9355.

Muzumdar, M.D. et al., 2007. A Global Double-Fluorescent Cre Reporter Mouse. *Genesis*, 605(September), pp.593–605.

Muzumdar, M.D. et al., 2016. Clonal dynamics following p53 loss of heterozygosity in Kras-driven cancers. *Nature communications*, 7, p.12685.

Nabhan, A.N. et al., 2018. Single-cell Wnt signaling niches maintain stemness of alveolar type 2 cells. *Science (New York, N.Y.)*, 359(6380), pp.1118–1123.

Nakamura, M., Ohsawa, S. & Igaki, T., 2014. Mitochondrial defects trigger proliferation of neighbouring cells via a senescence-associated secretory phenotype in Drosophila. *Nature Communications*, 5, p.5264.

Nakanishi, Y. et al., 2013. Dclk1 distinguishes between tumor and normal stem cells in the intestine. *Nature genetics*, 45(1), pp.98–103.

Nardella, C. et al., 2008. Aberrant Rheb-mediated mTORC1 activation and Pten haploinsufficiency are cooperative oncogenic events. *Genes & development*, 22(16), pp.2172–7.

Nardella, C. et al., 2008. Aberrant Rheb-mediated mTORC1 activation and Pten haploinsufficiency are cooperative oncogenic events. *Genes & Development*, 22(16), pp.2172–2177.

Narita, M. et al., 2003. Rb-mediated heterochromatin formation and silencing of E2F target genes during cellular senescence. *Cell*, 113(6), pp.703–716.

Newey, P.J. et al., Whole-exome sequencing studies of nonfunctioning pituitary adenomas. *The Journal of clinical endocrinology and metabolism*, 98(4), pp.E796-800.

Nicolas, M. et al., 2003. Notch1 functions as a tumor suppressor in mouse skin. *Nature Genetics*, 33(3), pp.416–421.

Nielsen, E.H. et al., 2011. Incidence of craniopharyngioma in Denmark (n = 189) and estimated world incidence of craniopharyngioma in children and adults. *Journal of neuro-oncology*, 104(3), pp.755–63.

Nochols, K.E. et al., 2001. Germ-line p53 mutations predispose to a wide spectrum of early-onset cancers. *Cancer Epidemiology Biomarkers and Prevention*, 10(2), pp.83–87.

Nolan, L.A. et al., 1998. Anterior pituitary cell population control: basal cell turnover and the effects of adrenalectomy and dexamethasone treatment. *Journal of neuroendocrinology*, 10(3), pp.207–15.

Nomura, R., Yoshida, D. & Teramoto, A., 2009. Stromal cell-derived factor-1 expression in pituitary adenoma tissues and upregulation in hypoxia. *Journal of Neuro-Oncology*, 94(2), pp.173–181.

Norlin, S., Nordström, U. & Edlund, T., 2000. Fibroblast growth factor signaling is required for the proliferation and patterning of progenitor cells in the developing anterior pituitary. *Mechanisms of development*, 96(2), pp.175–82.

Nusse, R. & Varmus, H.E., 1982. Many tumors induced by the mouse mammary tumor virus contain a provirus integrated in the same region of the host genome. *Cell*, 31(1), pp.99–109.

O'Callaghan, M., 2015. Cancer risk: Accuracy of literature. *Science*, 347(6223), pp.729–729.

Ohanna, M. et al., 2013. Secretome from senescent melanoma engages the STAT3 pathway to favor reprogramming of naive melanoma towards a tumor-initiating cell phenotype . *Oncotarget*, 4(12), pp.2012–2224.

Ohanna, M. et al., 2011. Senescent cells develop a PARP-1 and nuclear factor- k B-associated secretome (PNAS). *Genes & Development*, 25, pp.1245–1261.

Ohtani, N. & Hara, E., 2013. Roles and mechanisms of cellular senescence in regulation of tissue homeostasis. *Cancer Science*, 104(5), pp.525–530.

Ohuchi, H. et al., 2000. FGF10 Acts as a Major Ligand for FGF Receptor 2 IIIb in Mouse Multi-Organ Development. *Biochemical and Biophysical Research Communications*, 277(3), pp.643–649.

Oikonomou, E. et al., 2005. β-catenin mutations in craniopharyngiomas and pituitary adenomas. *Journal of Neuro-Oncology*, 73(3), pp.205–209.

Olivier, M., Hollstein, M. & Hainaut, P., 2010. TP53 Mutations in Human Cancers: Origins, Consequences, and Clinical Use. *Cold Spring Harbor Perspectives in Biology*, 2(1), pp.a001008--a001008.

Pao, W. & Miller, V.A., 2005. Epidermal growth factor receptor mutations, small-molecule kinase inhibitors, and non-small-cell lung cancer: current knowledge and future directions. *Journal of clinical oncology : official journal of the American Society of Clinical Oncology*, 23(11), pp.2556–68.

Park, W.-Y. et al., 2016. H3K27 Demethylase JMJD3 Employs the NF-$κ$B and BMP Signaling Pathways to Modulate the Tumor Microenvironment and Promote Melanoma Progression and Metastasis. *Cancer research*, 76(1), pp.161–170.

Parrinello, S. et al., 2003. Oxygen sensitivity severely limits the replicative lifespan of murine fibroblasts. *Nature cell biology*, 5(8), pp.741–7.

Parrinello, S. et al., 2005. Stromal-epithelial interactions in aging and cancer: senescent fibroblasts alter epithelial cell differentiation. *Journal of cell science*, 118(Pt 3), pp.485–496.

Patel, D.M., Shah, J. & Srivastava, A.S., 2013. Therapeutic Potential of Mesenchymal Stem Cells in Regenerative Medicine. *Stem Cells International*, 2013, pp.1–15.

Pathway, R.E.R.K. et al., 2011. Control of Mitotic Spindle Angle by. *Science*, 333(July), pp.342–345.

Pearson, G. et al., 2001. Mitogen-Activated Protein (MAP) Kinase Pathways: Regulation and Physiological Functions [1]. *Endocrine Reviews*, 22(2), pp.153–183.

Perez-Castro, C. et al., 2012. Cellular and Molecular Specificity of Pituitary Gland Physiology. *Physiological Reviews*, 92(1), pp.1–38.

Pérez Millán, M.I. et al., 2016. PROP1 triggers epithelial-mesenchymal transition-like process in pituitary stem cells. *eLife*, 5.

Perkins, N.D., 2007. Integrating cell-signalling pathways with NF-$κ$B and IKK function. *Nature Reviews Molecular Cell Biology*, 8(1), pp.49–62.

Pfeifer, A. et al., 2001. Delivery of the Cre recombinase by a self-deleting lentiviral vector: efficient gene targeting in vivo. *Proceedings of the National Academy of Sciences of the United States of America*, 98(20), pp.11450–5.

Pluquet, O., Pourtier, A. & Abbadie, C., 2015. The unfolded protein response and cellular senescence. A Review in the Theme: Cellular Mechanisms of Endoplasmic Reticulum Stress Signaling in Health and Disease. *American Journal of Physiology-Cell Physiology*, 308(6), pp.C415–C425.

te Poele, R.H. et al., 2002. DNA damage is able to induce senescence in tumor cells in vitro and in vivo. *Cancer research*, 62(6), pp.1876–1883.

Polakis, P., 2007. The many ways of Wnt in cancer. *Current Opinion in Genetics & Development*, 17(1), pp.45–51.

Polakis, P., 2012. Wnt Signaling in Cancer. *Cold Spring Harbor Perspectives in Biology*, 4(5), pp.a008052–a008052.

Politi, K. et al., 2006. Lung adenocarcinomas induced in mice by mutant EGF receptors found in human lung cancers respond to a tyrosine kinase inhibitor or to down-regulation of the receptors. *Genes & Development*, 20(11), pp.1496–1510.

Pollina, E.A. & Brunet, A., 2011. Epigenetic regulation of aging stem cells. *Oncogene*, 30(28), pp.3105–3126.

Potter, J.D. & Prentice, R.L., 2015. Cancer risk: Tumors excluded. *Science*, 347(6223), pp.727–727.

Prieur, A. et al., 2011. p53 and p16(INK4A) independent induction of senescence by chromatin-dependent alteration of S-phase progression. *Nature communications*, 2(May), p.473.

Qi, S. et al., 2013. Growth and weight of children with craniopharyngiomas based on the tumour location and growth pattern. *Journal of Clinical Neuroscience*, 20(12), pp.1702–1708.

Reimann, M. et al., 2010. Tumor Stroma-Derived TGF-β Limits Myc-Driven Lymphomagenesis via Suv39h1-Dependent Senescence. *Cancer Cell*, 17(3), pp.262–272.

Reincke, M. et al., Mutations in the deubiquitinase gene USP8 cause Cushing's disease. *Nature genetics*, 47(1), pp.31–38.

Reya, T. & Clevers, H., 2005. Wnt signalling in stem cells and cancer. *Nature*, 434(7035), pp.843–50.

van Rhee, F. et al., 2014. Siltuximab for multicentric Castleman's disease: a randomised, double-blind, placebo-controlled trial. *The Lancet Oncology*, 15(9), pp.966–974.

Ritschka, B. et al., 2017. The senescence-associated secretory phenotype induces cellular plasticity and tissue regeneration. *Genes and Development*, 31, pp.1–12.

Rizzoti, K., 2015. Genetic regulation of murine pituitary development. *Journal of Molecular Endocrinology*, 54(2), pp.R55–R73.

Rizzoti, K., Akiyama, H. & Lovell-Badge, R., 2013. Mobilized adult pituitary stem cells contribute to endocrine regeneration in response to physiological demand. *Cell stem cell*, 13(4), pp.419–32.

Roberson, R.S. et al., 2005. Escape from therapy-induced accelerated cellular senescence in p53-null lung cancer cells and in human lung cancers. *Cancer research*, 65(7), pp.2795–803.

Robinson, M.J. & Cobb, M.H., 1997. Mitogen-activated protein kinase pathways. *Current opinion in cell biology*, 9(2), pp.180–6.

Rodier, F. et al., 2009. Persistent DNA damage signalling triggers senescence-associated inflammatory cytokine secretion. *Nature cell biology*, 11(8), pp.973–979.

Ronchi, C.L. et al., Landscape of somatic mutations in sporadic GH-secreting pituitary adenomas. *European journal of endocrinology*, 174(3), pp.363–372. Articles&IdsFromResult=26701869&ordinalpos=3&itool=EntrezSystem2.PEntrez.Pubmed.Pubmed_ResultsPanel.Pubmed_RVDocSum.

Ronkina, N., Kotlyarov, A. & Gaestel, M., 2008. MK2 and MK3--a pair of

isoenzymes? *Frontiers in bioscience : a journal and virtual library*, 13, pp.5511–21.

Roos, C.M. et al., 2016. Chronic senolytic treatment alleviates established vasomotor dysfunction in aged or atherosclerotic mice. *Aging Cell*, 15(5), pp.973–977.

Roque, A. & Odia, Y., 2017. BRAF-V600E mutant papillary craniopharyngioma dramatically responds to combination BRAF and MEK inhibitors. *CNS oncology*, 6(2), pp.95–99.

Rostami, E. et al., 2017. Recurrent papillary craniopharyngioma with BRAFV600E mutation treated with neoadjuvant-targeted therapy. *Acta Neurochirurgica*, 159(11), pp.2217–2221.

Rovillain, E. et al., 2011. Activation of nuclear factor-kappa B signalling promotes cellular senescence. *Oncogene*, 30(20), pp.2356–2366.

Rubinfeld, B. et al., 1993. Association of the APC gene product with beta-catenin. *Science (New York, N.Y.)*, 262(5140), pp.1731–4.

Ruhland, M.K. et al., 2016. Stromal senescence establishes an immunosuppressive microenvironment that drives tumorigenesis. *Nature communications*, 7, p.11762.

Saab, R. et al., 2009. p18Ink4c and p53 Act as tumor suppressors in cyclin D1-driven primitive neuroectodermal tumor. *Cancer research*, 69(2), pp.440–8.

Safari, R. & Meuwissen, R., 2015. Practical Use of Advanced Mouse Models for Lung Cancer. In *Methods in molecular biology (Clifton, N.J.)*. pp. 93–124.

Sage, J. et al., 2003. Acute mutation of retinoblastoma gene function is sufficient for cell cycle re-entry. *Nature*, 424(6945), pp.223–8.

Sagiv, A. et al., 2013. Granule exocytosis mediates immune surveillance of senescent cells. *Oncogene*, 32(15), pp.1971–7.

Sajedi, E. et al., 2013. Analysis of mouse models carrying the I26T and R160C substitutions in the transcriptional repressor HESX1 as models for septo-optic dysplasia and hypopituitarism. *Disease models & mechanisms*, 1(4–5), pp.241–254.

Sajedi, E. et al., 2008. DNMT1 interacts with the developmental transcriptional repressor HESX1. *Biochimica et Biophysica Acta (BBA) - Molecular Cell Research*, 1783(1), pp.131–143.

Salama, R. et al., 2014. Cellular senescence and its effector programs. *Genes & Development*, 28(2), pp.99–114.

Saland, L.C., 2001. The mammalian pituitary intermediate lobe: an update on innervation and regulation. *Brain research bulletin*, 54(6), pp.587–93.

Salminen, A. et al., 2008. Activation of innate immunity system during aging: NF-kB signaling is the molecular culprit of inflamm-aging. *Ageing research reviews*, 7(2), pp.83–105.

Salminen, A., Kauppinen, A. & Kaarniranta, K., 2012. Emerging role of NF-κB signaling in the induction of senescence-associated secretory phenotype (SASP). *Cellular signalling*, 24(4), pp.835–45.

Sarkisian, C.J. et al., 2007. Dose-dependent oncogene-induced senescence in vivo

and its evasion during mammary tumorigenesis. *Nature Cell Biology*, 9(5), pp.493–505.

Sato, S. et al., 2015. Ablation of the p16INK4a tumour suppressor reverses ageing phenotypes of klotho mice. *Nature Communications*, 6, p.7035.

Sauer, B. & Henderson, N., 1988. Site-specific DNA recombination in mammalian cells by the Cre recombinase of bacteriophage P1. *Proceedings of the National Academy of Sciences of the United States of America*, 85(14), pp.5166–70.

Scagliotti, V. et al., 2016. Histopathology and molecular characterisation of intrauterine-diagnosed congenital craniopharyngioma. *Pituitary*, 19(1), pp.50–56.

Schafer, M.J. et al., 2017. Cellular senescence mediates fibrotic pulmonary disease. *Nature Communications*, 8, p.14532.

Schepers, A.G. et al., 2012. Lineage Tracing Reveals Lgr5+ Stem Cell Activity in Mouse Intestinal Adenomas. *Science*, 337(October), pp.449–452.

Schimmer, B.P. & White, P.C., 2010. Minireview: steroidogenic factor 1: its roles in differentiation, development, and disease. *Molecular endocrinology (Baltimore, Md.)*, 24(7), pp.1322–37.

Schindelin, J. et al., 2012. Fiji: an open-source platform for biological-image analysis. *Nature Methods*, 9(7), pp.676–682.

Schuster, K. et al., 2014. Nullifying the CDKN2AB locus promotes mutant K-ras lung tumorigenesis. *Molecular cancer research : MCR*, 12(6), pp.912–23.

Sekine, S. et al., 2002. Craniopharyngiomas of adamantinomatous type harbor beta-catenin gene mutations. *The American journal of pathology*, 161(6), pp.1997–2001.

Serrano, M. et al., 1997. Oncogenic ras provokes premature cell senescence associated with accumulation of p53 and p16(INK4a). *Cell*, 88(5), pp.593–602.

Serrano, M. et al., 1996. Role of the INK4a locus in tumor suppression and cell mortality. *Cell*, 85(1), pp.27–37.

Serrano, M., Hannon, G.J. & Beach, D., 1993. A new regulatory motif in cell-cycle control causing specific inhibition of cyclin D/CDK4. *Nature*, 366(6456), pp.704–707.

Seymour, P.A. et al., 2007. SOX9 is required for maintenance of the pancreatic progenitor cell pool. *Proceedings of the National Academy of Sciences*, 104(6), pp.1865–1870.

Sharpless, N.E. et al., 2004. The differential impact of p16 INK4a or p19 ARF deficiency on cell growth and tumorigenesis. *Oncogene*, 23(2), pp.379–385.

Sharpless, N.E. & Sherr, C.J., 2015. Forging a signature of in vivo senescence. *Nature Reviews Cancer*, 15(7), pp.397–408.

Shaw, A.C. et al., 2010. Aging of the innate immune system. *Current Opinion in Immunology*, 22(4), pp.507–513.

Shaw, A.T. & Engelman, J.A., 2013. *ALK* in Lung Cancer: Past, Present, and Future. *Journal of Clinical Oncology*, 31(8), pp.1105–1111.

Shelton, D.N. et al., 1999. Microarray analysis of replicative senescence. *Current*

biology : CB, 9(17), pp.939–45.

Shepherd, F.A. et al., 2007. The International Association for the Study of Lung Cancer lung cancer staging project: proposals regarding the clinical staging of small cell lung cancer in the forthcoming (seventh) edition of the tumor, node, metastasis classification for lung cancer. *Journal of thoracic oncology : official publication of the International Association for the Study of Lung Cancer*, 2(12), pp.1067–77.

Shigematsu, H. & Gazdar, A.F., 2006. Somatic mutations of epidermal growth factor receptor signaling pathway in lung cancers. *International Journal of Cancer*, 118(2), pp.257–262.

Shlomo Melmed, 2011. Pathogenesis of pituitary tumors. *Nature Reviews Endocrinology*, 7(10), pp.207–227.

Singer, O. & Verma, I.M., 2008. Applications of lentiviral vectors for shRNA delivery and transgenesis. *Current gene therapy*, 8(6), pp.483–8.

Song, M. & Giovannucci, E.L., 2015. Cancer risk: Many factors contribute. *Science*, 347(6223), pp.728–729.

Soriano, P., 1999. Generalized lacZ expression with the ROSA26 Cre reporter strain. *Nature genetics*, 21(1), pp.70–1.

Spike, B.T. & Wahl, G.M., 2011. p53, Stem Cells, and Reprogramming: Tumor Suppression beyond Guarding the Genome. *Genes & cancer*, 2(4), pp.404–419.

Stache, C. et al., 2015. Insights into the infiltrative behavior of adamantinomatous craniopharyngioma in a new xenotransplant mouse model. *Brain pathology (Zurich, Switzerland)*, 25(1), pp.1–10.

Stamos, J.L. & Weis, W.I., 2013. The β-catenin destruction complex. *Cold Spring Harbor perspectives in biology*, 5(1), p.a007898.

Stolt, C.C. et al., 2003. The Sox9 transcription factor determines glial fate choice in the developing spinal cord. *Genes & development*, 17(13), pp.1677–89.

Storer, M. et al., 2013. Senescence is a developmental mechanism that contributes to embryonic growth and patterning. *Cell*, 155(5), pp.1119–1130.

Su, L.K. et al., 1992. Multiple intestinal neoplasia caused by a mutation in the murine homolog of the APC gene. *Science (New York, N.Y.)*, 256(5057), pp.668–70.

Su, L.K., Vogelstein, B. & Kinzler, K.W., 1993. Association of the APC tumor suppressor protein with catenins. *Science (New York, N.Y.)*, 262(5140), pp.1734–7..

Subramanian, A. et al., 2005. Gene set enrichment analysis: a knowledge-based approach for interpreting genome-wide expression profiles. *Proceedings of the National Academy of Sciences of the United States of America*, 102(43), pp.15545–50.

Sun, D. et al., 2013. Sox9-related signaling controls zebrafish juvenile ovary–testis transformation. *Cell Death & Disease*, 4(11), pp.e930–e930.

Sutherland, K.D. et al., 2014. Multiple cells-of-origin of mutant K-Ras-induced mouse lung adenocarcinoma. *Proceedings of the National Academy of Sciences of the United States of America*, 111(13), pp.4952–7.

Sutherland, K.D. & Berns, A., 2010. Cell of origin of lung cancer. *Molecular Oncology*, 4(5), pp.397–403.

Syro, L. V et al., 2015. Progress in the Diagnosis and Classification of Pituitary Adenomas. *Frontiers in endocrinology*, 6, p.97.

Tammela, T. et al., 2017. A Wnt-producing niche drives proliferative potential and progression in lung adenocarcinoma. *Nature*, 545(7654), pp.355–359.

Tariq, M.U. et al., 2017. Papillary craniopharyngioma: A clinicopathologic study of a rare entity from a major tertiary care center in Pakistan. *Neurology India*, 65(3), pp.570–576.

Tasdemir, N. et al., 2016. BRD4 connects enhancer remodeling to senescence immune surveillance. *Cancer Discovery*.

Tateyama, H. et al., 2001. Different keratin profiles in craniopharyngioma subtypes and ameloblastomas. *Pathology, research and practice*, 197(11), pp.735–42.

Tchkonia, T. et al., 2013. Cellular senescence and the senescent secretory phenotype: therapeutic opportunities. *Journal of Clinical Investigation*, 123(3), pp.966–972.

Theveneau, E. & Mayor, R., 2012. Neural crest delamination and migration: From epithelium-to-mesenchyme transition to collective cell migration. *Developmental Biology*, 366(1), pp.34–54.

Thomas, P. & Beddington, R., 1996. Anterior primitive endoderm may be responsible for patterning the anterior neural plate in the mouse embryo. *Current Biology*, 6(11), pp.1487–1496.

Tiozzo, C. et al., 2009. Deletion of *Pten* Expands Lung Epithelial Progenitor Pools and Confers Resistance to Airway Injury. *American Journal of Respiratory and Critical Care Medicine*, 180(8), pp.701–712.

Tomasetti, C. & Vogelstein, B., 2015. Variation in cancer risk among tissues can be explained by the number of stem cell divisions. *Science*, 347(6217), pp.78–81.

Travis, W.D. et al., 2015. The 2015 World Health Organization Classification of Lung Tumors: Impact of Genetic, Clinical and Radiologic Advances Since the 2004 Classification. *Journal of thoracic oncology : official publication of the International Association for the Study of Lung Cancer*, 10(9), pp.1243–1260.

Travis, W.D., Brambilla, E. & Riely, G.J., 2013. New Pathologic Classification of Lung Cancer: Relevance for Clinical Practice and Clinical Trials. *Journal of Clinical Oncology*, 31(8), pp.992–1001.

Treier, M., O'Connell, S., Gleiberman, a, et al., 2001. Hedgehog signaling is required for pituitary gland development. *Development (Cambridge, England)*, 128(3), pp.377–386.

Treier, M., O'Connell, S., Gleiberman, A., et al., 2001. Hedgehog signaling is required for pituitary gland development. *Development (Cambridge, England)*, 128(3), pp.377–86.].

Treier, M. et al., 1998. Multistep signaling requirements for pituitary organogenesis in vivo. *Genes & development*, 12(11), pp.1691–704.

Trejo, C.L. et al., 2012. MEK1/2 Inhibition Elicits Regression of Autochthonous Lung Tumors Induced by KRASG12D or BRAFV600E. *Cancer Research*, 72(12), pp.3048–3059.

Trowe, M.-O. et al., 2013. Inhibition of Sox2-dependent activation of Shh in the ventral diencephalon by Tbx3 is required for formation of the neurohypophysis. *Development (Cambridge, England)*, 140(11), pp.2299–309.

Tuveson, D.A. et al., 2004. Endogenous oncogenic K-ras(G12D) stimulates proliferation and widespread neoplastic and developmental defects. *Cancer cell*, 5(4), pp.375–87.

Tuveson, D.A. et al., Endogenous oncogenic K-ras(G12D) stimulates proliferation and widespread neoplastic and developmental defects. *Cancer cell*, 5(4), pp.375–387.

Välimäki, N. et al., Whole-Genome Sequencing of Growth Hormone (GH)-Secreting Pituitary Adenomas. *The Journal of clinical endocrinology and metabolism*, 100(10), pp.3918–3927.

Vankelecom, H., 2010. Pituitary stem/progenitor cells: embryonic players in the adult gland? *The European journal of neuroscience*, 32(12), pp.2063–81.

Ventura, J.J. et al., 2007. p38alpha MAP kinase is essential in lung stem and progenitor cell proliferation and differentiation. *Nature genetics*, 39(6), pp.750–8.

Vicent, S. et al., 2004. ERK1/2 is activated in non-small-cell lung cancer and associated with advanced tumours. *British Journal of Cancer*, 90(5), pp.1047–1052.

Vital, P. et al., 2014. The senescence-associated secretory phenotype promotes benign prostatic hyperplasia. *American Journal of Pathology*, 184(3), pp.721–731.

Vizioli, M.G. et al., 2011. Evidence of oncogene-induced senescence in thyroid carcinogenesis. *Endocrine-Related Cancer*, 18(6), pp.743–757.

Vousden, K.H. & Ryan, K.M., 2009. P53 and Metabolism. *Nature reviews. Cancer*, 9(10), pp.691–700.

Wagner, J. et al., 2015. Overexpression of the novel senescence marker $β$-galactosidase (GLB1) in prostate cancer predicts reduced PSA recurrence. *PloS one*, 10(4), p.e0124366.

Wajapeyee, N. et al., 2008. Oncogenic BRAF induces senescence and apoptosis through pathways mediated by the secreted protein IGFBP7. *Cell*, 132(3), pp.363–74.

Wang, C. et al., 2009. DNA damage response and cellular senescence in tissues of aging mice. *Aging Cell*, 8(3), pp.311–323.

Ward, R.D. et al., 2006. Cell proliferation and vascularization in mouse models of pituitary hormone deficiency. *Molecular endocrinology (Baltimore, Md.)*, 20(6), pp.1378–1390.

Weaver, A.N. & Yang, E.S., 2013. Beyond DNA Repair: Additional Functions of PARP-1 in Cancer. *Frontiers in oncology*, 3(November), p.290.

Weiss, S. et al., Evidence for a progenitor cell population in the human pituitary. *Clinical neuropathology*, 28(4), pp.309–18.

Wesche, J., Haglund, K. & Haugsten, E.M., 2011. Fibroblast growth factors and their receptors in cancer. *Biochemical Journal*, 437(2), pp.199–213.

White, E., 2012. Deconvoluting the context-dependent role for autophagy in cancer. *Nat Rev Cancer*, 12(6), pp.401–410.

Widmann, C. et al., 1999. Mitogen-activated protein kinase: conservation of a three-kinase module from yeast to human. *Physiological reviews*, 79(1), pp.143–80.

Wild, C. et al., 2015. Cancer risk: Role of chance overstated. *Science*, 347(6223), pp.728–728.

Winslow, M.M. et al., 2011. Suppression of lung adenocarcinoma progression by Nkx2-1. *Nature*, 473(7345), pp.101–104.

Wirawan, E. et al., 2012. Autophagy: for better or for worse. *Cell research*, 22(1), pp.43–61.

Wistuba, I.I. & Gazdar, A.F., 2006. Lung cancer preneoplasia. *Annual review of pathology*, 1(1), pp.331–48.

Wood, L.D. et al., 2007. The Genomic Landscapes of Human Breast and Colorectal Cancers. *Science*, 318(5853), pp.1108–1113.

Wu, S. et al., 2016. Substantial contribution of extrinsic risk factors to cancer development. *Nature*, 529(7584), pp.43–7.

Xu, M. et al., 2008a. Beta-catenin expression results in p53-independent DNA damage and oncogene-induced senescence in prelymphomagenic thymocytes in vivo. *Molecular and cellular biology*, 28(5), pp.1713–23.

Xu, M. et al., 2008b. Beta-catenin expression results in p53-independent DNA damage and oncogene-induced senescence in prelymphomagenic thymocytes in vivo. *Molecular and cellular biology*, 28(5), pp.1713–23.

Xu, M. et al., 2018. Senolytics improve physical function and increase lifespan in old age. *Nature Medicine*, 24(8), pp.1246–1256.

Xu, Q. et al., 2009. Isolation of tumour stem-like cells from benign tumours. *British journal of cancer*, 101(2), pp.303–11.

Xu, X. et al., 2012. Evidence for type II cells as cells of origin of K-Ras-induced distal lung adenocarcinoma. *Proceedings of the National Academy of Sciences*, 109(13), pp.4910–4915.

Xue, W. et al., 2007a. Senescence and tumour clearance is triggered by p53 restoration in murine liver carcinomas. *Nature*, 445(7128), pp.656–60.

Xue, W. et al., 2007b. Senescence and tumour clearance is triggered by p53 restoration in murine liver carcinomas. *Nature*, 445(7128), pp.656–60.

Yang, G. et al., 2006. The chemokine growth-regulated oncogene 1 (Gro-1) links RAS signaling to the senescence of stromal fibroblasts and ovarian tumorigenesis. *Proceedings of the National Academy of Sciences of the United States of America*, 103(44), pp.16472–16477.

Yauch, R.L. et al., 2008. A paracrine requirement for hedgehog signalling in cancer. *Nature*, 455(7211), pp.406–10.

Yosef, R. et al., 2016. Directed elimination of senescent cells by inhibition of BCL-W and BCL-XL. *Nature Communications*, 7(1), p.11190.

Yosef, R. et al., 2017. p21 maintains senescent cell viability under persistent DNA damage response by restraining JNK and caspase signaling. *The EMBO*

Journal, 36(15), pp.2280–2295.

Young, M.D. et al., 2010. Gene ontology analysis for RNA-seq: accounting for selection bias. *Genome Biology*, 11(2), p.R14.

Yu, Y.-C. et al., 2013. Radiation-induced senescence in securin-deficient cancer cells promotes cell invasion involving the IL-6/STAT3 and PDGF-BB/PDGFR pathways. *Scientific Reports*, 3.

Yun, M.H., Davaapil, H. & Brockes, J.P., 2015. Recurrent turnover of senescent cells during regeneration of a complex structure. *eLife*, 4.

Zhang, D., Wang, H. & Tan, Y., 2011. Wnt/β-catenin signaling induces the aging of mesenchymal stem cells through the DNA damage response and the p53/p21 pathway. A. J. Cooney, ed. *PloS one*, 6(6), p.e21397.

Zhang, S. & Cui, W., 2014. Sox2, a key factor in the regulation of pluripotency and neural differentiation. *World Journal of Stem Cells*, 6(3), p.305.

Zhao, R. et al., 2016. Implications of Genetic and Epigenetic Alterations of CDKN2A (p16(INK4a)) in Cancer. *EBioMedicine*, 8, pp.30–39.

Zhou, C. et al., 2013. The Rac1 splice form Rac1b promotes K-ras-induced lung tumorigenesis. *Oncogene*, 32(7), pp.903–9.

Zhu, J. & You, C., 2015. Craniopharyngioma: Survivin expression and ultrastructure. *Oncology letters*, 9(1), pp.75–80.

Zhu, L. et al., 2016. Multi-organ Mapping of Cancer Risk. *Cell*, 166(5), p.1132–1146.e7.

Zhu, X. et al., 2007. Signaling and epigenetic regulation of pituitary development. *Current Opinion in Cell Biology*, 19(6), pp.605–611.

Zhu, Y. et al., 2016. Identification of a novel senolytic agent, navitoclax, targeting the Bcl-2 family of anti-apoptotic factors. *Aging Cell*, 15(3), pp.428–435.

Zhu, Y. et al., 2015. The Achilles' Heel of Senescent Cells: From Transcriptome to Senolytic Drugs. *Aging Cell*,

Zoicas, F. & Schöfl, C., 2012. Craniopharyngioma in adults. *Frontiers in endocrinology*, 3, p.46.

Zomer, A. et al., 2013. Brief report: Intravital imaging of cancer stem cell plasticity in mammary tumors. *Stem Cells*, 31(3), pp.602–606.